Does it Stick?

Macromolecular Building Blocks for Antifouling Coatings

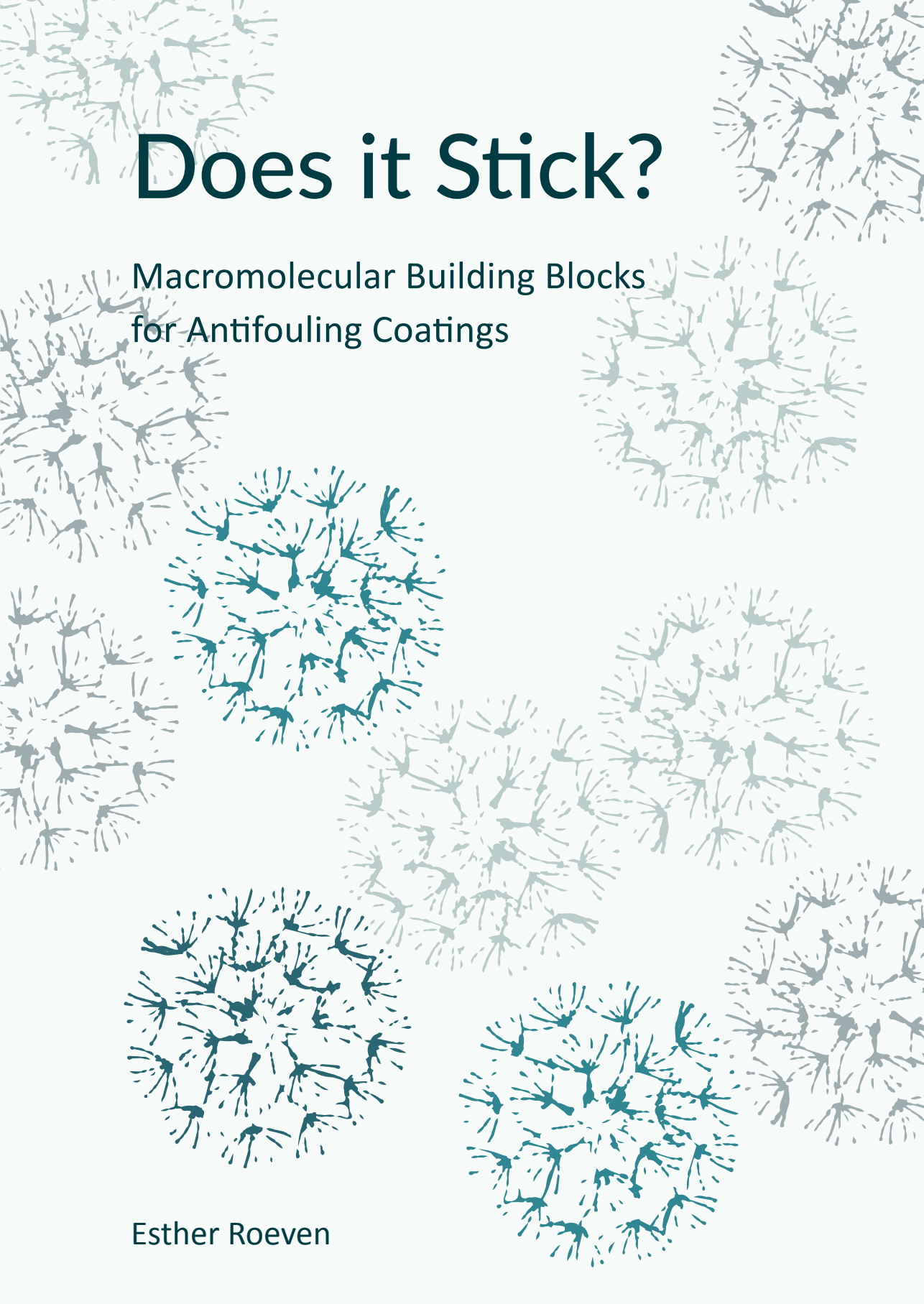

Esther Roeven

Propositions

1. Dendrimers are not as well defined as generally claimed in literature.
   (this thesis)

2. The choice of reference surface is equally important to assess the degree of fouling as the choice of the antifouling coating itself.
   (this thesis)

3. Application-driven research trumps research-driven applications.

4. Deconvolution to individual peaks for all chemical species in X-ray photoelectron spectroscopy narrow spectra leads to "wishful fitting".

5. Scientific publications need to be judged like wine: quality over quantity.

6. We have only scratched the surface regarding the possible impact of surface chemistry in many industries.

7. In both family and chemistry, breaking bonds opens up possibilities for new ones.

Propositions belonging to the thesis, entitled

Does it Stick? – Macromolecular Building Blocks for Antifouling Coatings

Esther Roeven,
Wageningen, 1 December 2021

Does it Stick?

Macromolecular Building Blocks for Antifouling Coatings

Esther Roeven

Thesis committee

Promotor

Prof. Dr H. Zuilhof

Professor of Organic Chemistry

Wageningen University & Research

Co-promotor

Dr M.M.J. Smulders

Associate Professor, Laboratory of Organic Chemistry

Wageningen University & Research

Other members

Prof. Dr J.R. de Vries, Wageningen University & Research

Prof. Dr Dr P.Y.W. Dankers, Eindhoven University of Technology

Prof. Dr P. Jonkheijm, University of Twente, Enschede

Dr C. Rodriguez-Emmenegger, RWTH Aachen University, Germany

This research was conducted under the auspices of the Graduate School VLAG (Advanced studies in Food Technology, Agrobiotechnology, Nutrition and Health Sciences).

Does it Stick?

Macromolecular Building Blocks for Antifouling Coatings

Esther Roeven

Thesis

Submitted in fulfilment of the requirements of the degree of doctor

at Wageningen University

by the authority of the Rector Magnificus,

Prof. Dr A.P.J. Mol,

in the presence of the

Thesis Committee appointed by the Academic Board

to be defended in public

on Wednesday 1 December 2021

at 4.00 p.m. in the Aula.

Esther Roeven
Does it Stick? - Macromolecular Building Blocks for Antifouling Coatings
182 pages.

PhD thesis, Wageningen University, Wageningen, the Netherlands (2021)
With references, with summary in English

ISBN 978-94-6395-943-8
DOI 10.18174/551763

Table of Contents

Chapter 1	**General Introduction**	**7**
Chapter 2	**Design, Synthesis, and Characterization of Fully Zwitterionic, Functionalized Dendrimers**	**23**
Chapter 3	**Surface Immobilization Strategies for Zwitterionic Dendrimers**	**57**
Chapter 4	**Zwitterionic Dendrimer – Polymer Hybrid Copolymers for Self-Assembling Antifouling Coatings**	**87**
Chapter 5	**PLL-poly(HPMA) Bottlebrush-Based Antifouling Coatings: Three Grafting Routes**	**119**
Chapter 6	**General Discussion**	**151**
	Summaries	**163**
	Summary	165
	Samenvatting	167
	About the Author	**171**
	Curriculum Vitae	173
	List of Publications	174
	Overview of Completed Training Activities	175
	Dankwoord	**177**

Chapter 1

General Introduction

Abstract

In this chapter, a brief introduction to the concepts of fouling and antifouling is given. The most commonly used antifouling coatings are discussed alongside the most promising, state-of-the-art materials. Furthermore, macromolecules that make interesting candidates to serve as building blocks for antifouling coatings are introduced. At the end of this chapter, the overall aims of this research and a short outline of this Thesis are given.

1.1 Fouling and Antifouling

Fouling generally refers to the undesired deposition of material onto a surface, such as non-organic materials (e.g. dust or soil) or organic (bio)materials. Notably, this Thesis is focused on the prevention of organic (bio)fouling in aqueous media. Especially when operating in biomedical systems, one has to deal with interactions at the solid-liquid interface. Contact between a solid surface and a biological medium, such as blood (plasma), interstitial fluids or clinical samples, rapidly leads to the adsorption of small (bio)molecular components on the solid's surface.[1–3] In some cases these interactions are desired, e.g. biomarkers that have to contact a biosensor's surface in order to provoke a signal.[4,5] Nonetheless, most of the spontaneous interactions are undesired. In the example of biosensors, unwanted interactions of components in the operation medium lead to undesirably high noise levels, which lower the sensitivity and selectivity of the assay, obstructing the proper functioning of the sensor platform.[6–8] In the case of fouling of surgical tools and implants, settlements on the surface can lead to inflammations or even rejection responses of the concerning organism.[3,9,10] However, adsorption of specific biomolecules on a biomaterial surface, is not always harmful and, in some cases, even beneficial. For example, formed bio-films on artificial joints can have lubricating effects,[11] and bone cell attachment and proliferation on orthopedic implants can be enhanced by protein adsorption.[12] Therefore, by looking at the examples of biosensors and medical tools, it is obvious that developing knowledge on how to control protein adsorption on a material surface is crucial.[13]

In order to prevent unwanted interactions, it is first of all important to understand the underlying mechanism of (bio)fouling. On hydrophobic or moderately hydrophilic surfaces it is energetically more favorable for water molecules to interact with each other rather than contacting the surface.[1] Simultaneously, proteins and other biomaterials adsorb to surfaces in order to reduce the interfacial energy with their hydrophilic aqueous environment. By a change in conformation of the protein structures, hydrophobic domains can be exposed, which leads to hydrophobic interactions (Van der Waals interactions) with the surface at the exclusion of water molecules.[14] Whereas single hydrophobic interactions are only weak, collectively they can form a substantial driving force for the overall adsorption of proteins to surfaces, especially since 40–50% of the surface area of most small proteins is non-polar.[15] Therefore, one of the basic requirements for a surface to be *antifouling* is a low interfacial energy with aqueous medium, i.e. to be hydrophilic. One way to control the interactions between a material and its surroundings is by engineering the material's surface by applying a thin coating layer.

1.2 Antifouling Coatings

In order to minimize the interfacial energy of a surface with an aqueous environment, hydrophilic coatings have been developed that are designed to create a so called "hydration layer".[8,16–19] The developed coatings usually contain functional groups like *e.g.* ethylene glycols,[20] polysaccharides,[21] amino acids,[22,23] and mixed charged groups.[24] Fundamental studies by the group of Whitesides using thin, self-assembling monolayers (SAMs) led to insights that are now known as 'Whitesides rules' listing the general properties for antifouling coatings, which should: (i) contain hydrogen bond acceptors, but not hydrogen bond donors, (ii) be charge neutral and (iii) be polar.[25–27] Later, based on computational models, Le *et al.* added to these guidelines the advice to use *relatively large, conformationally mobile and polarizable functional groups*.[28] Independently, other studies also showed thickness-dependent antifouling properties, in which thicker coating layers outperformed their thin analogs.[29–31]

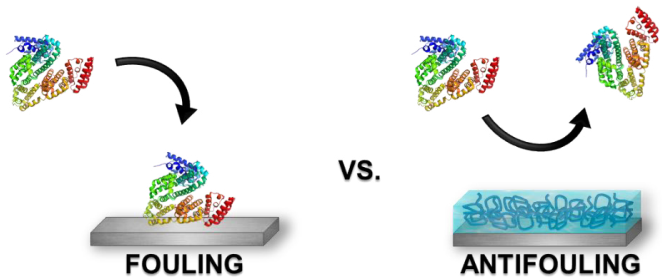

Figure 1.1 Schematic representation of the undesired adsorption of proteins (fouling) versus repellence (antifouling) upon the application of a hydrated, hydrophilic coating.

Poly(ethylene glycol)

One of the most applied antifouling materials is based on oligo- or poly(ethylene glycol) (OEG or PEG).[32,33] Next to the hydrophilic nature of the PEG coatings, the mechanism for protein repellence of PEG systems can also be attributed to the "steric repulsion" between hydrated neutral PEG chains and proteins.[34] Indeed, during protein adsorption, physisorbed water has to be removed from the PEG structure, a process which is thermodynamically unfavorable.[20,35,36] For the abovementioned reasons, PEG was for quite some time considered as the golden standard for protein-resistant surfaces. However, since 1983, also disadvantages became visible, including the expression of antibodies and oxidative degradation, yielding toxic compounds.[27,37,38] Furthermore, the use of PEG *in vivo* leads to the expression of antibodies specific for PEGs.[39–41] Hence, in the recent decades, strong interests towards alternatives to PEG based antifouling coatings have developed.

Zwitterionic materials

Among the recently developed coatings, one of the most successfully applied materials complying with all of the Whitesides rules are *zwitterionic coatings*.[42] A zwitterionic material carries both one or more positive and negative charge, whilst being overall neutral under physiological conditions.[43] Charge neutrality is an important property for an antifouling coating in order to minimize the charge-based drive for adsorption of proteins.[3,16,17,44] In surface chemistry, mainly *betaines* are being used since these

zwitterion pairs cannot isomerize to an uncharged form.[45,46] In betaines the positive charge is generally located on a quaternary ammonium group, while the negative charge usually is a carboxylate (carboxybetaine), sulfonate (sulfobetaine) or phosphonate (phosphocholine) (Figure 1.2).[42,47] Applied as a coating, especially carboxybetaine zwitterionic materials have shown to drastically reduce (bio)fouling, even in complex media such as plasma or blood serum.[18,29,48–50] In comparative studies, zwitterionic-based antifouling coatings outperformed PEG, likely because of their electrically induced and stronger solvation of water compared to solely hydrogen bond driven hydration of PEG.[51,52]

Poly(*N*-(2-hydroxypropyl)methacrylamide)

More recently, poly(*N*-(2-hydroxypropyl)methacrylamide) (polyHPMA) polymer coatings have been reported to be highly antifouling, on a par with - and in some cases outperforming - zwitterionic polymer coatings.[13,42,53–56] Although the antifouling properties of poly(HPMA) are not entirely understood,[55] since their earliest days, poly(HPMA) has been functioning as excellent bioinert polymers for drug delivery systems.[57,58] These bioinert properties were later related to low protein adsorption at the interface with the biological medium.[54,59] Since poly(HPMA) is lacking ionic moieties, its antifouling mechanism might rely on a different mechanism than zwitterionic materials. Thermodynamic analysis by the group of Rodriguez-Emmenegger indicated strong interactions between poly(HPMA) coated surfaces and water and suggested that poly(HPMA) was a poor H-bond donor.[60]

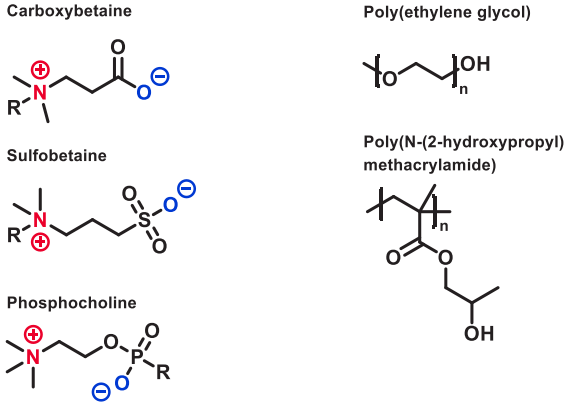

Figure 1.2 Left: Chemical structures of the most commonly used zwitterionic motifs in antifouling coatings. Right: chemical structure of poly(ethylene glycol) and poly(*N*-(2-hydroxypropyl)methacrylamide).

1.3 Polymeric Antifouling Coatings

As mentioned before, thicker polymeric PEG and zwitterionic coating layers outperform their thinner chemical analogs,[29] most possibly because the thicker polymer layer benefits from the increased number of antifouling groups per square unit of surface area. In addition, the adsorption of proteins is entropically unfavorable on thick layers, as it leads to the compression of the highly flexible, "sponge-like" polymer structure.[28,30,31] These polymer layers are typically made by *grafting-to* or *grafting-from* the surface (Figure 1.3).

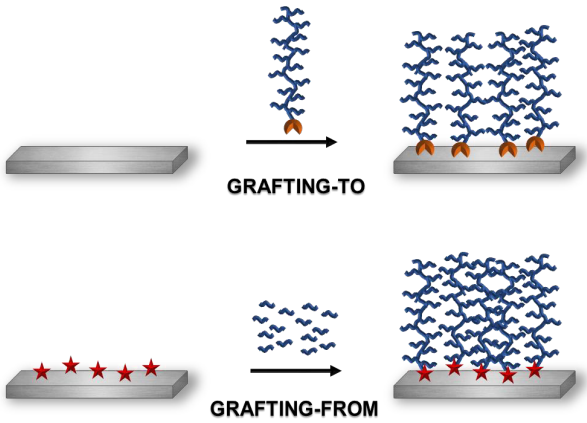

Figure 1.3 Schematic representation of grafting-to and grafting-from approaches to immobilize polymers onto surfaces. Polymer chains are depicted in blue, the orange clamps represent the functional end-groups of a polymer that bind to the surface (in the case of grafting-to) and the red stars represent reactive groups that could be immobilized onto the surface as a point for the chain growth (in the case of grafting-from).

The first approach relies on the binding, either physical or chemical, of polymers containing a functional group with affinity for the surface.[61,62] The second uses *in situ* polymerization of monomers on a surface-immobilized initiator.[18,63,64] Growing polymers from the surface leads to a densely packed *polymer brush* structure with tunable thickness, thereby making it a promising route towards antifouling coatings.[65–67] Currently, the best performing antifouling coatings are prepared by the use of grafting-from methods.[33,43,52] However, despite the advantageous properties of polymer brushes grown via the grafting-from method, there is a major hurdle to be overcome when applying these antifouling coatings on large, industrially relevant scales.[69] Namely, grafting-from polymer brushes are typically synthesized by surface-initiated, controlled living polymerization in the presence of a (metal) catalysts and in an oxygen-free environment.[53,55,63,70,71] Since these conditions make it a demanding technique, it is difficult to scale up and implement it in, *e.g.*, industrial production lines in a reproducible manner.[18,67] Very recently, surface-initiated polymerizations have been developed that can be performed in ambient conditions.[72,73] The biggest advantage of the grafting-to method is its potentially simple application step, using only small amounts of a carefully pre-synthesized polymer that can self-assemble on a surface under mild conditions.[18,53,63,70] However, in contrast to grafting-from, the main challenge of this method is to reach a sufficient grafting-density of the resulting coating, which depends on the molecular weight and affinity of the polymer towards the surface.[3]

1.4 Macromolecules as Antifouling Materials

Dendrimers

To overcome the challenges related to the grafting-from approach, we explore macromolecular systems that allow for grafting-to approaches, whilst also possessing antifouling properties. We chose to work with a special class of polymers called *dendrimers*. Dendrimers are multivalent (macro)molecules in which the repeated units are not connected in a linear fashion, but form a well-defined, branched three-dimensional architecture of nanometer size (Figure 1.4).[74–77] As a result, they possess a distinct molecular architecture that consists of a central core, branches and terminal functional groups, present at the outer surface of the macromolecule.

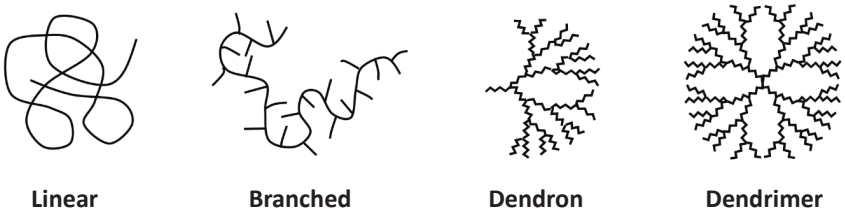

Figure 1.4 Examples of different classes of macromolecules, from linear polymers to dendrimers.[78]

Dendrimers of different sizes can be engineered by a stepwise, versatile chemical synthesis approach. Generally, dendrimers are synthesized *via* two conceptually different approaches, namely *divergent* or *convergent* routes.[79] Divergent syntheses start from a multifunctional core, followed by creating one monomer layer or *generation* at the time.[80] In contrast, in the convergent approach the dendrimer synthesis starts from the end groups and terminates at the core. This is made possible by two or more subunits reacting with a single joining unit, which will thereby form the core of the dendrimer.[81]

Due to their highly defined 3D structure, several types of dendrimers have found use in biomedical applications such as drug delivery, sensing and MRI contrast agents.[82–91] However, most commonly used dendrimers, like *e.g.* poly(propylene imine) (PPI) and poly(amido amine) (PAMAM),[81] are not biocompatible.[92,93] As a result, to reduce their toxicity, the exterior of these dendrimers had to be modified with, polyethylene glycol (PEG)[94,95,96] or charged groups[82,87,91,97–99] for their *in vivo* use. Because of their highly organized structure and the possibilities for functionalization at their terminal ends, we envisioned to modify dendrimers to become fully zwitterionic, in order to be able to test their potential as building blocks for antifouling coatings, which so far has not been reported.

Hybrid Copolymers

In search for a method to bind macromolecular building blocks to a surface in one step - in a grafting-to fashion - they could be coupled to a polymer prior to surface immobilization.[100] The polymer of choice should have affinity towards the surface and allow for the coupling of multiple building blocks. Poly(L-lysine) (PLL) is known for its affinity towards, for example, silicon oxide, metal oxide and polymeric surfaces driven by multiple electrostatic attractions between the negatively charged surface and the positively charged pendant amine groups present in PLL.[34,62,101–106] A well-known and widely used combination of PLL with antifouling side groups is poly(L-lysine)-*graft*-poly(ethylene glycol) (PLL-

g-PEG).[34,62,101–104] In other studies, also the coupling of other antifouling polymers to a PLL backbone was shown to result in coatings with antifouling properties.[62,107] For drug delivery purposes, PLL-poly(HPMA) block copolymers were synthesized in order to obtain transfection agents with minimal toxicity.[108]

The combination of linear and dendritic copolymers, was first described in the beginning of 1990s by the group of Fréchet.[109–111] Other research groups have developed block,[112–114] star,[115,116] linearly alternating linear-dendrimer hybrid architectures,[111] crosslinked superstructures,[117] and brush-like polymers with dendritic side chains[118–120] to control self-assembly, to enhance solubility and to reduce toxicity and immunogenicity of polymeric materials.[110,121]

1.5 Outline of this Thesis

In this Thesis, we combine the fields of organic chemistry and surface chemistry to cover the development of antifouling coatings: from the synthesis of the macromolecular building blocks to the application in surface coatings and testing of antifouling properties. The synthesis of these building blocks was allowed to involve multiple steps, while the main focus throughout our research was on the development of robust and yet mild surface functionalization and effective coatings.

In **Chapter 2** we describe the design and subsequent synthesis of dendrimers that are highly charged whilst having zero net charge, *i.e.* zwitterionic dendrimers (ZIDs). These ZIDs are potential candidates for biomedical applications such as antifouling coating, but also for *e.g.* drug delivery. First we fully optimized the synthesis of charge-neutral carboxybetaine and sulfobetaine zwitterionic dendrimers. However, in order to have a functional “handle” on the ZIDs, we subsequently synthesized ZIDs that contain a variable number of alkyne and azide groups that allow straightforward (bio)functionalization or surface coupling via click chemistry.

To form a coating, the developed macromolecules need to be coupled to a surface. **Chapter 3** reports different strategies to enable covalent immobilization of the ZID on a surface to create a stable and potentially durable coating. The first explored method was amide bond-mediated binding of the ZID’s carboxylates to amine-terminated surfaces. Next to this, two types of click-reactions, CuAAC and thiol-yne chemistry, between pre-installed functional groups on the ZIDs and the surfaces were tested. Finally, mono- and multilayer coatings were formed by free radical polymerization of methacrylate functionalized ZIDs on pre-modified surfaces. Antifouling properties of the most promising coatings were preliminarily tested using fluorescently labelled proteins and fluorescence microscopy.

The work in Chapter 3, however, showed that to immobilize ZIDs, a pre-functionalization step was needed, which is undesirable. To circumvent this, the macromolecules themself should be designed as such that they have an intrinsic affinity towards the surface. Therefore, in **Chapter 4** we used a *linear polymer* as a coupling agent to a surface. We showed two different routes to synthesize polymer-dendrimer hybrids by the coupling of poly(L-lysine) and ZIDs. The PLL-ZID macromolecules were self-assembled on silicon oxide surfaces from aqueous solutions in a single step. Their potential use as antifouling coatings was tested by fluorescence microscopy and quartz crystal microbalance (QCM) with foulants such a single proteins and diluted human serum. Finally, by performing an on-surface

biofunctionalization step with biotin, we demonstrated it is possible to use these polymer-dendrimer hybrids for selective detection of target analytes.

As already discussed in this chapter, poly(HPMA) is known for having excellent antifouling properties. Hence, in **Chapter 5** we explored possibilities to create such a coating without having to perform sensitive polymerization reactions on-surface. We pre-synthesized HPMA polymers onto a PLL backbone to create a so-called "bottlebrush" branched polymer which could self-assemble onto a surface likewise to the PLL-ZID copolymers. We compare three routes towards such PLL-HPMA-coated surfaces, ranging from "classic" *grafting-from* to entirely *grafting-to* in order to compare differences in outcome and overall antifouling performance of the coatings. Additionally, we designed and synthesized a bottlebrush polymer that eventually allowed for additional (bio)functionalization in solution or after surface immobilization.

Finally, in **Chapter 6** we compare the differently developed building blocks and synthesized coatings in terms of antifouling properties. The findings of our research are placed in a broader context and recommendations for further research are given.

1.6 References

1. Kyriakides, T. R. *Molecular Events at Tissue-Biomaterial Interface*; Elsevier Inc., 2015.
2. Horbett, T. A. Fibrinogen Adsorption to Biomaterials. *J. Biomed. Mater. Res. A.* **2018**, *106* (10), 2777–2788.
3. Söder, D.; Garay-Sarmiento, M.; Rahimi, K.; Obstals, F.; Dedisch, S.; Haraszti, T.; Davari, M. D.; Jakob, F.; Heß, C.; Schwaneberg, U.; Rodriguez-Emmenegger, C. Unraveling the Mechanism and Kinetics of Binding of an LCI-EGFP-Polymer for Antifouling Coatings. *Macromol. Biosci.* **2021**, *2100158*, 1–10.
4. Liu, N.; Xu, Z.; Morrin, A.; Luo, X. Low Fouling Strategies for Electrochemical Biosensors Targeting Disease Biomarkers. *Anal. Methods* **2019**, *11* (6), 702–711.
5. Bhakta, S. A.; Evans, E.; Benavidez, T. E.; Garcia, C. D. Protein Adsorption onto Nanomaterials for the Development of Biosensors and Analytical Devices: A Review. *Anal. Chim. Acta* **2015**, *872*, 7–25.
6. Agata, R. D.; Bellassai, N.; Giuffrida, M. C.; Aura, A. M.; Petri, C.; Kögler, P.; Vecchio, G.; Jonas, U.; Spoto, G. A New Ultralow Fouling Surface for the Analysis of Human Plasma Samples with Surface Plasmon Resonance. *Talanta* **2021**, *221* (1), 121483.
7. Paloni, J. M.; Dong, X. H.; Olsen, B. D. Protein-Polymer Block Copolymer Thin Films for Highly Sensitive Detection of Small Proteins in Biological Fluids. *ACS Sensors* **2019**, *4* (11), 2869–2878.
8. Hower, J. C.; Bernards, M. T.; Chen, S.; Tsao, H. K.; Sheng, Y. J.; Jiang, S. Hydration of "Nonfouling" Functional Groups. *J. Phys. Chem. B* **2009**, *113* (1), 197–201.
9. Maddikeri, R. R.; Tosatti, S.; Schuler, M.; Chessari, S.; Textor, M.; Richards, R. G.; Harris, L. G. Reduced Medical Infection Related Bacterial Strains Adhesion on Bioactive RGD Modified Titanium Surfaces: A First Step toward Cell Selective Surfaces. *J. Biomed. Mater. Res. Part A* **2007**, *84A* (2), 425–435.
10. Healthcare-associated Infections (HAI) Data https://www.cdc.gov/hai/data/index.html.
11. Wang, Z.; Yan, Y.; Su, Y.; Qiao, L. Effect of Proteins on the Surface Microstructure Evolution of a CoCrMo Alloy in Bio-Tribocorrosion Processes. *Colloids Surfaces B Biointerfaces* **2016**, *145*, 176–184.
12. Anbazhagan, E.; Rajendran, A.; Natarajan, D.; Kiran, M. S.; Pattanayak, D. K. Divalent Ion Encapsulated Nano Titania on Ti Metal as a Bioactive Surface with Enhanced Protein Adsorption. *Colloids Surfaces B Biointerfaces* **2016**, *143*, 213–223.
13. Baggerman, J.; Smulders, M. M. J.; Zuilhof, H. Romantic Surfaces: A Systematic Overview of Stable, Biospecific, and Antifouling Zwitterionic Surfaces. *Langmuir* **2019**, *35* (5), 1072–1084.
14. Sivaraman, B.; Latour, R. A. The Relationship between Platelet Adhesion on Surfaces and the Structure versus the Amount of Adsorbed Fibrinogen. *Biomaterials* **2010**, *31* (5), 832–839.
15. Wilson, C. J.; Clegg, R. E.; Leavesley, D. I.; Pearcy, M. J. Mediation of Biomaterial–Cell Interactions by Adsorbed Proteins: A Review. *Tissue Eng.* **2005**, *11* (1–2), 1–18.
16. Magin, C. M.; Cooper, S. P.; Brennan, A. B. Non-Toxic Antifouling Strategies. *Mater. Today* **2010**, *13* (4), 36–44.

17. Baier, R. E. Surface Behaviour of Biomaterials: The Theta Surface for Biocompatibility. *J. Mater. Sci. Mater. Med.* **2006**, *17* (11), 1057–1062.
18. Jiang, S.; Cao, Z. Ultralow-Fouling, Functionalizable, and Hydrolyzable Zwitterionic Materials and Their Derivatives for Biological Applications. *Adv. Mater.* **2010**, *22* (9), 920–932.
19. Chen, S.; Li, L.; Zhao, C.; Zheng, J. Surface Hydration: Principles and Applications toward Low-Fouling/Nonfouling Biomaterials. *Polymer,* **2010**, *51* (23), 5283–5293.
20. Balamurugan, S.; Ista, L. K.; Yan, J.; López, G. P.; Fick, J.; Himmelhaus, M.; Grunze, M. Reversible Protein Adsorption and Bioadhesion on Monolayers Terminated with Mixtures of Oligo(Ethylene Glycol) and Methyl Groups. *J. Am. Chem. Soc.* **2005**, *127* (42), 14548–14549.
21. Piehler, J.; Brecht, A.; Hehl, K.; Gauglitz, G. Protein Interactions in Covalently Attached Dextran Layers. *Colloids Surfaces B Biointerfaces* **1999**, *13* (6), 325–336.
22. Xu, C.; Hu, X.; Wang, J.; Zhang, Y. M.; Liu, X. J.; Xie, B. Bin; Yao, C.; Li, Y.; Li, X. S. Library of Antifouling Surfaces Derived from Natural Amino Acids by Click Reaction. *ACS Appl. Mater. Interfaces* **2015**, *7* (31), 17337–17345.
23. Liu, Q.; Li, W.; Singh, A.; Cheng, G.; Liu, L. Two Amino Acid-Based Superlow Fouling Polymers: Poly(Lysine Methacrylamide) and Poly(Ornithine Methacrylamide). *Acta Biomater.* **2014**, *10* (7), 2956–2964.
24. Zhang, Z.; Zhang, M.; Chen, S.; Horbett, T. A.; Ratner, B. D.; Jiang, S. Blood Compatibility of Surfaces with Superlow Protein Adsorption. *Biomaterials* **2008**, *29* (32), 4285–4291.
25. Ostuni, E.; Chapman, R. G.; Liang, M. N.; Meluleni, G.; Pier, G.; Ingber, D. E.; Whitesides, G. M. Self-Assembled Monolayers That Resist the Adsorption of Cells. *Langmuir* **2001**, *17* (7), 6336–6343.
26. Prime, K. L.; Whitesides, G. M. Adsorption of Proteins onto Surfaces Containing End-Attached Oligo(Ethylene Oxide): A Model System Using Self-Assembled Monolayers. *J. Am. Chem. Soc.* **1993**, *115* (23), 10714–10721.
27. Wei, Q.; Becherer, T.; Angioletti-Uberti, S.; Dzubiella, J.; Wischke, C.; Neffe, A. T.; Lendlein, A.; Ballauff, M.; Haag, R. Protein Interactions with Polymer Coatings and Biomaterials. *Angew. Chemie - Int. Ed.* **2014**, *53* (31), 8004–8031.
28. Le, T. C.; Penna, M.; Winkler, D. A.; Yarovsky, I. Quantitative Design Rules for Protein-Resistant Surface Coatings Using Machine Learning. *Sci. Rep.* **2019**, *9* (1), 1–12.
29. Ladd, J.; Zhang, Z.; Chen, S.; Hower, J. C.; Jiang, S. Zwitterionic Polymers Exhibiting High Resistance to Nonspecific Protein Adsorption from Human Serum and Plasma. *Biomacromolecules* **2008**, *9* (5), 1357–1361.
30. Zhou, F.; Huck, W. T. S. Surface Grafted Polymer Brushes as Ideal Building Blocks for "Smart" Surfaces. *Phys. Chem. Chem. Phys.* **2006**, *8* (33), 3815–3823.
31. Yang, W.; Cheng, G.; Jiang, S. Film Thickness Dependence of Protein Adsorption from Blood Serum and Plasma onto Poly(Sulfobetaine) and Poly(Carboxybetaine)-Grafted Surfaces. *Langmuir* **2008**, No. 24, 9211–9214.
32. Ostuni, E.; Chapman, R. G.; Holmlin, R. E.; Takayama, S.; Whitesides, G. M. A Survey of Structure-Property Relationships of Surfaces That Resist the Adsorption of Protein. *Langmuir* **2001**, *17* (18), 5605–5620.
33. Joshi, S.; Pellacani, P.; van Beek, T. A.; Zuilhof, H.; Nielen, M. W. F. Surface Characterization and Antifouling Properties of Nanostructured Gold Chips for Imaging Surface Plasmon Resonance Biosensing. *Sens. Actuators B* **2015**, *209*, 505–514.
34. Kenausis, G. L.; Vo, J.; Elbert, D. L.; Huang, N.; Hofer, R.; Ruiz-taylor, L.; Textor, M.; Hubbell, J. A.; Spencer, N. D. Poly (L-Lysine)-g-Poly(Ethylene Glycol) Layers on Metal Oxide Surfaces: Attachment Mechanism and Effects of Polymer Architecture on Resistance to Protein Adsorption. *J. Phys. Chem. B* **2000**, *104* (14), 3298–3309.
35. Jeon, S. I.; Lee, J. H.; Andrade, J. D.; De Gennes, P. G. Protein-Surface Interactions in the Presence of Polyethylene Oxide. I. Simplified Theory. *J. Colloid Interface Sci.* **1991**, *142* (1), 149–158.
36. Zhou, F. *Antifouling Surfaces and Materials - From Land to Marine Environment*; Zhou, F., Ed.; Springer Berlin Heidelberg, 2015.
37. Richter, A. W.; Åkerblom, E. Antibodies Against Polyethylene Glycol Produced in Animals by Immunization with Monomethoxy Polyethylene Glycol Modified Proteins. *Int. Arch. Allergy Immunol.* **1983**, *70* (2), 124–131.
38. Branden, R.; Matthew, G.; Anirudha, S.; Janis, T.; Cecilia, F.; Melissa, M.; Jennifer, E. PEG Hydrogel Degradation and the Role of the Surrounding Tissue Environment. *J. Tissue Eng. Regen. Med.* **2015**, *9* (3), 315–318.
39. Lubich, C.; Allacher, P.; de la Rosa, M.; Bauer, A.; Prenninger, T.; Horling, F. M.; Siekmann, J.; Oldenburg, J.; Scheiflinger, F.; Reipert, B. M. The Mystery of Antibodies Against Polyethylene Glycol (PEG) - What Do We Know? *Pharm. Res.* **2016**, *33* (9), 2239–2249.
40. Webster, R.; Elliott, V.; Park, B. K.; Walker, D.; Hankin, M.; Taupin, P. PEG and PEG Conjugates Toxicity: Towards an Understanding of the Toxicity of PEG and Its Relevance to PEGylated Biologicals. *PEGylated Protein Drugs Basic Sci. Clin. Appl.* **2009**, 127–146.
41. Garay, R. P.; El-Gewely, R.; Armstrong, J. K.; Garratty, G.; Richette, P. Antibodies against Polyethylene Glycol in Healthy Subjects and in Patients Treated with PEG-Conjugated Agents. *Expert Opin. Drug Deliv.* **2012**, *9* (11), 1319–1323.
42. Van Andel, E.; Lange, S. C.; Pujari, S. P.; Tijhaar, E. J.; Smulders, M. M. J.; Savelkoul, H. F. J.; Zuilhof, H. Systematic

Comparison of Zwitterionic and Non-Zwitterionic Antifouling Polymer Brushes on a Bead-Based Platform. *Langmuir* **2019**, *35* (5), 1181–1191.

43. Erfani, A.; Seaberg, J.; Aichele, C. P.; Ramsey, J. D. Interactions between Biomolecules and Zwitterionic Moieties: A Review. *Biomacromolecules* **2020**, *21* (7), 2557–2573.
44. Halperin, A. Polymer Brushes That Resist Adsorption of Model Proteins: Design Parameters. *Langmuir* **1999**, *15* (7), 2525–2533.
45. Laschewsky, A.; Rosenhahn, A. Molecular Design of Zwitterionic Polymer Interfaces: Searching for the Difference. *Langmuir* **2018**.
46. Laschewsky, A. Structures and Synthesis of Zwitterionic Polymers. *Polymers.* **2014**, *6* (5), 1544–1601.
47. Wu, A.; Gao, Y.; Zheng, L. Zwitterionic Amphiphiles: Their Aggregation Behavior and Applications. *Green Chem.* **2019**, *21* (16), 4290–4312.
48. Schlenoff, J. B. Zwitteration: Coating Surfaces with Zwitterionic Functionality to Reduce Nonspecific Adsorption. *Langmuir* **2014**, *30* (32), 9625–9636.
49. Vaisocherová, H.; Zhang, Z.; Yang, W.; Cao, Z.; Cheng, G.; Taylor, A. D.; Piliarik, M.; Homola, J.; Jiang, S. Functionalizable Surface Platform with Reduced Nonspecific Protein Adsorption from Full Blood Plasma—Material Selection and Protein Immobilization Optimization. *Biosens. Bioelectron.* **2009**, *24*, 1924–1930.
50. Blackman, L. D.; Gunatillake, P. A.; Cass, P.; Locock, K. E. S. An Introduction to Zwitterionic Polymer Behavior and Applications in Solution and at Surfaces. *Chem. Soc. Rev.* **2019**, *48* (3), 757–770.
51. Chen, S.; Li, L.; Zhao, C.; Zheng, J. Surface Hydration: Principles and Applications toward Low-Fouling/Nonfouling Biomaterials. *Polymer (Guildf).* **2010**, *51* (23), 5283–5293.
52. Leng, C.; Hung, H. C.; Sun, S.; Wang, D.; Li, Y.; Jiang, S.; Chen, Z. Probing the Surface Hydration of Nonfouling Zwitterionic and PEG Materials in Contact with Proteins. *ACS Appl. Mater. Interfaces* **2015**, *7* (30), 16881–16888.
53. Kuzmyn, A. R.; Nguyen, A. T.; Zuilhof, H.; Baggerman, J. Bioactive Antifouling Surfaces by Visible-Light-Triggered Polymerization. *Adv. Mater. Interfaces* **2019**, *6* (12), 1900351.
54. Vorobii, M.; de los Santos Pereira, A.; Pop-Georgievski, O.; Kostina, N. Y.; Rodriguez-Emmenegger, C.; Percec, V. Synthesis of Non-Fouling Poly[N-(2-Hydroxypropyl)Methacrylamide] Brushes by Photoinduced SET-LRP. *Polym. Chem.* **2015**, *6* (23), 4210–4220.
55. Rodriguez-Emmenegger, C.; Brynda, E.; Riedel, T.; Houska, M.; Šubr, V.; Alles, A. B.; Hasan, E.; Gautrot, J. E.; Huck, W. T. S. Polymer Brushes Showing Non-Fouling in Blood Plasma Challenge the Currently Accepted Design of Protein Resistant Surfaces. *Macromol. Rapid Commun.* **2011**, *32* (13), 952–957.
56. Surman, F.; Riedel, T.; Bruns, M.; Kostina, N. Y.; Sedláková, Z.; Rodriguez-Emmenegger, C. Polymer Brushes Interfacing Blood as a Route toward High Performance Blood Contacting Devices. *Macromol. Biosci.* **2015**, *15* (5), 636–646.
57. Kopeckova, P.; Rathi, R.; Takada, S.; Říhová, B.; Berenson, M. M.; Kopeček, J. Bioadhesive N-(2-Hydroxypropyl) Methacrylamide Copolymers for Colon-Specific Drug Delivery Copolymers. *J. Control. Release* **1994**, *28* (93), 211–222.
58. Říhová, B.; Ulbrich, K.; Kopeček, J.; Mančal, P. Immunogenicity of N-(2-Hydroxypropyl)-Methacrylamide Copolymers-Potential Hapten or Drug Carriers. *Folia Microbiologica*. 1983, pp 217–227.
59. de Oliveira, F. A.; Albuquerque, L. J. C.; Riske, K. A.; Jäger, E.; Giacomelli, F. C. Outstanding Protein-Repellent Feature of Soft Nanoparticles Based on Poly(N-(2-Hydroxypropyl) Methacrylamide) Outer Shells. *J. Colloid Interface Sci.* **2020**, *574* (April), 260–271.
60. Lopez-Mila, B.; Alves, P.; Riedel, T.; Dittrich, B.; Mergulhão, F.; Rodriguez-Emmenegger, C. Effect of Shear Stress on the Reduction of Bacterial Adhesion to Antifouling Polymers. *Bioinspir. Biomim.* **2018**, *13* (6), 065001.
61. Taylor, W.; Jones, R. a L. Producing High-Density High-Molecular-Weight Polymer Brushes by a "Grafting to" Method from a Concentrated Homopolymer Solution. *Langmuir* **2010**, *26* (17), 13954–13958.
62. Morgese, G.; Verbraeken, B.; Ramakrishna, S. N.; Gombert, Y.; Cavalli, E.; Rosenboom, J. G.; Zenobi-Wong, M.; Spencer, N. D.; Hoogenboom, R.; Benetti, E. M. Chemical Design of Non-Ionic Polymer Brushes as Biointerfaces: Poly(2-Oxazine)s Outperform Both Poly(2-Oxazoline)s and PEG. *Angew. Chem. Int. Ed.* **2018**, *57* (36), 11667–11672.
63. Nguyen, A. T.; Baggerman, J.; Paulusse, J. M. J.; Rijn, C. J. M. Van; Zuilhof, H. Stable Protein-Repellent Zwitterionic Polymer Brushes Grafted from Silicon Nitride. *Langmuir* **2011**, *27* (6), 2587–2594.
64. van Andel, E.; de Bus, I.; Tijhaar, E. J.; Smulders, M. M. J.; Savelkoul, H. F. J.; Zuilhof, H. Highly Specific Binding on Antifouling Zwitterionic Polymer-Coated Microbeads as Measured by Flow Cytometry. *ACS Appl. Mater. Interfaces* **2017**, *9* (44), 38211–38221.
65. Yang, W.; Xue, H.; Li, W.; And, J. Z.; Jiang, S. Pursuing "Zero" Protein Adsorption of Poly(Carboxybetaine) from Undiluted Blood Serum and Plasma. *Langmuir* **2009**, *25* (19), 11911–11916.
66. Blaszykowski, C.; Sheikh, S.; Thompson, M. A Survey of State-of-the-Art Surface Chemistries to Minimize Fouling from Human and Animal Biofluids. *Biomater. Sci.* **2015**, *3* (10), 1335–1370.
67. Honda, T.; Nakao, A.; Ishihara, K.; Higaki, Y.; Higaki, K.; Takahara, A.; Iwasaki, Y.; Yusa, S. I. Polymer Coating Glass to

Improve the Protein Antifouling Effect. *Polym. J.* **2018**, *50* (5), 381–388.
68. Lísalová, H.; Brynda, E.; Houska, M.; Víšová, I.; Mrkvová, K.; Song, X. C.; Gedeonová, E.; Surman, F.; Riedel, T.; Pop-Georgievski, O.; Homola, J. Ultralow-Fouling Behavior of Biorecognition Coatings Based on Carboxy-Functional Brushes of Zwitterionic Homo- and Copolymers in Blood Plasma: Functionalization Matters. *Anal. Chem.* **2017**, *89* (6), 3524–3531.
69. Michalek, L.; Barner, L.; Barner-Kowollik, C. Polymer on Top: Current Limits and Future Perspectives of Quantitatively Evaluating Surface Grafting. *Adv. Mater.* **2018**, *30* (21), 1–18.
70. Lange, S. C.; Van Andel, E.; Smulders, M. M. J.; Zuilhof, H. Efficient and Tunable Three-Dimensional Functionalization of Fully Zwitterionic Antifouling Surface Coatings. *Langmuir* **2016**, *32* (40), 10199–10205.
71. Vorobii, M.; De Los Santos Pereira, A.; Pop-Georgievski, O.; Kostina, N. Y.; Rodriguez-Emmenegger, C.; Percec, V. Synthesis of Non-Fouling Poly[N-(2-Hydroxypropyl)Methacrylamide] Brushes by Photoinduced SET-LRP. *Polym. Chem.* **2015**, *6* (23), 4210–4220.
72. Szczepaniak, G.; Fu, L.; Jafari, H.; Kapil, K.; Matyjaszewski, K. Making ATRP More Practical: Oxygen Tolerance. *Acc. Chem. Res.* **2021**, *54* (7), 1779–1790.
73. Enciso, A. E.; Fu, L.; Russell, A. J.; Matyjaszewski, K. A Breathing Atom-Transfer Radical Polymerization: Fully Oxygen-Tolerant Polymerization Inspired by Aerobic Respiration of Cells. *Angew. Chemie - Int. Ed.* **2018**, *57* (4), 933–936.
74. Boas, U.; Christensen, J. B.; Heegaard, P. M. H. Dendrimers: Design, Synthesis and Chemical Properties. *J. Mater. Chem.* **2006**, *16* (38), 3785–3798.
75. Sato, K.; Anzai, J. I. Dendrimers in Layer-by-Layer Assemblies: Synthesis and Applications. *Molecules* **2013**, *18* (7), 8440–8460.
76. Abbasi, E.; Aval, S. F.; Akbarzadeh, A.; Milani, M.; Nasrabadi, H. T.; Joo, S. W.; Hanifehpour, Y.; Nejati-Koshki, K.; Pashaei-Asl, R. Dendrimers: Synthesis, Applications, and Properties. *Nanoscale Res. Lett.* **2014**, *9* (1), 1–10.
77. Lee, C. C.; MacKay, J. A.; Fréchet, J. M. J.; Szoka, F. C. Designing Dendrimers for Biological Applications. *Nat. Biotechnol.* **2005**, *23* (12), 1517–1526.
78. Gillani, S. S.; Munawar, M. A.; Khan, K. M.; Chaudhary, J. A. Synthesis, Characterization and Applications of Poly-Aliphatic Amine Dendrimers and Dendrons. *J. Iran. Chem. Soc.* **2020**, *17* (11), 2717–2736.
79. Nimesh, S. *Gene Therapy: Potential Applications of Nanotechnology*; Woodhead Publishing, 2013.
80. Hawker, C. J.; Frechet, J. M. J. Preparation of Polymers with Controlled Molecular Architecture. A New Convergent Approach to Dendritic Macromolecules. *J. Am. Chem. Soc.* **1990**, *112* (21), 7638–7647.
81. Newkome, G. R.; Shreiner, C. D. Poly(Amidoamine), Polypropylenimine, and Related Dendrimers and Dendrons Possessing Different 1 → 2 Branching Motifs: An Overview of the Divergent Procedures. *Polymer.* **2008**, *49* (1), 1–173.
82. Wang, L.; Wang, Z.; Ma, G.; Lin, W.; Chen, S. Reducing the Cytotoxity of Poly(Amidoamine) Dendrimers by Modification of a Single Layer of Carboxybetaine. *Langmuir* **2013**, *29* (28), 8914–8921.
83. Ramireddy, R. R.; Subrahmanyam, A. V.; Thayumanavan, S. Zwitterionic Moieties from the Huisgen Reaction: A Case Study with Amphiphilic Dendritic Assemblies. *Chem. Eur. J* **2013**, *19* (48), 16374–16381.
84. Li, L.; Wang, Y.; Ji, F.; Wen, Y.; Li, J.; Yang, B.; Yao, F. Synthesis and Characterization of Dendritic Star-Shaped Zwitterionic Polymers as Novel Anticancer Drug Delivery Carriers. *J. Biomater. Sci. Polym. Ed.* **2014**, *25* (14–15), 1641–1657.
85. Wang, L.; Zhang, J.; Lin, W.; Wang, Z.; Chen, S. Development of a Protein Mimic with Peptide Ligands to Enhance Specific Sensing and Targeting by the Zwitterionic Surface Engineering of Poly(Amido Amine) Dendrimers. *Adv. Mater. Interfaces* **2014**, *1* (1), 1300059.
86. Wang, Y.; Li, L.; Li, J.; Yang, B.; Wang, C.; Fang, W.; Ji, F.; Wen, Y.; Yao, F. Stable and PH-Responsive Polyamidoamine Based Unimolecular Micelles Capped with a Zwitterionic Polymer Shell for Anticancer Drug Delivery. *RSC Adv.* **2016**, *6* (21), 17728–17739.
87. Svenningsen, S. W.; Janaszewska, A.; Ficker, M.; Petersen, J. F.; Klajnert-Maculewicz, B.; Christensen, J. B. Two for the Price of One: PAMAM-Dendrimers with Mixed Phosphoryl Choline and Oligomeric Poly(Caprolactone) Surfaces. *Bioconjug. Chem.* **2016**, *27* (6), 1547–1557.
88. Huang, D.; Yang, F.; Wang, X.; Shen, H.; You, Y.; Wu, D. Facile Synthesis and Self-Assembly Behaviour of PH-Responsive Degradable Polyacetal Dendrimers. *Polym. Chem.* **2016**, *7* (40), 6154–6158.
89. Cao, W.; Huang, J.; Jiang, B.; Gao, X.; Yang, P. Highly Selective Enrichment of Glycopeptides Based on Zwitterionically Functionalized Soluble Nanopolymers. *Sci. Rep.* **2016**, *6* (29776), 1–8.
90. Han, Y.; Qian, Y.; Zhou, X.; Hu, H.; Liu, X.; Zhou, Z.; Tang, J.; Shen, Y. Facile Synthesis of Zwitterionic Polyglycerol Dendrimers with a β-Cyclodextrin Core as MRI Contrast Agent Carriers. *Polym. Chem.* **2016**, *7*, 6354.
91. Xiong, Z.; Wang, Y.; Zhu, J.; Li, X.; He, Y.; Qu, J.; Shen, M.; Xia, J.; Shi, X. Dendrimers Meet Zwitterions: Development of a Unique Antifouling Nanoplatform for Enhanced Blood Pool, Lymph Node and Tumor CT Imaging. *Nanoscale* **2017**, *9* (34), 12295–12301.

92. Tsai, H.-C.; Imae, T. Fabrication of Dendrimers Toward Biological Application. *Prog. Mol. Biol. Transl. Sci.* **2011**, *104*, 101–140.
93. Otto, D. P.; de Villiers, M. M. Poly(Amidoamine) Dendrimers as a Pharmaceutical Excipient. Are We There Yet? *J. Pharm. Sci.* **2018**, *107* (1), 75–83.
94. Stasko, N. A.; Johnson, C. B.; Schoenfisch, M. H.; Johnson, T. A.; Holmuhamedov, E. L. Cytotoxicity of Polypropylenimine Dendrimer Conjugates on Cultured Endothelial Cells. *Biomacromolecules* **2007**, *8* (12), 3853–3859.
95. Jevprasesphant, R.; Penny, J.; Jalal, R.; Attwood, D.; McKeown, N. .; D'Emanuele, A. The Influence of Surface Modification on the Cytotoxicity of PAMAM Dendrimers. *Int. J. Pharm.* **2003**, *252* (1–2), 263–266.
96. Geiger, B. C.; Wang, S.; Padera, R. F.; Grodzinsky, A. J.; Hammond, P. T. Cartilage-Penetrating Nanocarriers Improve Delivery and Efficacy of Growth Factor Treatment of Osteoarthritis. *Sci. Transl. Med.* **2018**, *10* (469), eaat8800.
97. Bodewein, L.; Schmelter, F.; Di Fiore, S.; Hollert, H.; Fischer, R.; Fenske, M. Differences in Toxicity of Anionic and Cationic PAMAM and PPI Dendrimers in Zebrafish Embryos and Cancer Cell Lines. *Toxicol. Appl. Pharmacol.* **2016**, *305*, 83–92.
98. Hu, J.; Su, Y.; Zhang, H.; Xu, T.; Cheng, Y. Design of Interior-Functionalized Fully Acetylated Dendrimers for Anticancer Drug Delivery. *Biomaterials* **2011**, *32* (36), 9950–9959.
99. Carr, L. R.; Zhou, Y.; Krause, J. E.; Xue, H.; Jiang, S. Uniform Zwitterionic Polymer Hydrogels with a Nonfouling and Functionalizable Crosslinker Using Photopolymerization. *Biomaterials* **2011**, *32* (29), 6893–6899.
100. Morell, M.; Puiggalí, J. Hybrid Block Copolymers Constituted by Peptides and Synthetic Polymers: An Overview of Synthetic Approaches, Supramolecular Behavior and Potential Applications. *Polymers (Basel).* **2013**, *5*, 188–224.
101. Paul, S. M. De; Vo, J.; Spencer, N. D.; Textor, M. Poly(L-Lysine)-Graft-Poly (Ethylene Glycol) Assembled Monolayers on Niobium Oxide Surfaces : A Quantitative Study of the Influence of Polymer Interfacial Architecture on Resistance to Protein Adsorption by ToF-SIMS and in Situ OWLS. *Langmuir* **2003**, *19* (20), 9216–9225.
102. Perry, S. S.; Yan, X.; Limpoco, F. T.; Lee, S.; Müller, M.; Spencer, N. D. Tribological Properties of Poly(l -Lysine)- Graft -Poly(Ethylene Glycol) Films: Influence of Polymer Architecture and Adsorbed Conformation. *ACS Appl. Mater. Interfaces* **2009**, *1* (6), 1224–1230.
103. Huang, W. M.; Gibson, S. J.; Facer, P.; Gu, J.; Polak, J. M. Improved Section Adhesion for Immunocytochemistry Using High Molecular Weight Polymers of L-Lysine as a Slide Coating. *Histochemistry* **1983**, *77* (2), 275–279.
104. Yan, X.; Perry, S. S.; Spencer, N. D.; Pasche, S.; De Paul, S. M.; Textor, M.; Lim, M. S. Reduction of Friction at Oxide Interfaces upon Polymer Adsorption from Aqueous Solutions. *Langmuir* **2004**, *20* (2), 423–428.
105. Parks, G. A. The Isoelectric Points of Solid Oxides, Solid Hydroxides, and Aqueous Hydroxo Complex Systems. *Chem. Rev.* **1965**, *65* (2), 177–198.
106. Weber, D.; Torger, B.; Richter, K.; Nessling, M.; Momburg, F.; Woltmann, B.; Müller, M.; Schwartz-Albiez, R. Interaction of Poly(L-Lysine)/Polysaccharide Complex Nanoparticles with Human Vascular Endothelial Cells. *Nanomaterials* **2018**, *8* (6), 358.
107. Roeven, E.; Kuzmyn, A. R.; Scheres, L.; Baggerman, J.; Smulders, M. M. J.; Zuilhof, H. PLL-Poly(HPMA) Bottlebrush-Based Antifouling Coatings: Three Grafting Routes. *Langmuir* **2020**, *36* (34), 10187–10199.
108. Tappertzhofen, K.; Weiser, F.; Montermann, E.; Reske-Kunz, A.; Bros, M.; Zentel, R. Poly-L-Lysine-Poly[HPMA] Block Copolymers Obtained by RAFT Polymerization as Polyplex-Transfection Reagents with Minimal Toxicity. *Macromol. Biosci.* **2015**, *15* (8), 1159–1173.
109. Gitsov, I.; Wooley, K. L. Novel Polyether Copolymers Consisting of Linear and Dendritic Blocks. *Angew. Chem. Int. Ed.* **1992**, *31* (9), 1200–1202.
110. Sousa-Herves, A.; Riguera, R.; Fernandez-Megia, E. PEG-Dendritic Block Copolymers for Biomedical Applications. *New J. Chem.* **2012**, *36* (2), 205–210.
111. Sun, H.; Haque, F. M.; Zhang, Y.; Commisso, A.; Mohamed, M. A.; Tsianou, M.; Cui, H.; Grayson, S. M.; Cheng, C. Linear-Dendritic Alternating Copolymers. *Angew. Chem. Int. Ed.* **2019**, *58* (31), 10572–10576.
112. Chapman, T. M.; Hillyer, G. L.; Mahan, E. J.; Shaffer, K. A. Hydraamphiphiles: Novel Linear Dendritic Block Copolymer Surfactants. *J. Am. Chem. Soc.* **1994**, *116* (24), 11195–11196.
113. van Hest, J. C. M.; Delnoye, D. A. P.; Baars, M. W. P. L.; van Genderen, M. H. P.; Meijer, E. W. Polystyrene-Dendrimer Amphiphilic Block Copolymers with a Generation-Dependent Aggregation. *Science.* **1995**, *268* (5217), 1592–1595.
114. Iyer, J.; Fleming, K.; Hammond, P. T. Synthesis and Solution Properties of New Linear-Dendritic Diblock Copolymers. *Macromolecules* **1998**, *31* (25), 8757–8765.
115. Hedden, R. C.; Bauer, B. J.; Paul Smith, A.; Gröhn, F.; Amis, E. Templating of Inorganic Nanoparticles by PAMAM/PEG Dendrimer - Star Polymers. *Polymer,* **2002**, *43* (20), 5473–5481.
116. Lee, C. C.; Gillies, E. R.; Fox, M. E.; Guillaudeu, S. J.; Fréchet, J. M. J.; Dy, E. E.; Szoka, F. C. A Single Dose of Doxorubicin-Functionalized Bow-Tie Dendrimer Cures Mice Bearing C-26 Colon Carcinomas. *Proc. Natl. Acad. Sci. U. S. A.* **2006**, *103* (45), 16649–16654.
117. Kaup, R.; Bart, J.; Velders, A. H. Dendroids, Discrete Covalently Cross-Linked Dendrimer Superstructures. *ACS Nano*

2020, *15* (1), 1666–1674.

118. Frauenrath, H. Dendronized Polymers - Building a New Bridge from Molecules to Nanoscopic Objects. *Prog. Polym. Sci.* **2005**, *30* (3–4), 325–384.
119. Zhang, Y.; Li, X.; Deng, G.; Chen, Y. Novel Hybrid Polymer Brushes with Alternating Dendritic Wedges and Linear Side Chains. *Macromol. Chem. Phys.* **2006**, *207* (15), 1394–1403.
120. Shi, Y.; Zhu, W.; Chen, Y. Synthesis of Cylindrical Polymer Brushes with Umbrella-like Side Chains via a Combination of Grafting-from and Grafting-onto Methods. *Macromolecules* **2013**, *46* (6), 2391–2398.
121. Andrén, O. C. J.; Zhang, Y.; Lundberg, P.; Hawker, C. J.; Nyström, A. M.; Malkoch, M. Therapeutic Nanocarriers via Cholesterol Directed Self-Assembly of Well-Defined Linear-Dendritic Polymeric Amphiphiles. *Chem. Mater.* **2017**, *29* (9), 3891–3898.

Chapter 2

Design, Synthesis and Characterization of Fully Zwitterionic, Functionalized Dendrimers

Esther Roeven | Luc Scheres | Maarten M. J. Smulders | Han Zuilhof

Published in: **ACS Omega 2019, 4, 3000-3011**
DOI: 10.1021/acsomega.8b03521

Abstract

Dendrimers are interesting candidates for various applications due to the high level of control over their architecture, the presence of internal cavities and the possibility for multivalent interactions. More specifically, zwitterionic dendrimers modified with an equal number of oppositely charged groups have found use in *in vivo* biomedical applications. However, the design and control over the synthesis of these dendrimers remains challenging, in particular with respect to achieving full modification of the dendrimer. In this work we show the design and subsequent synthesis of dendrimers that are highly charged whilst having zero net charge, *i.e.* zwitterionic dendrimers that are potential candidates for biomedical applications. First we designed and fully optimized the synthesis of charge-neutral carboxybetaine and sulfobetaine zwitterionic dendrimers. Following their synthesis, the various zwitterionic dendrimers were extensively characterized. In this study we also report for the first time the use of X-ray photoelectron spectroscopy (XPS) as an easy-to-use and quantitative tool for the compositional analysis of this type of macromolecules that can complement *e.g.* NMR and GPC. Finally, we designed and synthesized zwitterionic dendrimers that contain a variable number of alkyne and azide groups that allow straightforward (bio)functionalization via click chemistry.

2.1 Introduction

Dendrimers are multivalent (macro)molecules in which the repeat units are not connected in a linear fashion, but form a well-defined, branched three-dimensional architecture of nanometer size.[1–4] As a result, they possess a distinct molecular architecture that consists of a central core, branches and terminal functional groups, present at the outer surface of the macromolecule. Due to their unique, highly defined 3D structure, dendrimers have found use in a wide variety of applications ranging from dyes[5] to catalysts,[6] and from MRI contrast agents[7] to sensors for small molecules.[8] Furthermore, the high level of control over dendritic architectures, the presence of internal cavities and the possibility for multivalent binding have made dendrimers ideal candidates for carriers in biomedical applications.[3,4,9] Therefore, over the past few years, the use of dendrimers for gene and drug delivery has been extensively reported.[9–12] However, most commonly used dendrimers, which include PPI (poly(propylene imine)) and PAMAM (poly(amido amine)),[13] by themselves are not biocompatible and can induce cytotoxic effects.[10,14] As a result, for *in vivo* use the exterior of dendrimers then needs to be modified with, for instance, polyethylene glycol (PEG)[15,16,17] or charged groups[18–23] to reduce their toxicity.

While such dendrimers modified with charged groups have found use in biomedical applications such as drug delivery, sensing and MRI contrast agents,[18–20,24–30] the design and control over the synthesis of these dendrimers remains challenging and is still subject to further optimization. So far, only partially zwitterionic dendrimers (modification of either only the interior or of the exterior of the dendrimer), or dendrimers with non-permanent, pH-sensitive charged groups (*i.e.* protonated amines) have been reported.[18–20,24–30]

Given these limitations it is therefore still highly relevant to design and characterize dendrimers that are highly charged, yet could intrinsically have a zero net charge, *i.e.* zwitterionic dendrimers (ZID). We expect that the complete charge neutrality of such ZIDs can further diminish undesired interactions within a living system, thus making them more suitable for *in vitro* and *in vivo* applications, just like their larger, but less well defined polymer counterparts, zwitterionic polymers.[20,31,32] Building blocks for such a new type of zwitterionic materials should allow for a high density of oppositely charged moieties, creating a strong zwitterionic character, while remaining overall neutral. In addition, their inherently multivalent nature should, in principle, allow that ZIDs are functionalized in a controlled manner with multiple functional groups, including *e.g.* bio-recognition elements. Within this project, specifically poly(propylene imine) (PPI) dendrimers were found to be interesting candidates because of their high density of quaternizable amine groups and commercial availability.[1,13] Furthermore they have been found to more stable than and poly(amido amine) (PAMAM) dendrimers, which can undergo retro-Michael reactions (β-eliminations) at high temperature or pH, which may be detrimental during the synthesis of the ZID.[33,34]

In this chapter we report the first synthesis of a series of zwitterionic dendrimers as well as their characterization. We prepare 2nd and 3rd generation ZIDs with a near-equal number of positively charged (quaternary) nitrogen atoms and negatively charged carboxylates, so as to make an electrically neutral oligocarboxybetaine. Of course, such carboxylate moieties could be functionalized – *e.g.* via standard NHS/EDC chemistry – but only with concomitant loss of charge neutrality, which for such relatively small molecules would easily strengthen the interaction with biomolecules. To thus allow for a precisely controlled functionalization of intrinsically charge-neutral ZIDs, we subsequently developed a synthetic strategy that allows incorporation of a specific number of clickable azido or alkyne functional groups. In this work, we also present for the first time the use of X-ray photoelectron spectroscopy (XPS) for the quantitative compositional analysis of such three-dimensional oligomers, and show the power of this technique for the analysis of the chemical composition of large organic molecules. Due to their highly branched nature, dendrimeric building blocks have a large number of functional groups that all need to be converted during the synthesis. However, from an analytical perspective it is often far from trivial to accurately determine this degree of conversion. To complement limitations with conventionally used analytical methods like NMR, MS, GPC and IR, we thus invoked XPS. This technique, traditionally used for surface analysis, allowed us to precisely determine the nature and electronic environment of specific elements in the relevant functional group (nitrogen atoms in our case), from which we could accurately determine the overall conversion.

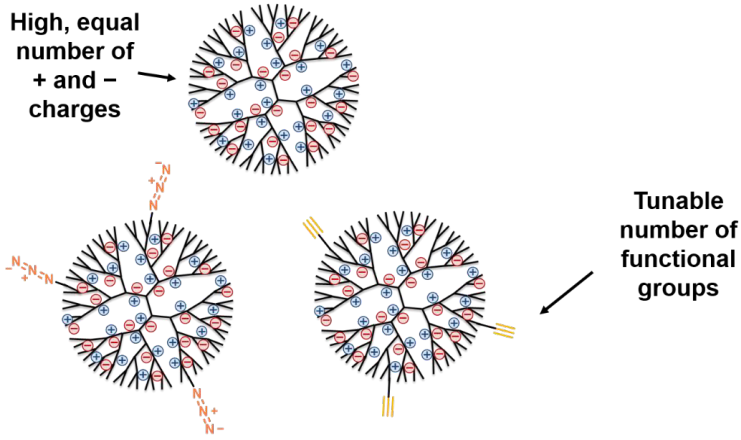

Figure 2.1 Schematic overview of the synthesized fully zwitterionic, functionalized dendrimers.

2.2 Results and Discussion

2.2.1 Design of synthesis of fully zwitterionic dendrimers (ZIDs).

Previously, PAMAM[18,19] or PPI dendrimers[19] and polyethyleneimine polymers[35] have been modified to become exteriorly zwitterionic by reacting only the outer primary amines with zwitterionic monomers in order to reduce their cytotoxicity. Alternatively, Hu *et al.* investigated the interior zwitterionic modification of both PPI and PAMAM dendrimers for drug delivery purposes by first acetylating the outer amines and subsequently reacting the inner tertiary amines with 1,3-propane sultone.[22] Carr *et al.* have reported the synthesis of zwitterionic cross linkers for hydrogels by performing a Michael addition on a secondary amine-containing monomer with a protected acid (which was later deprotected), followed by *N*-alkylation using methyl iodide.[23] While both these approaches could also be applied to dendrimers, they would not result in charge neutral products, which could be detrimental for their performance in biological systems,[36] since it could attract positively charged biomaterials.

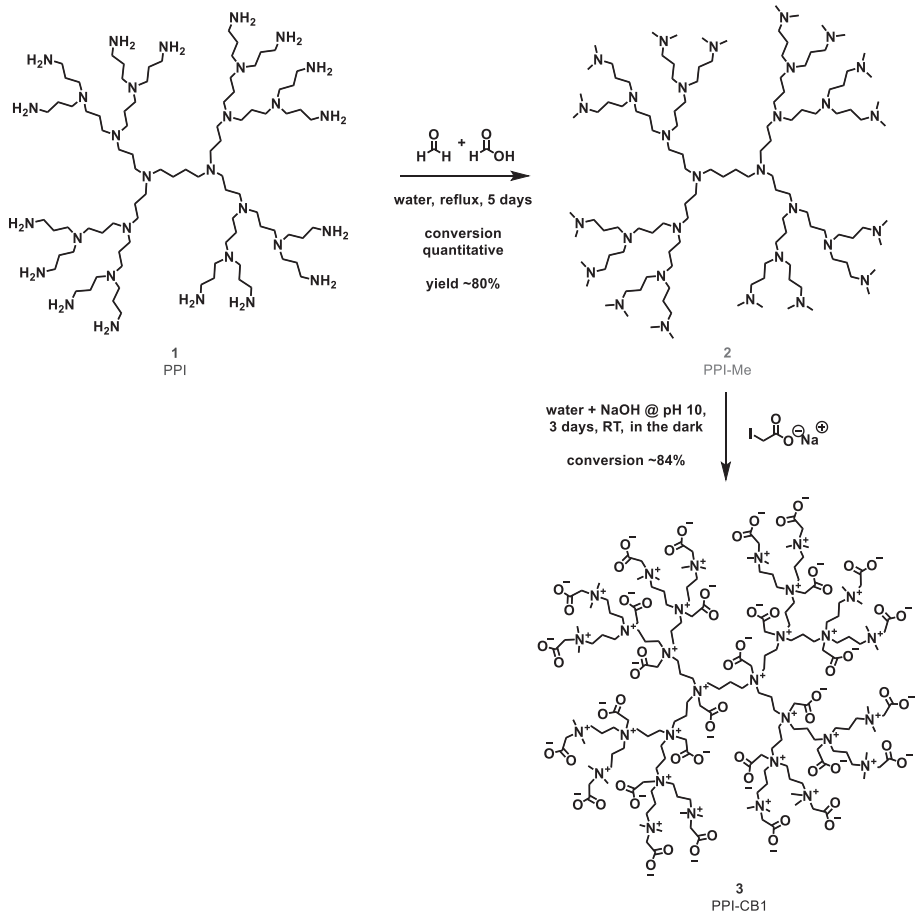

Scheme 2.1 Synthesis of zwitterionic PPI-CB1 dendrimers (colors for the different compounds are also used in the Results & Discussion section to label experimental data to the appropriate compound).

We chose the first step in the modification of the PPI dendrimers to be the (double) methylation of the outer, primary amines using the Eschweiler-Clarke reaction, as this can be run to full conversion to yield dendrimers with tertiary amines only (Scheme 2.1).[37,38] Subsequently, the dendrimers were made zwitterionic by reacting all the interior and exterior tertiary amines with an alkyl halide with a protected or free anionic group, possibly followed by a deprotection step (Scheme 2.1).[39]
For the synthesis of ZIDs, we chose to work with PPI generation 3 (G3) dendrimers (in line with the definition by Meijer and co-workers, a PPI dendrimer with 16 end groups is called a third-generation dendrimer [40]) because of their size and the trade-off between the stability under relevant conditions as mentioned before and low number of defects (since the latter increases with generation growth).[41]

2.2.2 Synthesis of zwitterionic dendrimer 3 PPI-CB1

As explained, the first step in the synthesis of the zwitterionic PPI-based dendrimers is the methylation of the primary amine groups under Eschweiler-Clarke conditions, leading to intermediate **2** PPI-Me (Scheme 2.1). This first intermediate, **2**, was subsequently characterized using NMR, IR and MS. The ^{1}H NMR spectrum of intermediate **2** showed the appearance of a new, sharp singlet at 2.48 ppm with corresponding integrals that could be assigned to the installed methyl groups, while the existing methylene peaks of the dendrimer showed the expected downfield shift (peak a in Figure 2.1b). Furthermore, IR spectroscopy also showed the presence of methyl groups as indicated by C–H bending vibrations at 1456 cm^{-1} for intermediate **2**. Indirectly, the intensity decrease of the N–H stretch (3360 and 3280 cm^{-1}) and N–H bend (1592 cm^{-1}) bands also indicated the disappearance of the primary amines of starting material **1** (Figure 2.2a). Dendrimer **2** could be converted into a zwitterionic dendrimer by reacting it with an appropriate alkylating agent that also features a negatively charged group (Scheme 2.1).
Initially, we selected sodium iodoacetate as the alkylation agent to introduce both the positive and negative charges in a single step. After the reaction, all dendrimer backbone peaks showed a downfield shift in the ^{1}H-NMR spectrum (Figure 2.2b). In addition, a new peak was observed at 3.97 ppm, corresponding to the CH_2 group of the carboxybetaines (peak e in Figure 2.2b and c). The presence of the carboxylate group was also confirmed by the C=O stretch peak at 1600 cm^{-1} in the IR spectrum (Figure 2.2a). Diffusion-ordered spectroscopy (DOSY) also indicated that all the assigned signals belonged to one macromolecular structure by showing the same diffusion coefficient (Figure 2.2d). Applying the Stokes-Einstein equation to data obtained by DOSY, we estimate the hydrodynamic diameter for PPI-CB1 **3** to be 3.2 nm (Table 2.2), which is in agreement with values reported in literature for related dendrimers of similar mass.[42,43]
Gel Permeation Chromatography (GPC) data also confirmed the estimated mass and desired monodispersity of product **3**. The observed molecular weight (MW, 4.1×10^3 g/mol) was in reasonable agreement with the proposed molecular weight at full conversion (3877), keeping in mind that the M_w of the zwitterionic, dendritic structure **3** was calculated using a linear, non-zwitterionic calibration system. The measured polydispersity (PDI) of dendrimer **3** was low (1.102), especially given the multiple consecutive modification steps that led to **3**.

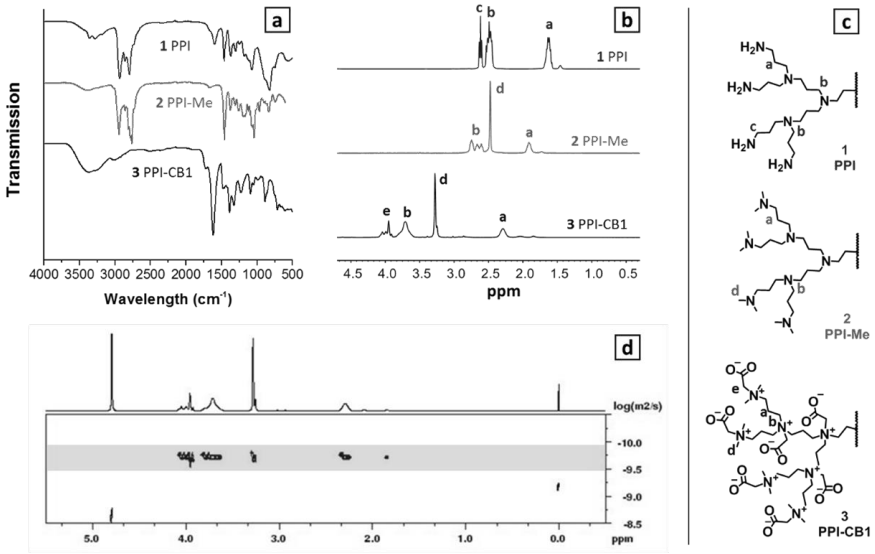

Figure 2.2 IR (a) and ^{1}H-NMR results (b) with corresponding peak assignment (c) of **1** PPI, **2** PPI-Me and **3** PPI-CB1; and DOSY (d) results of product **3** PPI-CB1. Full assignment of NMR and IR spectra is provided in the Supporting Information.

Determining the exact conversion of this second reaction step was found to be challenging, since IR is not a quantitative technique and ^{1}H-NMR signals became broad, preventing accurate integration. Therefore, we initially used ^{1}H-^{15}N Heteronuclear Multiple Bond Correlation (HMBC) to indirectly measure the ^{15}N-NMR spectrum of compound **3** PPI-CB1 (Figure 2.11). The indicative methyl ^{1}H peak at 3.28 ppm (also visible in Figure 2.2b) was found to correlate with multiple ^{15}N-NMR peaks. This implied that after modification still different N atoms were present, which suggests the presence of unreacted tertiary amines and a not fully complete conversion.

To be able to quantify this conversion, we made use of the unique information that X-ray photoelectron spectroscopy (XPS) can provide about the conversion from tertiary to quaternary amines, as XPS can reveal the electronic configuration of the nitrogen atoms. XPS provides both quantitative and qualitative information on the elemental composition and chemical environment of elements on a surface. The binding energy of the core electrons of an element is measured and from the obtained spectra, the amount of the element present can be calculated.[44,45] XPS is generally used to investigate the chemical composition of ca. the top-10 nm of surfaces, and is not employed as a standard characterization method for organic molecules. However, following earlier research in our labs that focused on the extensive characterization of polymers that are covalently bound to surfaces,[46–48] or that are strongly adsorbed onto surfaces,[49] we hypothesized that this technique might also provide unique information in the characterization of large (meaning: non-volatile) but well-defined compounds. We therefore used the technique to characterize organic macromolecules by dropcasting and drying them from solution on a silicon surface.

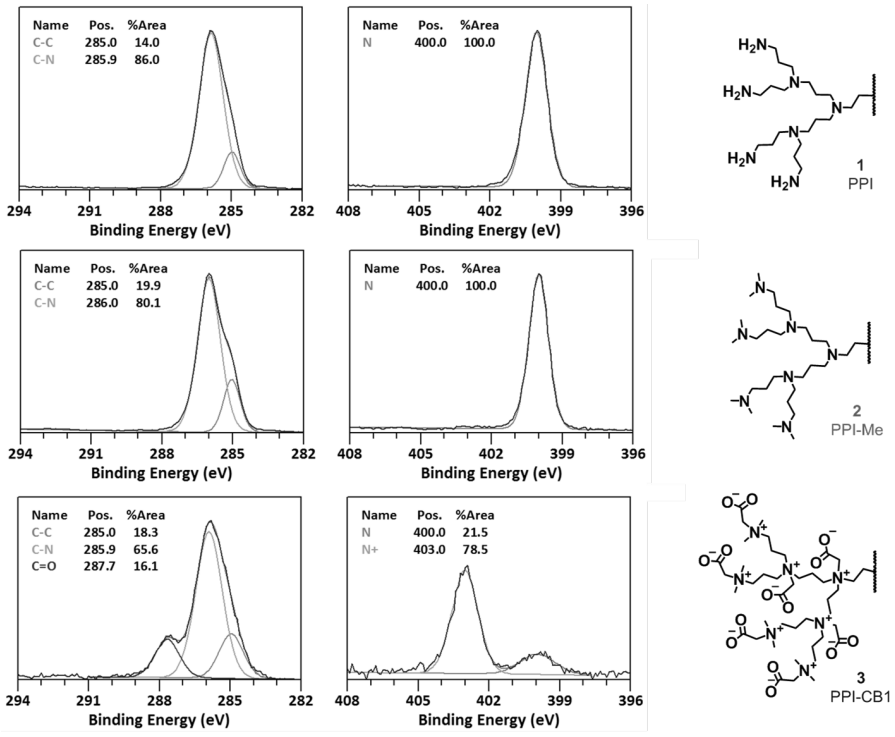

Figure 2.3 Narrow scan XPS C 1s (left) and N 1s (right) data of **1** (top), **2** (middle) and **3** (bottom).

In Figure 2.3 the XPS C 1s and N 1s narrow-range scans are displayed. By scanning the element peaks with high resolution, valuable quantitative information about the chemical state of the element involved can be obtained, which can be related to the electronic effects of its substituents and thereby its chemical structure. After methylation, the C 1s scan of intermediate **2** showed solely C–C (285.0 eV) and C–N (286.0 eV) carbon species, in accordance with the structure of **2**. In contrast, after alkylation with sodium iodoacetate, an additional peak in the C 1s narrow scan is visible at 287.7 eV, which points to the presence carboxylate carbons (–C(=O)–O. Furthermore, the C–N peak also broadened because of the increase in the variation of this type of carbon. More importantly, the XPS N 1s scans provided us with unique information about the fraction of quaternary nitrogen atoms. Before alkylation, structure **2** shows one sharp peak for tertiary amines (400.0 eV). After alkylation, compound **3** showed an additional major peak at 403.0 eV, corresponding to quaternary amines. The ratio of these two peaks shows that a conversion of approximately 80% was achieved when reacting **2** with sodium iodoacetate. Unfortunately, the quantitative information about the chemical state of N as obtained by XPS was unique with respect to the accuracy it offered in determining the degree of conversion. Such accuracy could not be achieved –and hence not compared– with results obtained by other, well known, techniques (*e.g.* NMR or MS).

Table 2.1 XPS results for the optimization of the alkylation/charge-neutralization reaction on **2**, via either the sodium salt (a-d) or the protected acid (e-h) of the indicated alkyl halides (see Figure 2.7).

	Reactant	Conversion [a]
a	Sodium iodoacetate	87%
b	Sodium bromoacetate	54%
c	Sodium bromoethane sulfonate	74%
d	Sodium bromopropane sulfonate	70%
e	*tert*-Butyl iodoacetate + deprotection	85%
f	*tert*-Butyl bromoacetate + deprotection	93%
g	Methyl iodoacetate + deprotection	79%
h	Methyl bromoacetate + deprotection	77%

[a] based on conversion to quaternary amine as measured by XPS N 1s narrow scans

As the conversion of the last step was not 100%, there will be tertiary amines left that can be protonated under physiological conditions, which will lead to dendrimers that are not permanently charge neutral since the carboxylate group is needed to compensate for the positively charged amine. Furthermore, since it is known that the performance of zwitterionic materials is enhanced with an increase in hydration of the brush that is linked to its charge density,[50] we set out to systematically explore a range of reaction conditions to optimize this last reaction step. XPS provided a very powerful and sensitive method to systematically screen conditions under which the last reaction step could be improved. In particular, we used XPS (Table 2.1) to study the influence of the following parameters:

1) *Steric hindrance within the dendrimer:* Generations 2, 3 and 4 of the PPI dendrimer were reacted with sodium iodoacetate. Steric hindrance within the dendrimer was found not to play a significant role, since the conversion did not increase significantly with decreased dendrimer size (Figure 2.6).

2) *Solvent effect:* The use of both methyl- and *tert*-butyl-protected carboxylates allowed us to use an aprotic polar solvent since both the reactant and the intermediate product (before deprotection) are soluble in such a solvent, enhancing the stability of the alkyl halide precursors. We indeed observed an increase in conversion up to roughly 90% when using protected acids (e-f), possibly due to the stability of the halide precursors in an aprotic solvent. However, when using this approach an extra deprotection is necessary, which then needs to be quantitative to yield a charge-neutral ZID (e-h).

3) *Reactivity:* We found a clear difference in conversion when comparing sodium iodo- and bromoacetate (87% vs. 54%) in water, which is in line with expectation since iodide is a better leaving group in this reaction (a-b). However, the corresponding reactions with protected acids in organic solvents, showed no significant difference when comparing halide leaving group (e-h). We postulate that due to the lack of (water-induced) competitive elimination reactions and the long reaction time (3 days), in this case both groups eventually reach the same high conversion.

4) *Nature and size of the anionic group:* We evaluated both the nature of the anionic head group, which was either a carboxylate or a sulfonate group, as well as the carbon spacer length between the opposite charges of the zwitterion pair. We chose to synthesize CB1 (carboxybetaine, one-carbon spacer) ZID, because it does not allow for Hofmann elimination (resulting in loss of $C_2H_3COO^-$), in

contrast to CB2 (carboxybetaine, two-carbon spacer) species.[51] On top of that, we compared SB2 and SB3 (sulfobetaine, with two- and three-carbon spacers, respectively) to study steric effects caused by the precursor. We indeed found a lower conversion when using the slightly bigger SB3 compound (c-d). Unfortunately, the precursor for SB1 was not available.

To further evaluate the effect of sterics we also reacted an ~80% converted ZID with methyl iodide as a small, strong alkylation agent, resulting in near 100% conversion towards quaternary amines (Figure S4). This suggest that indeed for steric reasons it is practically hard to reach full conversion (for **2**, a 93% conversion of the 30 N atoms effectively means that 28 N atoms will be quaternized). While the final product after reaction with methyl iodide is fully quaternized, it is no longer charge neutral, likely thus on average +2, and therefore we did not use it as such for further studies.

Overall, from this comparative study we concluded that the sodium iodoacetate reaction on **1** was most efficient. For this reaction the highest conversion was obtained without the need for an additional deprotection step. A reaction efficiency of 87% implies for an N_{30}-molecule like **3** that typically 26 tertiary N atoms have been converted to quaternary N atoms. As a result, under physiological conditions likely one or two N atoms will be protonated. The determination of the precise charge and charge distribution under these conditions are topics of future investigations in our labs.

2.2.3 Synthesis of functional, zwitterionic dendrimers

In order to use the zwitterionic dendrimers for biological or biomedical applications, functional groups at the dendrimer's periphery that allow easy modification are needed. In order to do this, fast, easy, orthogonal and water-compatible chemistry is required. Given the intrinsic multivalent nature of the PPI dendrimers, introduction of a functional group can be achieved through reaction with a pre-defined number of amine groups of the dendrimer, provided that both the installed bond and the functional group are compatible with the conditions of the subsequent reaction steps that alkylate and add the zwitterionic moieties (Scheme 2.1). On the basis of these provisions, we relied on the reaction of PPI with activated esters to form amide bonds to introduce a new functional group of choice. We chose to functionalize the dendrimers with alkyne and azido groups as they allow for a range of click chemistries (Scheme 2.2).[52]

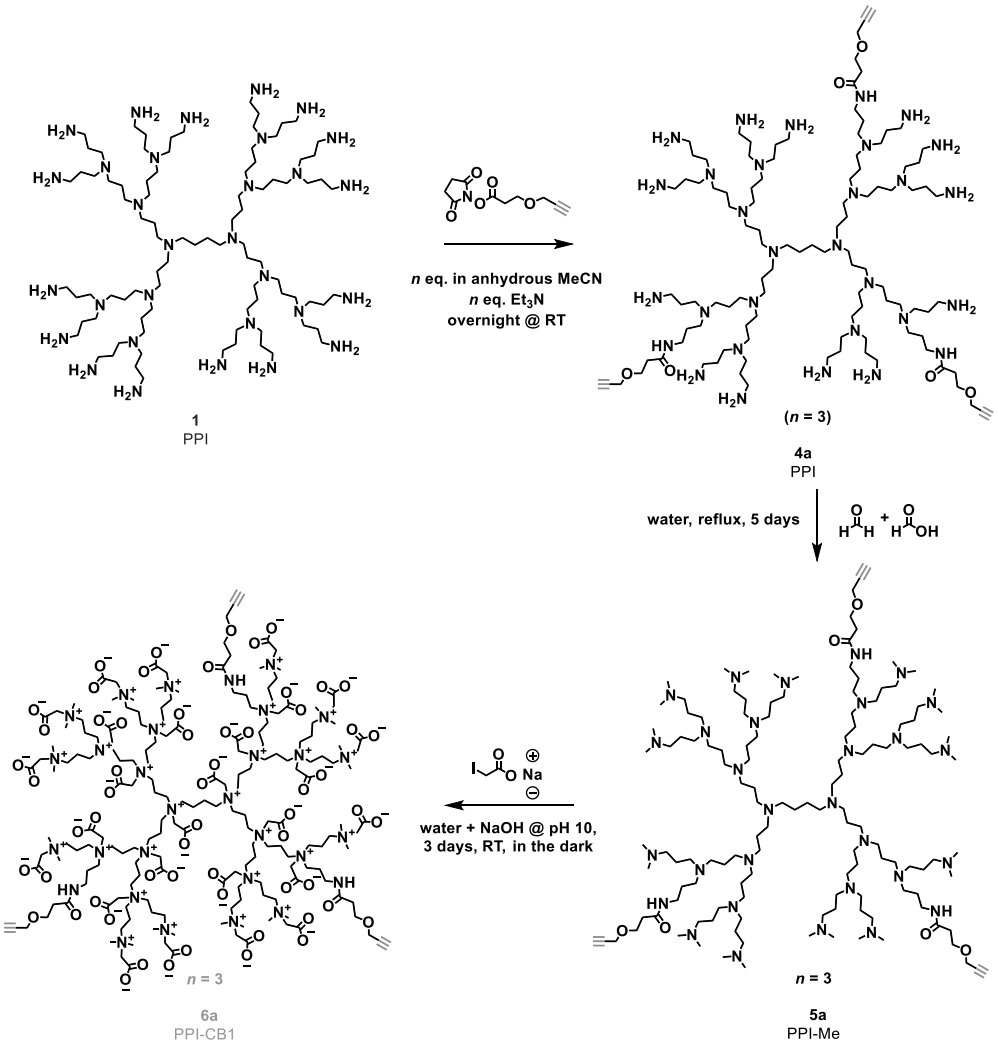

Scheme 2.2 Synthesis of alkyne-functionalized zwitterionic PPI-CB1 dendrimers. Note: n = 3 is shown as example, but other degrees of functionalization are possible; this synthesis was also performed with n = 2 and n = 6; see Supporting Information for details.

To install an alkyne click handle, PPI dendrimer **1** was first reacted with a predetermined number of equivalents of an NHS-activated ester featuring an alkyne group connected with a short linker (forming intermediate product **4a**). The formed product was directly reacted towards the fully methylated intermediate **5**, using the Eschweiler-Clarke conditions previously established for the non-functional dendrimer **3** (Scheme 2.1). Finally the functionalized, zwitterionic dendrimers with an alkyne (**6a**) handle were obtained through reaction with sodium iodoacetate (again following procedures previously employed in the synthesis of **3**).

In the ^{1}H-NMR spectrum (Figure 2.15) of the reaction product **6a** we observed characteristic signals for the alkyne groups (3.33 ppm), as well as for the formed amide bonds (CH_2 next to the amide, 3.36 ppm). Based on NMR integration, an average degree of incorporation of 2.9 for **6a** (*n* = 3) could be determined. To confirm with another technique and to obtain information about the distribution of the number of functional groups per dendrimer, we used mass spectrometry (MS). Unfortunately, the ESI-MS of methylated intermediate **5a** lead to fragmentation due to rearrangements within the dendrimer, most probably due to ionization[53] or methylation.[54] This prompted us to isolate intermediates **4a** (both *n* = 2 and *n* = 3) for MS analysis to study the distribution of functional groups over the ZID. MS data nicely showed a fairly small range of distribution of *n* = 2 and *n* = 3 with the desired number of *n* as center of the distribution (Figure 2.23 and Figure 2.24). The final product **6a** itself could not be measured, which we attribute to ionization difficulties of the highly zwitterionic dendrimers; unfortunately, also with MALDI–ToF we were unable to get signal.
GPC confirmed the estimated mass and desired PDI of products **3** and **6a** (both for *n* = 2 and *n* = 3). The observed molecular weight was in good agreement with the molecular weight at full conversion. As also observed for **3**, the PDI of all three products; 1.102 (**3**), 1.193 (**6a** *n* = 2) and 1.138 (**6a** *n* = 3) were rather low, which is even more remarkable since these are macromolecules that underwent several consecutive modification steps (Table 2.3 in the Supporting Information).

To quantify the incorporation of the functional groups, XPS again proved to be a valuable technique. Since the carbonyl–carbon that forms upon forming the amide bond gives a signal that is found at a sufficiently high binding energy (~288 eV) to be discerned as a separate peak in C 1s XPS spectra, it is possible to determine the relative number of C=O carbons present in the dendrimer.

In Figure 2.4, the XPS C 1s data confirm an average incorporation of 2 and 3 alkyne groups by showing a similar amount of carbonyl–carbon signals (*n* = 2 carbonyls out of 128 carbons in total = 1.6% theoretically, 1.9% is observed) (*n* = 3 carbonyls out of 132 carbons in total = 2.2% theoretically, 3.6% is observed) at 288.2 and 288.1 eV in the upper graphs for intermediate **5a**. Furthermore, both C 1s scans of compound **6a** *n* = 2 and *n* = 3 show a similar transformation upon alkylation as described before for compound **3**. To extend the versatility of click reaction-based dendrimer modification, we also synthesized ZIDs with azide groups. By reacting PPI dendrimer **1** with an NHS-activated ester that was linked to an azide group via a short oligo(ethylene oxide) chain (NHS-EO_8-azide) group, intermediate **4b** was formed. This intermediate **4b** was further reacted following procedures previously employed in the synthesis of both **3** and **6a** to eventually yield product **6b** (Scheme 2.3).

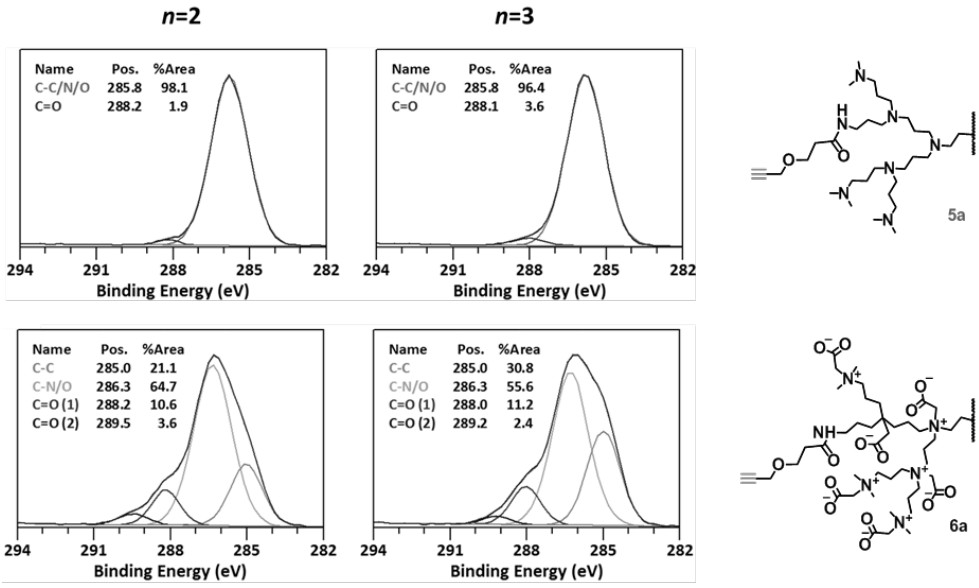

Figure 2.4. XPS narrow scan C 1s data of **5a** (top) and **6a** (bottom) of *n* = 2 (left) and *n* = 3 (right) alkyne-modified dendrimer. For reference, a characteristic part of the modified dendrimer is shown.

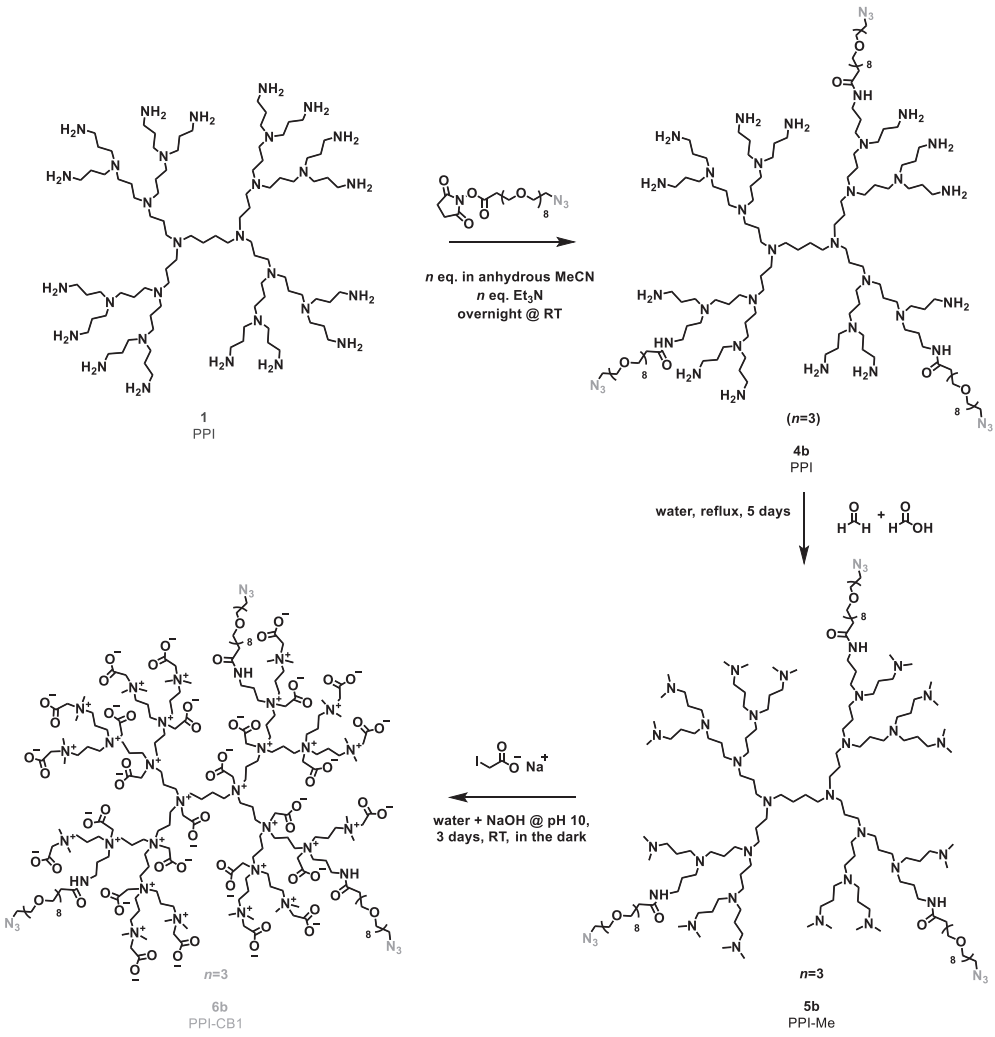

Scheme 2.3. Synthesis of azido-functionalized zwitterionic PPI-CB1 dendrimers. *Note: n* = 3 is shown as example, but other degrees of functionalization are possible; this synthesis was also performed with *n* = 2 and *n* = 6; see Supporting Information for details.

In the ^{1}H-NMR spectrum (Figure 2.17) of reaction product **6b** (*n* = 3) we observed characteristic signals for the ethylene glycol spacers (3.69 ppm), as well as for the formed amide bonds (3.37 ppm). DOSY indicated that all the assigned signals, including the functional groups, belong to one macromolecular structure by showing the same diffusion coefficient (Figure 2.5), confirming that the low-molecular weight functional groups were successfully linked to the high-molecular weight dendrimer. We also observed a trend in increased diffusion constant with increasing size and expected molecular weight of the ZID (Figure 2.5): applying the Stokes-Einstein equation, the hydrodynamic diameters for **3**, **6a** and **6b** were estimated to be 3.2, 4.1 and 5.1 nm, respectively (Table 2.2).

Unfortunately, dynamic light scattering (DLS) proved to be impossible to use as a complementary technique to determine the dimensions of our dendrimers, which is most likely the result of the relatively small size of the dendrimers. As a result, we also could not determine the zeta potential to get more insight into the charge distribution within the dendrimer structures.

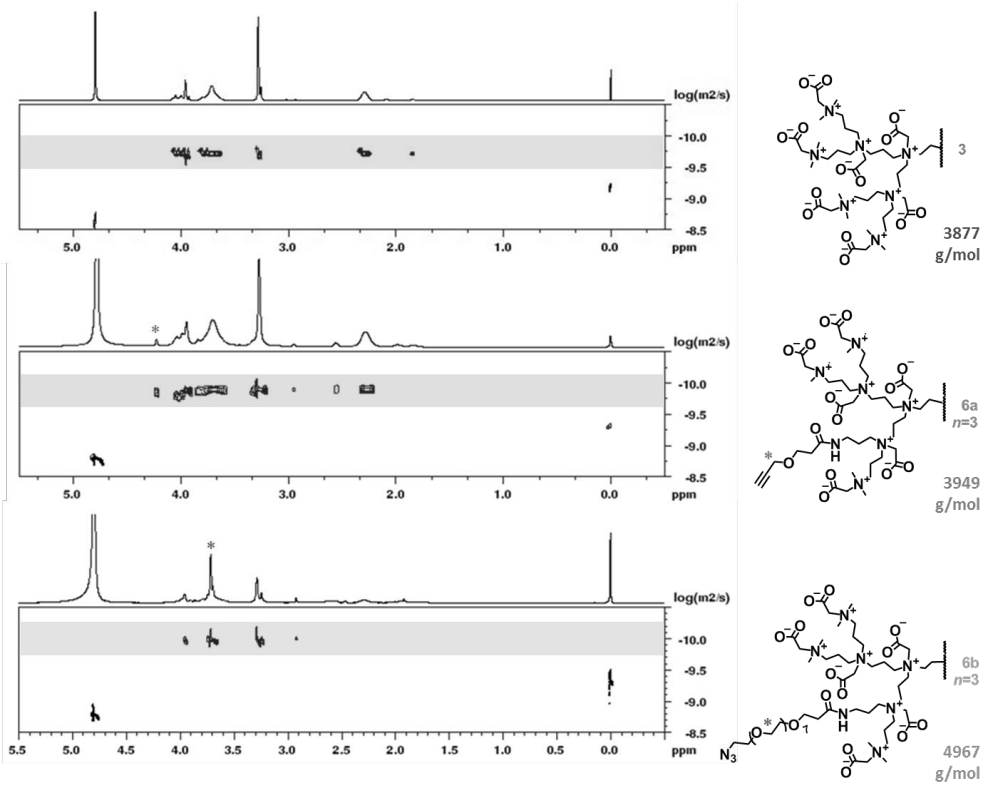

Figure 2.5 DOSY spectra of unmodified PPI-CB1 dendrimer **3**, alkyne-modified **6a** PPI-CB1 and azide-modified **6b** PPI-CB1 (both *n* = 3). In the functionalized dendrimers the most indicative ^{1}H signal is labeled by a star (*). In all three spectra, the signals in the highlighted band correspond to the ZID, the signals at 4.8 ppm and 0.0 ppm represent water and TMS, respectively. Furthermore, theoretical molecular masses (at full conversion) are given.

Unfortunately, though not fully unexpectedly, in the IR spectrum, the alkyne and azide signals could hardly be discerned for **6a** and **6b** (both *n* = 2 or *n* = 3), since the abundance of these groups in the large dendrimer is relatively low (namely only 2 or 3 alkyne or azide groups per 4000 - 5000 g/mol structure). Fortunately, due to the modularity of the synthetic route (Scheme 2.2), the synthesis of functional dendrimers with a higher number of functional groups (reaction with 6 eq. instead of 2 or 3 eq.) was straightforward. For these *n* = 6 dendrimers it was possible to observe by IR spectroscopy the alkyne and azide groups at 2115 and 2106 cm^{-1}, respectively (Figure 2.22). Hence, these IR measurements provided further experimental evidence for the successful incorporation of the functional alkyne and azide moieties.

As a proof-of-principle experiment to demonstrate that our installed click handles can indeed be used for (bio)functionalization, we introduced a biotin moiety onto the alkyne-containing ZID **6a** (*n* = 3) by reacting the latter with an azide-functionalized PEG-biotin derivative as shown in Scheme 2.4. NMR data nicely showed the corresponding signal for the proton in the formed triazole at 8.13 ppm in the ^{1}H NMR spectrum after extensive dialysis, providing evidence that the biotin was successfully coupled to the ZID (see Figure 2.19 and Figure 2.20).

2.3 Conclusion

In this work, we showed the design and optimized synthesis of (nearly) charge neutral, multivalently clickable zwitterionic dendrimers (ZID). The effect of different parameters on the conversion towards a fully zwitterionic system was established, leading to an optimized synthesis protocol. In this optimization study, X-ray photoelectron spectroscopy (XPS), which so far was mainly employed for surface characterization, proved to be a very valuable technique to analyze macromolecules by providing information about the degree of conversion in these highly functional dendrimer structures. Furthermore, we developed a modular synthetic approach to incorporate a variable number of alkyne or azide functional groups, which allow for covalent (bio)functionalization. Proof-of-principle coupling of an azide-biotin conjugate by click chemistry showed that the ZID indeed can be further functionalized. The fact that multiple, or ultimately even different, functional groups can be incorporated, will further enhance the (bio)applicability of this kind of zwitterionic dendrimers.

2.4 Acknowledgements

The authors thank Dr. Pieter de Waard and Prof. Aldrik Velders for assistance with the ^{15}N and 2D-NMR measurements, and Margaux Tellez and Maaike van Slagmaat for their contributions to this work. This project was supported by NWO (LIFT program, grant 731.015.042) with Surfix BV as a partner.

2.5 References

1. Boas, U.; Christensen, J. B.; Heegaard, P. M. H. Dendrimers: Design, Synthesis and Chemical Properties. *J. Mater. Chem.* **2006**, *16* (38), 3785–3798.
2. Sato, K.; Anzai, J. I. Dendrimers in Layer-by-Layer Assemblies: Synthesis and Applications. *Molecules* **2013**, *18* (7), 8440–8460.
3. Abbasi, E.; Aval, S. F.; Akbarzadeh, A.; Milani, M.; Nasrabadi, H. T.; Joo, S. W.; Hanifehpour, Y.; Nejati-Koshki, K.; Pashaei-Asl, R. Dendrimers: Synthesis, Applications, and Properties. *Nanoscale Res. Lett.* **2014**, *9* (1), 1–10.
4. Lee, C. C.; MacKay, J. A.; Fréchet, J. M. J.; Szoka, F. C. Designing Dendrimers for Biological Applications. *Nat. Biotechnol.* **2005**, *23* (12), 1517–1526.
5. Froehling, P. E. Dendrimers and Dyes — a Review. *Dye. Pigment.* **2001**, *48* (3), 187–195.
6. Knapen, J. W. J.; van der Made, A. W.; de Wilde, J. C.; van Leeuwen, P. W. N. M.; Wijkens, P.; Grove, D. M.; van Koten, G. Homogeneous Catalyst Based on Silane Dendrimers Functioanlized with Arylnickel(II) Complexes. *Nature* **1994**, *372*, 659–663.
7. Kobayashi, H.; Brechbiel, M. W. Nano-Sized MRI Contrast Agents with Dendrimer Cores. *Adv. Drug Deliv. Rev.* **2005**, *57* (15), 2271–2286.
8. Fernandes, E. G. R.; Vieira, N. C. S.; de Queiroz, A. A. A.; Guimarães, F. E. G.; Zucolotto, V. Immobilization of Poly (Propylene Imine) Dendrimer / Nickel Phtalocyanine as Nanostructured Multilayer Films To Be Used as Gate Membranes for SEGFET PH Sensors. *J. Phys. Chem. C* **2010**, *114* (14), 6478–6483.

9. Nimesh, S. *Gene Therapy: Potential Applications of Nanotechnology*; Woodhead Publishing, 2013.
10. Tsai, H.-C.; Imae, T. Fabrication of Dendrimers Toward Biological Application. *Prog. Mol. Biol. Transl. Sci.* **2011**, *104*, 101–140.
11. Sharma, A. K.; Gothwal, A.; Kesharwani, P.; Alsaab, H.; Iyer, A. K.; Gupta, U. Dendrimer Nanoarchitectures for Cancer Diagnosis and Anticancer Drug Delivery. *Drug Discov. Today* **2017**, *22* (2), 314–326.
12. Wang, T.; Zhang, Y.; Wei, L.; Teng, Y. G.; Honda, T.; Ojima, I. Design, Synthesis, and Biological Evaluations of Asymmetric Bow-Tie PAMAM Dendrimer-Based Conjugates for Tumor-Targeted Drug Delivery. *ACS Omega* **2018**, *3* (4), 3717–3736.
13. Newkome, G. R.; Shreiner, C. D. Poly(Amidoamine), Polypropylenimine, and Related Dendrimers and Dendrons Possessing Different 1 → 2 Branching Motifs: An Overview of the Divergent Procedures. *Polymer.* **2008**, *49* (1), 1–173.
14. Otto, D. P.; de Villiers, M. M. Poly(Amidoamine) Dendrimers as a Pharmaceutical Excipient. Are We There Yet? *J. Pharm. Sci.* **2018**, *107* (1), 75–83.
15. Stasko, N. A.; Johnson, C. B.; Schoenfisch, M. H.; Johnson, T. A.; Holmuhamedov, E. L. Cytotoxicity of Polypropylenimine Dendrimer Conjugates on Cultured Endothelial Cells. *Biomacromolecules* **2007**, *8* (12), 3853–3859.
16. Jevprasesphant, R.; Penny, J.; Jalal, R.; Attwood, D.; McKeown, N. .; D'Emanuele, A. The Influence of Surface Modification on the Cytotoxicity of PAMAM Dendrimers. *Int. J. Pharm.* **2003**, *252* (1–2), 263–266.
17. Geiger, B. C.; Wang, S.; Padera, R. F.; Grodzinsky, A. J.; Hammond, P. T. Cartilage-Penetrating Nanocarriers Improve Delivery and Efficacy of Growth Factor Treatment of Osteoarthritis. *Sci. Transl. Med.* **2018**, *10* (469), eaat8800.
18. Wang, L.; Wang, Z.; Ma, G.; Lin, W.; Chen, S. Reducing the Cytotoxity of Poly(Amidoamine) Dendrimers by Modification of a Single Layer of Carboxybetaine. *Langmuir* **2013**, *29* (28), 8914–8921.
19. Svenningsen, S. W.; Janaszewska, A.; Ficker, M.; Petersen, J. F.; Klajnert-Maculewicz, B.; Christensen, J. B. Two for the Price of One: PAMAM-Dendrimers with Mixed Phosphoryl Choline and Oligomeric Poly(Caprolactone) Surfaces. *Bioconjug. Chem.* **2016**, *27* (6), 1547–1557.
20. Xiong, Z.; Wang, Y.; Zhu, J.; Li, X.; He, Y.; Qu, J.; Shen, M.; Xia, J.; Shi, X. Dendrimers Meet Zwitterions: Development of a Unique Antifouling Nanoplatform for Enhanced Blood Pool, Lymph Node and Tumor CT Imaging. *Nanoscale* **2017**, *9* (34), 12295–12301.
21. Bodewein, L.; Schmelter, F.; Di Fiore, S.; Hollert, H.; Fischer, R.; Fenske, M. Differences in Toxicity of Anionic and Cationic PAMAM and PPI Dendrimers in Zebrafish Embryos and Cancer Cell Lines. *Toxicol. Appl. Pharmacol.* **2016**, *305*, 83–92.
22. Hu, J.; Su, Y.; Zhang, H.; Xu, T.; Cheng, Y. Design of Interior-Functionalized Fully Acetylated Dendrimers for Anticancer Drug Delivery. *Biomaterials* **2011**, *32* (36), 9950–9959.
23. Carr, L. R.; Zhou, Y.; Krause, J. E.; Xue, H.; Jiang, S. Uniform Zwitterionic Polymer Hydrogels with a Nonfouling and Functionalizable Crosslinker Using Photopolymerization. *Biomaterials* **2011**, *32* (29), 6893–6899.
24. Ramireddy, R. R.; Subrahmanyam, A. V.; Thayumanavan, S. Zwitterionic Moieties from the Huisgen Reaction: A Case Study with Amphiphilic Dendritic Assemblies. *Chem. Eur. J* **2013**, *19* (48), 16374–16381.
25. Li, L.; Wang, Y.; Ji, F.; Wen, Y.; Li, J.; Yang, B.; Yao, F. Synthesis and Characterization of Dendritic Star-Shaped Zwitterionic Polymers as Novel Anticancer Drug Delivery Carriers. *J. Biomater. Sci. Polym. Ed.* **2014**, *25* (14–15), 1641–1657.
26. Wang, L.; Zhang, J.; Lin, W.; Wang, Z.; Chen, S. Development of a Protein Mimic with Peptide Ligands to Enhance Specific Sensing and Targeting by the Zwitterionic Surface Engineering of Poly(Amido Amine) Dendrimers. *Adv. Mater. Interfaces* **2014**, *1* (1), 1300059.
27. Wang, Y.; Li, L.; Li, J.; Yang, B.; Wang, C.; Fang, W.; Ji, F.; Wen, Y.; Yao, F. Stable and PH-Responsive Polyamidoamine Based Unimolecular Micelles Capped with a Zwitterionic Polymer Shell for Anticancer Drug Delivery. *RSC Adv.* **2016**, *6* (21), 17728–17739.
28. Huang, D.; Yang, F.; Wang, X.; Shen, H.; You, Y.; Wu, D. Facile Synthesis and Self-Assembly Behaviour of PH-Responsive Degradable Polyacetal Dendrimers. *Polym. Chem.* **2016**, *7* (40), 6154–6158.
29. Cao, W.; Huang, J.; Jiang, B.; Gao, X.; Yang, P. Highly Selective Enrichment of Glycopeptides Based on Zwitterionically Functionalized Soluble Nanopolymers. *Sci. Rep.* **2016**, *6* (29776), 1–8.
30. Han, Y.; Qian, Y.; Zhou, X.; Hu, H.; Liu, X.; Zhou, Z.; Tang, J.; Shen, Y. Facile Synthesis of Zwitterionic Polyglycerol Dendrimers with a β-Cyclodextrin Core as MRI Contrast Agent Carriers. *Polym. Chem.* **2016**, *7*, 6354.
31. Zhang, P.; Sun, F.; Tsao, C.; Liu, S.; Jain, P.; Sinclair, A.; Hung, H.-C.; Bai, T.; Wu, K.; Jiang, S. Zwitterionic Gel Encapsulation Promotes Protein Stability, Enhances Pharmacokinetics, and Reduces Immunogenicity. *Proc. Natl. Acad. Sci.* **2015**, *112* (39), 12046–12051.
32. Ramasamy, T.; Ruttala, H. B.; Gupta, B.; Poudel, B. K.; Choi, H. G.; Yong, C. S.; Kim, J. O. Smart Chemistry-Based Nanosized Drug Delivery Systems for Systemic Applications: A Comprehensive Review. *J. Control. Release* **2017**, *258* (April), 226–253.
33. Astruc, D.; Boisselier, E.; Ornelas, C. Dendrimers Designed for Functions: From Physical, Photophysical, and Supramolecular Properties to Applications in Sensing, Catalysis, Molecular Electronics, Photonics, and Nanomedicine. *Chem. Rev.* **2010**, *110* (4), 1857–1959.
34. Patil, M. L.; Zhang, M.; Taratula, O.; Garbuzenko, O. B.; He, H.; Minko, T. Internally Cationic Polyamidoamine PAMAM-OH Dendrimers for SiRNA Delivery: Effect of the Degree of Quaternization and Cancer Targeting. *Biomacromolecules*

2009, *10* (2), 258–266.
35. Sun, J.; Zeng, F.; Jian, H.; Wu, S. Conjugation with Betaine: A Facile and Effective Approach to Significant Improvement of Gene Delivery Properties of PEI. *Biomacromolecules* **2013**, *14* (3), 728–736.
36. Magin, C. M.; Cooper, S. P.; Brennan, A. B. Non-Toxic Antifouling Strategies. *Mater. Today* **2010**, *13* (4), 36–44.
37. Pine, S. H.; Sanchez, B. L. Formic Acid-Formaldehyde Methylation of Amines. *J. Org. Chem.* **1971**, *36* (6), 829–832.
38. Zhou, X.; Chen, Y.; Han, J.; Wu, X.; Wang, G.; Jiang, D. Betaine Ester-Shell Functionalized Hyperbranched Polymers for Potential Antimicrobial Usage: Guest Loading Capability, PH Controlled Release and Adjustable Compatibility. *Polymer (Guildf).* **2014**, *55* (24), 6261–6270.
39. Wu, L.; Jasinski, J.; Krishnan, S. Carboxybetaine, Sulfobetaine, and Cationic Block Copolymer Coatings: A Comparison of the Surface Properties and Antibiofouling Behavior. *J. Appl. Polym. Sci.* **2012**, *124* (3), 2154–2170.
40. Bosman, A. W.; Janssen, H. M.; Meijer, E. W. About Dendrimers : Structure , Physical Properties , and Applications. *Chem. Rev.* **1999**, *99*, 1665–1688.
41. de Brabander-van den Berg, E. M. M.; Meijer, E. W. Poly(Propylene Imine) Dendrimers: Large-Scale Synthesis by Hetereogeneously Catalyzed Hydrogenations. *Angew. Chem. Int. Ed. Engl.* **1993**, *32* (9), 1308–1311.
42. Wrobel, D.; Appelhans, D.; Signorelli, M.; Wiesner, B.; Fessas, D.; Scheler, U.; Voit, B.; Maly, J. Interaction Study between Maltose-Modified PPI Dendrimers and Lipidic Model Membranes. *Biochim. Biophys. Acta - Biomembr.* **2015**, *1848* (7), 1490–1501.
43. Müller, R.; Laschober, C.; Szymanski, W. W.; Allmaier, G. Determination of Molecular Weight, Particle Size, and Density of High Number Generation PAMAM Dendrimers Using MALDI-TOF-MS and NES-GEMMA. *Macromolecules* **2007**, *40* (15), 5599–5605.
44. Briggs, D.; Grant, J. T. Perspectives and Basic Principles. In *Surface analysis by Auger and x-ray photoelectron spectroscopy*; IM Publications and SurfaceSpectra Limited, 2003; pp 1–88.
45. Giesbers, M.; Marcelis, A. T. M.; Zuilhof, H. Simulation of XPS C1s Spectra of Organic Monolayers by Quantum Chemical Methods. *Langmuir* **2013**, *29* (15), 4782–4788.
46. Joshi, S.; Pellacani, P.; van Beek, T. A.; Zuilhof, H.; Nielen, M. W. F. Surface Characterization and Antifouling Properties of Nanostructured Gold Chips for Imaging Surface Plasmon Resonance Biosensing. *Sens. Actuators B* **2015**, *209*, 505–514.
47. van Andel, E.; de Bus, I.; Tijhaar, E. J.; Smulders, M. M. J.; Savelkoul, H. F. J.; Zuilhof, H. Highly Specific Binding on Antifouling Zwitterionic Polymer-Coated Microbeads as Measured by Flow Cytometry. *ACS Appl. Mater. Interfaces* **2017**, *9* (44), 38211–38221.
48. Nguyen, A. T.; Baggerman, J.; Paulusse, J. M. J.; Zuilhof, H.; Van Rijn, C. J. M. Bioconjugation of Protein-Repellent Zwitterionic Polymer Brushes Grafted from Silicon Nitride. *Langmuir* **2012**, *28* (1), 604–610.
49. Slagman, S.; Jonkers, W. A.; Zuilhof, H.; Franssen, M. C. R. Elucidating the Mechanism behind the Laccase-Mediated Modification of Poly(Ethersulfone). *RSC Adv.* **2018**, *8* (48), 27101–27110.
50. Shao, Q.; Mi, L.; Han, X.; Bai, T.; Liu, S.; Li, Y.; Jiang, S. Differences in Cationic and Anionic Charge Densities Dictate Zwitterionic Associations and Stimuli Responses. *J. Phys. Chem. B* **2014**, *118* (24), 6956–6962.
51. Cao, B.; Li, L.; Tang, Q.; Cheng, G. The Impact of Structure on Elasticity, Switchability, Stability and Functionality of an All-in-One Carboxybetaine Elastomer. *Biomaterials* **2013**, *34* (31), 7592–7600.
52. Kolb, H. C.; Finn, M. G.; Sharpless, K. B. Click Chemistry: Diverse Chemical Function from a Few Good Reactions. *Angew. Chemie - Int. Ed.* **2001**, *40* (11), 2004–2021.
53. Weener, J.; Dongen, J. L. J. Van; Meijer, E. W. Electrospray Mass Spectrometry Studies of Poly (Propylene Imine) Dendrimers : Probing Reactivity in the Gas Phase. *J. Am. Chem. Soc.* **1999**, *121* (44), 10346–10355.
54. Alder, R. W.; Colclough, D.; Mowfam, R. W. Fragmentation During the Formic Acid/Formaldehyde (Eschweiler-Clarke) Methylation of Polyamines. *Tetrahedron Lett.* **1991**, *32* (52), 7755–7758.
55. Boisselier, E.; Ornelas, C.; Pianet, I.; Aranzaes, J. R.; Astruc, D. Four Generations of Water-Soluble Dendrimers with 9 to 243 Benzoate Tethers: Synthesis and Dendritic Effects on Their Ion Pairing with Acetylcholine, Benzyltriethylammonium, and Dopamine in Water. *Chem. - A Eur. J.* **2008**, *14* (18), 5577–5587.
56. Salorinne, K.; Lahtinen, T.; Malola, S.; Koivisto, J.; Häkkinen, H. Solvation Chemistry of Water-Soluble Thiol-Protected Gold Nanocluster Au102 from DOSY NMR Spectroscopy and DFT Calculations. *Nanoscale* **2014**, *6* (14), 7823–7826.
57. Holz, M.; Weingartner, H. Calibration in Accurate Spin-Echo Self-Diffusion Measurements Using 1H and Less-Common Nuclei. *J. Magn. Reson.* **1991**, *92* (1), 115–125.

2.6 Supporting Information

2.6.1 Experimental Section

2.6.1.1 Materials

Milli-Q water was purified by a Barnsted water purification system, with a resistivity of <18.3 MΩ·cm. The reported plasma cleaner was a Diener Femto plasma system. Molecular sieves (10 Å) were oven-dried (120 °C, overnight) prior to use. Sonication steps were performed in an Elmasonic P 30 H ultrasonic unit at 80 kHz. Float-a-lyzer G2 dialysis membranes (VWR) with a 500-1000D DE (default) or 1000-5000D CE (when specifically mentioned) were used for the final purification step. Commercially available reagents were used without purification, unless mentioned otherwise: Poly(propylene imine) dendrimers G2, G3 and G4 (PPI, SyMOChem); ethanol (EtOH, absolute, dried over molecular sieves, Merck); hydrochloric acid (HCl, 37% in water, Acros Organics); dichloromethane (DCM, GPR Rectapur, Fisher Scientific); n-hexane (≥99%, Sigma Aldrich); acetone (Semiconductor grade, Sigma Aldrich); deuterium oxide (D2O, 99.9 atom% D, Sigma Aldrich); 3-(trimethylsilyl)-1-propanesulfonic acid-d6 sodium salt (TMS salt, 98 atom% D, Sigma Aldrich); formaldehyde (37 wt% in water, 10-15% methanol, Fisher Scientific); formic acid (99%, VWR); tert-Butyl bromoacetate (98%, Sigma Aldrich); tert-Butyl 2-iodoacetate (Sigma Aldrich); trifluoroacetic acid (Biosolve B.V.); methyl bromoacetate (96%, Sigma Aldrich); methyl 2-iodoacetate (95%, Sigma Aldrich); methyl iodide (99%, stabilized, Fisher Scientific); sodium bromoacetate (98%, Sigma Aldrich); sodium iodoacetate (≥98%, Sigma Aldrich); sodium 2-bromoethylsulfonate (98%, Sigma Aldrich); sodium 3-bromopropanesulfonate (≥97%, Sigma Aldrich); propargyl-N-hydroxysuccinimidyl ester (NHS-alkyne, Sigma Aldrich); azido-PEG®8-NHS ester (NHS-PEG-azide, Sigma Aldrich); sodium hydroxide (NaOH, 98.5% pellets, Fisher Scientific); sodium sulfate (Na_2SO_4, anhydrous, Fisher Scientific); triethylamine (99%, distilled, on KOH, Fisher Scientific); azide-PEG3-biotin (Sigma Aldrich); sodium L-ascorbate (sodium ascorbate, ≥98%, Sigma Aldrich); copper sulfate pentahydrate (≥98%, Sigma Aldrich)

2.6.1.2 Characterization methods

Nuclear Magnetic Resonance Spectroscopy (NMR)
^{1}H NMR measurements were recorded on a Bruker Avance III NMR at 400 MHz, ^{13}C NMR spectra were recorded at 100 MHz. For the ^{1}H–^{15}N HMBC measurements settings of 600 and 60 MHz were used, respectively, on a 600 MHz Bruker Avance III Ultrashield Plus equipped with a cryoprobe. Chemical shifts are reported in parts per million (ppm), and are referred to the methyl signal of the sodium salt of 3-(trimethylsilyl)-1-propanesulfonic acid-d_6 (δ = 0).

Infrared Spectroscopy (IR)
IR analyses were performed on a Bruker Tensor 27 spectrometer with platinum ATR accessory.

X-ray Photoelectron Spectroscopy (XPS)
Samples for dendrimer analysis were prepared by concentrating the dendrimers (in milli-Q water) and drop-casting 3 µL of this suspension onto a piece of Si(111) (Siltronix, N-type, phosphorus doped), which was cleaned by rinsing and sonicating for 5 min in semiconductor grade acetone followed by oxygen plasma treatment (Diener electronic, Femto A) for 1 min at 100% power. The dropcast samples were subsequently dried in vacuum overnight before XPS measurements were started. XPS spectra were obtained using a JPS-9200 photoelectron spectrometer (JEOL, Japan) with monochromatic Al-Kα X-Ray radiation at 12 kV and 20 mA. The obtained spectra were analyzed using CASA XPS software (version 2.3.16 PR 1.6). In C1s and N1s narrow-range spectra, the positions are set to 285 eV and 400 eV for the C–C and N–C signals, respectively.

Gel Permeation Chromatography (GPC)
The polymer molecular weight and polydispersity index (PDI) were determined using gel permeation chromatography (Agilent G5654A quaternary pump, G7162A refractive index detector), where a PSS SUPREMA Combination medium (P/N 206-0002) 1000 Å single porosity column was employed (0.05% NaN_3 in milli-Q water as eluent, 1 mL/min). Dendrimer in Milli-Q solutions were freshly prepared. 20 µL was used for each analysis. An Agilent PL2080-0101 PEO calibration kit was used for calibration purposes.

Mass Spectrometry (MS)
MS data were recorded on an Exactive high-resolution MS instrument (Thermo Scientific) equipped with a ESI probe. The MS was calibrated daily using Proteomass LTQ/FT-hybrid ESI Pos. Mode Cal Mix and Pierce ESI Neg. Ion Cal. solutions. Thermo XCalibur Browser software (version 4.0.27.19) was used for instrument control, data acquisition and data processing.

2.6.1.3 Synthesis of ZID 3

*Synthesis of **2** PPI-Me*
A solution of 0.500 g of **1** PPI G3 dendrimer (0.296 mmol) in 10 mL demi water was prepared. A 100 mL 3-neck round bottom flask with a cooler and a stirring bar were flushed with argon by applying 3 vacuum-argon cycles, ending with a final argon refill. Under argon overpressure, 20 mL demi water, 6.35 mL formaldehyde (37% aqueous solution; 75 mmol, 15 eq. per PPI primary amine) and 6.12 mL formic acid (150 mmol, 30 eq. per PPI primary amine) were added. The mixture was cooled on ice before the **1** PPI G3 in 10 mL demi water was added dropwise. The reaction mixture was allowed to warm up to room temperature, after which the setup was closed under argon and refluxed using an oil bath for 5 continuous days to assure full conversion.
Afterwards, the mixture was cooled on ice and the pH was raised to 11 by the slow addition of a saturated NaOH solution. The solution became cloudy since the methylated dendrimers were less water soluble after deprotonation at this concentration. The aqueous solution was extracted with DCM for three times. The combined organic layers were washed with water and dried over Na_2SO_4. After evaporation of the solvent, 0.474 g (0.22 mmol) of a yellow oil was obtained with a yield of 80%.
For the synthesis of **2** PPI-Me G2 and G4 the amounts were adjusted in order to retain 15 eq. of formaldehyde and 30 eq. formic acid per PPI primary amine.

***2** PPI-Me characterization*
^{1}H-NMR (400 MHz, D_2O, 298K) δ 1.73 (H_1; s, 4H), δ 1.91 (H_2; t-overlapping, 56.0H), δ 2.48 (H_3;s, 96H), δ 2.60, 2.67, 2.75 (H_4; t-overlapping, 116H) (Figure 2.9), **^{13}C-NMR (**100 MHz, D_2O, 298K) δ 23.39, δ 41.45-44.28, δ 51.74, δ 54.94, δ 57.14 see Figure 2.10, **^{13}C-HSQC** (100 MHz, D_2O, 298K) see Figure 2.10, **IR** see Figure 2.21, **XPS** C 1s and N 1s narrow scans are provided in Figure 2.3.

*Synthesis of **3** PPI-CB1*
0.200 g of **2** PPI-Me (0.094 mmol) was dissolved in 3 ml aqueous NaOH solution at pH 10 by stirring in a 10 ml round bottom flask. 2.08 g (10 mmol) sodium iodoacetate was added and the solution was stirred at room temperature in the dark for 3 days. Afterwards, the pH was adjusted to ~7 using an HCl solution to assure compatibility with the dialysis membrane and the volume of the mixture was increased to 10 mL by addition of demi water. The mixture was dialyzed against 500 mL demi water for 3 days with 3 medium exchanges. After evaporation of the solvent and lyophilization, 0.238 g of a fluffy white powder was obtained with a yield of 68%.
For the synthesis of **3** PPI-CB1 G2 and G4 with sodium iodoacetate, the amounts were adjusted in order to retain 4 eq. of sodium iodoacetate per **2** PPI-Me tertiary amine.

***3** PPI-CB1 characterization*
^{1}H-NMR (400 MHz, D_2O, 298K) δ 2.29 (H_1; s, 56.0H), δ 3.27 (H_2**;** s-overlapping, 96H), δ 3.71 (H_3; s, 116H), δ 3.97 (H_4; s-overlapping, 60H) see Figure 2.11, **^{13}C-NMR** (100 MHz, D_2O, 298K) (δ 16.45, δ 51.99, δ 56.74-59.80, δ 60.28, δ 61.69, δ 64.00) see Figure 2.12, **^{13}C-HSQC** (100 MHz, D_2O, 298K) see Figure 2.12, **DOSY** (400 MHz, D_2O, 298K) see Figure 2.5, **COSY** (400 MHz, D_2O, 298K) see Figure 2.13, **^{1}H-^{15}N HMBC** (600 MHz, D_2O, 298K) see Figure 2.14, **IR** see Figure 2.21, **XPS** C1s and N1s narrow scans are provided in Figure 2.3, **GPC** see Table 2.3.

Optimization Menschutskin alkylation of methylated dendrimers using different alkyl halides
To optimize the conversion of the alkylation reaction, we tested different dendrimer sizes and alkylation agents and studied the results by XPS N1s high-resolution scans (see Figure 2.6 and Figure 2.7). For the sodium salts sodium bromoacetate, sodium bromoethane sulfonate and sodium bromopropane sulfonate a similar procedure as described for sodium iodoacetate was used, keeping the same equivalents: 0.200 g of **2** PPI (0.094 mmol) was dissolved in 3 mL aqueous NaOH solution at pH 10 by stirring in a 10 mL round bottom flask. 10 mmol of the alkyl halide sodium salt was added and the solution was stirred at room temperature in the dark for 3 days. Afterwards, the pH was adjusted to ~7 using an aqueous HCl solution to assure compatibility with the dialysis membrane and the volume of the mixture was increased to 10 mL by addition of demi water. The mixture was dialyzed against 500 mL demi water for 3 days with 3 medium exchanges. After evaporation of the solvent and

lyophilization, the products were obtained with various yields and conversions.
For the reaction with protected acids or *methyl iodide* instead of free acetates (*tert-butyl iodoacetate*, *tert-butyl bromoacetate*, *metyl iodoacetate*, *metyl bromoacetate*) an adjusted protocol was followed, using the same equivalents. For solubility reasons, acetonitrile was used as a solvent instead of aqueous NaOH solution. Afterwards, the solvent and other volatiles were evaporated *in vacuo* and a deprotection step was performed before purification. To this end, *tert*-butyl-protected CB1 dendrimers were stirred in 50 mmol TFA in 15 mL acetonitrile (3.3M) at room temperature for 3 days, followed by evaporation of solvent, TFA and *tert*-butanol. After dissolving the product in demi water, the pH was adjusted to ~7 using a NaOH solution before purification by dialysis. Deprotection of methyl-protected CB1 dendrimers was achieved by refluxing in a pH 10 NaOH solution for 3 days, the pH was adjusted to ~7 using an HCl solution before purification by dialysis. The dendrimer solutions were dialyzed against 500 mL demi water for 3 days with 3 medium exchanges. After evaporation of the solvent and lyophilization, the products were obtained with various conversions (see Table 2.1).

XPS results alkylation

In this section the XPS N 1S wide scan spectra are shown that were obtained during the optimization study to establish the optimal conditions for the second reaction step, during which the tertiary amine groups become quarternized with concomitant installation of negatively charged group (Scheme 2.1).

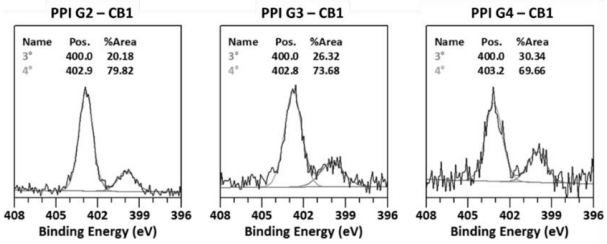

Figure 2.6 Effect of dendrimer generation on the conversion of the second reaction step (3° = tertiary amine, 4° = quaternary amine).

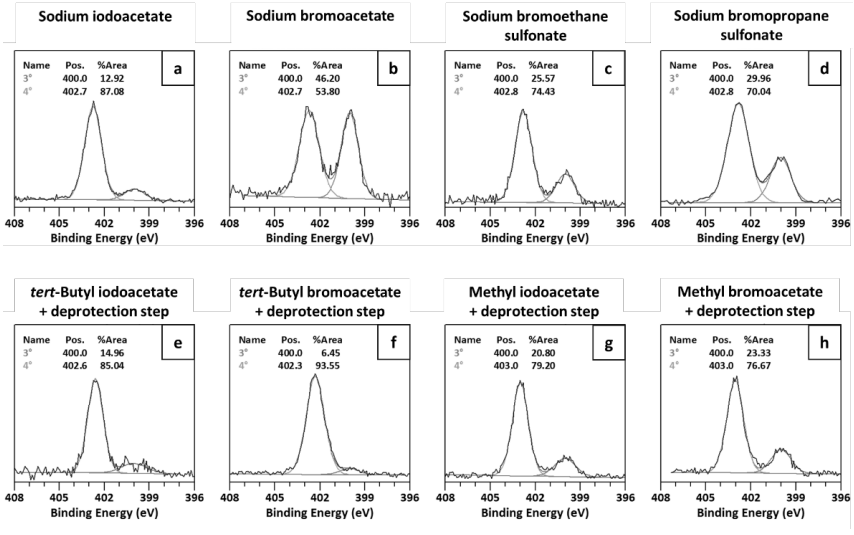

Figure 2.7 XPS results for the optimization study of the second reaction step, which was achieved using either the sodium salt (a-d) or the protected acid (e-h) of the indicated alkyl halides (3° = tertiary amine, 4° = quaternary amine).

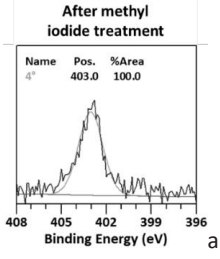

Figure 2.8 XPS results after treatment of an almost 100% quaternary zwitterionic dendrimer with methyl iodide as strong alkylating agent (4° = quaternary amine).

2.6.1.4 Synthesis of ZID 6a

*Synthesis of alkyne-functionalized PPI dendrimer **4a***
50 mg of **1** PPI G3 (0.029 mmol) was dissolved in 5 mL dry acetonitrile by stirring in an argon-flushed 25 mL round bottom flask. Then, 9 µL (0.062 mmol, *n* = 2), 13 µL (0.093 mmol, *n* = 3), or 26 µL (0.186 mmol, *n* = 6) of triethylamine was added and the solution was cooled on ice. A solution of 13.5 mg (0.060 mmol, *n* = 2), 20.3 mg (0.090 mmol, *n* = 3) or 40.5 mg (0.180 mmol, *n* = 6) of alkyne-NHS in 5 mL dry acetonitrile was slowly added to the **1** PPI G3 solution while stirring vigorously to assure well distribution of the functional click handles over the dendrimers. The mixture was allowed to warm up to room temperature and stirring was continued overnight under argon. The solvent and triethylamine were removed by rotavap and oil pump vacuum until a viscous colorless oil was left. 10% of the crude was purified using dialysis as described before for MS analysis purposes. From this fraction, an average yields of ~90% could be calculated. The rest of the crude product was used for the next reaction step without further purification.

*Synthesis of alkyne-functionalized PPI-Me **5a***
The functionalized dendrimer **4a** was methylated as described before for compound **2**, using the same equivalents, conditions and purification by extraction (Note: after extraction there were still some minor impurities present in NMR, which were fully removed after extensive dialysis in the next modification step). This lead to methylated, functionalized dendrimers with typical yields of ~70%.

*Synthesis of alkyne-functionalized PPI-CB1 **6a***
The methylated, functionalized dendrimers were alkylated using sodium iodoacetate as described previously for compound **3**. This yielded alkyne-modified ZID with typical yields of 30% (not taking into account that the conversion in the last step is not quantitative).

***6a** PPI-CB1 characterization*
^{1}H-NMR (400 MHz, D_2O, 300 K) δ 2.29 (H_1; m, 50H), δ 2.56 (H_2; m, 6H), δ 2.95 (H_3; t, 6H), δ 3.28 (H_4; s, 78H), δ 3.33 (H_5; s, 3H), δ 3.39 (H_6; t, 6H), δ 3.70 (H_7; t, 110H), δ 3.95 (H_8; s-overlapping, 54H), δ 4.04 (H_9; t-overlapping, 6H), δ 4.23 (H_{10}; s, 6H) (Figure 2.15), **^{13}C-NMR** see Figure 2.16, **DEPT-HSQC** see Figure 2.16, **IR** see Figure 2.22, **XPS** C1s and N1s narrow scans are provided Figure 2.4, **MS** see Figure 2.23 and Figure 2.24, **GPC** see Table 2.3.

2.6.1.5 Synthesis of ZID 6b

*Synthesis of azide-functionalized PPI dendrimer **4b***
50 mg of **1** PPI G3 (0.029 mmol) was dissolved in 5 mL dry acetonitrile by stirring in an argon-flushed 25 mL round bottom flask. Then, 13 µL (0.093 mmol, *n* = 3) or 26 µL (0.186 mmol, *n* = 6) of triethylamine was added and the solution was cooled on ice. A solution of 50.8 mg (0.090 mmol, *n* = 3) or 101.6 mg (0.180 mmol, *n* = 6) of azide-PEG-NHS in 5 mL dry acetonitrile was slowly added to the **1** PPI G3 solution while stirring vigorously to assure well distribution of the functional handles over the dendrimers. The mixture was allowed to warm up to room temperature, and stirring was continued overnight under argon. The solvent and triethylamine were removed by rotavap and oil pump vacuum until a viscous colorless oil was left. The crude product was used for the next reaction step without further purification.

*Synthesis of azide-functionalized PPI-Me **5b***
The functionalized dendrimer **4b** was methylated as described before for compound **2**, using the same equivalents, conditions and purification by extraction (Note: after extraction there were still some minor impurities present in NMR, which were fully removed after extensive dialysis in the next modification step). This lead to methylated, functionalized dendrimers with an average yield of ~89%.

*Synthesis of azide-functionalized PPI-CB1 **6b***
The methylated, functionalized dendrimers were alkylated using sodium iodoacetate as described previously for compound **3**. This yielded alkyne-modified ZID with an average yield of ~68%.

***6b** PPI-CB1 characterization*
^{1}H-NMR (400 MHz, D_2O, 300 K) δ 2.27 (H_1**;** m, 50H), δ 2.54 (H_2; s, 6H), δ 2.92 (H_3; m, 6H), δ 3.26 (H_4; t, 78H), δ 3.37 (H_5; s, 6H), δ 3.69 (H_6; t, 108H), δ 3.77 + δ 3.84 (H_{7+8}; t-overlapping, 113H), δ 3.93 (H_9; d, 54H) (Figure 2.17), **^{13}C-NMR** see Figure 2.18, **DEPT-HSQC** see Figure 2.18, **IR** see Figure 2.22.

2.6.1.6 Synthesis of ZID 7

*Synthesis of biotin-functionalized PPI dendrimer **7***

A solution of 21.6 mg (0.005 mmol) alkyne functionalized ZID **6a** (*n* = 3) in 1.6 ml milli-Q water was prepared. To this solution. Next, 0.2 ml of a 1 mg/ml solution (0.001 mmol) of copper(II) sulfate pentahydrate in milli-Q water was mixed with 0.2 ml of a 200 mg/ml solution (0.2 mmol) of sodium ascorbate in milli-Q water. This mixture was added to the dendrimer **6a** solution after which 10.8 mg (0.024 mmol) azide-PEG3-biotin was added. The solution was stirred overnight at room temperature. The mixture was dialyzed (MWCO 1000-5000 Da) against 500 mL demi water for 3 days with 3 medium exchanges. After evaporation of the solvent and lyophilization, 20.6 mg of a fluffy light yellow powder was obtained.

***7** PPI-CB1 n = 3 characterization*

^{1}H-NMR see Figure 2.9; **^{13}C-NMR** and **^{13}C-HSQC** see Figure 2.20 and Figure 2.10

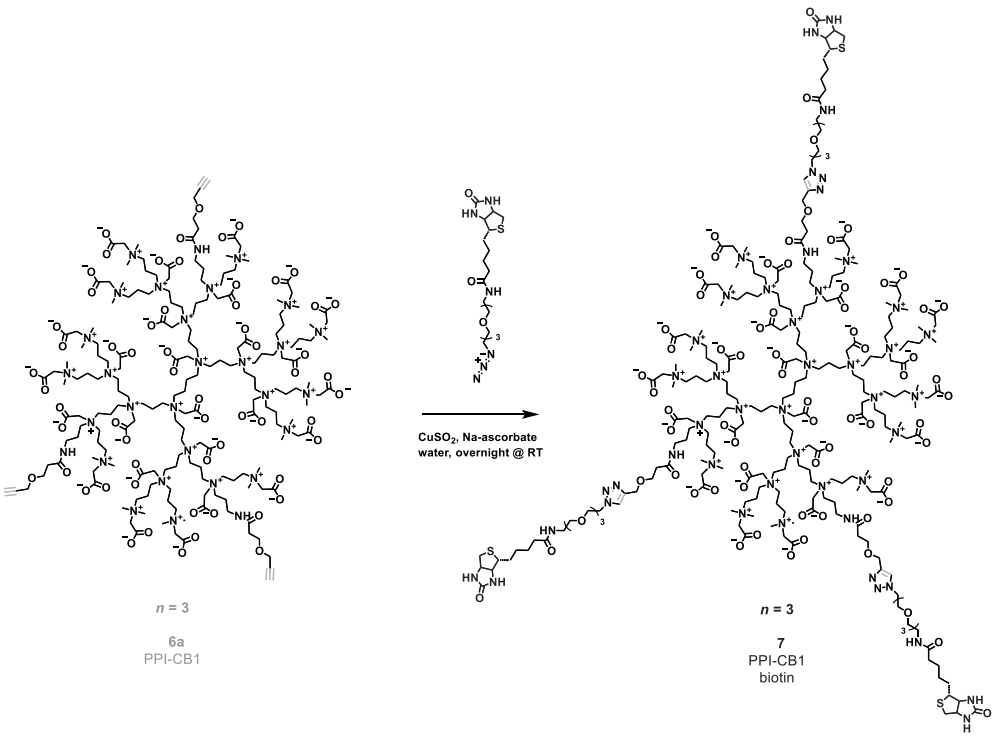

Scheme 2.4 Synthesis of biotin-functionalized zwitterionic PPI-CB1 dendrimers for *n* = 3

2.6.2 NMR data and calculations

*Dendrimer **2** PPI-Me*

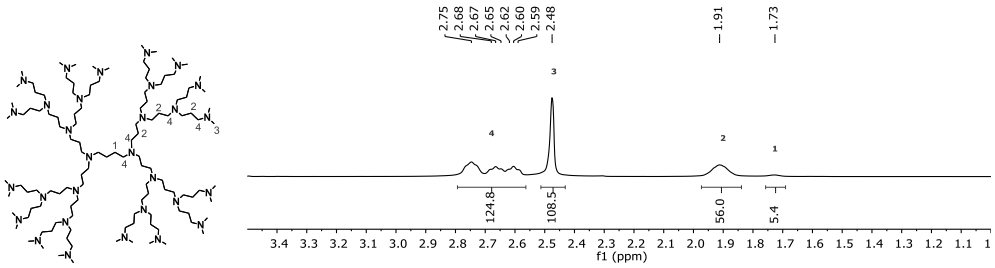

Figure 2.9 ^{1}H-NMR spectrum of **2** PPI-Me in D_2O (400 MHz, 298 K).

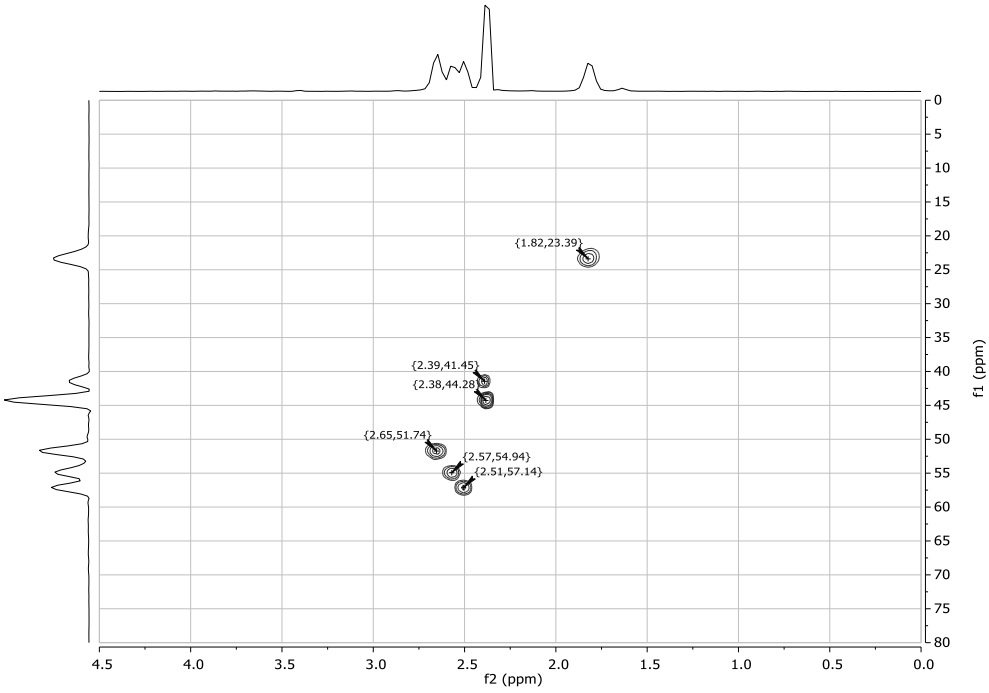

Figure 2.10 HSQC-NMR spectrum of **2** PPI-Me in D_2O (400 MHz, 298 K). The split up of peaks at 2.39,41.45 and 2.38,44.28 is caused by methyl peaks that are coupled to originally secondary amines (due to minor defects in the starting material 1 PPI [1] or rearrangements during the methylation [54]).

*Dendrimer **3** PPI-CB1*

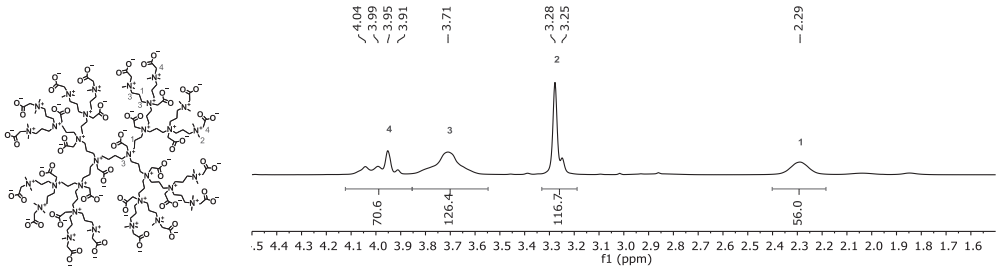

Figure 2.11 ^{1}H-NMR spectrum of **3** PPI-CB1 in D_2O (400 MHz, 298 K). The split up of peaks at 3.25 and 3.28 is caused by methyl peaks that are coupled to originally secondary amines (minor defects in the starting material 1 PPI). Peak H_4 is split up in multiple peaks because of the various shells in the dendrimer.

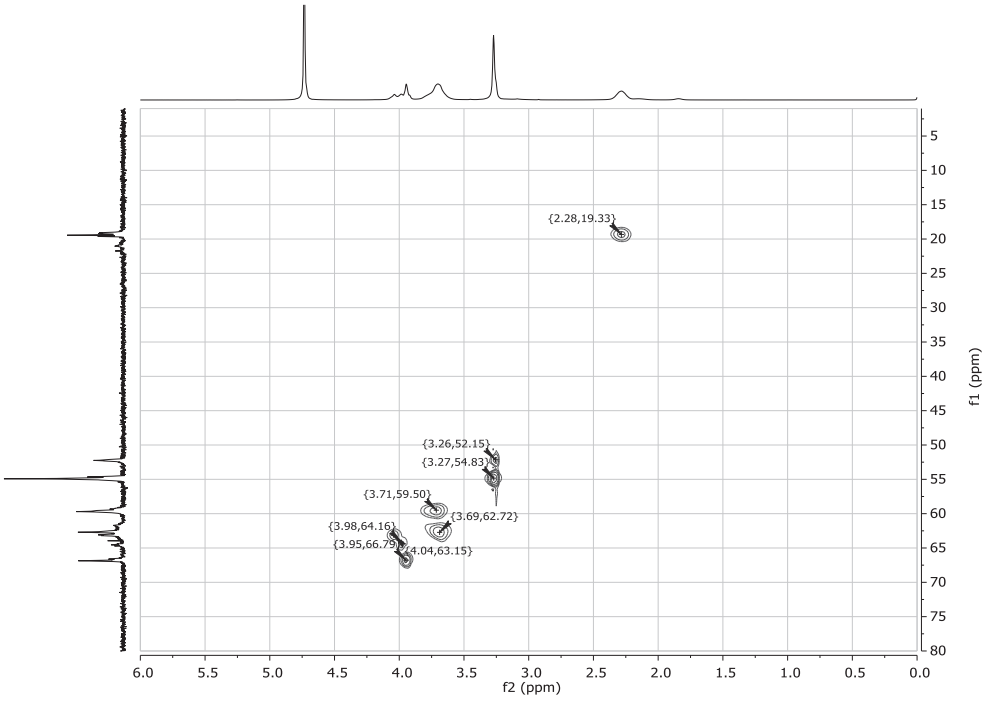

Figure 2.12 HSQC spectrum of **3** PPI-CB1 in D_2O (400 MHz, 298 K).

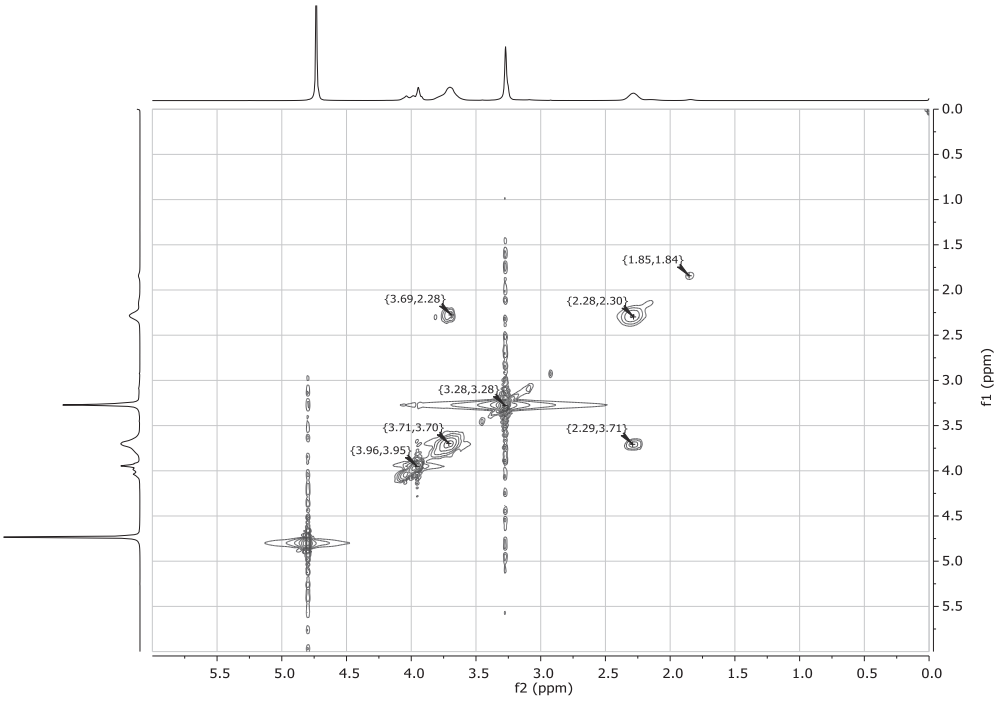

Figure 2.13 COSY spectrum of **3** PPI-CB1 in D_2O (400 MHz, 298 K).

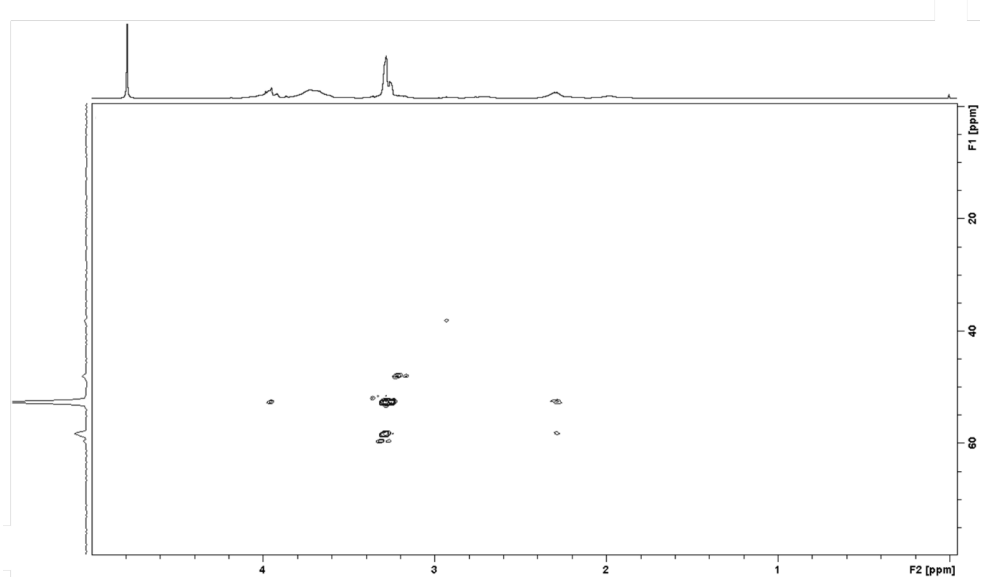

Figure 2.14 $^{1}H–^{15}N$ HMBC spectrum of **3** PPI-CB1 in D_2O (600 MHz, 298 K). On the vertical axis, a projection of the 2D-spectrum is shown.

*Dendrimer **6a** (n = 3) PPI-CB1*

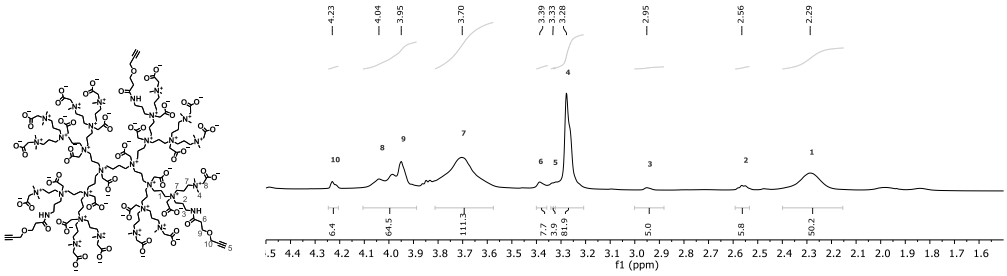

Figure 2.15 ^{1}H-NMR spectrum of **6a** (*n* = 3) PPI-CB1 in D_2O (400 MHz, 298 K). The spectrum was normalized by setting the combined integrals of peaks labelled 1 and 2 to a value of 56. For quantification of *n*, integrals of peak 3 and 10 (both free peaks originating from a CH_2 group present in the alkyne linker) were considered. Based on their average integral value of 5.7 an average value for *n* was calculated to be 2.9.

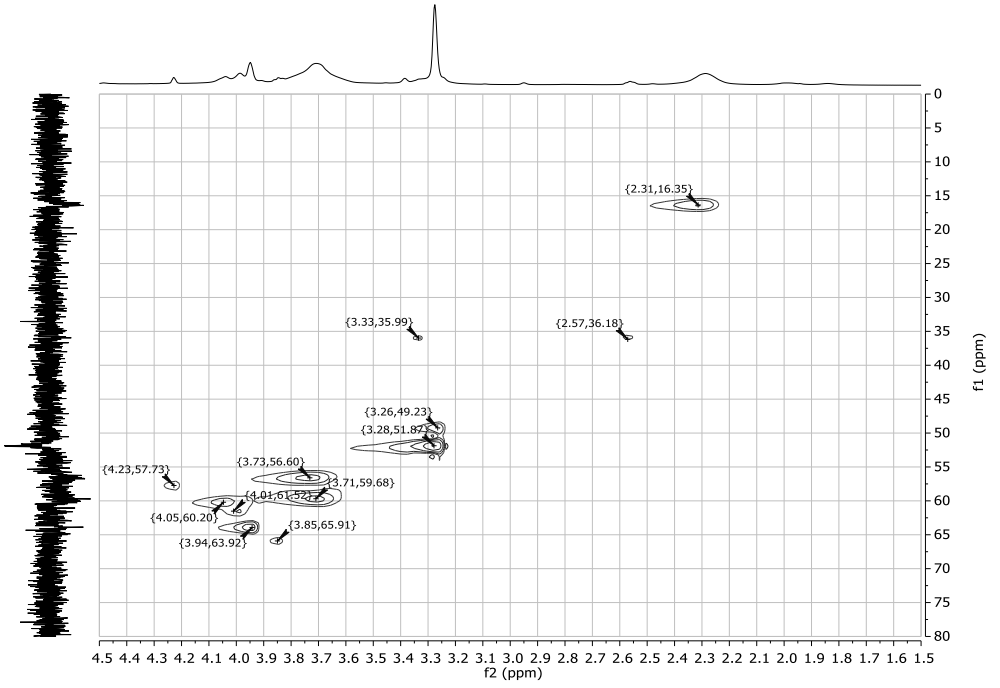

Figure 2.16 DEPT-HSQC spectrum of **6a** (*n* = 3) PPI-CB1 in D_2O (400 MHz, 298 K).

*Dendrimer **6b** (n = 3) PPI-CB1*

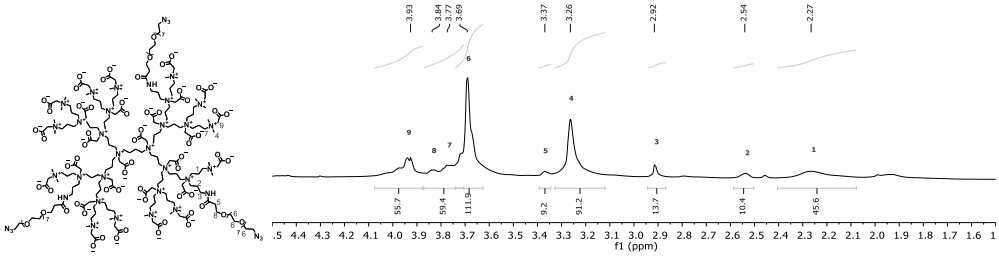

Figure 2.17 ^{1}H-NMR **6b** (*n* = 3) PPI-CB1 (400 MHz, 298 K).

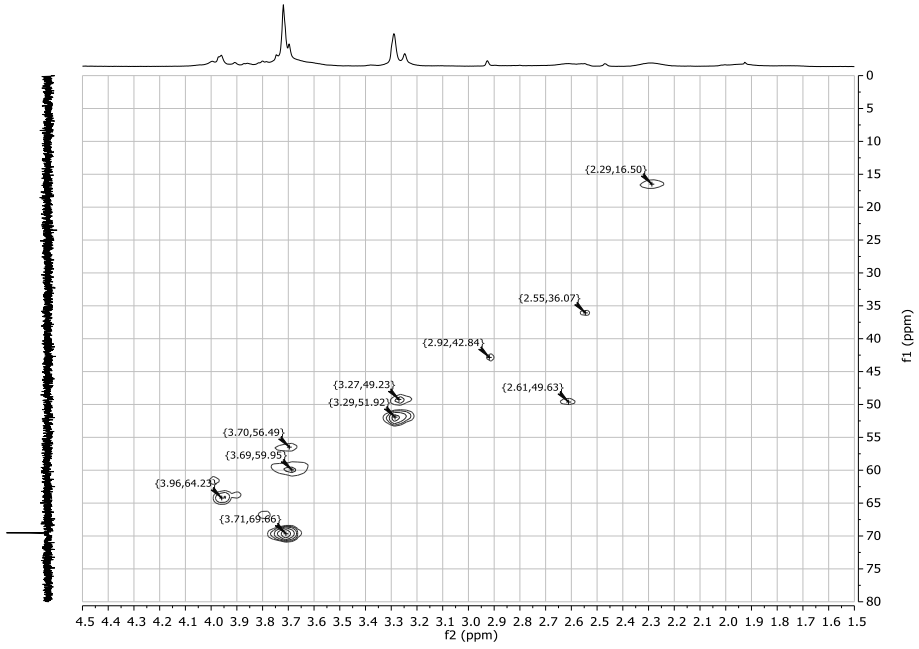

Figure 2.18 DEPT-HSQC spectrum of **6b** (*n* = 3) PPI-CB1 in D_2O (400 MHz, 298 K).

*Dendrimer **7** (n = 3) PPI-CB1 biotin*

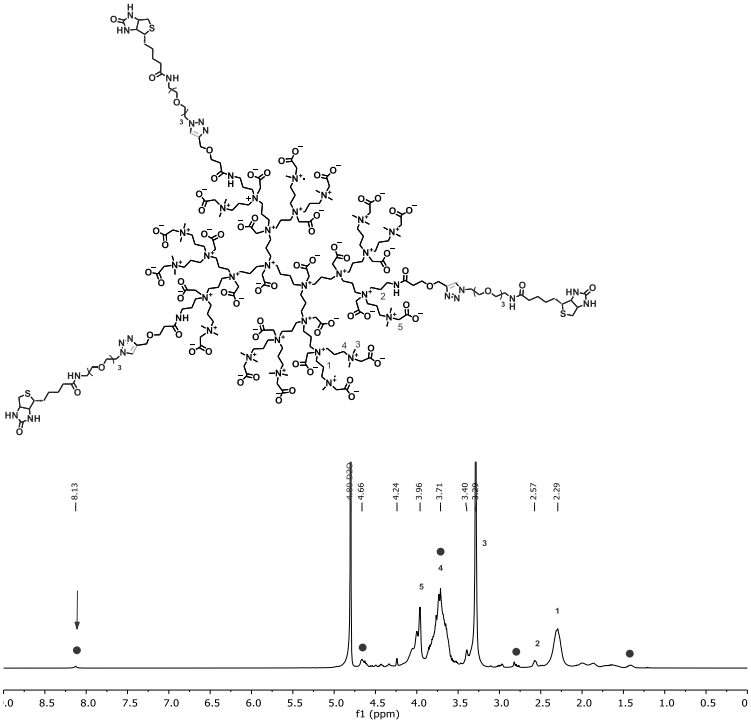

Figure 2.19 ^{1}H NMR spectrum of **7** (*n* = 3) PPI-CB1 biotin in D_2O (400 MHz, 298 K). Most important dendrimer backbone signals are indicated in red and signals coming from the biotin and the PEG linker are indicated in purple. The most indicative peak is assigned with a red arrow; the formed triazole (8.13 ppm).

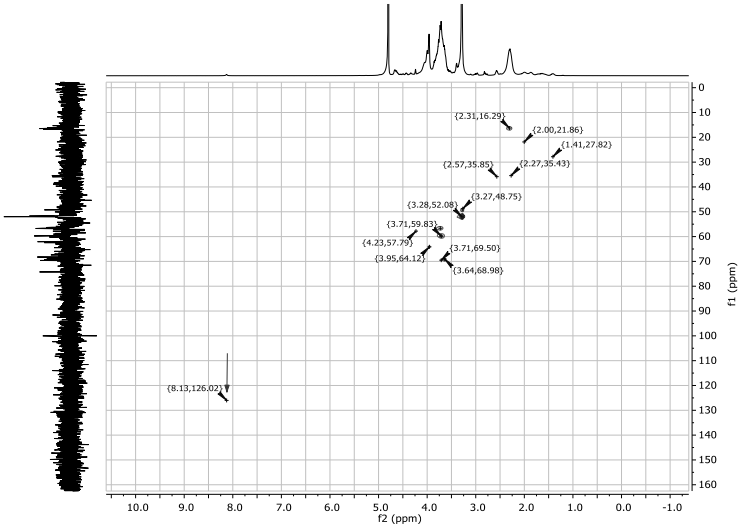

Figure 2.20 ^{13}C-HSQC spectrum of **7** (*n* = 3) PPI-CB1 biotin in D_2O (400 MHz, 298 K). The most indicative peak is assigned with a red arrow which originates from the formed triazole (8.13, 126.02 ppm), confirming the desired click reaction has taken place.

2.6.3 DOSY hydrodynamic radius calculation

Under the assumption that the zwitterionic dendrimers can be regarded as spherical objects, the hydrodynamic radius, r_H, of this sphere can be calculated from the measured diffusion coefficient, D, using the Stokes-Einstein equation: [55,56,57]

$$\boldsymbol{D = \frac{k_B \cdot T}{6\pi \cdot \eta \cdot r_H}} \qquad \text{(eq. 2.1)}$$

where D is the diffusion coefficient, k_B the Boltzmann constant, T the absolute temperature, η the solvent viscosity, and r_H the hydrodynamic radius of the molecule.

Table 2.2 lists the calculated hydrodynamic radius for zwitterionic dendrimers **3**, **6a** and **6b**, determined from the diffusion coefficient as obtained in the DOSY measurement (shown in Figure 2.5).

Table 2.2 Calculated hydrodynamic diameter based on average diffusion coefficients D (m^2/s) measured for ZID **3**, **6a** (n = 3) and **6b** (n = 3) in D_2O at 300 K.

ZID	Average D_{ZID} (m^2/s)	Hydrodynamic diameter (nm)
3	1.67×10^{-10}	3.2
6a (n = 3)	1.27×10^{-10}	4.1
6b (n = 3)	1.03×10^{-10}	5.1

2.6.6 Gel Permeation Chromatography data

Table 2.3 GPC data for ZID **3**, **6a** (n = 2) and **6a** (n = 3) in milli-Q water (containing 0.05% NaN_3).

ZID	Theoretical MW at full conversion (g/mol)	MW by GPC (g/mol)	PDI
3	3877	4133	1.102
6a (n = 2)	3925	3591	1.193
6a (n = 3)	3949	3692	1.138

2.6.4 IR spectroscopy data

*Dendrimer **1** PPI, **2** PPI-Me, **3** PPI–CB1*

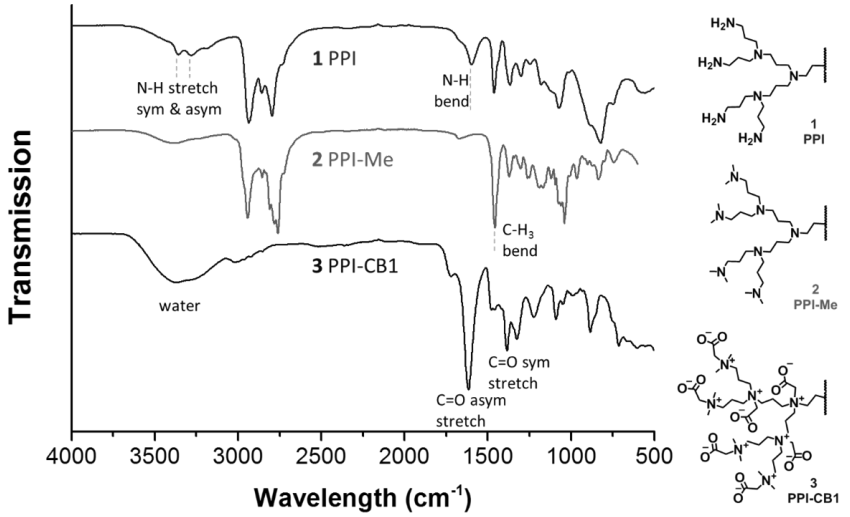

Figure 2.21 IR spectra of **1**, **2** and **3**. For clarity, on the *y*-axis the spectra are shown with an offset with respect to each other.

*Dendrimer **6a** (n = 6) PPI-CB1, **6b** (n = 6) PPI-CB1*

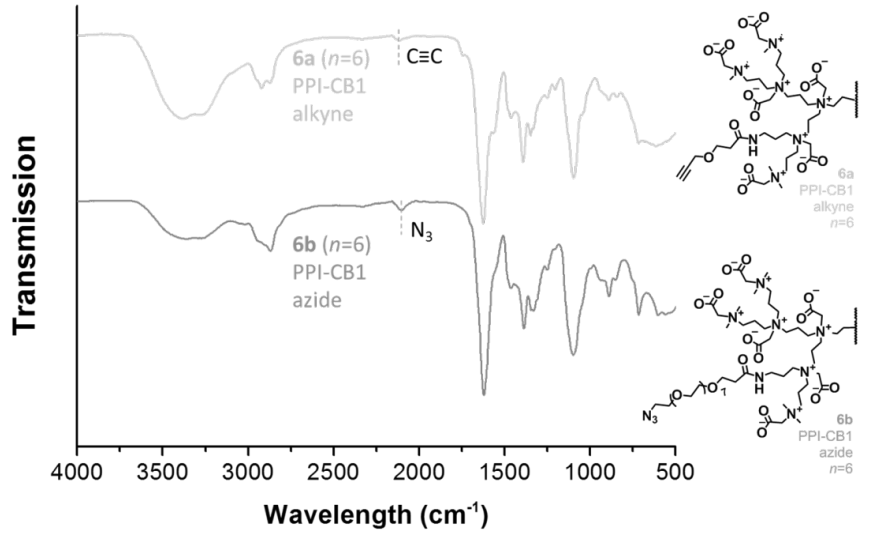

Figure 2.22 IR spectra of **6a** and **6b**. For clarity, on the *y*-axis the spectra are shown with an offset with respect to each other.

2.6.5 Mass Spectrometry data

*Dendrimer **6a** (n = 2) PPI-CB1*

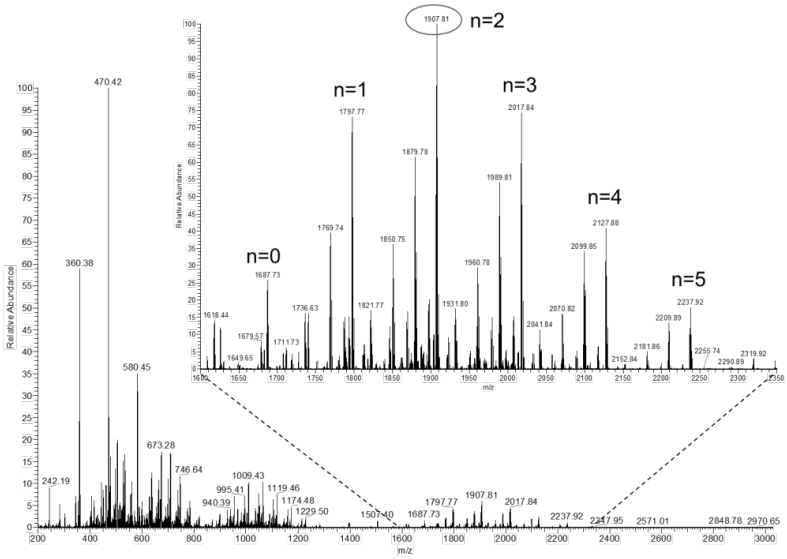

Figure 2.23 MS spectra of intermediate **4a** (*n* = 2) Proposed molecular weight for **4a** (*n* = 2) at full conversion is 1907.07. From the MS data, it can be concluded that the main species of functionalized dendrimer that can be observed in MS is indeed the *n* = 2 species, but that also species with *n* ranging from 0 to 5 can be seen.

*Dendrimer **6a** (n = 3) PPI-CB1*

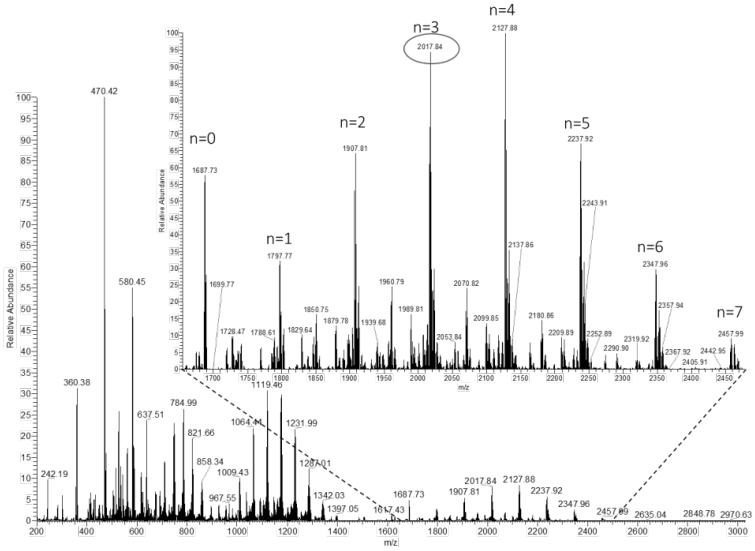

Figure 2.24 MS spectra of intermediate **4a** (*n* = 3). Proposed molecular weight for **4a** (*n* = 3) at full conversion is 2017.18. From the MS data, it can be concluded that the main species of functionalized dendrimer that can be observed in MS is indeed the *n* = 3 and 4 species, but that also species with *n* ranging from 0 to 7 can be seen.

Chapter 3

Surface Immobilization Strategies for Zwitterionic Dendrimers

Abstract

While zwitterionic dendrimers (ZID) are interesting building blocks for antifouling coatings, they need to be immobilized on a surface in order to be able to use them as such. In this chapter, we evaluated four different strategies to enable covalent immobilization of the ZID on a surface to create a stable and potentially durable coating. The first explored method was amide bond-mediated binding of the ZID's carboxylates to amine-terminated surfaces. Next to this, two types of click-reactions, copper-catalyzed azide-alkyne cycloadditions (CuAAC) and thiol-yne chemistry, between pre-installed functional groups on the ZIDs and the surfaces were tested. Finally, mono- and multilayer coatings were formed by free radical polymerization of methacrylate functionalized ZIDs on pre-modified surfaces. Antifouling properties of the most promising coatings were preliminarily tested using fluorescently labelled proteins and fluorescence microscopy.

3.1 Introduction

In the previous chapter, mainly the synthesis and characterization of zwitterionic dendrimers (ZID) was described. Additionally, their use in biomedical or drug delivery applications was discussed briefly.[1–8] However, these zwitterionic dendrimers also enable an entirely new application, namely as a coating to reduce unwanted surface interactions. Previously, zwitterionic polymers have been shown to be able to drastically reduce (bio)fouling of surfaces when applied as a coating.[9,10]

Our developed ZIDs are charge neutral, whilst containing a large number of zwitterionic groups that are densely packed, which are desired properties for building blocks for antifouling coatings.[11] Furthermore, their branched nature with carboxylate end groups allows for multivalent, preferably covalent, surface anchoring or even crosslinking. One can think of several ways to immobilize these ZIDs on a surface to form a coating. In the field of biosensors, several strategies to immobilize biomacromolecules on sensor surfaces have been developed to monitor bio-interaction events. The adsorption of macromolecules such as proteins to surfaces can be a spontaneous process, depending on the intrinsic features of the protein such as charged or hydrophobic domains.[12] However, because of the inherent charge neutrality of the ZIDs – and therefore little tendency to assemble onto a surface based on charge – we chose to explore strategies that would lead to covalent bonds.

The presence of the carboxylates on the outside of the ZIDs allows for coupling via amide bond formation, as this is a widely used for the bioconjugation of carboxybetaine-based zwitterionic polymers,[13–16] and surface immobilization of, for instance, enzymes.[17] Inspired by site-specific and oriented immobilization of antibodies, ZIDs can also be immobilized by introducing functional groups with an inherent affinity for a functional group on a surface.[18] All these mentioned strategies will eventually lead to the formation of a ZID monolayer. However, from literature it is known that thicker layers lead to better antifouling coatings; zwitterionic polymer brush layers outperform their monolayer analogues in terms of antifouling properties.[19–22] In previous studies, multilayer coatings have often been prepared by adsorbing complementary functional groups onto a substrate, a process called layer-by-layer (LbL) assembly.[23] Stacked polyelectrolyte multilayers of *N*-alkylated polyethylenimine and poly(acrylic acid) have been shown to lower the amount of protein adsorption in a mechanistically study.[24] Alternating layers of polyanion and polycation polymers showed, for instance, a reduction of bio-fouling in catheter tubing.[25] Hence, it is of interest to also explore methods that can potentially lead to multilayers of ZIDs. Since our ZIDs are charge neutral, despite being polyelectrolytes, charge-driven self-assembled multilayers will unfortunately not form. Therefore, we aimed to covalently cross-react them on a surface by the use of a polymerizable group that is pre-installed on the ZIDs.[26–30]

In this chapter, we subsequently tested the following strategies to enable covalent immobilization of the ZID on a surface in order to create a stable and durable coating:

- *Amide bond-mediated binding of ZID onto amine-terminated surfaces.* The presence of the carboxylic acid groups on the ZIDs allows for coupling via amide bond formation onto amine-terminated surfaces, as this also is a widely used for the bioconjugation of carboxybetaine-based zwitterionic polymers.[13–16]
- *Cu-catalyzed azide/alkyne cycloaddition (CuAAC) click chemistry.* The previously developed ZIDs with multiple azide or alkyne groups[31] allow for click chemistry by reacting them with surfaces that have the appropriate CuAAC counterpart, namely an alkyne or azide moiety, on the surface.[32]
- *Thiol-yne click chemistry.* Similarly to the CuAAC strategy described above, alkyne-functionalized ZIDs allow for another type of (metal-free) click chemistry by reacting them with a thiol-terminated surface in the presence of a radical source.[33]
- *Free radical polymerization.* Post-synthesis, the alkyne-functionalized ZIDs were further functionalized by reacting the alkynes with an azide-methacrylate to obtain methacrylate-functionalized ZID. These ZIDs consequently allow for free radical polymerization reactions in the presence of a radical source. When a functional group on the surface is incorporated in this polymerization process, a coating can be formed.[26]

After coupling the abovementioned ZIDs to surfaces modified with the antagonistic handle, potentially antifouling coatings were formed. These coatings were investigated using water contact angle (WCA) measurements, IR spectroscopy and X-ray photoelectron spectroscopy (XPS). Antifouling properties were preliminarily tested by monitoring the attachment of fluorescently labelled proteins using fluorescence microscopy.

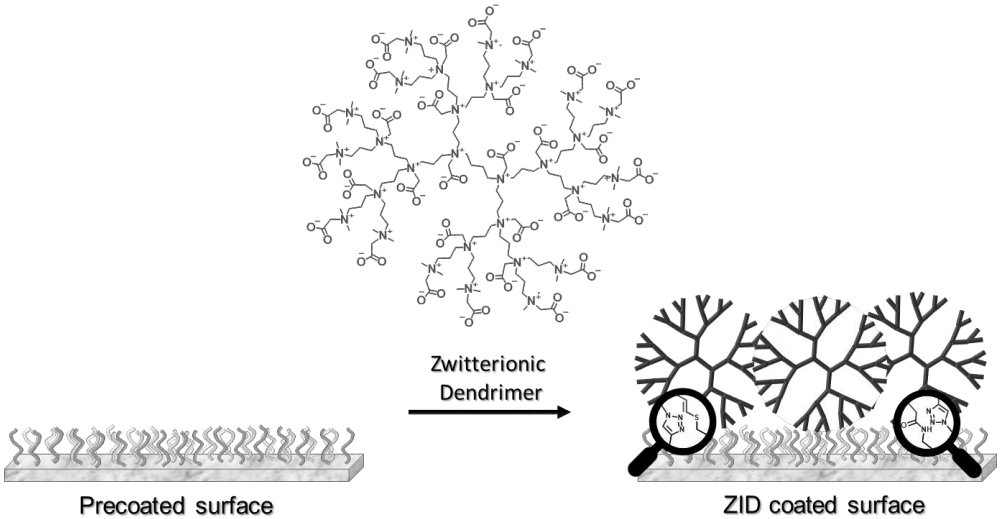

Figure 3.1 Schematic representation of the immobilization of ZID on a surface showing the possible covalent bonds enlarged.

3.2 Results and Discussion

We will first discuss the results of the formation of monolayers of ZID onto surfaces that were pre-coated with an anchoring layer in order to have the desired chemical groups for covalent binding present at the surface, as obtained via different routes. After that, the results of the approach to polymerize methacrylate-functionalized ZIDs onto pre-coated surfaces will be discussed.

3.2.1 Amide bond-mediated binding of ZID onto amine-terminated surfaces

In order to couple the ZID to a surface to form a coating, a straightforward route was to use the carboxylate groups on the ZIDs for coupling via amide bond formation[13–16] with the primary amines on an aminopropyl dimethyl ethoxysilane (APDMES) modified silicon oxide surface.[34]

To this aim, first an APDMES layer was formed on silicon oxide by the reaction of the ethoxy groups with the hydroxyl-terminated silica surface. The resulting amine-terminated surface was characterized by X-ray photoelectron spectroscopy (XPS) to study the chemical composition. Next to the expected silicon (at 103 eV) and oxygen signals (at 532 eV) coming from the glass substrate, we found additional signals corresponding to the presence of nitrogen (at 400 eV) and carbon (285 eV) that originate from the APDMES monolayer on the surface (Figure 3.3). Furthermore, the N_{1s} narrow scan showed only one peak, indicating the presence of only one type of nitrogen, namely the primary amine. The Si/C ratio in the XPS wide scan was used to calculate the average thickness of the layer,[35,36] which was found to be 0.6 nm. The static water contact angle (SWCA) was determined to be 52°. Both the layer thickness and SWCA are in good agreement with findings in literature.[34]

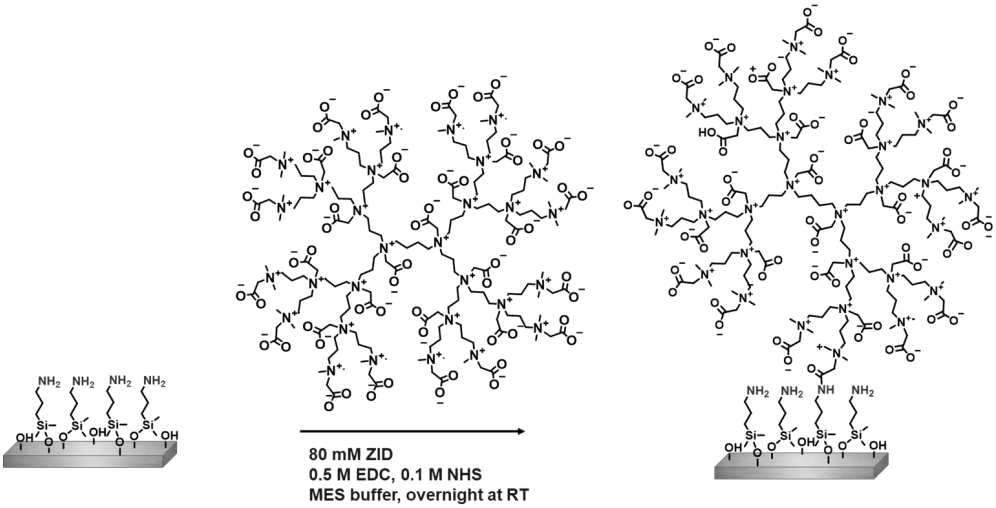

Figure 3.2 The immobilization of ZIDs onto APDMES-modified silicon oxide by NHS/EDC-mediated amide bond formation.

Upon formation of an APDMES monolayer, the ZIDs were immobilized by using *N*-hydroxysuccinimide (NHS) activation with *N*-(3-dimethylaminopropyl)-*N*'-ethylcarbodiimide hydrochloride (EDC) as a carboxyl-activating agent in a MES buffer (Figure 3.2). The APDMES-modified silicon oxide surfaces

were incubated in the reaction mixture overnight at room temperature, followed by washing and sonication with Milli-Q water. XPS analysis of the coatings was performed (Figure 3.3) and the obtained coatings showed increased signals for N (N_{1s} at 399 eV) and C (C_{1s} at 285 eV) on the wide scans on the silicon oxide surfaces, which is in agreement with the presence of the ZID on the surface. In the C_{1s} narrow scan, the C–hetero atom signals at 286.4 (C–O and C–N) and 288.2 eV (C=O) increased. More interestingly, the N_{1s} narrow scans showed an additional peak at 402.5 eV compared to the APDMES coating, which can be attributed to the dendrimer's quaternary N^+ atom. The layer thickness of the ZID coating was calculated using the Si/C ratio in the XPS widescan[35,36] and found to be 2.3 nm. This relatively low layer thickness increase of 1.7 nm can be understood by considering that the hydrodynamic diameter of the immobilized ZID was estimated to be approximately 3.2 nm,[31] whilst the XPS spectra were acquired under ultra-high vacuum conditions, which induce a collapse of the ZID layer. Unfortunately, the SWCA had not decreased as could be expected for a zwitterionic coating covering the entire surface. The obtained value after the immobilization of the ZID was still 50°, which decreased thus only marginally compared to the APDMES coating. Despite efforts to improve the reaction by varying, *e.g.*, reactant concentration, buffer and salt concentration, we concluded that the conversion of the immobilization reaction was not as high as expected. We hypothesized that the applied chemistry was not efficient enough to immobilize these macromolecular ZID on the static surfaces. To improve upon this initial immobilization strategy, we decided to explore the advantages of faster and more efficient "click" chemistry, which refers to covalent reactions with high reaction yields that can be performed under mild conditions.[32]

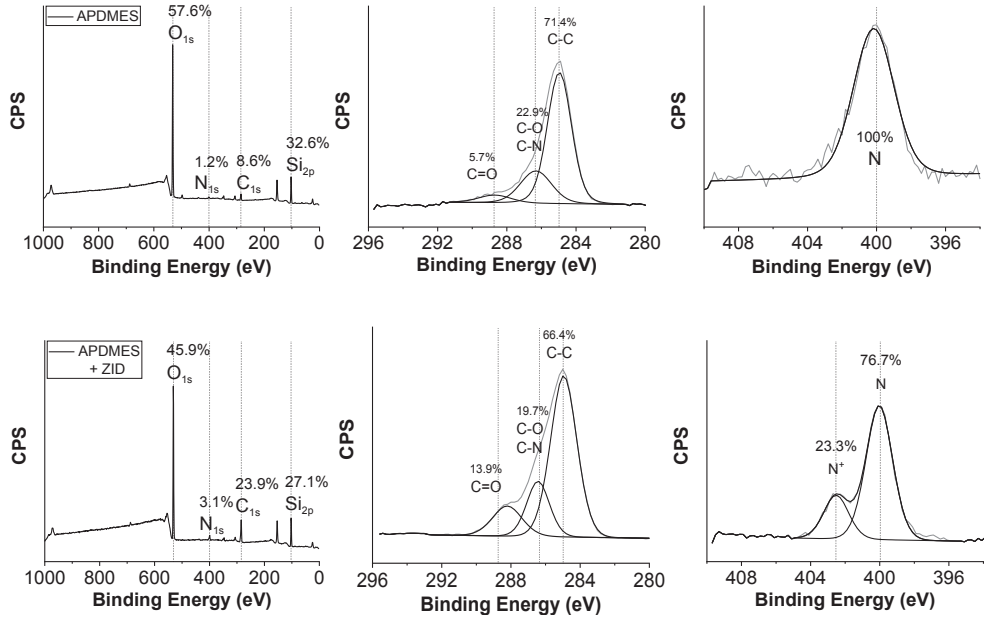

Figure 3.3 XPS wide scan (left), C_{1s} narrow (middle) and N_{1s} narrow (right) spectra of APDMES (top) and ZID (bottom) on silicon oxide.

3.2.2 Copper-catalyzed azide/alkyne cycloaddition (CuAAC) click chemistry

One of the most well-documented click reactions is the Cu^{I}-catalyzed variant of the Huisgen 1,3-dipolar azide-alkyne cycloaddition (CuAAC) to form 1,2,3-triazoles.[37] This CuAAC reaction previously showed to be an ideal candidate for surface modification[38] and polymer immobilization.[39] The previously developed ZIDs, reported in Chapter 2 of this Thesis, with multiple azide- or alkyne-groups[31] allow for click chemistry by reacting them with surfaces that have the CuAAC reactions' counterpart on the surface, namely an alkyne or azide group, respectively.[32] Since infrared (IR) spectroscopy is a very valuable tool to study both azides and alkynes, we used an IR-transparent substrate to monitor this approach of covalent surface binding of ZIDs, namely porous alumina oxide (PAO).[40] First, a phosphonic acid layer was formed on the PAO, having the ZID's CuAAC counter reactive group: an azide or an alkyne.[41] Previous studies by our group showed that it is worthwhile to dilute the functional groups to allow them to "stick out" from the surface in order to minimize surface-induced sterics.[42] To that end, we diluted the functionalized phosphonic acids with aliphatic octylphosphonic acids to obtain 25% functionality on the surface. Since both alkyne- and azide-functionalized ZIDs were developed, two strategies were investigated: (1) Alkyne-modified ZIDs on azide-modified surfaces and the opposite scenario (2) Azide-modified ZIDs on alkyne-modified surfaces. All resulting surfaces were characterized by X-ray photoelectron spectroscopy (XPS) and IR spectroscopy to study the chemical composition.

1. Alkyne-modified ZIDs on an azide-modified surface

In order to have the desired azide functionality on the surface, the PAO was modified with octylphosphonic acid and 12-azidododecylphosphonic acid (azido-PA) (resulting in 25% azide functionality on the surface) to function as an anchoring layer to bind via the CuAAC click reaction alkyne-functionalized ZIDs that were functionalized with on average three alkyne groups per ZID (**ZID-alkyne**).

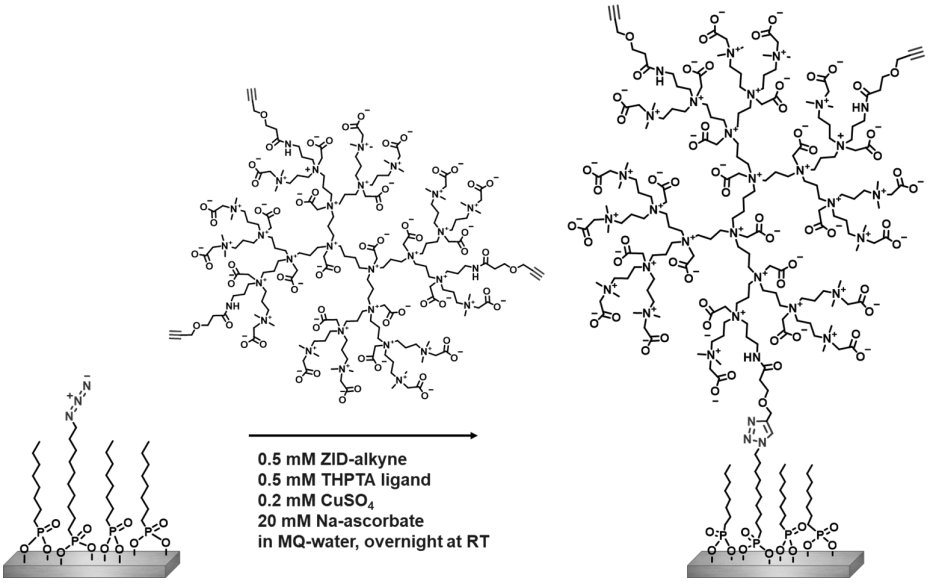

Figure 3.4 The immobilization of **ZID-alkyne** onto azide-modified PAO by Cu^{I}-catalyzed CuAAC reaction.

The XPS results of forming an azido-phosphonic acid layer on PAO are shown in Figure 3.5. After formation of the azido-PA layer we found signals corresponding to 35.8% carbon (285 eV), 2.9% nitrogen (at 401 eV) and 3.5% phosphor (at 192 eV) that originate from the octylphosponic acid-diluted coating, in line with the expected theoretical C/N/P ratio of 36 : 3 : 4. Furthermore, the expected aluminum (at 119 eV) and oxygen signals (at 531 eV) coming from the PAO substrate were present. Unfortunately, no XPS-based layer thickness calculations could be performed due to the porous nature of the substrate. The N_{1s} narrow scan also showed the expected 1:2 ratio of the electron configuration of the azide group.[38] The presence of the azide was also confirmed by IR spectroscopy (Figure 3.22 in the Supporting Information) by showing a clear peak at 2100 cm^{-1}.

The static water contact angle (SWCA) was determined to be 137°, which is in good agreement with previously reported SWCA of 140° for aliphatic coated PAO in literature.[43] (Please note that the PAO's surface roughness enhances the hydrophobic character of the coating, which is originally induced by the surface chemistry[44]).

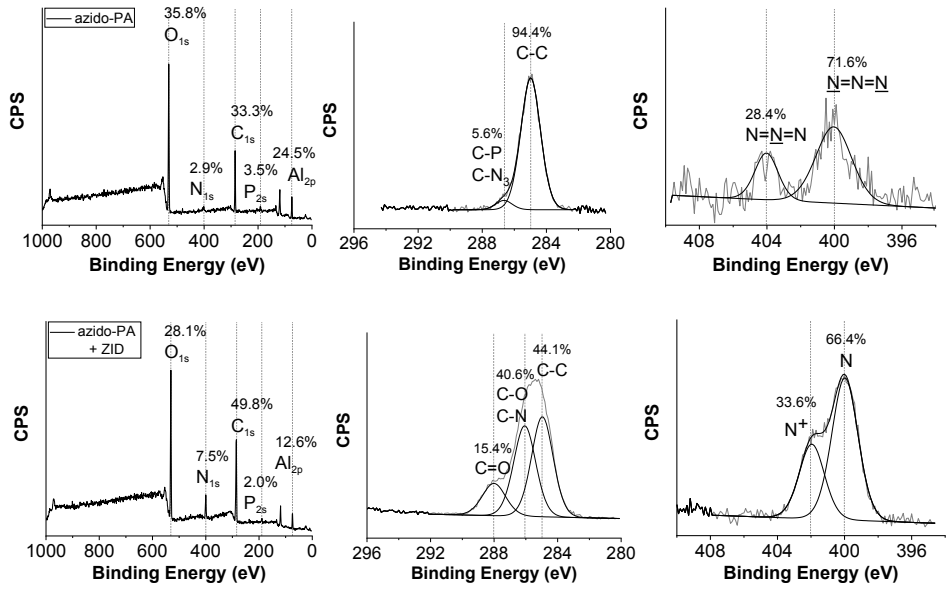

Figure 3.5 XPS wide scan (left), C_{1s} (middle) and N_{1s} narrow (right) spectra of azido-phosphonic acid (top) and **ZID-alkyne** (bottom) on PAO.

In the previous chapter, the synthesis of alkyne-functionalized ZIDs by installing an alkyne group on the native dendrimers prior to zwitterionic modification, was reported.[31] The **ZID-alkyne** was immobilized on the azide-functionalized monolayer by using the CuAAC reaction in water with sodium ascorbate as reducing agent (Figure 3.4). The azide-terminated PAO surfaces were incubated in the reaction mixture overnight at room temperature, followed by washing and sonication with Milli-Q water and ethanol, followed by a drying step under vacuum. XPS analysis of the coatings showed increased signals for N (N_{1s} at 400 eV) and C (C_{1s} at 285 eV) on the PAO surfaces (Figure 3.5), which is

in agreement with the chemical composition of the **ZID-alkyne**. Furthermore, the N_{1s} narrow scans showed an additional peak at 402 eV, which was attributed to the dendrimer's quaternary N^+ atom (Figure 3.5). Remarkably, the SWCA dramatically decreased to <20° because of the added hydrophilicity of the ZID's carboxylates. Please note that this increased hydrophilicity is not only the result of the immobilized ZID, but also of PAO's intrinsic surface roughness.[44] Unfortunately, the hydrophilicity of thus modified PAO automatically led to the adsorption of water from the atmosphere – despite flushing the setup with nitrogen – giving rise to dominant interfering water signals in the IR measurements. Overall, this attachment strategy seemed promising as concluded form the data by the XPS and the WCA results.

2. Azide-modified ZIDs on an alkyne-modified surface

Analogously to the previously discussed "alkyne-modified ZIDs on an azide-modified surface" approach, the opposite strategy was also tested. To that aim, the PAO was modified with octylphosphonic acid and 10-undecylphosphonic acid (alkyne-PA) (resulting in 25% alkyne functionality on the surface) to function as an anchoring layer to bind azide-functionalized ZIDs functionalized with on average three azide groups (**ZID-azide**) via the CuAAC click reaction.

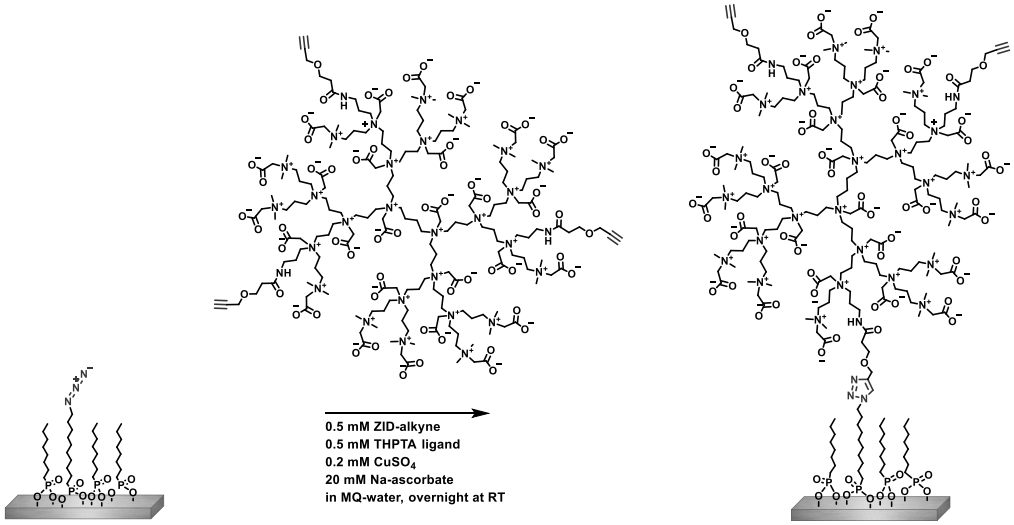

Figure 3.6 The immobilization of **ZID-azide** onto alkyne-modified PAO by Cu^I-catalyzed CuAAC reaction.

The XPS results of the alkyne-terminated phosphonic acid layer and that formed after CuAAC coupling of **ZID-azide** are shown in Figure 3.7. After formation of the alkyne-PA layer, the expected signals corresponding to carbon (285 eV) and phosphor (at 192 eV) C/P in a ratio of 33.5 : 6 that originate from the octylphosponic acid diluted coating are in line with the expected ratio of 35:4. Furthermore, the expected aluminum (at 119 eV) and oxygen signals (at 531 eV) coming from the PAO substrate were present. Also here, no XPS-based layer thickness calculations could be performed due to the porous nature of the substrate. The presence of the alkyne was confirmed by IR spectroscopy (Figure 3.23 in the Supporting Information) by showing the C≡C–H stretch signal at 3325 cm^{-1}. Since it is difficult to quantify these IR signals, due to the surface roughness and concomitant variation in attachment

angles, and since XPS gave no direct evidence of the presence of the alkyne group, it was not possible to quantify the amount of alkyne on the surface.

The static water contact angle (SWCA) was determined to be >160°, which means the surface has superhydrophobic properties because of the aliphatic coating combined with the PAO's surface roughness.[44]

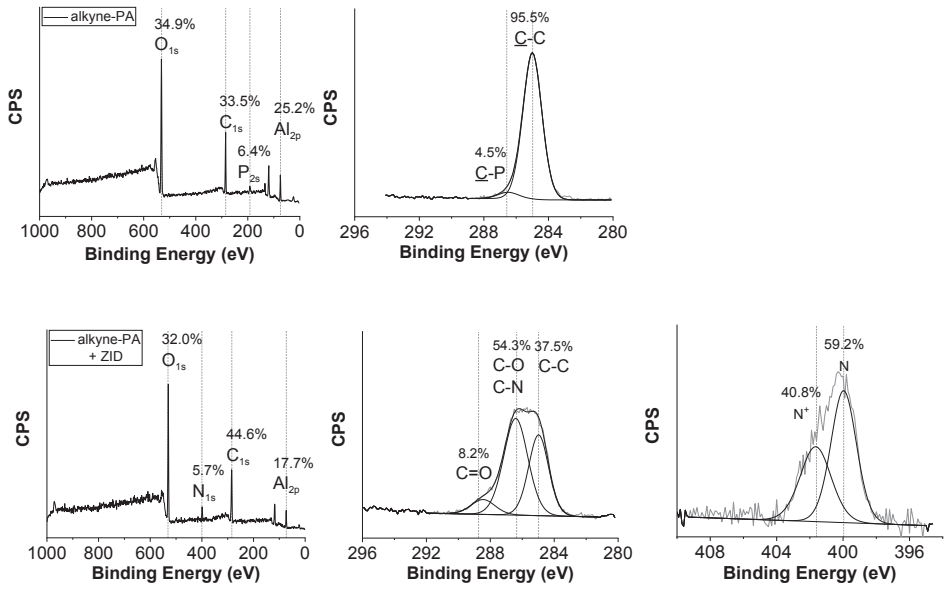

Figure 3.7 XPS wide scan (left), C_{1s} (middle) and N_{1s} narrow (right) spectra of alkyne-phosphonic acid (top) and **ZID-azide** (bottom) on PAO.

In Chapter 2, the synthesis of azide-functionalized ZIDs (**ZID-azide**), by installing an azide group on the native dendrimers prior to zwitterionic modification, was described.[31] Upon formation of the alkyne-functional monolayer, the **ZID-azide** was immobilized by using the same CuAAC reaction as described in the previous section. XPS analysis of the coatings showed the appearance of the N signal (N_{1s} at 399 eV) and an increase in C (C_{1s} at 285 eV) on the PAO surfaces. Furthermore, the C_{1s} narrow scan showed additional peaks at 286.4 and 288.4 eV and the recognizable peaks in the N_{1s} narrow scan from the dendrimer's amine species. The SWCA decreased to 90° because of the added hydrophilicity of the ZID's carboxylate moieties.

Based on the SWCA of the resulting ZID-modified surfaces, the conversion of "(1) azide-modified ZIDs on an alkyne-modified surface" appears lower than the opposite "(2) alkyne-modified ZID on an azide-modified surface" approach. Likely, the hydrophobic nature of the alkyne-modified PAO (WCA > 160°) hampered wetting by the aqueous ZID solution and thereby decreased the conversion. To explore the versatility and scope of click chemistry to immobilize these ZID, also another type of click chemistry was explored. We chose to apply the thiol-yne click reaction, which was previously applied for surface chemistry purposes in our group.[45]

3.2.3 Thiol-yne click chemistry

Similar to the CuAAC strategy described above, the **ZID-alkyne** allow for another type of click chemistry. That is, thiol-yne click chemistry is possible by reacting the terminal alkyne group with a thiol-terminated surface in the presence of a radical source.[33,45–47] In order to have the desired thiol functionality on the surface, flat aluminum oxide (AO) was modified with 25% 12-mercaptododecyl-phosphonic acid and 75% (2-{2-[2-hydroxy-ethoxy]-ethoxy}-ethyl)phosphonic acid (thiol-PA; Figure 3.8).[42]

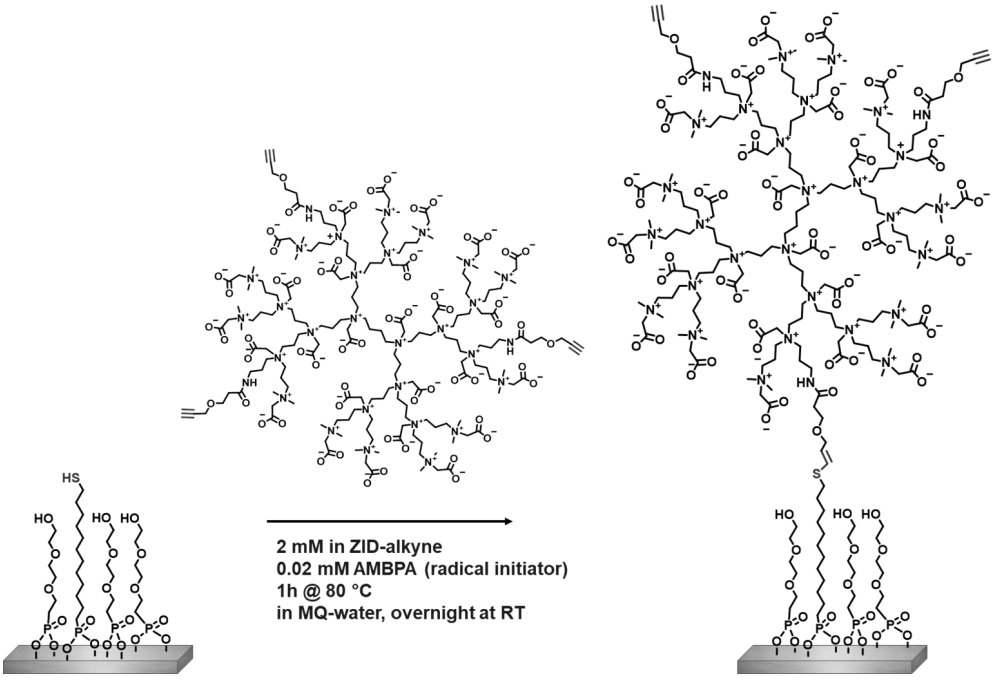

Figure 3.8 The immobilization of **ZID-alkyne** on thiol-modified aluminum oxide by the use of thiol-yne click chemistry.

The XPS results of the resulting surface are shown in Figure 3.9. After formation of the thiol-PA layer we found the expected signals for aluminum (at 119 eV) and oxygen (at 531 eV) coming from the AO substrate, next to the signals that originate from the phosphonic acid coating: carbon (285 eV), sulphur (at 228 eV) and phosphor (at 191 eV). Surprisingly, the found S/P ratio (3.2 : 4.5) did not correspond to the 25% dilution in the reaction mixture, but it suggested a dilution of approximately 70%. This suggested that the thiol-phosphonic acid was more reactive compared to the hydroxy-EG_3 dilutant. The Al/C ratio in the XPS wide scan was used to calculate the average thickness of the layer,[35,36] which was found to be 2.2 nm.

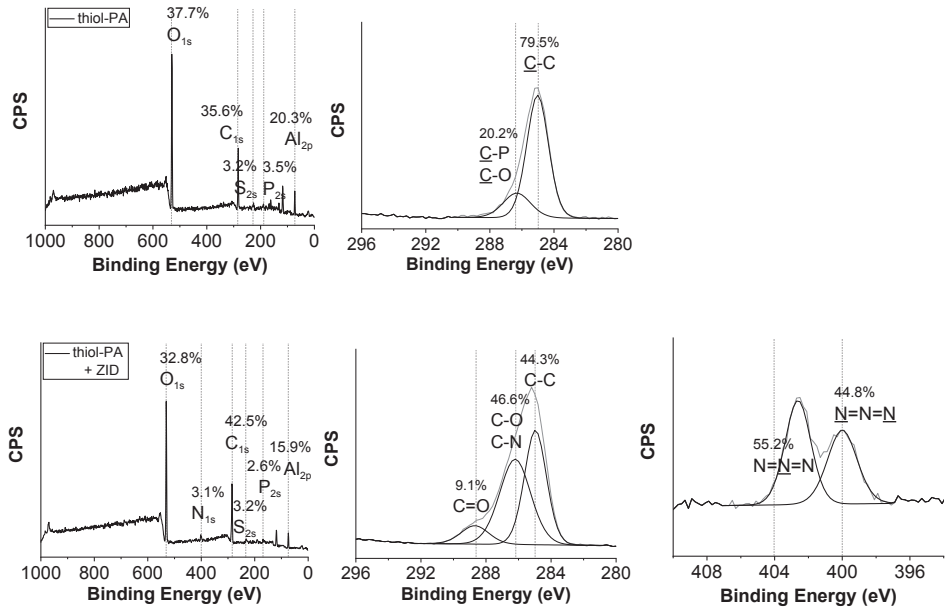

Figure 3.9 XPS wide scan (left), C_{1s} (middle) and N_{1s} narrow (right) spectra of mercapto-phosphonic acid (top) and **ZID-alkyne** (bottom) on AO.

Since thiols have the tendency to form disulfide bonds, a washing step with the reducing agent TCEP (tris(2-carboxyethyl)phosphine hydrochloride) was performed to reduce the potentially present disulfides. However, this did not lead to changes in the XPS results. The C_{1s} narrow scan confirmed the unintentional 70% coverage by the lack of a dominant C–O peak at 286 eV, which would have been induced by abundant ethylene glycol groups when present at the expected ratio. The 70% coverage was also reflected in the static water contact angle (SWCA) of 116°, which is in agreement with the hydrophobic composition of the layer.

Upon formation of the thiol-functional monolayer, the **ZID-alkyne** were immobilized by the thiol-yne click reaction in water with 2,2'-azobis(2-methylpropionamide)dihydrochloride (ABMPA) as a water-soluble radical initiator (Figure 3.8). The thiol-terminated AO surfaces were incubated in the reaction mixture for 1 h at 80 °C under an argon atmosphere, followed by washing and sonication with Milli-Q water and methanol, followed by a drying step under vacuum. XPS analysis of the coatings showed a new peak for N (N_{1s} at 400 eV) and an increased signal for C (C_{1s} at 285 eV) on the AO surfaces. The calculated layer thickness derived from the Al/C ratio in the XPS wide scan was found to be 3.8 nm. The layer thickness increase of 1.6 nm was found to be very similar to that of the previously discussed amide-bond mediated approach (1.7 nm).

In the N_{1s} narrow-scan spectrum we found the characteristic double peaks at 400.0 eV and 402.6 eV for the dendrimer's neutral and quaternary amines respectively. Furthermore, the C_{1s} showed an increase in the C–heteroatom signal at 286.4 eV and an additional peak at 288.7 eV for the C=O, which are in agreement with the structure of the ZID. Remarkably, the SWCA significantly decreased to 30°, because of the added hydrophilicity of the ZID's carboxylate groups. Combining the XPS and WCA

results, thiol-yne click chemistry appeared to be suitable for the immobilization of ZIDs to form a coating. However, in order to form thicker coatings, we subsequently explored methods to form multilayers by using polymerization techniques.

3.2.4 Free radical polymerization

All previously described strategies focused on making ZID monolayers. From literature it is known that thicker, zwitterionic polymer brush layer outperform their monolayer analogues in terms of antifouling properties.[19] Therefore, an approach that could potentially form multilayers was tested, namely, free-radical polymerization of ZIDs. ZIDs that contain polymerizable groups allow for free-radical polymerization reactions in the presence of a radical source.[48] When incorporating a functional group on the surface in this polymerization process, a coating could be formed. This approached is based on a process called *grafting-through polymerization*, a mechanism in which monomers are supplied to a surface that has a similar monomer attached.[27,28,49–52]

To this aim, **ZID-alkyne** with on average four alkyne groups was further functionalized by reacting the alkynes with an azido-methacrylate in a CuAAC reaction in solution to obtain methacrylate-functionalized ZIDs (**ZID-MA**) (Figure 3.10). The required 3-azidopropyl methacrylate was synthesized by reacting commercially available 3-azidopropan-1-ol with methacryloyl chloride (see Supporting Information for synthesis).[53]

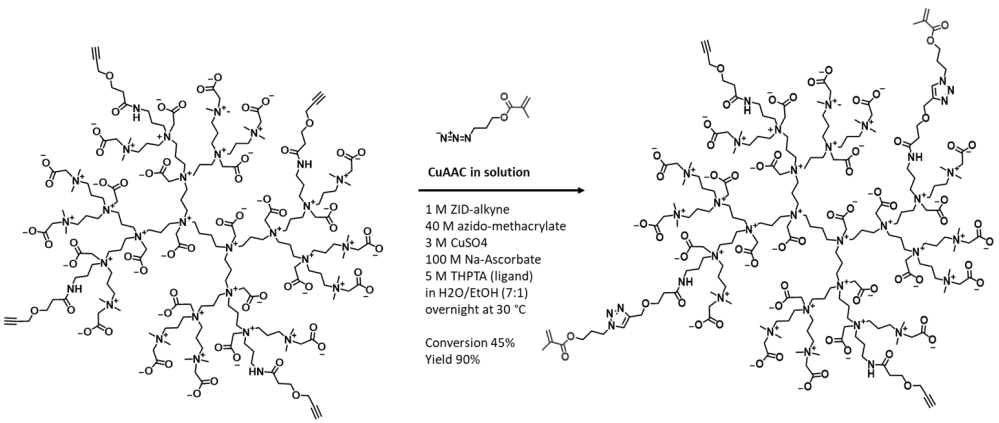

Figure 3.10 Methacrylate functionalization of **ZID-alkyne** by the use of CuAAC click chemistry to form **ZID-MA**. (Conversion and yield are based on ^{1}H-NMR data)

ZID-MA was purified by extensive dialysis and subsequently characterized using nuclear magnetic resonance (NMR). In the ^{1}H-NMR spectrum (Figure 3.11) of the reaction product **ZID-MA**, we observed characteristic signals for the methacrylate groups (peaks *h,* 5.66 and 5.97 ppm), as well as for the formed triazole (peak *i*, 8.06 ppm). Diffusion-ordered spectroscopy (DOSY) was used to verify that the assigned triazole signal indeed belonged to one macromolecular structure by showing the same diffusion coefficient as the proton signals originating from the ZIDs (Figure 3.20 in the Supporting Information). Furthermore, there was a clear decrease in alkyne-originating signals *d* (3.39 ppm) and *g* (4.23 ppm) which are expected to disappear during the CuAAC reaction. At full conversion, the

normalized integrals of the methacrylate signals should have been 4. However, an integral of approximately 1.8 was determined, which corresponds to a conversion of ~45%. Since one of the starting materials of the reactions is a macromolecule of almost 4000 Da,[31] the conversion is likely hampered by steric effects despite using excess of azidopropyl methacrylate and catalyst. Since we aimed for having on average >1 methacrylate groups in order to form crosslinks, we decided to explore **ZID-MA** as a building block to potentially grow multilayered ZID antifouling coatings.

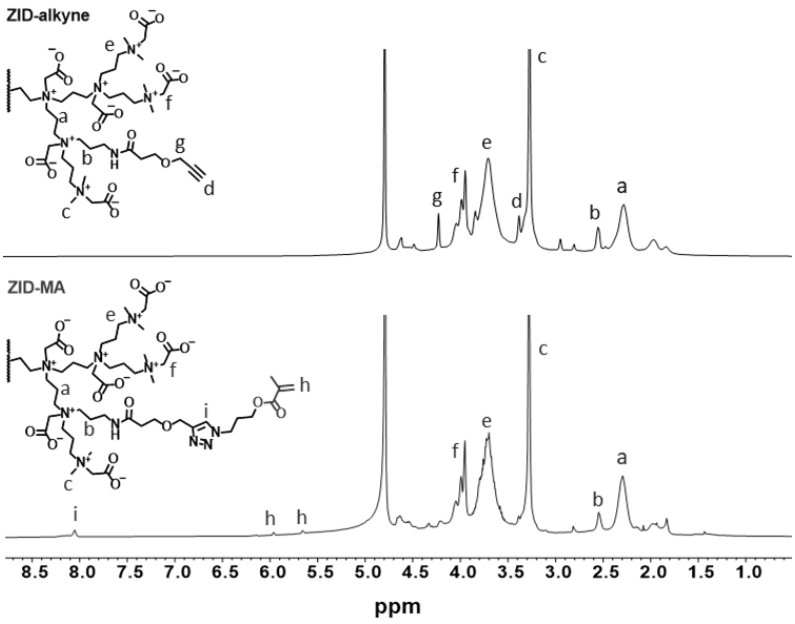

Figure 3.11 ^{1}H-NMR spectrum of **ZID-alkyne** and **ZID-MA** in D_2O (400 MHz, 298 K) accompanied by a branch of the concerning dendrimer. The spectra were normalized by setting the combined integrals of peaks labelled *a* and *b* to a value of 56. Full assignment of the spectra, including peak integration, is provided in the Supporting Information.

In order to covalently bind **ZID-MA** to the surface, the surface was first provided with a monolayer with functional groups that should be able to participate in a free-radical polymerization process. We chose to work with thiols since this functional group has proven to be able to react with acrylates in Michael-addition and thiol-ene click reactions.[54,55] First, a thiol-terminated coating was prepared by reacting (3-mercaptopropyl)trimethoxysilane (MPTMS) on silicon oxide surfaces in a similar way described for the APDMES coating.

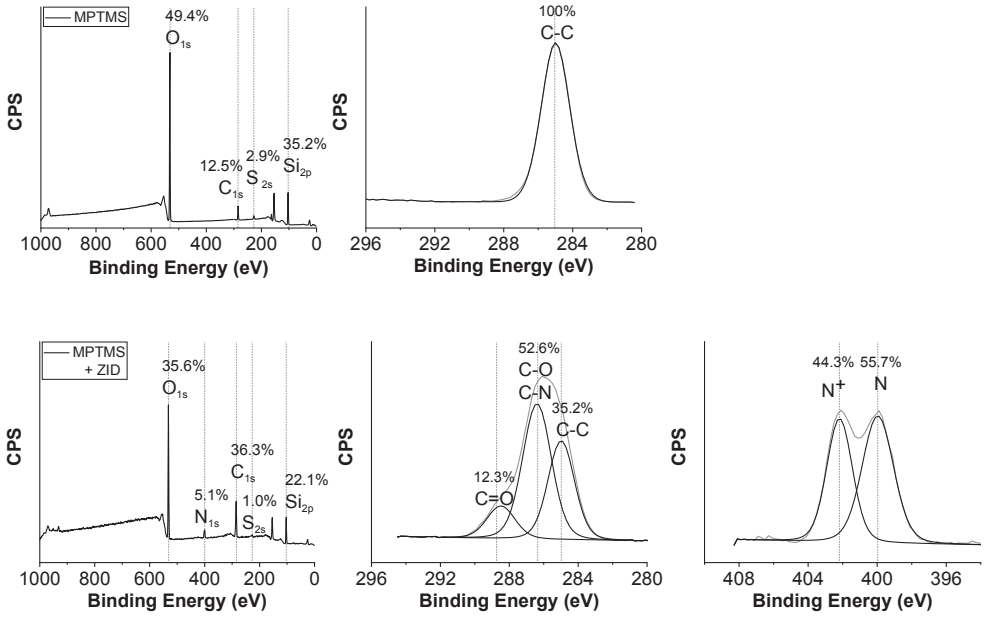

Figure 3.12 XPS wide scan (left), C_{1s} (middle) and N_{1s} narrow (right) spectra of (3-mercaptopropyl) trimethoxysilane (top) and **ZID-MA** (bottom) on silicon oxide.

When investigating the thiol-terminated coating by XPS, we found the expected silicon (at 103 eV) and oxygen signals (at 532 eV) coming from the glass substrate and additional signals corresponding to sulfur (at 228 eV) and carbon (285 eV) that originate from the MPTMS monolayer on the surface close to the expected ratio of 1:3 (Figure 3.12). The average layer thickness was calculated using the Si/C ratio in the XPS wide scan and found to be 1.1 nm.[35,36] The layer thickness was slightly thicker than expected, most likely due to hydrolysis-mediated side reactions of the trimethoxysilanes in the presence of small amounts of water.[34] The static water contact angle (SWCA) was determined to be 62°, which is in agreement with literature.[56,57]

After providing the silicon oxide surfaces with thiol groups, the **ZID-MA** were polymerized on these surfaces via a grafting-through polymerization process using the water-soluble cationic azo initiator 2,2'-azobis(2-methylpropionamidine)dihydrochloride (ABMPA) in water at 80 °C for 1 h under an argon atmosphere, followed by a final UV curing step for 10 min (Figure 3.13). Afterwards, the surfaces were cleaned by rinsing and sonication with Milli-Q water, dried in a stream of argon and directly used for analysis or further reaction. Experiments without this additional UV curing step resulted in significantly less attachment of **ZID-MA** (see Figure 3.21 in the Supporting Information for details).

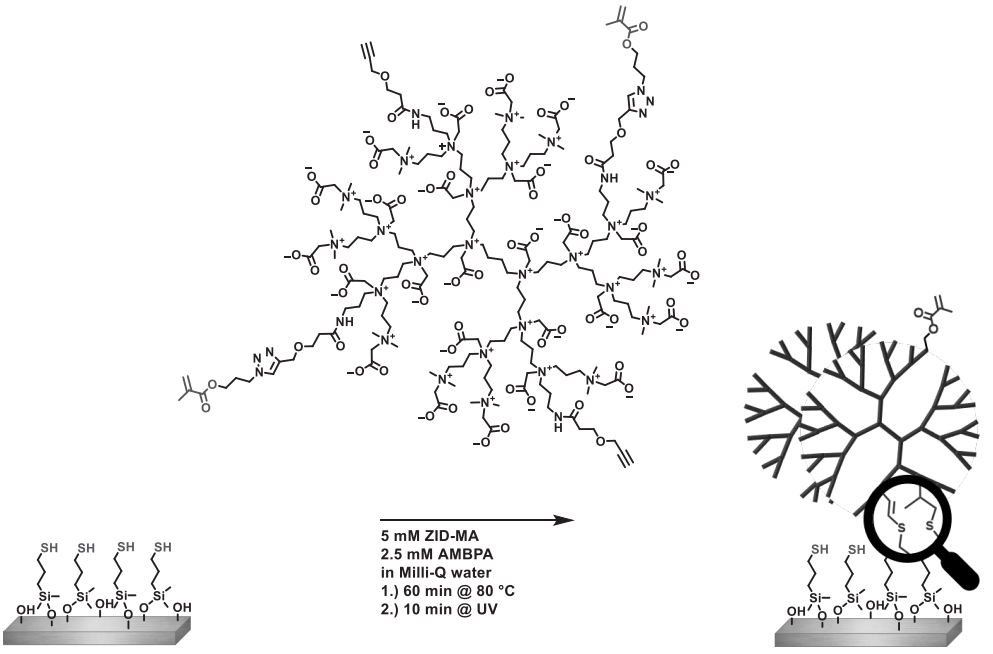

Figure 3.13 The immobilization of **ZID-MA** on thiol-modified silicon oxide by the use of free-radical polymerization.

Wide scan XPS analysis after ZID-MA immobilization showed a new peak for N (N1s at 400 eV) and an increased signal for C (C1s at 285 eV) on the silicon oxide surfaces, corresponding to a thickness of 3.7 nm. Since XPS measures a collapsed state of the formed coating under UHV and the hydrodynamic diameter of the used ZID-MA was estimated to be approximately 3.2 nm,[31] this immobilization technique resulted in a coating that consists of more than a single monolayer of ZID. In comparison, the formation of a monolayer of ZID on silicon oxide by amide bond formation resulted in layer thicknesses of 2.3 nm, with a corresponding increase of 1.7 nm (as discussed earlier in this chapter). In the N1s XPS we found the expected characteristic double peaks at 400.0 eV and 402.6 eV for the dendrimer's neutral and quaternary amines, respectively. The C_{1s} narrow scan spectrum showed a new C–heteroatom signal at 286.4 and an additional peak at 288.4 eV for the C=O, which are in agreement with the structure of the ZID (Figure 3.12). Furthermore, the SWCA decreased to 33° because of the added hydrophilicity of the ZID's carboxylate groups. Under the assumption that the formed **ZID-MA** coating could fulfil a role likewise to the mercaptosilane, *i.e.* participate in a free-radical polymerization process, the exact same **ZID-MA** polymerization procedure was repeated three more times to eventually form 4 layers (L1, L2, L3 and L4) in a procedure similar to a layer-by-layer (LbL) process (Figure 3.14).[23]

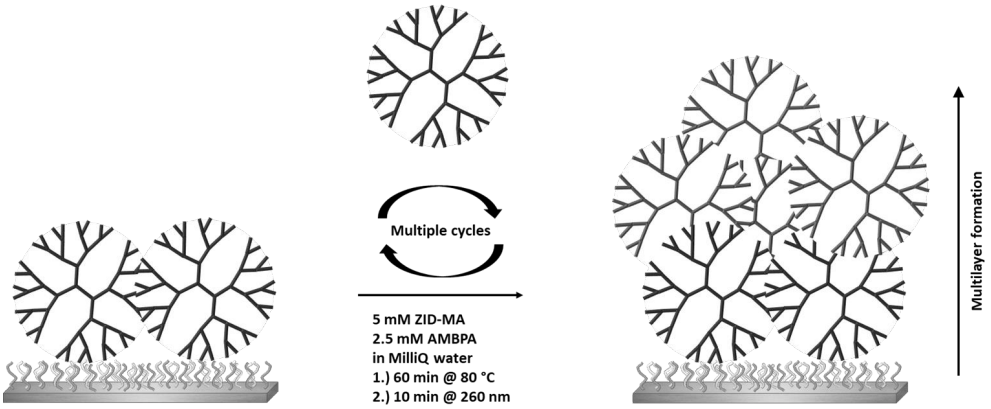

Figure 3.14 Multilayer formation by repeating cycles of **ZID-MA** attachment on SiO_2.

In Figure 3.15, the results of XPS analysis after the **ZID-MA** layer L1 to L4 build-up are shown. As expected, the layers grew thicker after every cycle. This could be inferred from the increase of both the C (C_{1s} at 285 eV) and N (N_{1s} at 400 eV) signals in the wide scans with each newly formed layer. The atomic ratio of the elements C and N in the ZID-MA dendrimer are 202 : 36, which match the found ratios in the XPS wide scans (60 : 10 in the case of L4) reasonably well, keeping in mind that excess carbon is expected from the underlying MPTMS layer. Overall, the increasing C content with every step logically translates into an increase in layer thickness up to 8.2 nm, as is also summarized in Table 3.1 and Figure 3.16. When investigating the chemical composition of the formed layer by analyzing the N_{1s} and C_{1s} narrow scans, it was also noticeable that there is an increase in ZID character, *i.e.*, the amount of quaternary amine (N^+ at 402 eV) and carboxylate (C=O at 288.7 eV) both increase with increasing number of layers. We unfortunately did not reach the 72% of N^+ (based on the structure of ZID-MA as drawn in Figure 3.10), possibly due to damage to the structure by the UV light. Investigating the hydrophilicity of the formed layers showed that an increasing amount of layers naturally gave rise to more hydrophilic layers, which is reflected in decreasing WCA to a final value of 20° (see Table 3.1 and Figure 3.16).

Table 3.1 WCA and XPS results for the layer-by-layer formation by using **ZID-MA**.

Coating	WCA	Thickness (nm)*	C_{1s} (%) wide scan	N_{1s} (%) wide scan	N^+ (%) N_{1s} narrow scan
Mercaptosilane	62°	1.1	13	-	-
ZID-MA LbL 1	33°	3.7	37	5	44
ZID-MA LbL 2	30°	4.8	44	7	52
ZID-MA LbL 3	29°	7.0	57	8	54
ZID-MA LbL 4	20°	8.2	60	10	58
100 % ZID-MA (theoretically)	-	-	85	15	72

Calculated with C/Si ratios in the XPS wide scan.[31]

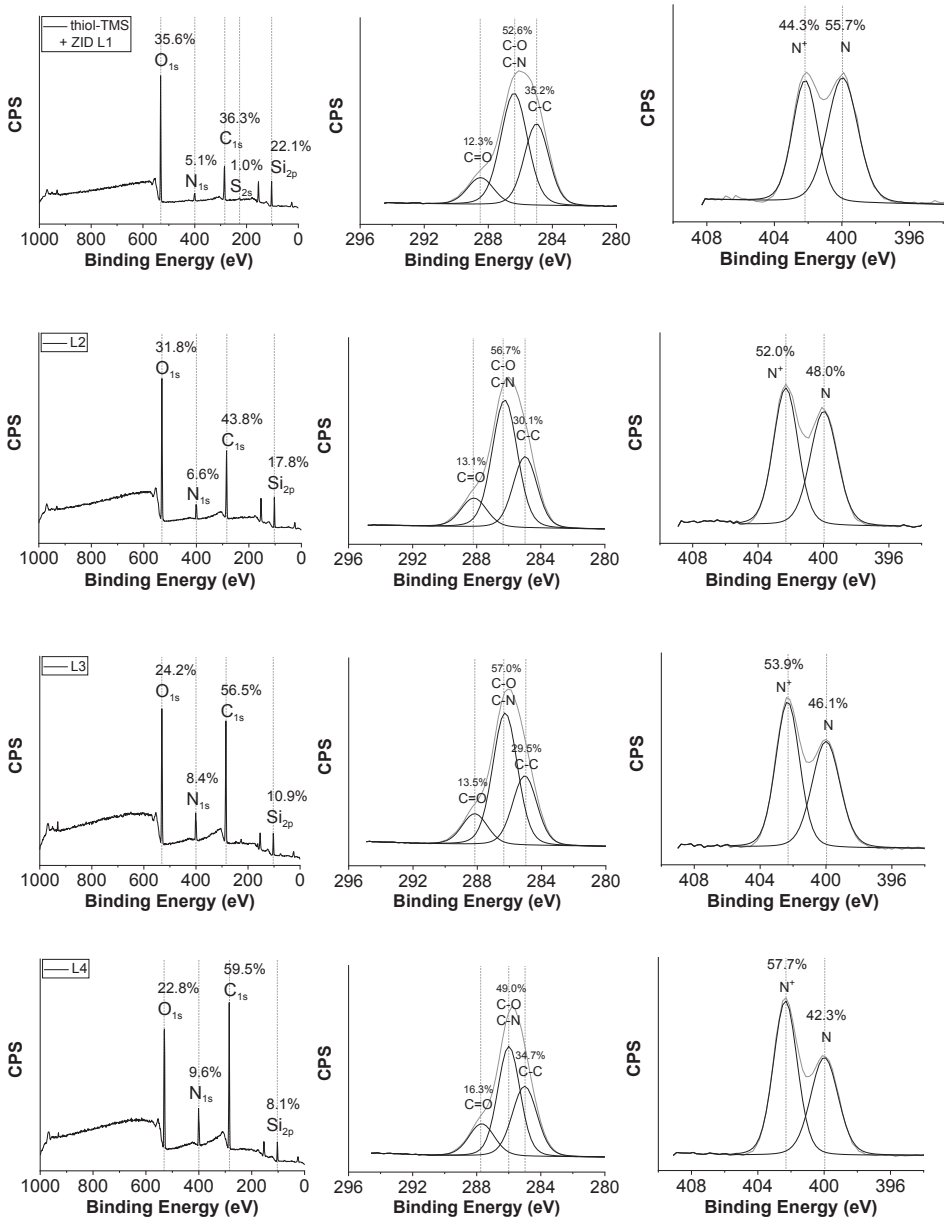

Figure 3.15 XPS wide scan (left), C1s (middle) and N1s narrow (right) spectra of **ZID-MA** L1, L2, L3 and L4 coatings (ascending from top to bottom) on silicon oxide.

Based on the XPS data and WCA, we concluded that it was possible to form a coating in a *layer-by-layer* fashion. By polymerizing methacrylate-functionalized ZID **ZID-MA**, incorporating a functional group on the surface, a stable, likely covalently bound coating was formed. By repeating this process, eventually even multilayers were formed. The resulting coatings were hydrophilic and had the expected chemical composition as measured by XPS and showed an increasing layer thickness.

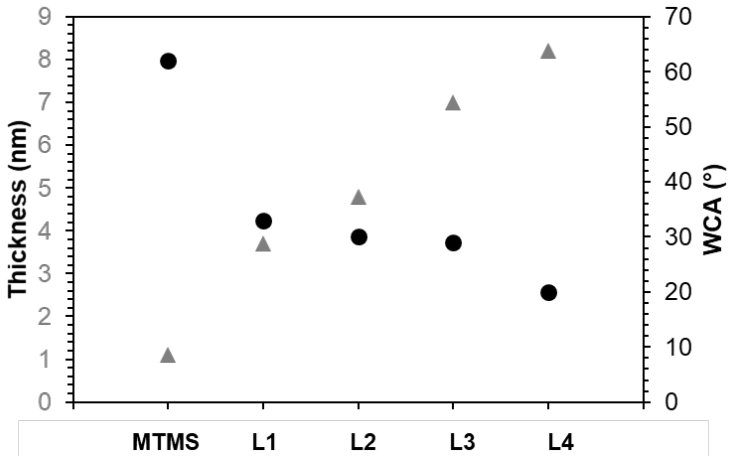

Figure 3.16 Layer thickness (triangles) and WCA (spheres) data for the layer-by-layer formation by using **ZID-MA**.

3.2.5 Antifouling studies

In order to preliminarily test the potential application of the developed ZID-MA LbL layers as antifouling coatings, we performed a study in which we undertook a series of antifouling studies. To this end, the surfaces were exposed to fluorescently labeled proteins in single-protein solutions, after which the degree of fouling was related to the amount of protein adsorption as measured by fluorescence microscopy.[16,58–60] In this study Alexa Fluor 488-labeled bovine serum albumin and fibrinogen were used as model proteins at concentrations of 1 mg/mL in phosphate-buffered saline (PBS) and contacted with the surfaces for 15 min before washing with PBS with Tween®20, PBS and water. Bovine serum albumin (BSA) was chosen since it is one of the most common proteins in blood plasma.[61] Fibrinogen (FIB) was used as a more challenging fouling model protein since it plays a major role in clotting of the blood due to formation of fibrin networks.[62] The amount of fouling of the four LbL-derived ZID coatings by these protein was compared with the fouling of a methoxy-oligo(ethylenoxy)propyl dimethylsilane monolayer ($EO_{6\text{-}9}$ SAM), which is known to add single-protein antifouling properties to silicon oxide surfaces (Figure 3.17).[63,64]

In the fluorescence study, we observed fouling levels for BSA on the first **ZID-MA** layer that were in the same order of magnitude as the EO SAM reference. Furthermore, the amount of fouling decreased upon increasing number of applied layers. The amount of fouling by FIB on all **ZID-MA** LbL coatings appeared to be below the fouling level of FIB on the EO SAM and was lowest on **ZID-MA** L4. Based on these initial results, it can be concluded that introduction of the ZID-based coatings imparts antifouling character to the surface and confirms the potential to further explore ZID as building blocks for antifouling coatings.

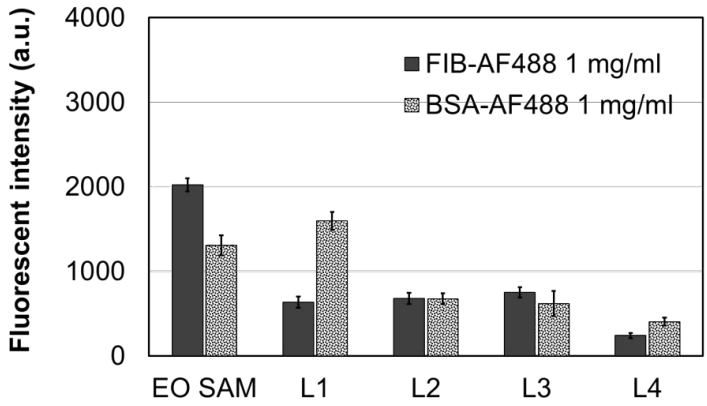

Figure 3.17 Fluorescence intensities of differently coated silicon oxide surfaces after exposure to a solution containing FIB-AF488 and BSA-AF488.

3.3 Conclusion

In this chapter we explored four strategies to immobilize ZIDs on surface to enable their use as a coating. The first three approaches – hinging on amide bond formation, Cu^{I}-catalyzed azide/alkyne cycloaddition (CuAAC), or thiol-yne click chemistry – all resulted in monolayers of ZID. The two "click" variants yielded higher levels of immobilized ZID, *i.e.*, thicker and more hydrophilic layers. In case of the CuAAC reactions, the conversion of "alkyne-modified ZID on an azide-modified surface" was found to be more efficient (WCA <20°) compared to "azide-modified ZID on an alkyne-modified surface". Likely, the hydrophobic (WCA > 160°) nature of the alkyne-terminated starting layer PAO hampered proper interaction by the aqueous ZID solution, thereby decreasing the conversion. The thiol-yne click chemistry also led to ZID layers, which showed the characteristic ZID character in XPS by displaying N^{+} atoms in the N_{1s} narrow scan and the desired hydrophilicity (WCA 30°).

To further increase the immobilization load of the ZID, we tested a grafting-through approach that led to multilayers of ZID by cross-reacting methacrylate-functionalized ZID (**ZID-MA)** onto a pre-coated surface. This led to a total of four stacked layers that showed increasing thicknesses and hydrophilicity with each newly formed layer, and antifouling properties slightly better than oligoethylene oxide SAMs.

However, all the above discussed immobilization strategies have one thing in common, namely the necessity of a precoated surface in order to tune the correct reactivity towards the ZIDs. This is not ideal since it involves an additional pretreatment step under critical conditions. Ideally, we develop a system which self-assembles on a surface in a single step, under ambient conditions. This implies the incorporation of a functional part, with an intrinsic affinity towards the surface, to the ZIDs. The results of this strategy are discussed in Chapter 4 and Chapter 5.

3.4 Acknowledgements

The authors gratefully thank Dr. Anke K. Schütz-Trilling for assistance with the antifouling studies measurements, and Margaux Tellez for contributions to the synthesis part of this work. This project was supported by NWO (LIFT program, grant 731.015.042) with Surfix BV as a partner.

3.5 References

1. Li, F.; Meng, J.; Ye, J.; Yang, B.; Tian, Q.; Deng, C. Surface Modification of PES Ultrafiltration Membrane by Polydopamine Coating and Poly(Ethylene Glycol) Grafting: Morphology, Stability, and Anti-Fouling. *Desalination* **2014**, *344*, 422–430.
2. Wang, Y.; Li, L.; Li, J.; Yang, B.; Wang, C.; Fang, W.; Ji, F.; Wen, Y.; Yao, F. Stable and PH-Responsive Polyamidoamine Based Unimolecular Micelles Capped with a Zwitterionic Polymer Shell for Anticancer Drug Delivery. *RSC Adv.* **2016**, *6* (21), 17728–17739.
3. Svenningsen, S. W.; Janaszewska, A.; Ficker, M.; Petersen, J. F.; Klajnert-Maculewicz, B.; Christensen, J. B. Two for the Price of One: PAMAM-Dendrimers with Mixed Phosphoryl Choline and Oligomeric Poly(Caprolactone) Surfaces. *Bioconjug. Chem.* **2016**, *27* (6), 1547–1557.
4. Huang, D.; Yang, F.; Wang, X.; Shen, H.; You, Y.; Wu, D. Facile Synthesis and Self-Assembly Behaviour of PH-Responsive Degradable Polyacetal Dendrimers. *Polym. Chem.* **2016**, *7* (40), 6154–6158.
5. Cao, W.; Huang, J.; Jiang, B.; Gao, X.; Yang, P. Highly Selective Enrichment of Glycopeptides Based on Zwitterionically Functionalized Soluble Nanopolymers. *Sci. Rep.* **2016**, *6* (29776), 1–8.
6. Han, Y.; Qian, Y.; Zhou, X.; Hu, H.; Liu, X.; Zhou, Z.; Tang, J.; Shen, Y. Facile Synthesis of Zwitterionic Polyglycerol Dendrimers with a β-Cyclodextrin Core as MRI Contrast Agent Carriers. *Polym. Chem.* **2016**, *7*, 6354.
7. Xiong, Z.; Wang, Y.; Zhu, J.; Li, X.; He, Y.; Qu, J.; Shen, M.; Xia, J.; Shi, X. Dendrimers Meet Zwitterions: Development of a Unique Antifouling Nanoplatform for Enhanced Blood Pool, Lymph Node and Tumor CT Imaging. *Nanoscale* **2017**, *9* (34), 12295–12301.
8. Roeven, E.; Scheres, L.; Smulders, M. M. J.; Zuilhof, H. Design, Synthesis, and Characterization of Fully Zwitterionic, Functionalized Dendrimers. *ACS Omega* **2019**, *4* (2), 3000–3011.
9. Jiang, S.; Cao, Z. Ultralow-Fouling, Functionalizable, and Hydrolyzable Zwitterionic Materials and Their Derivatives for Biological Applications. *Adv. Mater.* **2010**, *22* (9), 920–932.
10. Schlenoff, J. B. Zwitteration: Coating Surfaces with Zwitterionic Functionality to Reduce Nonspecific Adsorption. *Langmuir* **2014**, *30* (32), 9625–9636.
11. Holmlin, R. E.; Chen, X.; Chapman, R. G.; Takayama, S.; Whitesides, G. M. Zwitterionic SAMs That Resist Nonspecific Adsorption of Protein from Aqueous Buffer. *Langmuir* **2001**, *17* (13), 2841–2850.
12. Byrne, B.; Stack, E.; Gilmartin, N.; O'Kennedy, R. Antibody-Based Sensors: Principles, Problems and Potential for Detection of Pathogens and Associated Toxins. *Sensors (Switzerland)* **2009**, *9* (6), 4407–4445.
13. Xu, J.; Yu, Q.; Jiang, S. Cellulose Paper Sensors Modified with Zwitterionic Poly(Carboxybetaine) for Sensing and Detection in Complex Media. *Anal. Chem.* **2014**, *86*, 2871–2875.
14. Zhang, Z.; Chen, S.; Jiang, S. Dual-Functional Biomimetic Materials: Nonfouling Poly (Carboxybetaine) with Active Functional Groups for Protein Immobilization. *Biomacromolecules* **2006**, *7* (12), 3311–3315.
15. Baggerman, J.; Smulders, M. M. J.; Zuilhof, H. Romantic Surfaces: A Systematic Overview of Stable, Biospecific, and Antifouling Zwitterionic Surfaces. *Langmuir* **2019**, *35* (5), 1072–1084.
16. Kuzmyn, A. R.; Nguyen, A. T.; Zuilhof, H.; Baggerman, J. Bioactive Antifouling Surfaces by Visible-Light-Triggered

Polymerization. *Adv. Mater. Interfaces* **2019**, *6* (12), 1900351.
17. Khaldi, K.; Sam, S.; Gouget-Laemmel, A. C.; Henry De Villeneuve, C.; Moraillon, A.; Ozanam, F.; Yang, J.; Kermad, A.; Ghellai, N.; Gabouze, N. Active Acetylcholinesterase Immobilization on a Functionalized Silicon Surface. *Langmuir* **2015**, *31* (30), 8421–8428.
18. Chen, S.; Liu, L.; Zhou, J.; Jiang, S. Controlling Antibody Orientation on Charged Self-Assembled Monolayers. *Langmuir* **2003**, *19* (7), 2859–2864.
19. Ladd, J.; Zhang, Z.; Chen, S.; Hower, J. C.; Jiang, S. Zwitterionic Polymers Exhibiting High Resistance to Nonspecific Protein Adsorption from Human Serum and Plasma. *Biomacromolecules* **2008**, *9* (5), 1357–1361.
20. Zhang, Z.; Vaisocherová, H.; Cheng, G.; Yang, W.; Xue, H.; Jiang, S. Nonfouling Behavior of Polycarboxybetaine-Grafted Surfaces: Structural and Environmental Effects. *Biomacromolecules* **2008**, *9* (10), 2686–2692.
21. Cheng, N.; Brown, A. A.; Azzaroni, O.; Huck, W. T. S. Thickness-Dependent Properties of Polyzwitterionic Brushes. *Macromolecules* **2008**, *41* (17), 6317–6321.
22. Roosjen, A.; Van Der Mei, H. C.; Busscher, H. J.; Norde, W. Microbial Adhesion to Poly(Ethylene Oxide) Brushes: Influence of Polymer Chain Length and Temperature. *Langmuir* **2004**, *20* (25), 10949–10955.
23. Richardson, J. J.; Bjornmalm, M.; Caruso, F. Technology-Driven Layer-by-Layer Assembly of Nanofilms. *Science (80-.).* **2015**, *348* (6233), aaa2491.
24. Wong, S. Y.; Han, L.; Timachova, K.; Veselinovic, J.; Hyder, M. N.; Ortiz, C.; Klibanov, A. M.; Hammond, P. T. Drastically Lowered Protein Adsorption on Microbicidal Hydrophobic/Hydrophilic Polyelectrolyte Multilayers. *Biomacromolecules* **2012**, *13* (3), 719–726.
25. Wang, Y.; Liu, Y.; Cheng, Y.; Kim, E.; Rubloff, G. W.; Bentley, W. E.; Payne, G. F. Coupling Electrodeposition with Layer-by-Layer Assembly to Address Proteins within Microfluidic Channels. *Adv. Mater.* **2011**, *23* (48), 5817–5821.
26. Valencia, L.; Kumar, S.; Jalvo, B.; Mautner, A.; Salazar-Alvarez, G.; Mathew, A. P. Fully Bio-Based Zwitterionic Membranes with Superior Antifouling and Antibacterial Properties Prepared via Surface-Initiated Free-Radical Polymerization of Poly(Cysteine Methacrylate). *J. Mater. Chem. A* **2018**, *6* (34), 16361–16370.
27. Grande, C. D.; Tria, M. C.; Felipe, M. J.; Zuluaga, F.; Advincula, R. RAFT "Grafting-through" Approach to Surface-Anchored Polymers: Electrodeposition of an Electroactive Methacrylate Monomer. *Eur. Phys. J. E* **2011**, *34* (2).
28. Mohammadi Sejoubsari, R.; Martinez, A. P.; Kutes, Y.; Wang, Z.; Dobrynin, A. V.; Adamson, D. H. "Grafting-Through": Growing Polymer Brushes by Supplying Monomers through the Surface. *Macromolecules* **2016**, *49* (7), 2477–2483.
29. Pérez-Perrino, M.; Navarro, R.; Prucker, O.; Rühe, J. Binding of Functionalized Polymers to Surface-Attached Polymer Networks Containing Reactive Groups. *Macromolecules* **2014**, *47* (8), 2695–2702.
30. Ibrahim, K. a.; Al-Muhtaseb, A. H.; Prucker, O.; Rühe, J. Preparation of Hydrophilic Polymeric Nanolayers Attached to Solid Surfaces via Photochemical and ATRP Techniques. *J. Polym. Res.* **2013**, *20* (4), 28–31.
31. Roeven, E.; Scheres, L.; Smulders, M. M. J.; Zuilhof, H. Design, Synthesis, and Characterization of Fully Zwitterionic, Functionalized Dendrimers. *ACS Omega* **2019**, *4*, 3000–3011.
32. Rostovtsev, V. V.; Green, L. G.; Fokin, V. V.; Sharpless, K. B. A Stepwise Huisgen Cycloaddition Process: Copper(I)-Catalyzed Regioselective "Ligation" of Azides and Terminal Alkynes. *Angew. Chem. Int. Ed. Engl.* **2002**, *41* (14), 2596–2599.
33. Hensarling, R. M.; Doughty, V. A.; Chan, J. W.; Patton, D. L. "Clicking" Polymer Brushes with Thiol-Yne Chemistry: Indoors and Out. *J. Am. Chem. Soc.* **2009**, *131* (41), 14673–14675.
34. Yadav, A. R.; Sriram, R.; Carter, J. A.; Miller, B. L. Comparative Study of Solution-Phase and Vapor-Phase Deposition of Aminosilanes on Silicon Dioxide Surfaces. *Mater. Sci. Eng. C* **2014**, *35* (1), 283–290.
35. Wallart, X.; Henry de Villeneuve, C.; Allongue, P. Truly Quantitative XPS Characterization of Organic Monolayers on Silicon: Study of Alkyl and Alkoxy Monolayers on H-Si(111). *J. Am. Chem. Soc.* **2005**, *127* (21), 7871–7878.
36. Scheres, L.; Giesbers, M.; Zuilhof, H. Organic Monolayers onto Oxide-Free Silicon with Improved Surface Coverage: Alkynes versus Alkenes. *Langmuir* **2010**, *26* (7), 4790–4795.
37. Kolb, H. C.; Sharpless, K. B. The Growing Impact of Click Chemistry on Drug Discovery. *Drug Discov. Today* **2003**, *8* (24), 1128–1137.
38. Heinrich, T.; Traulsen, C. H. H.; Darlatt, E.; Richter, S.; Poppenberg, J.; Traulsen, N. L.; Linder, I.; Lippitz, A.; Dietrich, P. M.; Dib, B.; Unger, W. E. S.; Schalley, C. A. The Versatility of "Click" Reactions: Molecular Recognition at Interfaces. *RSC Adv.* **2014**, *4* (34), 17694–17702.
39. Such, G. K.; Quinn, J. F.; Quinn, A.; Tjipto, E.; Caruso, F. Assembly of Ultrathin Polymer Multilayer Films by Click Chemistry. *J. Am. Chem. Soc.* **2006**, *128* (29), 9318–9319.
40. Debrassi, A.; Roeven, E.; Thijssen, S.; Scheres, L.; De Vos, W. M.; Wennekes, T.; Zuilhof, H. Versatile (Bio)Functionalization of Bromo-Terminated Phosphonate-Modified Porous Aluminum Oxide. *Langmuir* **2015**, *31* (20), 5633–5644.
41. Debrassi, A.; Ribbera, A.; De Vos, W. M.; Wennekes, T.; Zuilhof, H. Stability of (Bio)Functionalized Porous Aluminum Oxide. *Langmuir* **2014**, *30* (5), 1311–1320.
42. Sen, R.; Gahtory, D.; Escorihuela, J.; Firet, J.; Pujari, S. P.; Zuilhof, H. Approach Matters: The Kinetics of Interfacial

Inverse-Electron Demand Diels–Alder Reactions. *Chem. - Eur. J.* **2017**, *23* (53), 13015–13022.
43. Debrassi, A.; Ribbera, A.; Vos, W. M. De; Wennekes, T.; Zuilhof, H. Stability of (Bio) Functionalized Porous Aluminum Oxide. *Langmuir* **2014**, *30* (5), 1311–1320.
44. Majhy, B.; Iqbal, R.; Sen, A. K. Facile Fabrication and Mechanistic Understanding of a Transparent Reversible Superhydrophobic – Superhydrophilic Surface. *Sci. Rep.* **2018**, *8* (1), 1–11.
45. Bhairamadgi, N. S.; Gangarapu, S.; Caipa Campos, M. A.; Paulusse, J. M. J.; Rijn, C. J. M. van; Zuilhof, H. Efficient Functionalization of Oxide-Free Silicon(111) Surfaces: Thiol−yne versus Thiol−ene Click Chemistry. *Langmuir* **2013**, *2013* (111), 4535–4542.
46. Fairbanks, B. D.; Sims, E. A.; Anseth, K. S.; Bowman, C. N. Reaction Rates and Mechanisms for Radical, Photoinitated Addition of Thiols to Alkynes, and Implications for Thiol-Yne Photopolymerizations and Click Reactions. *Macromolecules* **2010**, *43* (9), 4113–4119.
47. Fairbanks, B. D.; Scott, T. F.; Kloxin, C. J.; Anseth, K. S.; Bowman, C. N. Thiol-Yne Photopolymerizations: Novel Mechanism, Kinetics, and Step-Growth Formation of Highly Cross-Linked Networks. *Macromolecules* **2009**, *42* (1), 211–217.
48. Wang, Z.; van Andel, E.; Pujari, S. P.; Feng, H.; Dijksman, J. A.; Smulders, M. M. J.; Zuilhof, H. Water-Repairable Zwitterionic Polymer Coatings for Anti-Biofouling Surfaces. *J. Mater. Chem. B* **2017**, *5* (33), 6728–6733.
49. Henze, M.; Mädge, D.; Prucker, O.; Rühe, J. "Grafting through": Mechanistic Aspects of Radical Polymerization Reactions with Surface-Attached Monomers. *Macromolecules* **2014**, *47* (9), 2929–2937.
50. Pesek, S. L.; Li, X.; Hammouda, B.; Hong, K.; Verduzco, R. Small-Angle Neutron Scattering Analysis of Bottlebrush Polymers Prepared via Grafting-through Polymerization. *Macromolecules* **2013**, *46* (17), 6998–7005.
51. Datta, P.; Genzer, J. "Grafting Through" Polymerization Involving Surface-Bound Monomers. *J. Polym. Sci. Part A Polym. Chem.* **2016**, *54* (2), 263–274.
52. Chu, E.; Sidorenko, A. Surface Reconstruction by a "Grafting through" Approach: Polyacrylamide Grafted onto Chitosan Film. *Langmuir* **2013**, *29* (40), 12585–12592.
53. Peng, L.; DeSousa, J.; Su, Z.; Novak, B. M.; Nevzorov, A. A.; Garland, E. R.; Melander, C. Inhibition of Acinetobacter Baumannii Biofilm Formation on a Methacrylate Polymer Containing a 2-Aminoimidazole Subunit. *Chem. Commun. (Camb).* **2011**, *47*, 4896–4898.
54. Lowe, A. B. Thiol-Ene "Click" Reactions and Recent Applications in Polymer and Materials Synthesis. *Polym. Chem.* **2010**, *1* (1), 17.
55. Konuray, O.; Fernández-Francos, X.; Ramis, X.; Serra, À. State of the Art in Dual-Curing Acrylate Systems. *Polymers (Basel).* **2018**, *10* (2).
56. Hu, M.; Noda, S.; Okubo, T.; Yamaguchi, Y. Structure and Morphology of Self-Assembled Layers on Silicon Oxide. *Appl. Surf. Sci.* **2001**, *181*, 307–316.
57. Jian, L. Preparation and Tribological Characteristics of Sulfonated Self-Assembled Monolayer of 3-Mercaptopropyl Trimethoxysilane TiO2 Films. *J. Exp. Nanosci.* **2008**, *3* (4), 307–317.
58. Honda, T.; Nakao, A.; Ishihara, K.; Higaki, Y.; Higaki, K.; Takahara, A.; Iwasaki, Y.; Yusa, S. I. Polymer Coating Glass to Improve the Protein Antifouling Effect. *Polym. J.* **2018**, *50* (5), 381–388.
59. Xu, L. Q.; Pranantyo, D.; Neoh, K. G.; Kang, E. T.; Teo, S. L. M.; Fu, G. D. Synthesis of Catechol and Zwitterion-Bifunctionalized Poly(Ethylene Glycol) for the Construction of Antifouling Surfaces. *Polym. Chem.* **2016**, *7* (2), 493–501.
60. Kuzmyn, A. R.; Nguyen, A. T.; Teunissen, L. W.; Zuilhof, H.; Baggerman, J. Antifouling Polymer Brushes via Oxygen-Tolerant Surface-Initiated PET-RAFT. *Langmuir* **2020**, *36* (16), 4439–4446.
61. Kowalczyńska, H. M.; Nowak-Wyrzykowska, M.; Szczepankiewicz, A. A.; Dobkowski, J.; Dyda, M.; Kamiński, J.; Kołos, R. Albumin Adsorption on Unmodified and Sulfonated Polystyrene Surfaces, in Relation to Cell-Substratum Adhesion. *Colloids Surf. B Biointerfaces* **2011**, *84* (2), 536–544.
62. Horbett, T. A. Fibrinogen Adsorption to Biomaterials. *J. Biomed. Mater. Res. A.* **2018**, *106* (10), 2777–2788.
63. Prime, K. L.; Whitesides, G. M. Adsorption of Proteins onto Surfaces Containing End-Attached Oligo(Ethylene Oxide): A Model System Using Self-Assembled Monolayers. *J. Am. Chem. Soc.* **1993**, *115* (23), 10714–10721.
64. Balamurugan, S.; Ista, L. K.; Yan, J.; López, G. P.; Fick, J.; Himmelhaus, M.; Grunze, M. Reversible Protein Adsorption and Bioadhesion on Monolayers Terminated with Mixtures of Oligo(Ethylene Glycol) and Methyl Groups. *J. Am. Chem. Soc.* **2005**, *127* (42), 14548–14549.
65. Allahara, D.; Stapleton, J. Methods of IR Spectroscopy for Surfaces and Thin Films. In *Surface Science Techniques*; 2013; pp 59–98.
66. Stuart, B.; George, B.; McIntyre, P. *Modern Infrared Spectroscopy*; John Wiley & Sons, 1996.

3.6 Supporting Information

3.6.1 Experimental Section

3.6.1.1 Materials

Milli-Q water was purified by a Barnsted water purification system, with a resistivity of <18.3 MΩ.cm. The reported plasma cleaner was a Diener Femto plasma system. The UV curing step was performed using a collimated UV setup by Bachur using a 1000 W Hg/Xe lamp with mirror set resulting in a wavelength output of 260 nm. Molecular sieves (10 Å) were oven-dried (120 °C, overnight) prior to use. Float-a-lyzer G2 dialysis membranes with a 3.5k-5000k MWCO (VWR) were used for the final purification step of ZID-MA. Sonication steps were performed in an Elmasonic P 30 H ultrasonic unit at 80 kHz. Silicon single-side polished (Si(111), N-type, phosphorus-doped, Siltronix); porous aluminum oxide (PAO) substrates with dimensions of 36 × 8 mm2 and average pore size of 200 nm were purchased from MicroDish BV (Netherlands). Aluminium oxide (AO) surfaces (99.5% purity, mirror polished, Staalmarkt Beuningen BV) were cut using a mechanical cutter into pieces of 1 × 1 cm. Commercially available reagents were used without purification, unless mentioned otherwise: hydrogen peroxide solution (H2O2, 50 wt.% in H2O, Honeywell); sulfuric acid (H2SO4, 95.0-97.0%); phosphate-buffered saline (PBS, Sigma-Aldrich); bovine serum albumin-AlexaFluor488 (BSA-AF488, Fisher Thermo Scientific); methanol (MeOH, Normapure for synthesis, dehydrated, < 0,005 % water, VWR); ethanol (EtOH, absolute, dried over molecular sieves, Merck); hydrochloric acid (HCl, 37% in water, Acros Organics); dichloromethane (DCM, GPR Rectapur, Fisher Scientific); chloroform-d (CDCl3, 99.96 atom% D, Sigma Aldrich); deuterium oxide (D2O, 99.9 atom% D, Sigma Aldrich); 3-aminopropyl)dimethyl ethoxysilane (APDMES, 97%, ABCR); (3-mercaptopropyl)trimethoxysilane (MPTMS, 95%, Sigma Aldrich); 2-[Methoxy(polyethyleneoxy)propyl]dimethyl ethoxysilane, 6-9 PE units (EO6-9 SAM, ABCR); n-octylphosphonic acid (97%, Sigma Aldrich); 12-mercaptododecylphosphonic acid (thiol-PA, SiKemia); (2-{2-[2-(2-hydroxy-ethoxy)-ethoxy]-ethoxy}-ethyl)phosphonic acid (EO-PA, SiKemia); 2,2'-azobis(2-methylpropionamide)dihydrochloride (granular, 97%, Sigma Aldrich); tris(2-carboxyethyl)phosphine hydrochloride (TCEP ≥98% powder, Sigma Aldrich); MES buffer (1 M, Sigma Aldrich); N-hydroxysuccinimide (NHS, 98%, Sigma Aldrich); N-(3-dimethylaminopropyl)-N'-ethylcarbodiimide hydrochloride (EDC, purum, ≥98.0%, Sigma Aldrich); copper(II) sulfate pentahydrate (CuSO4·5H2O, ≥98.0%, Sigma Aldrich); sodium ascorbate (Na-Asc, (+)-Sodium L-ascorbate, crystalline, ≥98%, Sigma Aldrich); tris(3-hydroxypropyltriazolylmethyl)amine (THPTA, 95%, Sigma Aldrich); phosphate-buffered saline tablets (PBS, Sigma Aldrich); 3-Azido-1-propanol (≥96%, Sigma Aldrich); Tween (Tween® 20, Sigma Aldrich).

3.6.1.2 Characterization methods

Nuclear magnetic resonance (NMR)

^{1}H NMR measurements were recorded on a Bruker Avance III NMR at 400 MHz, ^{13}C NMR spectra were recorded at 100 MHz. Chemical shifts are reported in parts per million (ppm), and are referred to the methyl signal of the sodium salt of 3-(trimethylsilyl)-1-propanesulfonic acid-d_6 (δ = 0).

Infrared (IR)

IR analyses were performed on a Bruker Tensor 27 FT-IR spectrometer. Spectra were obtained in transmission mode using a spectral resolution of 2 cm^{-1} and 256 scans per measurement. The raw spectra were divided by the spectrum of a freshly cleaned and etched bare PAO reference substrate.

X-ray Photoelectron Spectroscopy (XPS)

XPS spectra were obtained using a JPS-9200 photoelectron spectrometer (JEOL, Japan) with monochromatic Al-Kα X-Ray radiation at 12 kV and 20 mA. The obtained spectra were analyzed using CASA XPS software (version 2.3.16 PR 1.6). In C1s and N1s narrow-range spectra, the positions are set to 285 eV and 400 eV for the C–C and N–C signals, respectively. For layers <15 nm, the thickness was calculated based on the attenuation of the Si signal in XPS, according to a published procedure.[36]

Gel Permeation Chromatography (GPC)

The polymer molecular weight and polydispersity index (PDI) were determined using gel permeation chromatography (Agilent G5654A quaternary pump, G7162A refractive index detector), where a PSS SUPREMA Combination medium (P/N 206-0002) 1000 Å single porosity column was employed (0.05% NaN_3 in milli-Q water

as eluent, 1 mL/min). Dendrimer in Milli-Q solutions were freshly prepared. 20 µL was used for each analysis. An Agilent PL2080-0101 PEO calibration kit was used for calibration purposes.

Fluorescence microscopy
Imaging was performed in a Zeiss Axio Scope A1 microscope equipped with a 20×/0.75 Fluar objectives. Excitation wavelengths of 450-490 nm were combined with a dichroic mirror (FT 495 nm) and achromatic lenses, and delivered to the microscope. An Axiocam 503 monochromatic CCD camera was used for detection. Exposure time for all samples was 0.1 s. Zen 2.3 Lite software was used for acquisition. Image analysis and fluorescence quantification after background correction (fluorescent intensity of the non-contacted, dark area) was performed by using ImageJ 1.51h – Fiji.z

3.6.1.3 Surface modification

Modification of silicon oxide with (3-Aminopropyl)dimethyl ethoxysilane
Silicon wafers were cut into 1×1 cm pieces and cleaned by sonication in acetone for 5 min and dried in an argon stream, subsequently oxidized by air plasma for 5 min and cleaned in a piranha solution (3 : 1 mixture by volume of H_2SO_4 : H_2O_2) for 15 min, after which they were soaked in and extensively rinsed with Milli-Q water and MeOH, finally dried by a stream of argon and immediately transferred into an oven dried reactor under argon atmosphere. The freshly cleaned surfaces were immediately used for modification by being covered with a solution of 150 µL (3-aminopropyl)dimethyl ethoxysilane in 15 mL dry toluene in the argon filled reactor overnight at room temperature. Afterwards, the modified surfaces were cleaned by sonication in DCM, followed by a DCM rinsing step and dried by a stream of argon.

ZID modification of amide-modified silicon oxide
First, the carboxylate groups of the ZID were activated with EDC and NHS in solution. A fresh solution containing ZID (80 mM), EDC (0.5 M) and NHS (0.1 M) in MES buffer (0.1 M) was prepared.
The freshly prepared APDMES-modified silicon oxide surfaces were covered with the reaction mixture and incubated overnight at room temperature in a humidity chamber. After rinsing and sonication with Milli-Q water, the samples were dried in a stream of argon and directly used for analysis.

Modification of PAO with 12-azidododecylphosphonic acid
PAO surfaces were cleaned by mild (80 Hz) sonication in acetone and Milli-Q water for 5 min each. Subsequently the surfaced were etched in a freshly prepared mixture of 37% hydrochloric acid and methanol (1:1 v/v) for 30 min. Afterwards, they were rinsed and sonicated in Milli-Q water and dry ethanol for 5 min each after which the surfaces were transferred into an oven dried reactor and dried under vacuum for 15 min. The reactor was backfilled with argon and the PAO substrates were immersed in a 1 mM solution of mixed phosphonic acid for 16 h at room temperature under argon atmosphere. The mixed phosphonic acid solution was freshly prepared and consisted of one equivalent of 12-azidododecylphosphonic acid (2.2 mg) and three equivalents of octylphosphonic acid (4.4 mg) in 30 ml dry ethanol. After immersion, the surfaces were rinsed and sonicated with absolute ethanol and heated to 130 °C under vacuum for 1 h. The substrates were rinsed and sonicated in again with ethanol and dried by vacuum.

ZID-alkyne modification of azide-modified PAO by CuAAC
In Chapter 2, we described the synthesis of ZID-alkyne with on average three alkyne groups. This ZID was immobilized by immersing an azido-modified PAO surface in a freshly prepared CuAAC reaction mixture. This mixture contained $CuSO_4$ (0.2 mM), Na-Ascorbate (20 mM), THPTA ligand (0.5 mM) and ZID-alkyne (0.5 mM) dissolved in Milli-Q water. The PAO surface was incubated overnight at room temperature. Afterwards, the surface was rinsed and sonicated with Milli-Q water and ethanol and dried by vacuum.

Modification of PAO with 10-undecylphosphonic acid
PAO surfaces were cleaned by mild (80 Hz) sonication in acetone and Milli-Q water for 5 min each. Subsequently the surfaced were etched in a freshly prepared mixture of 37% hydrochloric acid and methanol (1:1 v/v) for 30 min. Afterwards, they were rinsed and sonicated in Milli-Q water and dry ethanol for 5 min each after which the surfaces were transferred into an oven dried reactor and dried under vacuum for 15 min. The reactor was backfilled with argon and the PAO substrates were immersed in a 1 mM solution of mixed phosphonic acid for 16 h at room temperature under argon atmosphere. The mixed phosphonic acid solution was freshly prepared and consisted of one equivalent 10-undecylphosphonic acid (1.75 mg) and three equivalents octylphosphonic acid (4.4 mg) in 30 ml dry ethanol. After immersion, the surfaces were rinsed and sonicated with ethanol and

heated to 130 °C under vacuum for 1 h. The substrates were rinsed and sonicated in again with ethanol and dried by vacuum.

ZID-azide modification of alkyne-modified PAO by CuAAC
In Chapter 2, we described the synthesis of ZID-azide with on average three alkyne groups. This ZID was immobilized by immersing an alkyne-modified PAO surface in a freshly prepared CuAAC reaction mixture. This mixture contained $CuSO_4$ (0.2 mM), Na-Ascorbate (20 mM), THPTA ligand (0.5 mM) and ZID-azide (0.5 mM) dissolved in Milli-Q water. The PAO surface was incubated overnight at room temperature. Afterwards, the surface was rinsed and sonicated with Milli-Q water and ethanol and dried by vacuum.

Modification of AO with 12-mercaptododecylphosphonic acid
Aluminum oxide surfaces were cleaned by sonication in DCM twice (to remove the protective foil) for 5 min each. Subsequently the surfaced were etched in a freshly prepared mixture of 37% hydrochloric acid and methanol (1:1 v/v) for 5 min. Afterwards, they were rinsed and sonicated in Milli-Q water and dry ethanol for 5 min each, dried by a stream of argon and transferred into an argon-filled reactor. A 1 mM solution of mixed phosphonic acid was added under argon overpressure and the reactor was closed under argon atmosphere for 16 h at room temperature. The mixed phosphonic acid solution was freshly prepared and consisted of one equivalent 12-mercaptododecylphosphonic acid (1.6 mg) and three equivalents of (2-{2-[2-hydroxy-ethoxy]-ethoxy}-ethyl)phosphonic acid (3.6 mg) in 6 ml dry ethanol. After immersion, the surfaces were rinsed and sonicated with ethanol and heated at 130 °C under vacuum for 1 h. The substrates were rinsed and sonicated again with ethanol and dried by a stream of argon.

ZID-alkyne modification of thiol-modified AO by thiol-yne click chemistry
In Chapter 2, we described the synthesis of ZID-alkyne with on average three alkyne groups. A solution containing ZID-alkyne (2.0 mM) and radical initiator ABMPA (0.02 mM) in milli-Q water was freshly prepared. The thiol-modified AO surfaces were covered with this solution and heated to 80 °C for 1 h under an argon atmosphere. Afterwards, the surfaces were rinsed and sonicated in Milli-Q water and ethanol for 5 min each and dried by vacuum.

Modification of silicon oxide with (3-mercaptopropyl)trimethoxysilane
Silicon wafers were cut into 1×1 cm pieces and cleaned by sonication in acetone for 5 min and dried in an argon stream, subsequently oxidized by air plasma for 5 min and cleaned in a piranha solution (3 : 1 mixture by volume of H_2SO_4 : H_2O_2) for 15 min, after which they were soaked in and extensively rinsed with Milli-Q water and MeOH, finally dried by a stream of argon and immediately transferred into an oven dried reactor under argon atmosphere. The freshly cleaned surfaces were immediately used for modification by being covered with a solution of 150 µL (3-mercaptopropyl)trimethoxysilane in 15 mL dry toluene in the argon filled reactor overnight at room temperature. Afterwards, the modified surfaces were cleaned by sonication in DCM followed by a DCM rinsing step and dried by a stream of argon.

ZID-methacrylate modification of thiol-modified silicon oxide by free radical polymerization
A solution containing ZID-MA (5.0 mM) and radical initiator ABMPA (2.5 mM) in milli-Q water was freshly prepared. The thiol-modified silicon oxide surfaces were covered with this solution and heated to 80 °C for 1 hour under argon atmosphere, immediately followed by a UV curing step at 260 nm for 10 min. Afterwards, the surfaces were cleaned by rinsing and sonication with Milli-Q water and dried by a stream of argon.

ZID-methacrylate multilayer formation on silicon oxide by free radical polymerization
For the formation of multilayers (L2, L3 and L4), the above described procedure – including the washing steps – was repeated two, three or four times respectively.

3.6.1.4 Protein fouling studies

Fouling of the coated surfaces was investigated by spotting the surfaces in the single-protein solution of Alexa Fluor 488-labeled bovine serum albumin (BSA-AF488, 1 mg·mL^{-1}) and fibrinogen (FIB-AF488, 1 mg·mL^{-1}) and incubation in a humidity chamber for 15 min at room temperature. The surfaces were then washed with PBST (0.05% Tween®20 in PBS buffer), PBS buffer (pH 7.4) and Milli-Q water and subsequently dried in a stream of argon. The fluorescence intensity of the adsorbed proteins was measured.

3.6.1.5 Syntheses

Synthesis of 3-azidopropyl methacrylate

First, 3-azidopropyl methacrylate was synthesized by stirring a solution of 2.273 g 3-azido-1-propanol (22.5 mol), 1.72 ml methacrylic acid (20 mmol) and 0.825 g DMAP in 20 ml dry DCM in a round bottom flask on an ice bath. A solution of 4.64 g DCC (22.5 mol) in 15 ml DCM was added dropwise and slowly allowed to warm up to room temperature overnight. The next day, the precipitate was removed by filtering the reaction mixture and the DCM was removed by rotavap. The obtained impure product was purified over a silica gel column using a 9:1 mixture of hexane and ethyl acetate (R_f value of product 0.4 based on TLC). The solvents were removed by rotavap and the product was collected as 2.474 g of a colorless liquid with a yield of 73%.*

* After purification there were still some minor solvent impurities present in NMR, which were fully remove after extensive drying prior to yield determination.

^{1}H-NMR (400 MHz, CDCl3, 300 K) δ 1.96 (5,12; m, 5H), δ 3.42 (4; t, 2H), δ 4.24 (6; t, 2H), δ 5.58 (13; s, 1H), δ 6.11 (14; s, 1H) (Figure 3.18)

Synthesis of ZID-MA

ZID-alkyne was further functionalized by reacting the alkynes with 3-azidopropyl methacrylate in a CuAAC reaction in solution to obtain methacrylate-functionalized ZID (**ZID-MA**). In a round-bottom flask, 8 mg of ZID-alkyne (0.002 mol) was dissolved in 1.4 mL Milli-Q water. 0.2 mL of the following solutions each were added to the round-bottom flask: 1) a solution of 16.2 mL 3-azidopropyl methacrylate in 0.4 mL ethanol; 2) a solution of 1 mg $CuSO_4$ and 4.34 mg THPTA in 1 mL Milli-Q water; 3) a solution of 1 g Na-ascorbate in 5 mL Milli-Q water. The solution was stirred overnight at 30 °C. The obtained mixture was dialyzed against 500 mL demi water for three days with three medium exchanges. After evaporation of the solvent and lyophilization, 7.8 mg of a fluffy white powder was obtained with a yield of 90%. Based on ^{1}H-NMR, the conversion of alkyne to methacrylate groups was approximately 45%.

^{1}H-NMR (400 MHz, D_2O, 300 K) δ 2.30 (a; m, 45H), δ 2.50 (b; m, 10.5H), δ 3.29 (c; s, 77.3H), δ 3.71 (e; m, 113.8H), δ 3.96 (f; m, 52.2H), δ 5.66 and 5.97 (h; s, 4H), δ 8.06 (1; s, 1.8H) (Figure 3.19), **DOSY** (400 MHz, D_2O, 298K) (Figure 3.20)

3.6.2 NMR data

3-Azidopropyl methacrylate

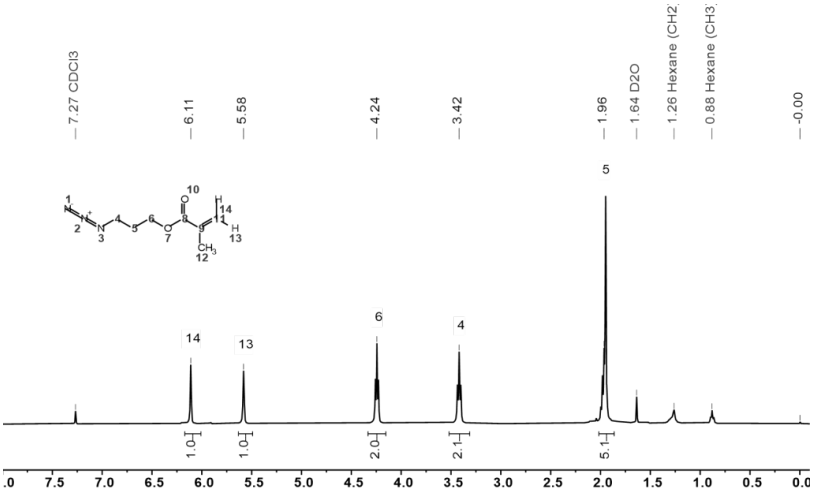

Figure 3.18 ^{1}H-NMR spectrum of 3-azidopropyl methacrylate in $CDCl_3$ (400 MHz, 298 K).

*Methacrylate-functionalized ZID (**ZID-MA**)*

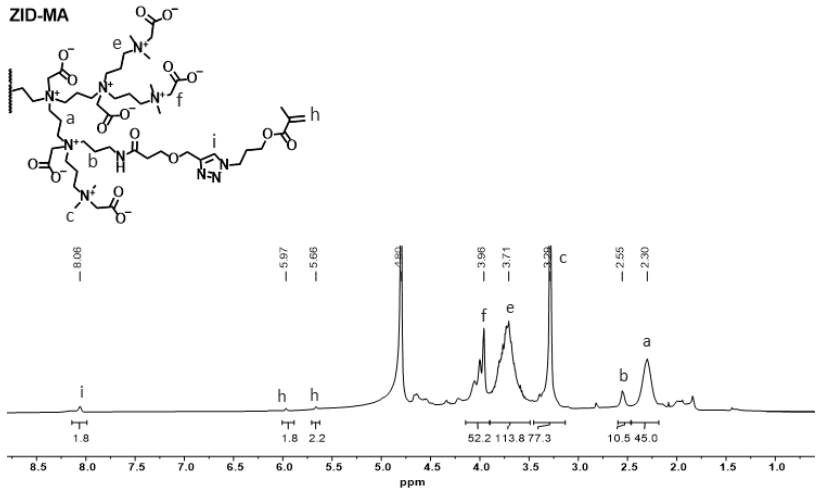

Figure 3.19 ^{1}H-NMR spectrum of **ZID-MA** in D_2O. (400 MHz, 298 K). The spectra was normalized by setting the combined integrals of peaks labelled *a* and *b* to a value of 56.

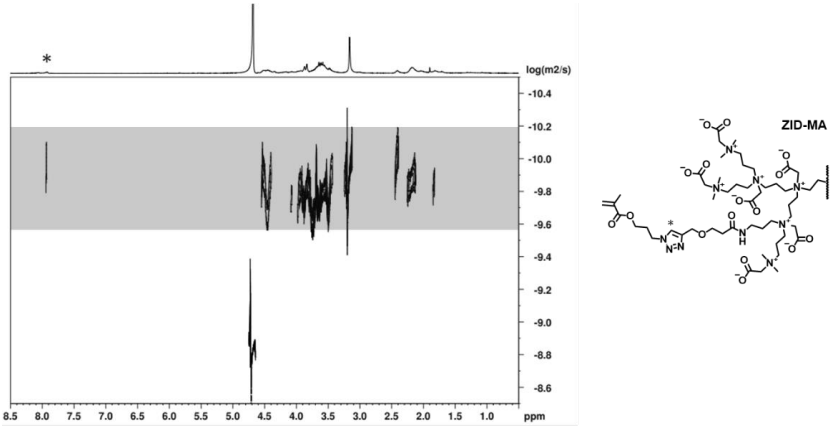

Figure 3.20 DOSY spectra of **ZID-MA**. The signals in the highlighted band correspond to the ZID and the indicative triazole ^{1}H signal is labeled by a star (*).

3.6.3 XPS data

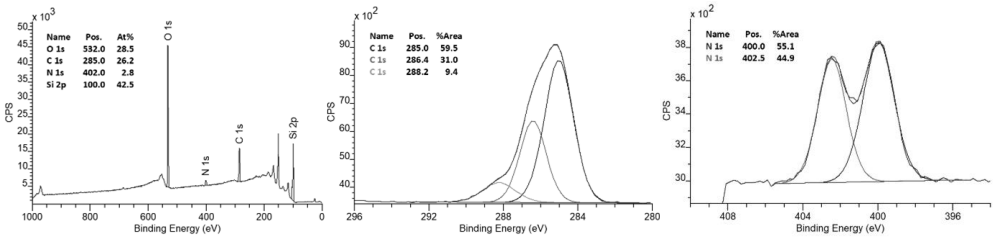

Figure 3.21 XPS wide scan (left), C_{1s} (middle) and N_{1s} narrow (right) spectra of ZID-MA on silicon oxide without additional UV curing step. This ZID-MA layer had a thickness of approximately 1.8 nm and a WCA of 35°.

3.6.4 IR data

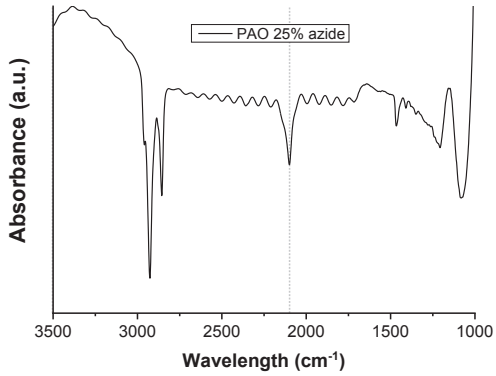

Figure 3.22 IR spectra of the octyl-diluted azidophosphonic acid (25%) modified PAO with the azide-signal at 2100 cm^{-1}. The interference- or fringing effects originate from reflections within the porous substrate.[65,66]

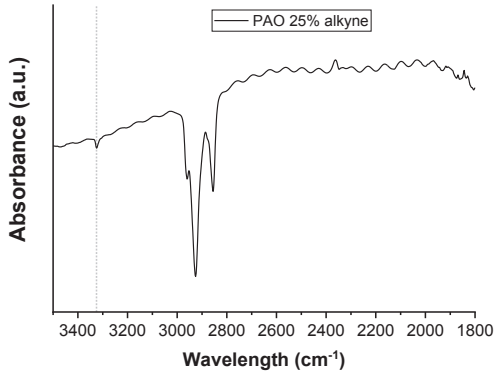

Figure 3.23 IR spectra of the octyl-diluted (25%) alkyne phosphonic acid modified PAO with the alkyne C≡C–H stretch signal at 3325 cm^{-1}. The interference- or fringing effects originate from reflections within the porous substrate.[65,66]

Chapter 4

Zwitterionic Dendrimer – Polymer Hybrid Copolymers for Self-Assembling Antifouling Coatings

Esther Roeven | Luc Scheres | Maarten M. J. Smulders | Han Zuilhof

Published in **European Polymer Journal 2021, 156, 110578**
DOI:10.1016/j.eurpolymj.2021.110578

Abstract

In this chapter, we show two different routes to synthesize polymer-dendrimer hybrids by the coupling of poly(L-lysine) and zwitterionic dendrimers (ZIDs). Poly(L-lysine) (PLL) is used because of its advantageous self-assembly properties onto silicon oxide by charged-based interactions between the lysine groups and the negatively charged surface, whilst the coupled ZIDs provide antifouling properties. The first route yields network-like structures in which PLL and ZIDs are crosslinked by multiple amide bonds. By using different ratios of PLL and ZID, we vary the size of the formed networks. A more defined, linear PLL-ZID macromolecule is formed via coupling of multiple ZIDs to PLL in a controlled way by a copper-catalyzed azide/alkyne cycloaddition (CuAAC) "click" reaction. Following synthesis and characterization of the two different types of PLL-ZID macromolecules, they are self-assembled on silicon oxide surfaces from aqueous solutions in a single step, to form thin, hydrophilic coatings. Their potential use as antifouling coatings is tested by fluorescence microscopy and quartz crystal microbalance (QCM) with foulants such a single proteins and diluted human serum. Finally, by performing an on-surface biofunctionalization step by biotin we demonstrate it is possible to use these polymer-dendrimer hybrids for selective detection of target analytes (here: streptavidin), while the underlying coating maintains its antifouling properties.

This method presents a new, straightforward approach for the manufacturing of PLL-ZID based coatings that can be pre-synthesized partly or fully and applied as coating in a single self-assembly step. Both steps can take place in aqueous solution and under ambient conditions, and result in stable coatings that not only display antifouling properties but also maintain the possibility of further functionalization.

4.1 Introduction

Most synthetic polymers are linear or only moderately branched. In contrast, dendrimers are a class of macromolecules with precisely defined, highly branched structures and are obtained by sequential reactions through divergent or convergent synthesis.[1–5] As a result, they possess a distinct molecular architecture with a core, branches and terminal functional groups. The high level of control over dendritic architectures, the presence of internal cavities and the possibility for multivalent binding have, for example, focused attention on dendrimers as potential carriers in biomedical applications.[3,4,6] While dendrimers modified with charged groups have found use for *in vivo* drug delivery, the presence of a high density of charged groups on the dendrimer structure also enables an entirely new application that has so far been largely overlooked. That is, highly charged dendrimers with no net charge, *i.e.* zwitterionic dendrimers (ZID) are potentially very interesting for surface chemistry applications since zwitterionic coatings have been shown to drastically reduce (bio)fouling of surfaces when applied as a coating.[7,8] Previously, charged dendrimers have been used as coating, although mainly in layer-by-layer approaches where alternating layers of positively and negatively charged dendrimers were assembled on a surface.[2,9,10] In contrast, the use of a fully and permanently zwitterionic dendrimer-based coating has not been reported in literature. So far, only the use of (partially) zwitterionic dendrimers has been reported for use in other biomedical applications such as drug delivery, sensing and MRI contrast agents.[11–21]

Building blocks for a new type of zwitterionic antifouling coating should have a high density of opposite charges, creating a strong zwitterionic character, while remaining overall neutral.[22] We chose to work with zwitterionic dendrimers as building blocks as they uniquely combine a well-defined and monodisperse nature with a relatively large size, and the possibility for multivalent coupling towards surface immobilization, crosslinking or eventually biofunctionalization. In our lab, fully zwitterionic, carboxybetaine dendrimers were previously developed.[13] Additionally, also zwitterionic dendrimers (ZID) that contain a variable number of alkyne and azide groups that allow coupling by click chemistry were synthesized.[13] In search for a method to strongly bind these ZIDs to a surface as a coating, we selected poly(L-lysine) (PLL) to covalently couple the ZID to. PLL is known for its affinity towards, *e.g.*, silicon oxide, metal oxide and polymeric surfaces.[23–28] The polymer self-assembles to silicon oxide at pH > 2, driven by multiple electrostatic attractions between the negatively charged surface and the positively charged pendant amine groups present in PLL.[29,30] For example, a well-known and widely used combination of PLL with antifouling side groups is poly(L-lysine)-*graft*-poly(ethylene glycol) (PLL-*g*-PEG).[23–28] In other studies, also the coupling of different antifouling polymers to a PLL backbone was shown to result in coatings with antifouling properties.[25,31] However, to the best of our knowledge, no combination of linear polymers and zwitterionic dendrimers has been investigated before for use as antifouling coating. For other applications, the unique combination of linear and dendritic copolymers was first described in the beginning of 1990s by the group of Fréchet.[32–34] Subsequently, other research groups have been developing block,[35–37] star,[38,39] linearly alternating linear-dendrimer hybrid architectures,[34] crosslinked superstructures,[40] and brush-like polymers with dendritic side chains.[41–43] These resulting linear-dendritic hybrids showed very interesting properties in terms of self-assembly, enhanced solubility and reduced toxicity and immunogenicity.[33,44]

Here we report the synthesis of two different architectures of dendrimer-PLL hybrids that were connected in two different ways (Figure 4.1). First we explored the random cross-coupling of the carboxylic acid groups of the carboxybetaine ZIDs and the terminal amine groups on the PLL in three different ZID : PLL ratios. This should create a large polymer network in which the ZID acts as crosslinking agent of the linear PLL chains. Next to this, a more controlled way of coupling the ZID to PLL was investigated. Namely, via the creation of specific covalent bonds to obtain a well-defined, non-networked macrostructure. The coupling between the ZID and PLL was established by a copper-catalyzed azide/alkyne cycloaddition (CuAAC) reaction[45] between a single terminal alkyne group on the ZID [13] and terminal azide groups on a commercially available azide-modified PLL. These two PLL-ZID macromolecules were first synthesized and characterized in solution (by techniques including NMR, DOSY and IR) prior to surface immobilization. In this study, silicon oxide was used as a model substrate because of its relevance in, *e.g.*, biosensors[46] and microfluidic devices.[47] After self-assembly on silicon oxide surfaces, the formed coatings were investigated using water contact angle (WCA) measurements and X-ray photoelectron spectroscopy (XPS). To investigate the potential perspective of the use of such PLL-ZID macromolecular coatings for antifouling purposes, we performed an investigation of the antifouling performance obtained for these hybrid PLL-ZID copolymer approaches. Quantitative protein adsorption onto a surface has been investigated by a variety of techniques, such as surface plasmon resonance (SPR), optical waveguide devices, atomic force microscopy (AFM) and ellipsometry.[25,48–51] Here, we first used fluorescence to study the protein repellence of fluorescently labeled proteins. The antifouling properties of selected PLL-ZID coatings against single proteins and human serum were subsequently studied in more detail with quartz crystal microbalance (QCM) studies. Finally, an on-surface biofunctionalization step by biotin was performed by activation of the carboxylate groups and reacting them with amino-biotin for the selective detection of streptavidin, while maintaining antifouling properties.

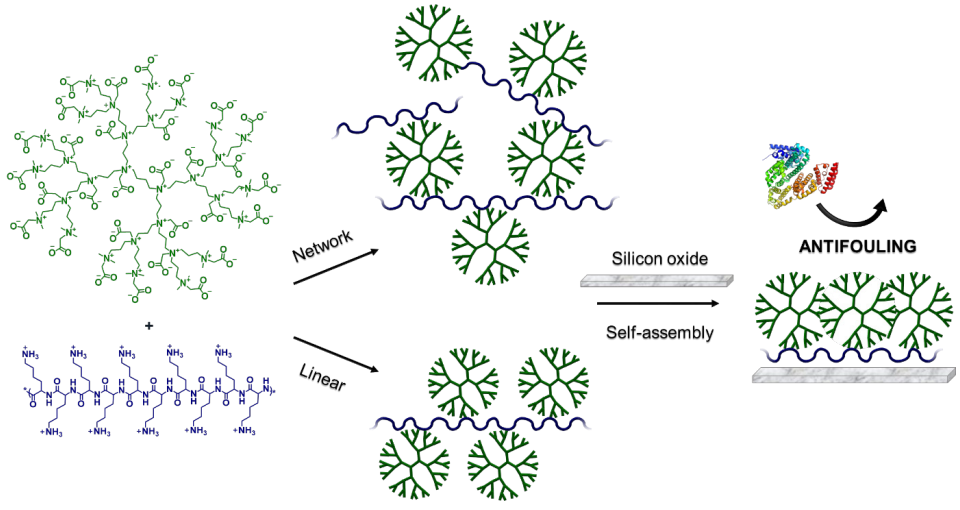

Figure 4.1 Molecular structure of ZID and PLL (left), and the formation of hybrid PLL-ZID macromolecules (as network or linear structure) and subsequent surface immobilization to create antifouling coatings.

4.2 Results and Discussion

We will first discuss the synthesis, characterization and surface immobilization of the poly(L-lysine)-zwitterionic dendrimer (PLL-ZID) networks. After that, the linear PLL-ZID macrostructures will be discussed in a similar fashion. Subsequently, the antifouling studies on the formed coatings as measured by fluorescence and QCM will be discussed and evaluated.

4.2.1 Synthesis and characterization of PLL-ZID networks

To obtain the poly(L-lysine)-zwitterionic dendrimer (PLL-ZID) networks, a suitable coupling reaction between the zwitterionic dendrimer and the PLL polymer backbone was needed. The presence of a carboxylic acid group on the former, and an amine group on the latter, prompted us to achieve the coupling via amide bond formation, as this is a widely used for the bioconjugation of carboxybetaine zwitterionic polymers (Figure 4.2).[52–55]

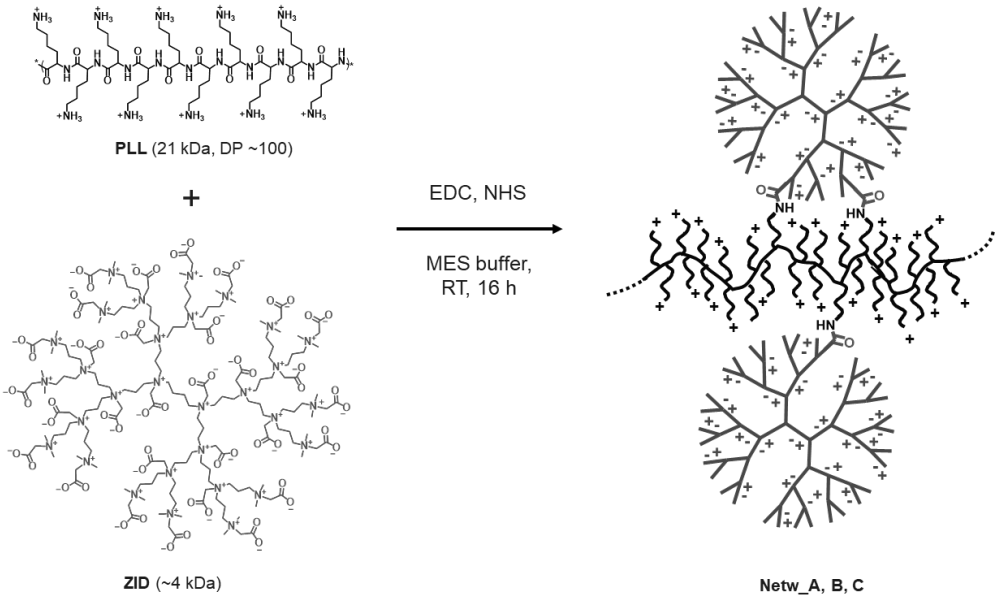

Figure 4.2 Schematic depiction of the formation of the PLL-ZID networks via NHS/EDC mediated amide bond formation.

The amide bond formation was performed by activation of the carboxylate groups on the dendrimer using *N*-hydroxysuccinimide (NHS) / 1-ethyl-3-[3-dimethylaminopropyl]-carbodiimide hydro-chloride (EDC) chemistry.[53] As both reactants in this coupling reaction contain a high number of (potentially) reacting groups (*i.e.* ~100 lysines on PLL and ~30 carboxylate groups on the dendrimer), it was anticipated that depending on the ratio between the two reactants different network structures could be formed. Therefore, three different ratios of ZID : PLL were explored to form the networks, which we labelled as **Netw_A**, **Netw_B** and **Netw_C** (see Table 4.1 for their feed ratio).

Table 4.1 Different ratios of ZID : PLL used in the formation of PLL-ZID networks expressed in molar, reactive group and mass ratios.

	Molar ratio			Reactive group ratio			Mass ratio		
	PLL	**:**	**ZID**	**LYS**	**:**	**COO^-**	**PLL**	**:**	**ZID**
Netw_A	1	:	5000	1	:	1500	1	:	720
Netw_B	1	:	500	1	:	150	1	:	72
Netw_C	1	:	50	1	:	15	1	:	7.2

After letting the NHS-mediated amide coupling reaction run for 24 h, the mixture was extensively dialyzed against water to remove all low-molecular weight species (unreacted EDC and NHS, buffer salts, etc.). After freeze-drying, the obtained product was first of all characterized by ^{1}H NMR spectroscopy, revealing the presence of both the ZID and PLL component in the product. The ratio between the ZID and PLL signals showed an expected trend in line with the different ratios in starting materials (Figure 4.3).

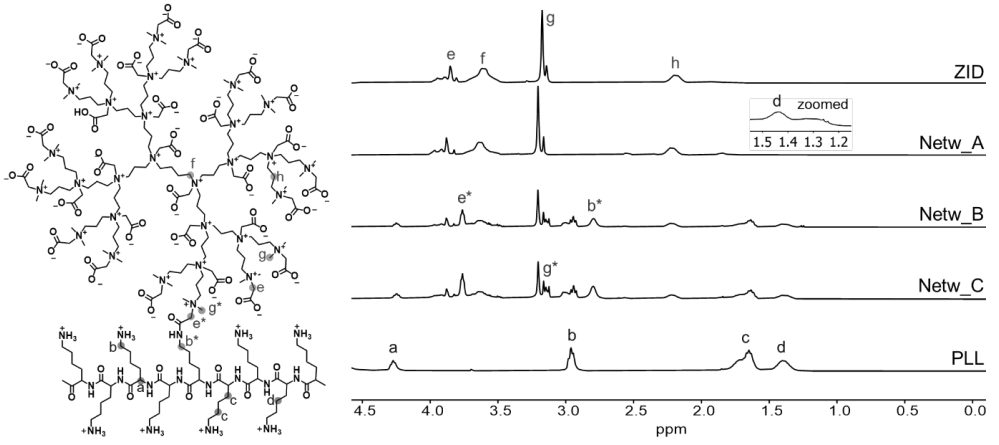

Figure 4.3 ^{1}H-NMR spectrum of the PLL-ZID networks and starting materials. From top to bottom: ZID, **Netw_A**, **Netw_B**, **Netw_C** and PLL (in D_2O, 400 MHz, 298 K). The inset for **Netw_A** is a zoomed-in fraction of the **Netw_A** spectrum to show the presence of the small PLL signal *d*.

The shift of peaks *e*, *b* and *g* to *e**, *b** and *g**, respectively, in Figure 4.3 indicates binding of ZID to PLL via amide bonds. Although all PLL-ZID networks were extensively dialyzed, especially in **Netw_A**, there seems to be more ZID present than can be explained by the amide bond formation. This suggests that, apart from the formed covalent bonds, most likely also charged-based interactions contribute to binding between PLL and ZID, which is not unsurprising given the highly charged nature of both components. Apart from the newly formed signals *e**, *b** and *g**, also the original signals were still present, implying that not all available amide and carboxylate groups reacted, which can be understood considering the steric clash that would occur at high or full conversion. The incomplete conversion can be further attributed to the fact that this reaction was performed at pH 6, meaning

that not all reactive groups are in the correct protonation state (pK_a^{LYS} ~10 and pK_a^{COO-} ~2 due to the short distance between the carboxyl group and the cationic site),[56,57] whereas the NHS coupling reaction is unsuccessful at both acidic and alkaline pH.[58] Such incomplete conversion is, however, in this case desirable, as for the surface binding it is essential to still have unreacted lysine groups available. Additionally, infrared (IR) spectroscopy on the three networks also showed the expected varying in signals origination from PLL and ZID (see SI). However, no newly formed amide signals could be observed since PLL as one of the starting materials already is a polyamide.

Diffusion-ordered spectroscopy (DOSY) allowed us to assess the dimensions of the three formed networks. The PLL-ZID networks with **Netw_B** and **Netw_C** yielded hydrodynamic volumes of 1.5×10^3 and 1.2×10^3 nm^3, respectively, whereas the PLL starting material had a hydrodynamic volume of 8.6×10^2 nm^3 (see Supporting Information, Table 4.2). An individual ZID molecule has an estimated volume of 20 nm^3.[13] Based on the increase in hydrodynamic volume, we infer that –on average– some tens of dendrimers are linked to the PLL backbone. Unfortunately, for **Netw_A** the ^{1}H spectrum was dominated by residual unbound ZID in such a way that no DOSY trace for the PLL-ZID network signals could be obtained.

4.2.2 Surface immobilization of the PLL-ZID networks

In order to form an antifouling coating by PLL-ZID networks, this crosslinked polymer network was self-assembled onto the surface by charged-based interactions between the free (protonated) terminal amine moieties of the lysine groups of PLL and the negatively charged silicon oxide surface, according to established protocols (Figure 4.4).[28,59]

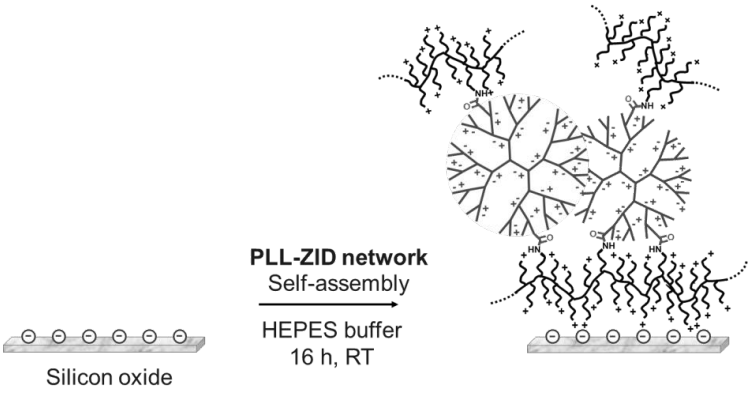

Figure 4.4 Schematic depiction of the self-assembly of a PLL-ZID network onto a silicon oxide surface.

Once immobilized, the ZIDs should provide antifouling properties to the surface. To this end, PLL-ZID networks were self-assembled by overnight immersion of freshly cleaned, negatively charged silicon oxide surfaces in a 0.1 mg/mL solution of PLL-ZID in HEPES buffer, followed by washing with HEPES buffer and MilliQ water (following previously reported procedures.[25,31]) XPS analysis of the coatings made by **Netw_A**, **Netw_B** and **Netw_C** was performed. Additionally, coatings with unfunctionalized PLL were made as a reference and also characterized by XPS. All the obtained coatings showed signals

for N (N_{1s} at 400 eV) and C (C_{1s} at 285 eV) on the silicon oxide surfaces, which is in agreement with the presence of the polymer network (Figure 4.5). Furthermore, the three PLL-ZID network coatings have a higher signal for O (O_{1s} at 530 eV), which can be ascribed to the carboxylate groups in ZID. The layer thickness of the PLL and PLL-ZID network coatings were calculated using the Si/C ratio in the XPS wide scan to calculate the average thickness of the layers,[60,61] and was found to be 0.7 nm for PLL and approximately 0.8 nm for all the networks. Such a low layer thickness for a surface-immobilized polymer is in agreement with other types of surface-immobilized PLL-based bottlebrushes reported in literature,[23–25] and typically attributed to the ultra-high vacuum conditions of XPS thickness measurements that yield a collapsed polymer layer that will expand upon immersion in solution.

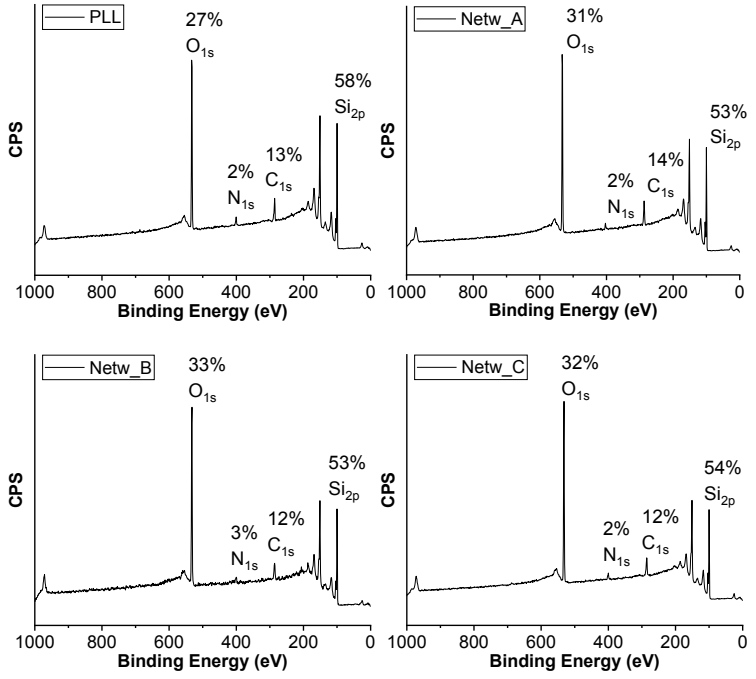

Figure 4.5 XPS wide spectra of the surface-immobilized PLL and PLL-ZID networks Netw_A, Netw_B and Netw_C.

The N_{1s} narrow scan of the coating made by PLL revealed peaks at 399.8 eV and 402.0 eV, which originated from non-protonated and protonated lysine amine moieties, respectively. The ZID-PLL networks showed an additional peak at 403.0 eV, which can be attributed to the dendrimer's quaternary N^+. Similar to the trend observed by ^{1}H-NMR for the three networks, the N_{1s} narrow scans also showed an increase in the amount of incorporated ZIDs via an increased fraction of the ZID-based quaternary nitrogen atoms (Figure 4.6).

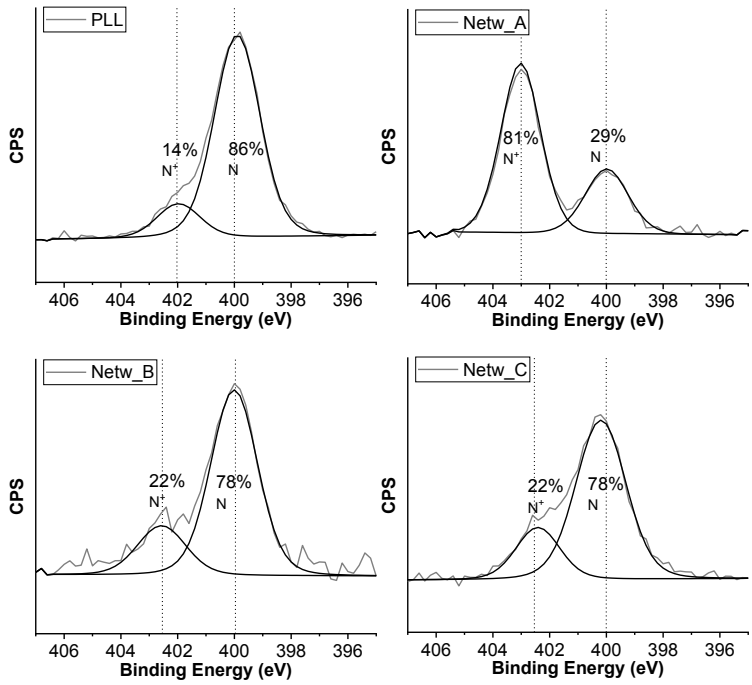

Figure 4.6 XPS N_{1s} narrow spectra of surface-immobilized **Netw_A**, **Netw_B** and **Netw_C** and PLL.

Additionally, the water contact angle (WCA) of all coatings made by **Netw_A**, **Netw_B** and **Netw_C** displayed full wetting, compared to the WCA of the PLL coating being <20°, but remaining a droplet on the surface. By eye, a clear difference in hydrophilicity was observed but unfortunately the difference could not be quantified due to the lower limit of angle detection of the WCA setup. The high hydrophilicity can be ascribed to the ZIDs which are attached to the PLL.

Combining all data shows that a macromolecular PLL-ZID network is formed via a combination of covalent amine bonds and charge-based interactions. These PLL-ZID networks can be applied as coatings that will self-assemble onto silicon oxide. While possible, the presence of charge-based binding of additional ZID units reduced the degree of definition of the resulting coatings. In order to find a more defined macromolecular structure, a second type binding strategy was studied. This strategy involved the incorporation of a defined number of complementary functional groups on PLL and ZID, respectively that will react to form a covalent bond, which should lead to linear PLL-ZID macrostructures.

4.2.3 Synthesis and characterization of linear PLL-ZID macrostructures by click chemistry

To obtain poly(L-lysine)-zwitterionic dendrimer (PLL-ZID) macrostructures with a well-defined, linear macrostructure, we set out to form covalent bonds by a Cu-catalyzed azide/alkyne cycloaddition (CuAAC) reaction between a single terminal alkyne group on the ZID and terminal azide groups on a commercially available azide-modified PLL (one out of five lysines contains an azide group).[45] Since we used ZIDs containing *one* alkyne group, as previously reported by our group.[13] This system leads to a better defined product compared to the more random networks that have multiple possible interactions between PLL and a single ZID (Figure 4.7).

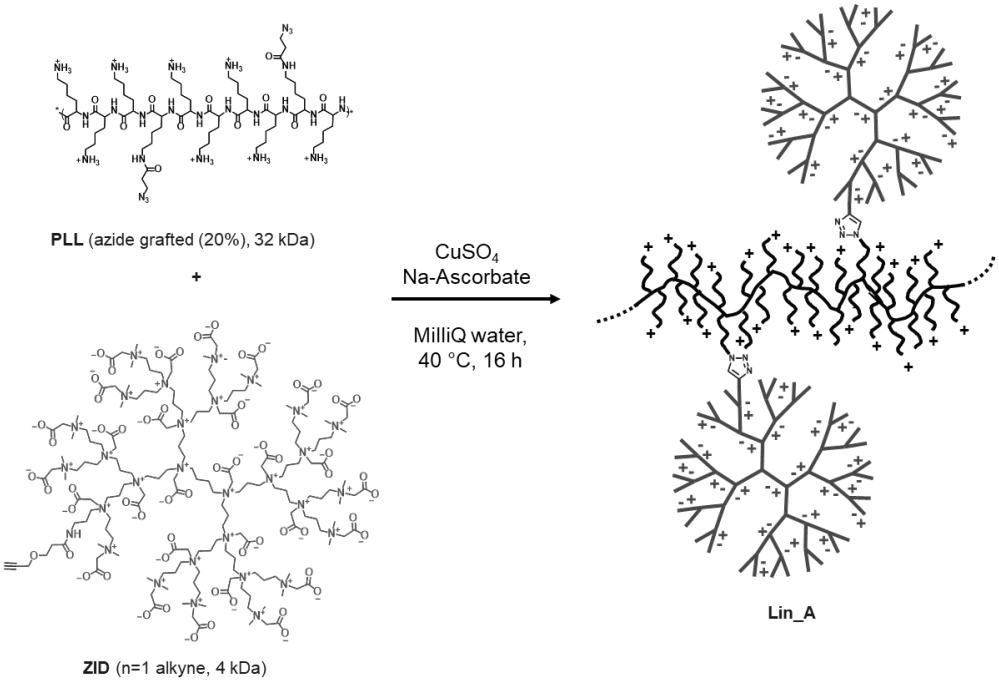

Figure 4.7 Schematic depiction of the formation of the linear PLL-ZID macrostructure **Lin_A** via copper(I)-mediated triazole ring formation.

After letting the CuAAC reaction run overnight at 40 °C, the mixture was extensively dialyzed against water to remove the copper sulfate and sodium ascorbate. After freeze-drying, the presence of both the ZID and PLL in the product was confirmed by ^{1}H NMR spectroscopy (Figure 4.8). Direct evidence for the success of the reaction is the triazole proton signal at δ 8.02 ppm. While this is a relatively small signal as a result of the large overall hybrid macromolecular structure, it could definitely be discerned in the ^{1}H NMR spectrum. When normalizing the integrals to the ZID signal *e* (δ 2.14 ppm), the integral ratio of this signal compared to *a* (triazole, δ 8.02 ppm) and *f* (PLL, δ 1.34 ppm) would imply a

conversion of approximately 90% of all PLL-based azide groups in the CuAAC reaction. Since the integration of peaks *a* and *f* is rather difficult, we treat this value only to mean that a significant fraction of the azide groups has reacted (see XPS-based data below for a more precise determination). Unfortunately, the ^{1}H spectrum was dominated by residual unbound ZID in such a way, that no DOSY trace for the **Lin_A** signals could be obtained. Infrared (IR) spectroscopy showed the disappearance of the characteristic azide signal (at 2108 cm^{-1}) upon reaction with the ZID's alkyne moiety in the CuAAC reaction, next to the expected signals for the ZID and PLL (Figure 4.24 in the Supporting Information).

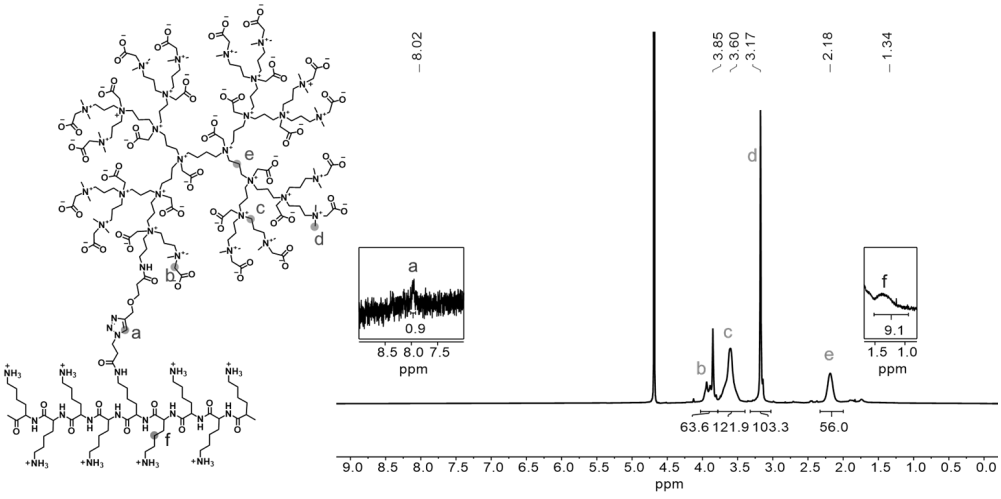

Figure 4.8 ^{1}H-NMR spectrum of the linear PLL-ZID macrostructure **Lin_A** (in D_2O, 400 MHz, 298 K).

4.2.4 Surface immobilization of linear PLL-ZID

The linear PLL-ZID **Lin_A** was self-assembled onto silicon oxide in a similar fashion as described for the PLL-ZID networks. Upon washing and drying, the coating made by **Lin_A** was analyzed using XPS. Again, the XPS wide scan showed signals for N (at 400 eV) and C (285 eV) on the silicon oxide surfaces, which confirms the formation of the polymer network (Figure 4.10). The layer thickness of the **Lin_A** PLL-ZID was calculated based om the Si/C ratio in the XPS wide scan and was found to be approximately 1.0 nm. Also here, the relatively thin layer is due to the collapsed polymer layer in the ultra-high vacuum within the XPS machine. The observed dry thickness was in line with the thicknesses of the PLL (0.7 nm) and the PLL-ZID networks **Netw_A**, **Netw_B**, **Netw_C** (all approximately 0.8 nm).

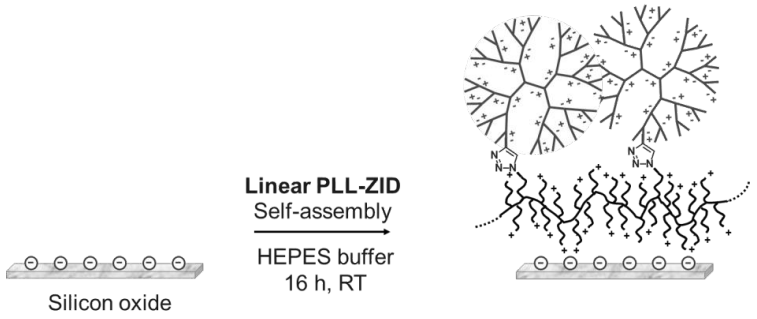

Figure 4.9 Schematic depiction of the self-assembly of linear PLL-ZID **Lin_A** on silicon oxide.

The XPS N_{1s} scan showed the characteristic peaks for neutral (400.0 eV), and quaternary (403.0 eV) amines with a ratio of 53 : 47. Since the theoretical ratio at full conversion is 17 : 25, the conversion of the click reaction was estimated to be roughly 60%. While this value is somewhat lower than the value obtained from the NMR integrations, this might be explained by the relatively small (and hence difficult to reliably integrate) azide signal needed for the NMR integration; in addition it means that loss of the IR azide signal does not imply full reaction, which can be partially attributed to peak broadening of the azide peaks due to the interaction of the polar azide groups with the highly polar ZID units.[62] Additionally, the coating made by linear PLL-ZID **Lin_A** was extremely hydrophilic and fully wetting when applying a droplet of water in order to determine the WCA. This extreme hydrophilicity is in line with the properties found for the PLL-ZID networks. In summary, we conclude the click conversion to have occurred with moderate to good yields. Given the size of the dendrimers that should click to the PLL backbone, and the concomitant steric hindrance, it is not surprising that the click reaction stopped before full conversion.

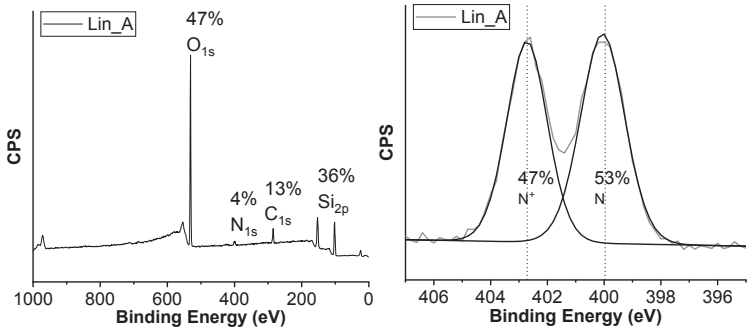

Figure 4.10 XPS wide (left) and N_{1s} narrow (right) spectra of surface-immobilized PLL-ZID **Lin_A**.

4.2.5 Antifouling properties of the PLL-ZID based coatings

Fluorescence microscopy

Having successfully synthesized and immobilized the different PLL-ZID coatings on silicon oxide surfaces, a preliminary investigation of their antifouling properties was performed. Firstly, the degree of fouling was related to the amount of protein adsorption by fluorescence microscopy, by exposing the coatings to fluorescently labelled single-protein solutions.[55,63–65] In this study, lysozyme (LYS), bovine serum albumin (BSA) and fibrinogen (FIB) were used as model proteins at concentrations of 1 mg/mL in phosphate-buffered saline (PBS) and contacted with the surfaces for 15 min before washing with PBS. BSA was chosen since it is one of the most common proteins in blood plasma with an overall negative charge at pH 7.4 (PBS buffer).[66] LYS is a relatively small, hydrophilic protein and was used because of its overall positive charge at pH 7.4 (PBS buffer).[67] FIB was used as a more challenging fouling model protein since it plays a major role in clotting of the blood due to formation of fibrin networks, and platelet plug formation.[68]

As controls for our single-protein adsorption experiments, we used bare silicon oxide surfaces and surfaces modified with commercially available PLL-PEG, which is known to have good single-protein antifouling properties.[24] In the fluorescence study, the unmodified blank silicon oxide surface showed higher fluorescence intensities from all protein solutions (Figure 4.11), indicating significant fouling compared to all coated silicon oxide surfaces. Furthermore, the coating made by **Netw_C** (which contains the least ZID) showed most fouling of all the coated surfaces, especially in the case of BSA and FIB, though it still performed better than the blank surface. The other coatings **Netw_B**, **Netw_A** and **Lin_A** performed very similar to coatings made by commercially available PLL-PEG. It should be noted, however, that these data are close to the limit of detection for this method and close to the autofluorescence intensity as measured for an unexposed, blank silicon oxide surface. Therefore, by using this method, we could not further differentiate between the antifouling performance of our synthesized coatings, in relation to the PLL-PEG coating.

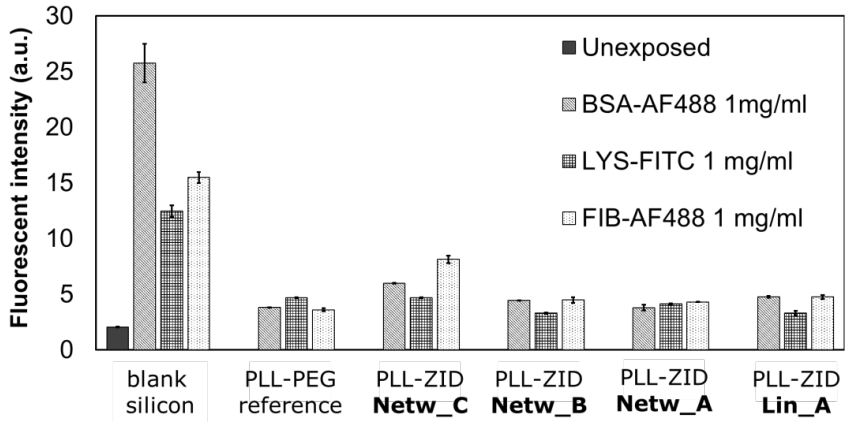

Figure 4.11 Fluorescence intensities of uncoated and coated silicon oxide surfaces after exposure to solutions containing BSA-AF488, LYS-FITC or FIB-AF488.

Quartz crystal microbalance

To overcome these limitations, both type of coatings were further tested by an additional, more quantitative method: quartz crystal microbalance with dissipation monitoring (QCM-D).[69] Recently, QCM-D has emerged as a precise and reliable method to monitor and quantify surface adsorption from aqueous solutions onto a broad variety of surfaces.[48,70–77] QCM-D measures real-time resonating frequency and dissipation shifts of a quartz crystal resonator. These shifts can provide information on mass (frequency related) and physical properties (dissipation related) of an adsorbed layer on the quartz surface.[69] The recorded data can be modelled to further calculate viscoelastic properties (*i.e.* viscosity, elastic modulus) as well as wet thickness of the adsorbed layer using the Sauerbrey equation.[78] Hence, QCM-D offers a suitable and convenient tool to investigate protein adsorption on silicon oxide surfaces.[70] **Netw_A** was chosen as a representative for the PLL-ZID networks and measured alongside linear PLL-ZID **Lin_A** – which showed promising initial results – to compare to blank silicon and PLL-PEG. Starting from QCM-D sensors with a silicon oxide top layer, we were able to use the previously described protocol to coat these sensors with **Lin_A**, **Netw_A** or PLL-PEG. The frequency change of the QCM-D crystal upon passing of a solution of foulant through the QCM-D cell was monitored and compared to the response of non-modified, blank silicon oxide. The surface adsorption of bovine serum albumin (BSA), lysozyme (LYS), fibrinogen (FIB) and diluted human serum (HS) foulant solutions were monitored and quantified (Figure 4.12).

All four tested foulant solutions showed a very similar response pattern. The sensor surface showed a stable baseline when being flushed with PBS buffer (0–500 sec). Upon switching to the foulant solution, a distinct change in frequency was observed, that could be related to binding of foulant to the surface. After 2400 sec, when the medium was switched back to PBS buffer, the frequency dropped, which can be explained by the release of weakly bound protein. After equilibration, a certain fraction of protein was still bound, which was referred to as the level of fouling. As expected –and in line with the fluorescence microscopy results– all modified sensors (**Lin_A**, **Netw_A** and PLL-PEG) showed clearly less adsorption compared to the blank silicon oxide sensor. Furthermore, **Lin_A** outperformed **Netw_A** consistently by adsorbing less protein mass upon contact with all fouling solutions. We attribute this to the less defined system and limited flexibility of **Netw_A** coatings: whereas the system in **Lin_A** is free to self-organize at the surface – meaning the lysines pointing towards the surfaces while the ZIDs having an upward orientation – the random 3D networks in **Netw_A** might not have this freedom, leading to a coating with a top-layer that possesses a lower density of ZID.

The low adsorption of BSA (10 mg/mL, isoelectric point: 4.7, MW: 66 kDa) on all modified sensors compared to the (less hydrophilic) unmodified silicon oxide sensor can be explained by the effective resistance of the coatings to fouling mediated by hydrophobic interactions. Especially the fact that the newly developed Lin_A outperforms the commercially available PLL-PEG (WCA = 31°), could be due to the more hydrophilic character of the **Lin_A**-based coating (WCA <20°). Lysozyme (10 mg/mL, isoelectric point: 11, MW: 14 kDa) was selected due to its net positive charge, in contrast to the negative charge of the other proteins tested, in order to assess the influence of electrostatic interactions. Both PLL-ZID-based coating showed increased adsorption in LYS fouling tests compared to BSA, but in both cases still lower than the uncoated silicon oxide surface. On the other hand, PLL-

PEG showed very similar fouling as observed for BSA. Fouling by FIB (10 mg/mL; isoelectric point 5.7, MW: 340 kDa) was strongly reduced by **Lin_A** and PLL-PEG coatings. The excellent antifouling by PEG is in agreement with previous works showing resistance to fouling from FIB.[79,80] Compared to **Lin_A** and PLL-PEG, a higher fouling was observed on **Netw_A**, probably due to the less defined system, which might logically also lead to less defined coatings. Amongst the tested single-protein solutions, FIB showed to be most fouling, especially on the uncoated blank surface, which was previously observed in literature by SPR.[81] Next to testing the antifouling behavior of the coatings against single protein solutions, we also tested human serum (5% in PBS) to more closely mimic the protein adsorption that would occur in biological fluids.[82] Both coatings by **Netw_A** and **Lin_A** showed clearly decreased fouling compared to the blank silicon oxide sensors. The newly developed **Lin_A** even performed equally well as the commercially available PLL-PEG, probably due to the more hydrophilic character of the **Lin_A**-based coating.

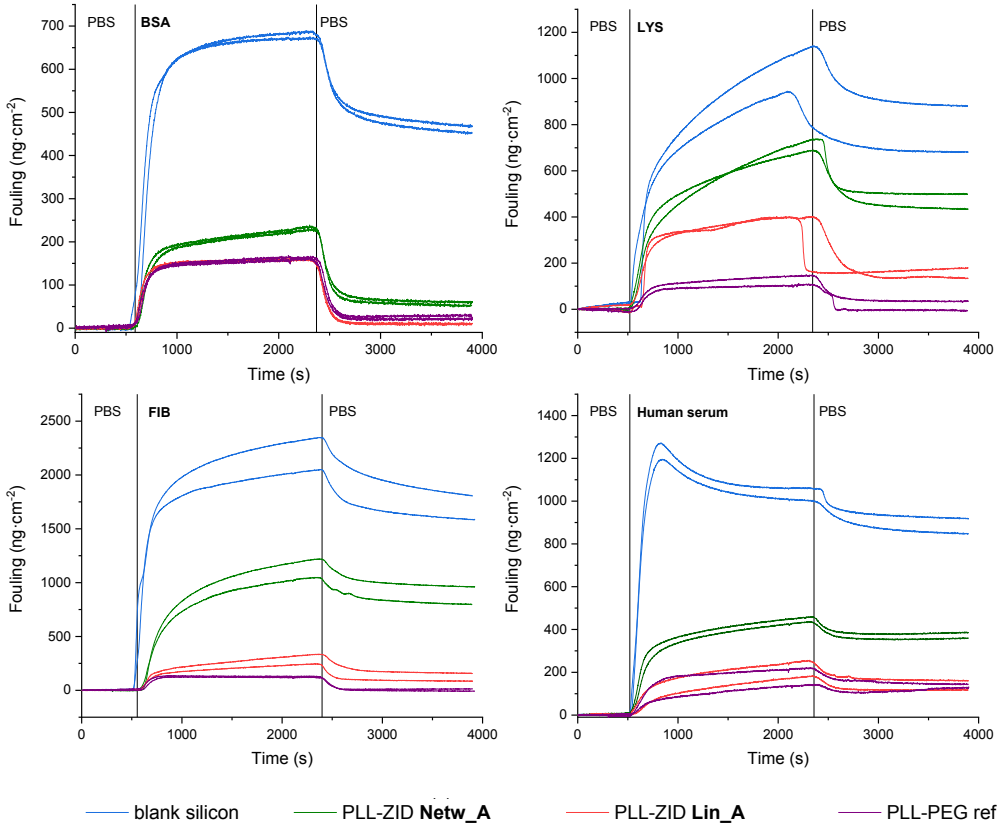

Figure 4.12 QCM-D protein adsorption of three protein solutions (BSA, LYS and FIB at 10 mg/mL in PBS) and human serum (5% in PBS) measured *in duplo*. Absolute mass adsorptions were calculated from the frequency changes by using the Sauerbrey equation (see SI).

The newly developed PLL-ZID macrostructures – particularly **Lin_A** – exhibited a decent resistance to fouling from single-protein solutions as well as diluted human serum, as revealed by fluorescence and QCM-D data. While the linear ZID-PLL platform does not yet meet the ultralow fouling levels as described in literature for the currently best performing coatings,[54,55,83–89] the results are obtained with physiologically relevant protein concentrations (10 mg/mL) and contact times (30 min) on a platform that involves only a single self-assembly step from an aqueous solution in an ambient atmosphere. Specifically, the low antifouling levels of <1 ng·cm^{-2} in single protein solutions such as BSA, LYS and FIB have frequently been shown for relatively thick (>30 nm) zwitterionic polymer brush coatings using lower concentrations of proteins, such as 0.1 mg/mL and 1.0 mg/mL [90] and shorter fouling exposure times (<30 min).[65,88,90,91] In addition, those coatings were obtained by multiple-step surface-initiated controlled radical polymerizations usually in an inert atmosphere, which makes it –in contrast to our approach– difficult to scale up.[7]

4.2.6 Biofunctionalization

To further develop the concept of PLL–ZID complexes as coatings, we also tested their potential for use as bio-interactive coatings which may find their application towards selective binding in, *e.g.*, biosensors and tissue engineering.[54,92,93] Since one of the most studied bio-interactions is that between biotin and streptavidin, biotin was chosen as a functional group to be immobilized on the surface of the coating to selectively capture streptavidin. The binding between biotin and streptavidin is rapid and robust and therefore and ideal candidate to test bio-selective interactions on our newly developed platform [94–96]. We selected the **Lin_A-**based coating to functionalize with biotin to be tested for bio-selective interactions with streptavidin, with the hypothesis that it would maintain its antifouling properties against BSA (1 mg/mL). After immobilizing **Lin_A** on a surface, free carboxylates on the dendrimer are still present on the surface. These carboxylate groups, allow for activation by NHS/EDC –in a manner similar to what we used for synthesis of the PLL-ZID networks– to couple a commercially available amino-functionalized biotin (Figure 4.13) [55,97,98].

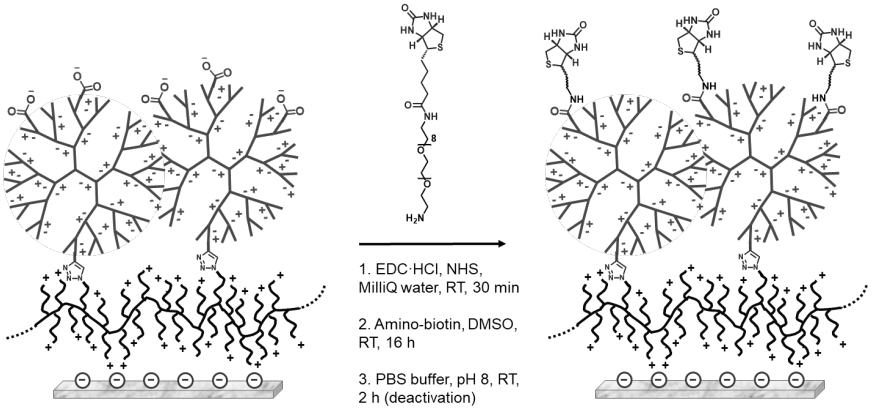

Figure 4.13 Biotinylation of **Lin_A** PLL-ZID coated silicon oxide.

After functionalizing the **Lin_A** based coating on the QCM-D sensor with biotin, the coating was tested for bio-selective interactions with streptavidin whilst maintaining its antifouling properties against BSA (1 mg/mL). As controls, blank silicon oxide, non-biotinylated **Lin_A** and PLL-PEG were also monitored for their response towards streptavidin (Figure 4.14). The sensors showed stable baselines when being flushed with PBS buffer (0–500 sec). Upon switching to a streptavidin solution (0.1 mg/mL), a distinct and very fast response was observed for *only* the biotinylated **Lin_A**. This indicated selective (and rapid) binding of streptavidin to the biotinylated **Lin_A**, whereas the other surfaces showed no clear signs of adsorption. After switching to PBS buffer, the signal remained stable, which indicates no release of streptavidin due to the strong binding of biotin-streptavidin.[99] To test if the **Lin_A** based coating maintained its antifouling properties after biotinylation and binding with streptavidin, a second test was performed by flushing a BSA solution (from 4100 to 5900 sec), followed by flushing with PBS for another 1500 sec. As anticipated, a similar response to the initial antifouling test (Figure 4.12) was observed: a distinct change in frequency, related to binding of BSA to the surface, followed by a drop in signal upon switching back to PBS buffer caused by release of weakly bound protein. A quantitative comparison between the unfunctionalized and biotin-functionalized **Lin_A** coatings yielded a BSA adsorption of approximately 6 and 10 ng·cm^{-2}, respectively. This indicates that the antifouling properties of the biotinylated **Lin_A** were maintained, also after binding of streptavidin.

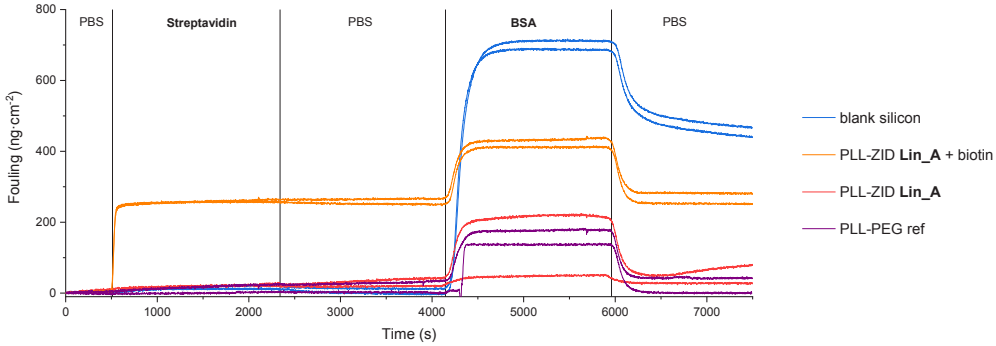

Figure 4.14 QCM-D plot of selective streptavidin binding (0.1 mg/mL), followed by an antifouling test with BSA (1 mg/mL in PBS). Absolute mass adsorptions were calculated from the frequency changes by using the Sauerbrey equation (see Supporting Information).

4.3 Conclusion

In this work we developed two different routes to synthesize polymer-dendrimer hybrids by the interconnection of PLL and ZID. The first route lead to network-like structures in which PLL and ZIDs were crosslinked by multiple amide bonds. By using different ratios of PLL and ZID, we could vary the size and PLL:ZID ratio in the formed networks. The second route lead to a more defined, linear PLL-ZID macromolecule, which was formed via click coupling of multiple ZIDs to a single PLL backbone. These two different types of PLL-ZID systems were then self-assembled onto silicon oxide surfaces from aqueous solutions in a single step, to form thin, hydrophilic coatings, which could be further bio-functionalized using the remaining carboxylate moieties in the coating. Especially the linear variant

yielded good antifouling properties towards single-protein solutions and diluted human serum, as shown in detail by using quartz crystal microbalance (QCM) for both the original as well as the biofunctionalized coatings. Given the ease with which these hybrid structures can be synthesized and surface-immobilized (single step, just immersing in aqueous solution under ambient conditions), these hybrid linear structures could be further studied, *e.g.*, by focusing on different (lengths of) polymer backbones and/or different dendrimer (generations).

4.4 Acknowledgements

The authors gratefully thank Hans Beijleveld, Dr. Andriy Kuzmyn, Sevil Sahin and Barend van Lagen for helpful discussions and instrumental support. This project was supported by NWO (LIFT program, grant 731.015.042) with Surfix BV as a partner.

4.5 References

1. Boas, U.; Christensen, J. B.; Heegaard, P. M. H. Dendrimers: Design, Synthesis and Chemical Properties. *J. Mater. Chem.* **2006**, *16* (38), 3785–3798.
2. Sato, K.; Anzai, J. I. Dendrimers in Layer-by-Layer Assemblies: Synthesis and Applications. *Molecules* **2013**, *18* (7), 8440–8460.
3. Abbasi, E.; Aval, S. F.; Akbarzadeh, A.; Milani, M.; Nasrabadi, H. T.; Joo, S. W.; Hanifehpour, Y.; Nejati-Koshki, K.; Pashaei-Asl, R. Dendrimers: Synthesis, Applications, and Properties. *Nanoscale Res. Lett.* **2014**, *9* (1), 1–10.
4. Lee, C. C.; MacKay, J. A.; Fréchet, J. M. J.; Szoka, F. C. Designing Dendrimers for Biological Applications. *Nat. Biotechnol.* **2005**, *23* (12), 1517–1526.
5. Newkome, G. R.; Shreiner, C. D. Poly(Amidoamine), Polypropylenimine, and Related Dendrimers and Dendrons Possessing Different 1 → 2 Branching Motifs: An Overview of the Divergent Procedures. *Polymer.* **2008**, *49* (1), 1–173.
6. Nimesh, S. *Gene Therapy: Potential Applications of Nanotechnology*; Woodhead Publishing, 2013.
7. Jiang, S.; Cao, Z. Ultralow-Fouling, Functionalizable, and Hydrolyzable Zwitterionic Materials and Their Derivatives for Biological Applications. *Adv. Mater.* **2010**, *22* (9), 920–932.
8. Schlenoff, J. B. Zwitteration: Coating Surfaces with Zwitterionic Functionality to Reduce Nonspecific Adsorption. *Langmuir* **2014**, *30* (32), 9625–9636.
9. Fernandes, E. G. R.; Vieira, N. C. S.; de Queiroz, A. A. A.; Guimarães, F. E. G.; Zucolotto, V. Immobilization of Poly (Propylene Imine) Dendrimer / Nickel Phtalocyanine as Nanostructured Multilayer Films To Be Used as Gate Membranes for SEGFET PH Sensors. *J. Phys. Chem. C* **2010**, *114* (14), 6478–6483.
10. Schlapak, R.; Armitage, D.; Saucedo-zeni, N.; Latini, G.; Gruber, H. J.; Mesquida, P.; Samotskaya, Y.; Hohage, M.; Cacialli, F.; Howorka, S. Preparation and Characterization of Dense Films of Poly (Amidoamine) Dendrimers on Indium Tin Oxide. *Langmuir* **2007**, *23* (17), 8916–8924.
11. Wang, L.; Wang, Z.; Ma, G.; Lin, W.; Chen, S. Reducing the Cytotoxity of Poly(Amidoamine) Dendrimers by Modification of a Single Layer of Carboxybetaine. *Langmuir* **2013**, *29* (28), 8914–8921.
12. Ramireddy, R. R.; Subrahmanyam, A. V.; Thayumanavan, S. Zwitterionic Moieties from the Huisgen Reaction: A Case Study with Amphiphilic Dendritic Assemblies. *Chem. Eur. J* **2013**, *19* (48), 16374–16381.
13. Roeven, E.; Scheres, L.; Smulders, M. M. J.; Zuilhof, H. Design, Synthesis, and Characterization of Fully Zwitterionic, Functionalized Dendrimers. *ACS Omega* **2019**, *4* (2), 3000–3011.
14. Li, L.; Wang, Y.; Ji, F.; Wen, Y.; Li, J.; Yang, B.; Yao, F. Synthesis and Characterization of Dendritic Star-Shaped Zwitterionic Polymers as Novel Anticancer Drug Delivery Carriers. *J. Biomater. Sci. Polym. Ed.* **2014**, *25* (14–15), 1641–1657.
15. Wang, L.; Zhang, J.; Lin, W.; Wang, Z.; Chen, S. Development of a Protein Mimic with Peptide Ligands to Enhance Specific Sensing and Targeting by the Zwitterionic Surface Engineering of Poly(Amido Amine) Dendrimers. *Adv. Mater. Interfaces* **2014**, *1* (1), 1300059.
16. Wang, Y.; Li, L.; Li, J.; Yang, B.; Wang, C.; Fang, W.; Ji, F.; Wen, Y.; Yao, F. Stable and PH-Responsive Polyamidoamine

Based Unimolecular Micelles Capped with a Zwitterionic Polymer Shell for Anticancer Drug Delivery. *RSC Adv.* **2016**, *6* (21), 17728–17739.

17. Svenningsen, S. W.; Janaszewska, A.; Ficker, M.; Petersen, J. F.; Klajnert-Maculewicz, B.; Christensen, J. B. Two for the Price of One: PAMAM-Dendrimers with Mixed Phosphoryl Choline and Oligomeric Poly(Caprolactone) Surfaces. *Bioconjug. Chem.* **2016**, *27* (6), 1547–1557.
18. Huang, D.; Yang, F.; Wang, X.; Shen, H.; You, Y.; Wu, D. Facile Synthesis and Self-Assembly Behaviour of PH-Responsive Degradable Polyacetal Dendrimers. *Polym. Chem.* **2016**, *7* (40), 6154–6158.
19. Cao, W.; Huang, J.; Jiang, B.; Gao, X.; Yang, P. Highly Selective Enrichment of Glycopeptides Based on Zwitterionically Functionalized Soluble Nanopolymers. *Sci. Rep.* **2016**, *6* (29776), 1–8.
20. Han, Y.; Qian, Y.; Zhou, X.; Hu, H.; Liu, X.; Zhou, Z.; Tang, J.; Shen, Y. Facile Synthesis of Zwitterionic Polyglycerol Dendrimers with a β-Cyclodextrin Core as MRI Contrast Agent Carriers. *Polym. Chem.* **2016**, *7*, 6354.
21. Xiong, Z.; Wang, Y.; Zhu, J.; Li, X.; He, Y.; Qu, J.; Shen, M.; Xia, J.; Shi, X. Dendrimers Meet Zwitterions: Development of a Unique Antifouling Nanoplatform for Enhanced Blood Pool, Lymph Node and Tumor CT Imaging. *Nanoscale* **2017**, *9* (34), 12295–12301.
22. Holmlin, R. E.; Chen, X.; Chapman, R. G.; Takayama, S.; Whitesides, G. M. Zwitterionic SAMs That Resist Nonspecific Adsorption of Protein from Aqueous Buffer. *Langmuir* **2001**, *17* (13), 2841–2850.
23. Kenausis, G. L.; Vo, J.; Elbert, D. L.; Huang, N.; Hofer, R.; Ruiz-taylor, L.; Textor, M.; Hubbell, J. A.; Spencer, N. D. Poly (L-Lysine)-g-Poly(Ethylene Glycol) Layers on Metal Oxide Surfaces: Attachment Mechanism and Effects of Polymer Architecture on Resistance to Protein Adsorption. *J. Phys. Chem. B* **2000**, *104* (14), 3298–3309.
24. Paul, S. M. De; Vo, J.; Spencer, N. D.; Textor, M. Poly(L-Lysine)-Graft-Poly (Ethylene Glycol) Assembled Monolayers on Niobium Oxide Surfaces : A Quantitative Study of the Influence of Polymer Interfacial Architecture on Resistance to Protein Adsorption by ToF-SIMS and in Situ OWLS. *Langmuir* **2003**, *19* (20), 9216–9225.
25. Morgese, G.; Verbraeken, B.; Ramakrishna, S. N.; Gombert, Y.; Cavalli, E.; Rosenboom, J. G.; Zenobi-Wong, M.; Spencer, N. D.; Hoogenboom, R.; Benetti, E. M. Chemical Design of Non-Ionic Polymer Brushes as Biointerfaces: Poly(2-Oxazine)s Outperform Both Poly(2-Oxazoline)s and PEG. *Angew. Chem. Int. Ed.* **2018**, *57* (36), 11667–11672.
26. Perry, S. S.; Yan, X.; Limpoco, F. T.; Lee, S.; Müller, M.; Spencer, N. D. Tribological Properties of Poly(l -Lysine)- Graft -Poly(Ethylene Glycol) Films: Influence of Polymer Architecture and Adsorbed Conformation. *ACS Appl. Mater. Interfaces* **2009**, *1* (6), 1224–1230.
27. Huang, W. M.; Gibson, S. J.; Facer, P.; Gu, J.; Polak, J. M. Improved Section Adhesion for Immunocytochemistry Using High Molecular Weight Polymers of L-Lysine as a Slide Coating. *Histochemistry* **1983**, *77* (2), 275–279.
28. Yan, X.; Perry, S. S.; Spencer, N. D.; Pasche, S.; De Paul, S. M.; Textor, M.; Lim, M. S. Reduction of Friction at Oxide Interfaces upon Polymer Adsorption from Aqueous Solutions. *Langmuir* **2004**, *20* (2), 423–428.
29. Parks, G. A. The Isoelectric Points of Solid Oxides, Solid Hydroxides, and Aqueous Hydroxo Complex Systems. *Chem. Rev.* **1965**, *65* (2), 177–198.
30. Weber, D.; Torger, B.; Richter, K.; Nessling, M.; Momburg, F.; Woltmann, B.; Müller, M.; Schwartz-Albiez, R. Interaction of Poly(L-Lysine)/Polysaccharide Complex Nanoparticles with Human Vascular Endothelial Cells. *Nanomaterials* **2018**, *8* (6), 358.
31. Roeven, E.; Kuzmyn, A. R.; Scheres, L.; Baggerman, J.; Smulders, M. M. J.; Zuilhof, H. PLL-Poly(HPMA) Bottlebrush-Based Antifouling Coatings: Three Grafting Routes. *Langmuir* **2020**, *36* (34), 10187–10199.
32. Gitsov, I.; Wooley, K. L. Novel Polyether Copolymers Consisting of Linear and Dendritic Blocks. *Angew. Chem. Int. Ed.* **1992**, *31* (9), 1200–1202.
33. Sousa-Herves, A.; Riguera, R.; Fernandez-Megia, E. PEG-Dendritic Block Copolymers for Biomedical Applications. *New J. Chem.* **2012**, *36* (2), 205–210.
34. Sun, H.; Haque, F. M.; Zhang, Y.; Commisso, A.; Mohamed, M. A.; Tsianou, M.; Cui, H.; Grayson, S. M.; Cheng, C. Linear-Dendritic Alternating Copolymers. *Angew. Chem. Int. Ed.* **2019**, *58* (31), 10572–10576.
35. Chapman, T. M.; Hillyer, G. L.; Mahan, E. J.; Shaffer, K. A. Hydraamphiphiles: Novel Linear Dendritic Block Copolymer Surfactants. *J. Am. Chem. Soc.* **1994**, *116* (24), 11195–11196.
36. van Hest, J. C. M.; Delnoye, D. A. P.; Baars, M. W. P. L.; van Genderen, M. H. P.; Meijer, E. W. Polystyrene-Dendrimer Amphiphilic Block Copolymers with a Generation-Dependent Aggregation. *Science.* **1995**, *268* (5217), 1592–1595.
37. Iyer, J.; Fleming, K.; Hammond, P. T. Synthesis and Solution Properties of New Linear-Dendritic Diblock Copolymers. *Macromolecules* **1998**, *31* (25), 8757–8765.
38. Hedden, R. C.; Bauer, B. J.; Paul Smith, A.; Gröhn, F.; Amis, E. Templating of Inorganic Nanoparticles by PAMAM/PEG Dendrimer - Star Polymers. *Polymer,* **2002**, *43* (20), 5473–5481.
39. Lee, C. C.; Gillies, E. R.; Fox, M. E.; Guillaudeu, S. J.; Fréchet, J. M. J.; Dy, E. E.; Szoka, F. C. A Single Dose of Doxorubicin-Functionalized Bow-Tie Dendrimer Cures Mice Bearing C-26 Colon Carcinomas. *Proc. Natl. Acad. Sci. U. S. A.* **2006**, *103* (45), 16649–16654.
40. Kaup, R.; Bart, J.; Velders, A. H. Dendroids, Discrete Covalently Cross-Linked Dendrimer Superstructures. *ACS Nano* **2020**, *15* (1), 1666–1674.

41. Frauenrath, H. Dendronized Polymers - Building a New Bridge from Molecules to Nanoscopic Objects. *Prog. Polym. Sci.* **2005**, *30* (3–4), 325–384.
42. Zhang, Y.; Li, X.; Deng, G.; Chen, Y. Novel Hybrid Polymer Brushes with Alternating Dendritic Wedges and Linear Side Chains. *Macromol. Chem. Phys.* **2006**, *207* (15), 1394–1403.
43. Shi, Y.; Zhu, W.; Chen, Y. Synthesis of Cylindrical Polymer Brushes with Umbrella-like Side Chains via a Combination of Grafting-from and Grafting-onto Methods. *Macromolecules* **2013**, *46* (6), 2391–2398.
44. Andrén, O. C. J.; Zhang, Y.; Lundberg, P.; Hawker, C. J.; Nyström, A. M.; Malkoch, M. Therapeutic Nanocarriers via Cholesterol Directed Self-Assembly of Well-Defined Linear-Dendritic Polymeric Amphiphiles. *Chem. Mater.* **2017**, *29* (9), 3891–3898.
45. Rostovtsev, V. V.; Green, L. G.; Fokin, V. V.; Sharpless, K. B. A Stepwise Huisgen Cycloaddition Process: Copper(I)-Catalyzed Regioselective "Ligation" of Azides and Terminal Alkynes. *Angew. Chem. Int. Ed. Engl.* **2002**, *41* (14), 2596–2599.
46. Thomson, D.; Zilkie, A.; Bowers, J. E.; Komljenovic, T.; Reed, G. T.; Vivien, L.; Marris-Morini, D.; Cassan, E.; Virot, L.; Fédéli, J. M.; Hartmann, J. M.; Schmid, J. H.; Xu, D. X.; Boeuf, F.; O'Brien, P.; Mashanovich, G. Z.; Nedeljkovic, M. Roadmap on Silicon Photonics. *J. Opt.* **2016**, *18* (7), 1–20.
47. Qi, Z. B.; Xu, L.; Xu, Y.; Zhong, J.; Abedini, A.; Cheng, X.; Sinton, D. Disposable Silicon-Glass Microfluidic Devices: Precise, Robust and Cheap. *Lab Chip* **2018**, *18* (24), 3872–3880.
48. Hook, F. F.; Vörös, J.; Rodahl, M.; Kurrat, R.; Böni, P.; Ramsden, J. J.; Textor, M.; Spencer, N. D.; Tengvall, P.; Gold, J.; Kasemo, B. A Comparative Study of Protein Adsorption on Titanium Oxide Surfaces Using in Situ Ellipsometry, Optical Waveguide Lightmode Spectroscopy, and Quartz Crystal Microbalance/Dissipation. *Colloids Surf. B Biointerfaces* **2002**, *24* (2), 155–170.
49. Besselink, G.; Heideman, R.; Schreuder, E.; Wevers, L.; Falke, F.; Van den Vlekkert, H. Performance of Arrayed Microring Resonator Sensors with the TriPleX Platform. *J. Biosens. Bioelectron.* **2016**, *7* (2), 1000209.
50. Gedig, E. Surface Chemistry in SPR Technology. *Handb. Surf. Plasmon Reson.* **2008**, 173–220.
51. Wörz, A.; Berchtold, B.; Moosmann, K.; Prucker, O.; Rühe, J. Protein-Resistant Polymer Surfaces. *J. Mater. Chem.* **2012**, *22* (37), 19547.
52. Xu, J.; Yu, Q.; Jiang, S. Cellulose Paper Sensors Modified with Zwitterionic Poly(Carboxybetaine) for Sensing and Detection in Complex Media. *Anal. Chem.* **2014**, *86*, 2871–2875.
53. Zhang, Z.; Chen, S.; Jiang, S. Dual-Functional Biomimetic Materials: Nonfouling Poly (Carboxybetaine) with Active Functional Groups for Protein Immobilization. *Biomacromolecules* **2006**, *7* (12), 3311–3315.
54. Baggerman, J.; Smulders, M. M. J.; Zuilhof, H. Romantic Surfaces: A Systematic Overview of Stable, Biospecific, and Antifouling Zwitterionic Surfaces. *Langmuir* **2019**, *35* (5), 1072–1084.
55. Kuzmyn, A. R.; Nguyen, A. T.; Zuilhof, H.; Baggerman, J. Bioactive Antifouling Surfaces by Visible-Light-Triggered Polymerization. *Adv. Mater. Interfaces* **2019**, *6* (12), 1900351.
56. Volodkin, D.; Ball, V.; Schaaf, P.; Voegel, J. C.; Mohwald, H. Complexation of Phosphocholine Liposomes with Polylysine. Stabilization by Surface Coverage versus Aggregation. *Biochim. Biophys. Acta* **2007**, *1768* (2), 280–290.
57. Laschewsky, A. Structures and Synthesis of Zwitterionic Polymers. *Polymers.* **2014**, *6* (5), 1544–1601.
58. Wickramathilaka, M. P.; Tao, B. Y. Characterization of Covalent Crosslinking Strategies for Synthesizing DNA-Based Bioconjugates. *J. Biol. Eng.* **2019**, *13* (1), 63.
59. Smith, R. K.; Lewis, P. a.; Weiss, P. S. Patterning Self-Assembled Monolayers. *Prog. Surf. Sci.* **2004**, *75* (1–2), 1–68.
60. Wallart, X.; Henry de Villeneuve, C.; Allongue, P. Truly Quantitative XPS Characterization of Organic Monolayers on Silicon: Study of Alkyl and Alkoxy Monolayers on H-Si(111). *J. Am. Chem. Soc.* **2005**, *127* (21), 7871–7878.
61. Scheres, L.; Giesbers, M.; Zuilhof, H. Organic Monolayers onto Oxide-Free Silicon with Improved Surface Coverage: Alkynes versus Alkenes. *Langmuir* **2010**, *26* (7), 4790–4795.
62. Scheres, L.; Giesbers, M.; Zuilhof, H. Self-Assembly of Organic Monolayers onto Hydrogen-Terminated Silicon: 1-Alkynes Are Better than 1-Alkenes. *Langmuir* **2010**, *26* (13), 10924–10929.
63. Honda, T.; Nakao, A.; Ishihara, K.; Higaki, Y.; Higaki, K.; Takahara, A.; Iwasaki, Y.; Yusa, S. I. Polymer Coating Glass to Improve the Protein Antifouling Effect. *Polym. J.* **2018**, *50* (5), 381–388.
64. Xu, L. Q.; Pranantyo, D.; Neoh, K. G.; Kang, E. T.; Teo, S. L. M.; Fu, G. D. Synthesis of Catechol and Zwitterion-Bifunctionalized Poly(Ethylene Glycol) for the Construction of Antifouling Surfaces. *Polym. Chem.* **2016**, *7* (2), 493–501.
65. Kuzmyn, A. R.; Nguyen, A. T.; Teunissen, L. W.; Zuilhof, H.; Baggerman, J. Antifouling Polymer Brushes via Oxygen-Tolerant Surface-Initiated PET-RAFT. *Langmuir* **2020**, *36* (16), 4439–4446.
66. Kowalczyńska, H. M.; Nowak-Wyrzykowska, M.; Szczepankiewicz, A. A.; Dobkowski, J.; Dyda, M.; Kamiński, J.; Kołos, R. Albumin Adsorption on Unmodified and Sulfonated Polystyrene Surfaces, in Relation to Cell-Substratum Adhesion. *Colloids Surf. B Biointerfaces* **2011**, *84* (2), 536–544.
67. Price, W. S.; Tsuchiya, F.; Arata, Y. Lysozyme Aggregation and Solution Properties Studied Using PGSE NMR Diffusion

Measurements. *J. Am. Chem. Soc.* **1999**, *121* (49), 11503–11512.
68. Horbett, T. A. Fibrinogen Adsorption to Biomaterials. *J. Biomed. Mater. Res. A.* **2018**, *106* (10), 2777–2788.
69. Tonda-Turo, C.; Carmagnola, I.; Ciardelli, G. Quartz Crystal Microbalance with Dissipation Monitoring: A Powerful Method to Predict the in Vivo Behavior of Bioengineered Surfaces. *Front. Bioeng. Biotechnol.* **2018**, *6*, 1–7.
70. Chandrasekaran, N.; Dimartino, S.; Fee, C. J. Study of the Adsorption of Proteins on Stainless Steel Surfaces Using QCM-D. *Chem. Eng. Res. Des.* **2013**, *91* (9), 1674–1683.
71. Janshoff, A.; Galla, H. J.; Steinem, C. Piezoelectric Mass-Sensing Devices as Biosensors - An Alternative to Optical Biosensors? *Angew. Chem. Int. Ed.* **2000**, *39* (22), 4004–4032.
72. Phan, H. T. M.; Bartelt-Hunt, S.; Rodenhausen, K. B.; Schubert, M.; Bartz, J. C. Investigation of Bovine Serum Albumin (BSA) Attachment onto Self-Assembled Monolayers (SAMs) Using Combinatorial Quartz Crystal Microbalance with Dissipation (QCM-D) and Spectroscopic Ellipsometry (SE). *PLoS One* **2015**, *10* (10).
73. Yang, R.; Gleason, K. K. Ultrathin Antifouling Coatings with Stable Surface Zwitterionic Functionality by Initiated Chemical Vapor Deposition (ICVD). *Langmuir* **2012**, *28* (33), 12266–12274.
74. Wang, X.; Cheng, B.; Ji, C.; Zhou, M.; Wang, L. Effects of Hydraulic Retention Time on Adsorption Behaviours of EPS in an A/O-MBR: Biofouling Study with QCM-D. *Sci. Rep.* **2017**, *7* (1), 1–9.
75. Alexander, T. E.; Lozeau, L. D.; Camesano, T. A. QCM-D Characterization of Time-Dependence of Bacterial Adhesion. *Cell Surf.* **2019**, *5* (April), 100024.
76. Shen, D.; Huang, M.; Chow, L.; Yang, M. Kinetic Profile of the Adsorption and Conformational Change of Lysozyme on Self-Assembled Monolayers as Revealed by Quartz Crystal Resonator. *Sens. Actuators B* **2001**, *77*, 664–670.
77. Bellassai, N.; Marti, A.; Spoto, G. Low-Fouling, Mixed-Charge Poly-l-Lysine Polymers with Anionic Oligopeptide Side-Chains. *J. Mater. Chem. B* **2018**, *6*, 7662–7673.
78. Rodahl, M.; Höök, F.; Kasemo, B. QCM Operation in Liquids: An Explanation of Measured Variations in Frequency and Q Factor with Liquid Conductivity. *Anal. Chem.* **1996**, *68* (13), 2219–2227.
79. Prime, K. L.; Whitesides, G. M. Adsorption of Proteins onto Surfaces Containing End-Attached Oligo(Ethylene Oxide): A Model System Using Self-Assembled Monolayers. *J. Am. Chem. Soc.* **1993**, *115* (23), 10714–10721.
80. Harder, P.; Grunze, M.; Dahint, R. Molecular Conformation in Oligo(Ethylene Glycol)-Terminated Self-Assembled Monolayers on Gold and Silver Surfaces Determines Their Ability To Resist Protein Adsorption. *J. Phys. Chem. B* **1998**, *5647* (97), 426–436.
81. Emmenegger, C. R.; Brynda, E.; Riedel, T.; Sedlakova, Z.; Houska, M.; Alles, A. B. Interaction of Blood Plasma with Antifouling Surfaces. *Langmuir* **2009**, *25* (7), 6328–6333.
82. Burzava, A. L. S.; Jasieniak, M.; Cockshell, M. P.; Voelcker, N. H.; Bonder, C. S.; Griesser, H. J.; Moore, E. Surface-Grafted Hyperbranched Polyglycerol Coating: Varying Extents of Fouling Resistance across a Range of Proteins and Cells. *ACS Appl. Bio Mater.* **2020**, *3*, 3718–3730.
83. van Andel, E.; de Bus, I.; Tijhaar, E. J.; Smulders, M. M. J.; Savelkoul, H. F. J.; Zuilhof, H. Highly Specific Binding on Antifouling Zwitterionic Polymer-Coated Microbeads as Measured by Flow Cytometry. *ACS Appl. Mater. Interfaces* **2017**, *9* (44), 38211–38221.
84. Yang, W.; Chen, S.; Cheng, G.; Vaisocherová, H.; Xue, H.; Li, W.; Zhang, J.; Jiang, S. Film Thickness Dependence of Protein Adsorption from Blood Serum and Plasma onto Poly(Sulfobetaine)-Grafted Surfaces. *Langmuir* **2008**, *24* (17), 9211–9214.
85. Koc, J.; Schönemann, E.; Amuthalingam, A.; Clarke, J.; Finlay, J. A.; Clare, A. S.; Laschewsky, A.; Rosenhahn, A. Low-Fouling Thin Hydrogel Coatings Made of Photo-Cross-Linked Polyzwitterions. *Langmuir* **2019**, *35* (5), 1552–1562.
86. Van Andel, E.; Lange, S. C.; Pujari, S. P.; Tijhaar, E. J.; Smulders, M. M. J.; Savelkoul, H. F. J.; Zuilhof, H. Systematic Comparison of Zwitterionic and Non-Zwitterionic Antifouling Polymer Brushes on a Bead-Based Platform. *Langmuir* **2019**, *35* (5), 1181–1191.
87. Vorobii, M.; de los Santos Pereira, A.; Pop-Georgievski, O.; Kostina, N. Y.; Rodriguez-Emmenegger, C.; Percec, V. Synthesis of Non-Fouling Poly[N-(2-Hydroxypropyl)Methacrylamide] Brushes by Photoinduced SET-LRP. *Polym. Chem.* **2015**, *6* (23), 4210–4220.
88. Rodriguez-Emmenegger, C.; Brynda, E.; Riedel, T.; Houska, M.; Šubr, V.; Alles, A. B.; Hasan, E.; Gautrot, J. E.; Huck, W. T. S. Polymer Brushes Showing Non-Fouling in Blood Plasma Challenge the Currently Accepted Design of Protein Resistant Surfaces. *Macromol. Rapid Commun.* **2011**, *32* (13), 952–957.
89. Surman, F.; Riedel, T.; Bruns, M.; Kostina, N. Y.; Sedláková, Z.; Rodriguez-Emmenegger, C. Polymer Brushes Interfacing Blood as a Route toward High Performance Blood Contacting Devices. *Macromol. Biosci.* **2015**, *15* (5), 636–646.
90. Cao, B.; Li, L.; Tang, Q.; Cheng, G. The Impact of Structure on Elasticity, Switchability, Stability and Functionality of an All-in-One Carboxybetaine Elastomer. *Biomaterials* **2013**, *34* (31), 7592–7600.
91. Chen, R.; Ma, Y.; Zhao, C.; Lin, Z.; Zhu, X.; Zhang, L.; Yang, W. Construction of DNA Microarrays on Cyclic Olefin Copolymer Surfaces Using Confined Photocatalytic Oxidation. *RSC Adv.* **2014**, *4* (87), 46653–46661.
92. Xiao, A.; Dhand, C.; Leung, C. M.; Beuerman, R. W.; Ramakrishna, S.; Lakshminarayanan, R. Strategies to Design

Antimicrobial Contact Lenses and Contact Lens Cases. *J. Mater. Chem. B* **2018**, *6* (15), 2171–2186.

93. Poręba, R.; de los Santos Pereira, A.; Pola, R.; Jiang, S.; Pop-Georgievski, O.; Sedláková, Z.; Schönherr, H. "Clickable" and Antifouling Block Copolymer Brushes as a Versatile Platform for Peptide-Specific Cell Attachment. *Macromol. Biosci.* **2020**, *20* (4), 1900354.
94. Lange, S. C.; Van Andel, E.; Smulders, M. M. J.; Zuilhof, H. Efficient and Tunable Three-Dimensional Functionalization of Fully Zwitterionic Antifouling Surface Coatings. *Langmuir* **2016**, *32* (40), 10199–10205.
95. Morag, E.; Bayer, E. A.; Wilchek, M. Reversibility of Biotin-Binding by Selective Modification of Tyrosine in Avidin. *Biochem. J.* **1996**, *316* (1), 193–199.
96. Piran, U.; Riordan, W. J. Dissociation Rate Constant of the Biotin-Streptavidin Complex. *J. Immunol. Methods* **1990**, *133* (1), 141–143.
97. Krishnamoorthy, M.; Hakobyan, S.; Ramstedt, M.; Gautrot, J. E. Surface-Initiated Polymer Brushes in the Biomedical Field: Applications in Membrane Science, Biosensing, Cell Culture, Regenerative Medicine and Antibacterial Coatings. *Chem. Rev.* **2014**, *114*, 10976–11026.
98. Vaisocherová, H.; Yang, W.; Zhang, Z.; Cao, Z.; Cheng, G.; Piliarik, M.; Homola, J.; Jiang, S. Ultralow Fouling and Functionalizable Surface Chemistry Based on a Zwitterionic Polymer Enabling Sensitive and Specific Protein Detection in Undiluted Blood Plasma. *Anal. Chem.* **2008**, *80* (20), 7894–7901.
99. Joshi, S.; Pellacani, P.; van Beek, T. A.; Zuilhof, H.; Nielen, M. W. F. Surface Characterization and Antifouling Properties of Nanostructured Gold Chips for Imaging Surface Plasmon Resonance Biosensing. *Sens. Actuators B* **2015**, *209*, 505–514.
100. Salorinne, K.; Lahtinen, T.; Malola, S.; Koivisto, J.; Häkkinen, H. Solvation Chemistry of Water-Soluble Thiol-Protected Gold Nanocluster Au102 from DOSY NMR Spectroscopy and DFT Calculations. *Nanoscale* **2014**, *6* (14), 7823–7826.
101. Holz, M.; Weingartner, H. Calibration in Accurate Spin-Echo Self-Diffusion Measurements Using 1H and Less-Common Nuclei. *J. Magn. Reson.* **1991**, *92* (1), 115–125.

4.6 Supporting Information

4.6.1 Experimental Section

4.6.1.1 Materials

Milli-Q water was purified by a Barnsted water purification system, with a resistivity of <18.3 MΩ·cm. Poly-l-lysine hydrobromide (PLL, MW of 20.9 kDa, Sigma Aldrich[1]); Poly- l-Lysine Azide grafted (PLL-azide, MW of 32 kDa, Nanosoft Polymers, purified by dialysis); 4-(2-hydroxyethyl)piperazine-1-ethanesulfonic acid (HEPES, ≥99.5%, Sigma Aldrich); Dimethyl sulfoxide (DMSO, anhydrous, 99.7%, Fisher Scientific); MES buffer (1 M, Sigma Aldrich); N-Hydroxysuccinimide (NHS, 98%, Sigma Aldrich); N-(3-Dimethylaminopropyl)-N'-ethylcarbodiimide hydrochloride (EDC, purum, ≥98.0%, Sigma Aldrich), Hydrogen peroxide solution (H2O2, 50 wt.% in H2O, Honeywell); Sulfuric acid (H2SO4, 95.0-97.0; phosphate-buffered saline (PBS, Sigma-Aldrich); Bovine serum albumin-AlexaFluor488 (BSA-AF488, Fisher Thermo Scientific); Lysozyme-FITC (LYS-FITC, NANOCS); Albumin bovine serum (BSA, for molecular biology, powder, Sigma Aldrich); Lysozyme from chicken egg white (LYS, Sigma Aldrich); Fibrinogen (FIB, from porcine plasma, Sigma Aldrich); Human Serum (from human male AB plasma, USA origin, sterile-filtered, Sigma Aldrich); Fibrinogen-AlexaFluor488 (FIB-AF488, Fisher Thermo Scientific); Silicon single side polished (Si(111), N-type, phosphorus-doped, Siltronix); QCM-D silicon dioxide sensors (QSX 303; QSense); deuterium oxide (D2O, 99.9 atom% D, Sigma Aldrich). Surfaces were plasma-cleaned by a Diener Femto plasma system. Sonication steps were performed in an Elmasonic P 30 H ultrasonic unit. Cellulose membrane dialysis tubing (25 mm flat width, Sigma-Aldrich) was used for ≥8 mL volume dialyses. Float-a-lyzer G2 8 mL dialysis membranes with a 3.5–5 kD MWCO (VWR) were used for the final purification step of the PLL-ZID macrostructures.

4.6.1.2 Characterization methods

Nuclear Magnetic Resonance Spectroscopy (NMR)
^{1}H NMR measurements were recorded on a Bruker Avance III NMR at 400 MHz, ^{13}C NMR spectra were recorded at 100 MHz. Chemical shifts are reported in parts per million (ppm), and are referred to the methyl signal of the sodium salt of 3-(trimethylsilyl)-1-propanesulfonic acid-d_6 (δ = 0).

Infrared Spectroscopy (IR)
IR analyses were performed on a Bruker Tensor 27 spectrometer with platinum ATR accessory.

X-ray Photoelectron Spectroscopy (XPS)
XPS spectra were obtained using a JPS-9200 photoelectron spectrometer (JEOL, Japan) with monochromatic Al-Kα X-Ray radiation at 12 kV and 20 mA. The obtained spectra were analyzed using CASA XPS software (version 2.3.16 PR 1.6). In C1s and N1s narrow-range spectra, the positions are set to 285 eV and 400 eV for the C–C and N–C signals, respectively. For layers <15 nm, the thickness was calculated based on the attenuation of the Si signal in XPS, according to a published procedure.[61]

Gel Permeation Chromatography (GPC)
The polymer molecular weight and polydispersity index (PDI) were determined using gel permeation chromatography (Agilent G5654A quaternary pump, G7162A refractive index detector), where a PSS SUPREMA Combination medium (P/N 206-0002) 1000 Å single porosity column was employed (0.05% NaN_3 in milli-Q water as eluent, 1 mL/min). Dendrimer in Milli-Q solutions were freshly prepared. 20 µL was used for each analysis. An Agilent PL2080-0101 PEO calibration kit was used for calibration purposes.

Fluorescence microscopy
A Leica TCS SP8 confocal laser scanning microscope (CLMS) (Leica Microsystems, Mannheim, Germany) was used to measure protein fouling and specific interactions of the coated surfaces. A Leica HyDTM hybrid detector was used in photon counting mode to measure the intensity of the fluorescence signal. The fluorescence was measured in the wavelength range from 500 to 535 nm with laser excitation wavelength at 488 nm. A 10×

[1] P7890 Certificate of Analysis (accessed 2021/02/01)
https://www.sigmaaldrich.com/Graphics/COfAInfo/SigmaSAPQM/COFA/P7/P7890/P7890-BULK_____SLCF0233__.pdf

objective was used, and the samples were set in focus by maximizing the reflected light intensity from the laser. Fluorescence images were obtained by accumulating ten consecutive images. Images were analyzed with the Leica LAS X Life Science software.

Quartz crystal microbalance with dissipation monitoring (QCM-D)
QCMD measurements were performed by using silicon dioxide-coated quartz resonators (QSX 303, Biolin Scientific, Sweden) in a QCM-D (Q-Sense E4, Biolin Scientific, Sweden) at 18 °C. The QCM-D sensors were cleaned with UV-ozone treatment (Procleaner UV.PC.220, Bioforce Nanosciences) for 10 minutes, soaked in 2% sodium dodecyl sulfate solution for 30 minutes and rinsed with demineralized water. After the sensors were dried in a stream of argon, they were again treated with UV-ozone cleaning for another 10 minutes. All solutions were bubbled with argon prior to the experiments. The setup was flushed with PBS buffer solution using a peristaltic pump (Ismatec high precision multichannel dispenser) with a flow rate of 50 $\mu L \cdot min^{-1}$ for at least 15 min before starting the measurement in order to have a stabile baseline. Throughout the experiment, a flow rate of 50 $\mu L \cdot min^{-1}$ was used. QSoft (version 2.8.0.913 Analyzer) and DFind (version 1.2.7) were used to record and process data, respectively.
Frequency (Δf) shifts were acquired real-time at the 3rd (15 MHz), 5th (25 MHz), 7th (35 MHz), 9th (45 MHz) and 11th (55 MHz) harmonic overtones. The 3rd (15 MHz) overtones were reported for comparison of different polymer coatings. The level of fouling was quantified as the difference in frequency shift of the quartz crystal between the buffer baselines before and after flowing the foulant solution, converted to surface coverage ($ng \cdot cm^{-2}$) using the Sauerbrey equation: [78]

$$\Delta \boldsymbol{m} = -\frac{\boldsymbol{C}}{\boldsymbol{n}} \Delta \boldsymbol{f} \quad \text{(eq. 4.1)}$$

where Δm is the areal mass density of the film, C is the mass sensitivity constant, n is the harmonic number and Δf is the frequency shift (based on the surface and bulk liquid phase of the system as provided by the software DFind).

4.6.1.3 Preparation of PLL coatings

Silicon wafers were cut into 1×1 cm pieces and cleaned by sonication in acetone for 5 min and drying in a argon stream, subsequently oxidized by air plasma for 5 min and cleaned in a piranha solution (3 : 1 mixture by volume of H_2SO_4 : H_2O_2) for 15 minutes, after which they were soaked in and extensively rinsed with Milli-Q water and finally dried by a stream of nitrogen. The freshly cleaned surfaces were immediately used for modification by being covered with a 0.1 $mg \cdot mL^{-1}$ solution of PLL-ZID macromolecule or PLL in HEPES buffer (10 mM, pH 7.4) and stored in a humidity chamber overnight at room temperature. Afterwards, they were again extensively rinsed with Milli-Q water and dried by a stream of nitrogen.

4.6.1.4 Protein fouling studies

Fouling of the coated surfaces was investigated by incubating surfaces in single-protein solutions of fluorescein isothiocyanate labeled lysozyme (LYS-FITC) (1.0 $mg \cdot mL^{-1}$), Alexa488 labeled bovine serum albumin (BSA-Alexa488) (1.0 $mg \cdot mL^{-1}$) or AlexaFluor488 labeled fibrinogen (FIB-AF488) (1.0 $mg \cdot mL^{-1}$) for 30 min at room temperature according to a published procedure.[65] The surfaces were then washed with PBS buffer (pH 7.4) and Milli-Q water and subsequently dried in a stream of argon. Subsequently, the samples were mounted on microscope slides using double sides tape and fluorescence intensity of the adsorbed proteins was measured. Each sample was produced and measured in duplo.

4.6.1.5 Syntheses

*Synthesis of PLL-ZID macrostructures **Netw_A**, **Netw_B** and **Netw_C***
The following solutions were prepared in falcon tubes:

1) 1 $mg–mL^{-1}$ PLL stock solution (20.9 kDa, degree of polymerization = 100) in MES 50 mM buffer. Resulting in a lysine monomer concentration of 5 mM), sonicated for 5 min to assure full solvation;
2) A solution of 1.14 mL MES buffer (50 mM) containing:
   - 216.6 mg ZID (3.9 kDa, ~0.056 mmol, containing ~30 COO^- groups) final concentration of COO^- of 1.5 M;
   - 98.5 mg EDC·HCl (191.7 $g \cdot mol^{-1}$, 0.51 mmol) final concentration of 0.44 M;
   - 52.4 mg NHS (115.09 $g \cdot mol^{-1}$, 0.46 mmol) final concentration of 53 M.

Solutions 1 and 2 were combined in three different ratios and mixed in a falcon tube to obtain PLL-ZID macrostructures **Netw_A**, **Netw_B** and **Netw_C** according to the table below:

	Solution 1	**Solution 2**	**MES buffer**
Netw_A	1 mL	0.5 mL	0.5 mL
Netw_B	1 mL	0.05 mL	0.95 mL
Netw_C	1 mL	0.005 mL	0.995 mL

The mixtures were shaken in an end-over-end shaker overnight (16 hours) at room temperature. The day after, the solutions were dialyzed against Milli-Q water for 3 days with 3 medium exchanges using dialysis membranes with a 3.5–5 kDa MWCO. After evaporation of the solvent and lyophilization, fluffy powders were obtained with yields of 46%, 26% and 12% for **Netw_A**, **Netw_B** and **Netw_C**, respectively.

PLL-ZID macrostructures **Netw_A** characterization:
^{1}H-NMR (400 MHz, D_2O, 298 K) δ 1.44 (H_d; m, 2H), δ 2.18 (H_h; m, 2H), δ 3.20 (H_g; s, 3H), δ 3.63 (H_f; t, 2H), δ 3.88 (H_e; m, 2H) see Figure 4.15; **^{1}H–^{13}C HSQC** (100 MHz, D_2O, 298 K) see Figure 4.16, **DOSY** (400 MHz, D_2O, 298 K) see Table 4.2, **IR** see Figure 4.23, **XPS** Surface immobilized (Figure 4.5 and Figure 4.6).

PLL-ZID macrostructures **Netw_B** characterization:
^{1}H-NMR (400 MHz, D_2O, 298 K) δ 1.39 (H_d; m, 2H), δ 1.64 (H_c; m, 4H), δ 2.22 (H_h; m, 2H), δ 2.73 (H_{b*}; m, 2H), δ 2.73 (H_b; m, 2H), δ 3.02 (H_{g*}; m, 3H), δ 3.21 (H_g; s, 3H), δ 3.63 (H_f; t, 2H), δ 3.76 (H_{e*}; s, 2H), δ 3.88 (H_e; s, 2H), δ 4.25 (H_a; t, 1H) see Figure 4.17, **^{1}H–^{13}C HSQC** (100 MHz, D_2O, 298 K) see Figure 4.18, **DOSY** (400 MHz, D_2O, 298 K) see Table 4.2, **IR** see Figure 4.23, **XPS** Surface immobilized (Figure 4.5 and 6).

PLL-ZID macrostructures **Netw_C** characterization:
^{1}H-NMR (400 MHz, D_2O, 298 K) δ 1.38 (H_d; m, 2H), δ 1.63 (H_c; m, 4H), δ 2.14 (H_h; m, 2H), δ 2.79 (H_{b*}; m, 2H), δ 2.94 (H_b; m, 2H), δ 3.00 (H_{g*}; m, 3H), δ 3.20 (H_g; s, 3H), δ 3.63 (H_f; t, 2H), δ 3.76 (H_{e*}; s, 2H), δ 3.88 (H_e; s, 2H), δ 4.25 (H_a; t, 1H) see Figure 4.19, **^{1}H-^{13}C HSQC** (100 MHz, D_2O, 298 K) see Figure 4.20, **DOSY** (400 MHz, D2O, 298 K) see Table 4.2, **IR** see Figure 4.23, **XPS** Surface immobilized (Figure 4.5 and Figure 4.6).

*Synthesis of PLL-ZID macrostructure **Lin_A***
The following solutions were prepared in falcon tubes:

25 mg of a 32 kDa PLL-azide (20% of the lysines is azide modified, resulting in 0.031 mmol azide) in 1 mL Milli-Q water, sonicated for 5 min to assure full dissolution);

- 400 mg (0.10 mmol) ZID-alkyne was dissolved in 1 mL Milli-Q water;
- 3.0 mL of a 1.0 mg·mL^{-1} $CuSO_4{\cdot}5H_2O$ solution in Milli-Q water (0.012 mmol $CuSO_4$);
- mL of a 0.2 g·mL^{-1} Na-Ascorbate solution in Milli-Q water (0.1 mmol Na-Ascorbate).

The above solutions were combined and stirred overnight in a falcon tube at 40 °C. The following day, the solutions were dialyzed against Milli-Q water for 3 days with 3 medium exchanges using dialysis membranes with a 14 kDa MWCO. After evaporation of the solvent and lyophilization, a fluffy powder was obtained with a yield of 59%.

PLL-ZID macrostructures **Lin_A** characterization:

^{1}H-NMR (400 MHz, D_2O, 298 K) δ 1.34 (H_f; m-overlapping, 2H), δ 2.18 (H_e; m, 2H), δ 3.17 (H_d; s, 3H), δ 3.60 (H_c; t, 2H), δ 3.85 (H_b; m-overlapping, 2H), δ 8.02 (H_a; s, 1H) see Figure 4.21, **^{1}H–^{13}C HSQC** (100 MHz, D_2O, 298 K) see Figure 4.22, **IR** see Figure 4.24, **XPS** Surface immobilized (Figure 4.10).

4.6.2 NMR data

PLL-ZID ***Netw_A***

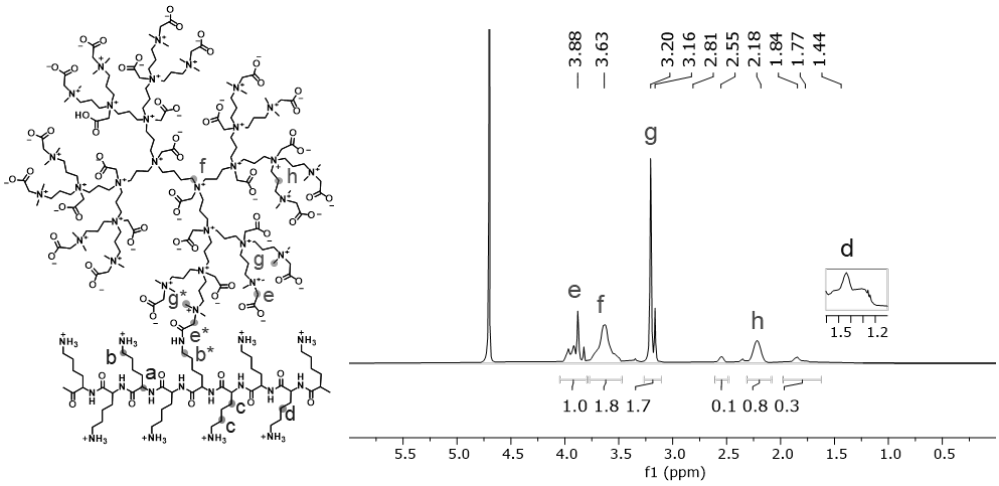

Figure 4.15 ^{1}H-NMR spectrum of PLL-ZID **Netw_A** measured in D_2O (400 MHz, 298 K).

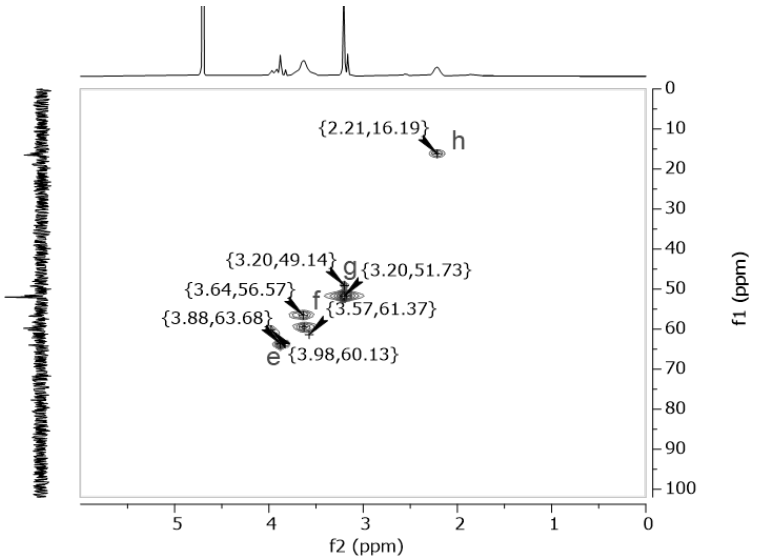

Figure 4.16 ^{1}H–^{13}C HSQC NMR spectrum of PLL-ZID **Netw_A** measured in D_2O (100 MHz, 298 K). Peaks were assigned following the labelling of the structure as shown in Figure 4.15.

PLL-ZID ***Netw_B***

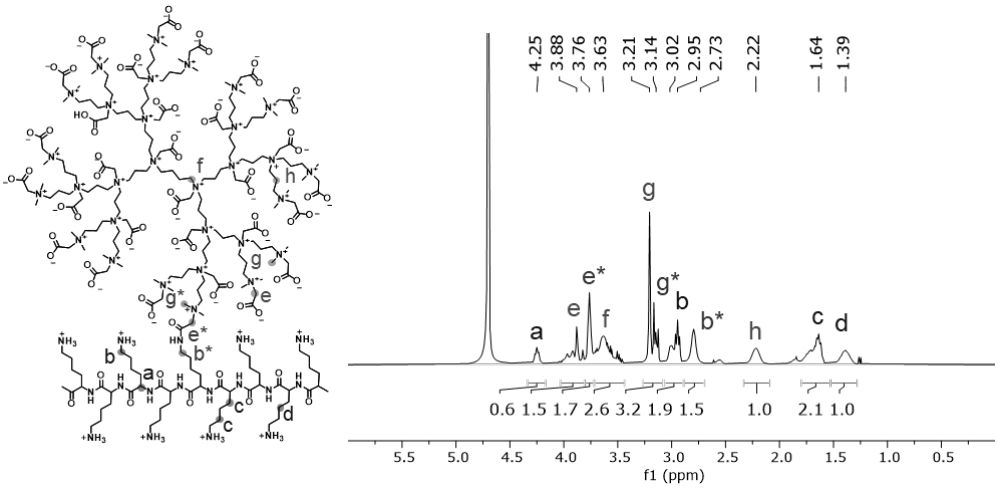

Figure 4.17 ^{1}H-NMR spectrum of PLL-ZID **Netw_B** measured in D_2O (400 MHz, 298 K).

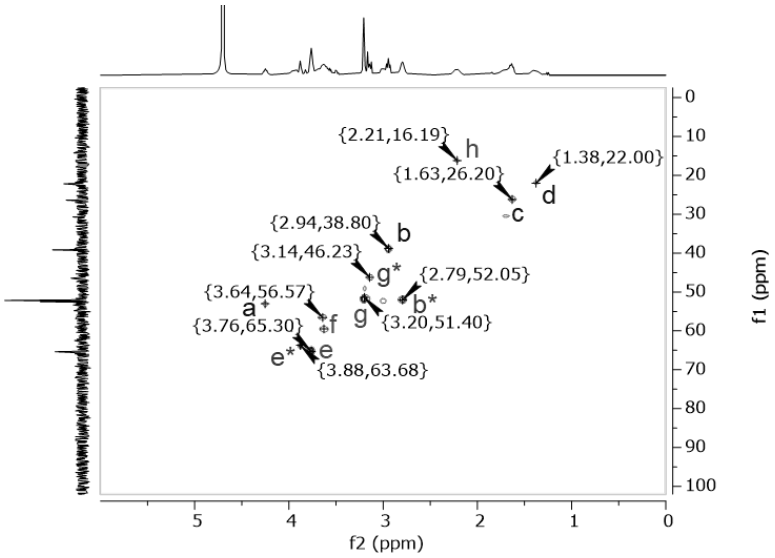

Figure 4.18 ^{1}H–^{13}C HSQC NMR spectrum of PLL-ZID **Netw_B** measured in D_2O (100 MHz, 298 K). Peaks were assigned following the labelling of the structure as shown in Figure 4.17.

PLL-ZID ***Netw_C***

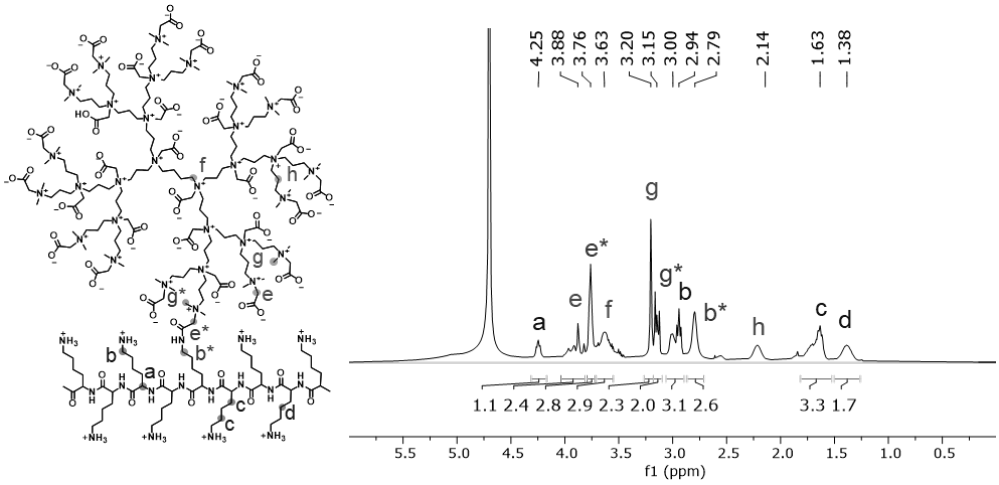

Figure 4.19 ^{1}H-NMR spectrum of PLL-ZID **Netw_C** measured in D_2O (400 MHz, 298 K).

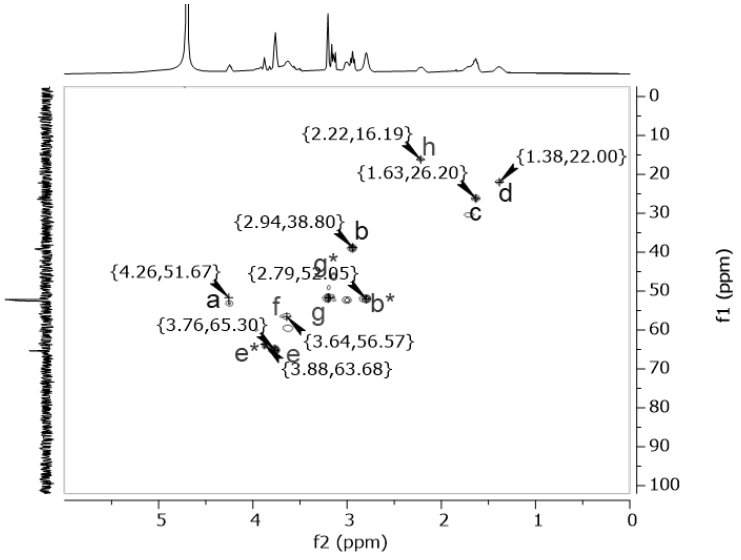

Figure 4.20 ^{1}H–^{13}C HSQC NMR spectrum of PLL-ZID **Netw_B** measured in D_2O (100 MHz, 298 K). Peaks were assigned following the labelling of the structure as shown in Figure 4.19.

*PLL-ZID **Lin_A***

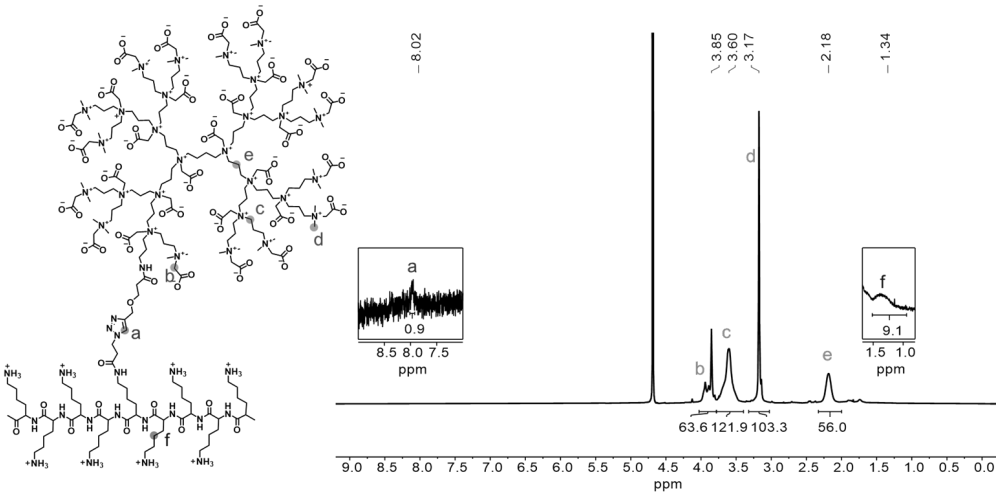

Figure 4.21 ^{1}H-NMR spectrum of PLL-ZID **Lin_A** measured in D_2O (400 MHz, 298 K).

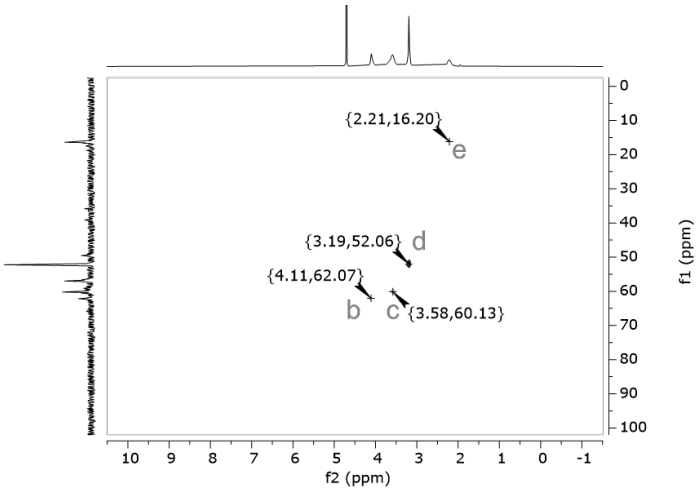

Figure 4.22 ^{1}H–^{13}C HSQC NMR spectrum of PLL-ZID **Lin_A** measured in D_2O (100 MHz, 298 K). Peaks were assigned following the labelling of the structure as shown in Figure 4.21.

4.6.3 DOSY hydrodynamic radius calculation

Under the assumption that the PLL-ZID macromolecules can be regarded as spherical objects, the hydrodynamic radius, r_H, of this sphere can be calculated from the measured diffusion coefficient, D, using the Stokes-Einstein equation:[100,101]

$$\boldsymbol{D = \frac{k_B \cdot T}{6\pi \cdot \eta \cdot r_H}} \qquad \text{(eq.4.2)}$$

where D is the diffusion coefficient, k_B the Boltzmann constant, T the absolute temperature, η the solvent viscosity, and r_H the hydrodynamic radius of the molecule. Using the hydrodynamic radius, the hydrodynamic volume can be calculated.
Table 4.2 lists the calculated hydrodynamic radius for PLL-ZID networks with **Netw_B** and **Netw_C**, determined from the diffusion coefficient as obtained in the DOSY measurement.

Table 4.2 Calculated hydrodynamic volumes based on diffusion coefficients D ($m^2 \cdot s^{-1}$) in D_2O at 300 K.

Structure	Diffusion coefficient D ($m^2 \cdot s^{-1}$)	Hydrodynamic volume (nm^3)
PLL	4.4×10^{-11}	8.6×10^{2}
Netw_A	n.a.*	n.a.*
Netw_B	3.7×10^{-11}	1.5×10^{3}
Netw_C	4.2×10^{-11}	1.2×10^{3}

* For **Netw_A** the spectrum was dominated by residual unbound ZID. Therefore, no PLL-ZID network DOSY trace could be obtained.

4.6.4 IR data

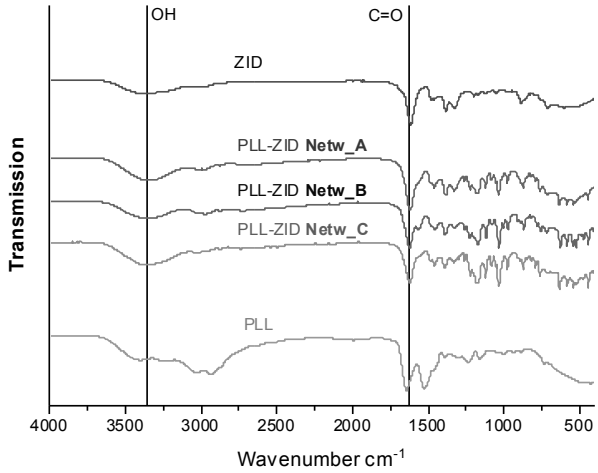

Figure 4.23 IR spectra of the ZID starting material, PLL-ZID **Netw_A**, **Netw_B**, **Netw_C** and starting material PLL. Characteristic signals are highlighted. On the *y*-axis the spectra are shown with an offset with respect to each other.

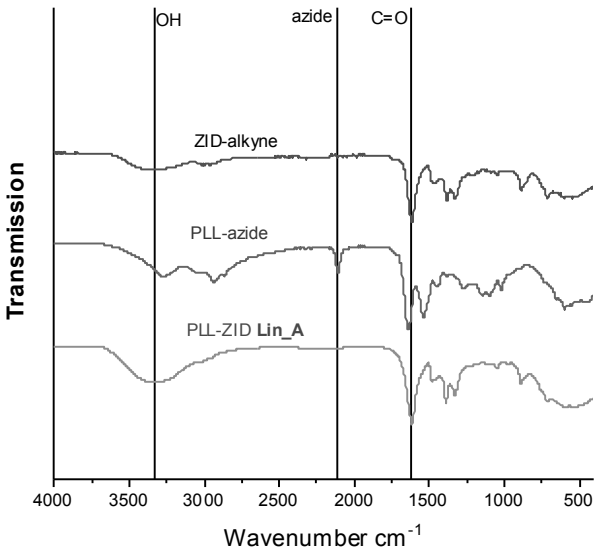

Figure 4.24 IR spectra of the ZID-alkyne and PLL-azide starting materials and PLL-ZID **Lin_A**. Characteristic signals are highlighted. On the *y*-axis the spectra are shown with an offset with respect to each other.

Chapter 5

PLL-poly(HPMA) Bottlebrush-Based Antifouling Coatings: Three Grafting Routes

Esther Roeven | Andriy R. Kuzmyn | Luc Scheres | Jacob Baggerman
Maarten M. J. Smulders | Han Zuilhof

Published in **Langmuir 2020, 36, 10187-10199**
DOI: 10.1021/acs.langmuir.0c01675

Abstract

In this chapter, we compare three routes to prepare antifouling coatings that consist of PLL-HPMA bottlebrushes. The poly(L-lysine) (PLL) backbone is self-assembled onto the surface by charged-based interactions between the lysine groups and the negatively charged silicon oxide surface, whereas the poly(N-(2-hydroxypropyl)methacrylamide) (HPMA) side chains, grown by RAFT polymerization, provide antifouling properties to the surface. First, the PLL-HPMA coatings are synthesized in a bottom-up fashion through a grafting-from approach. In this route, the PLL is self-assembled onto a surface, after which a polymerization agent is immobilized and finally HPMA is polymerized from the surface. In the second explored route the PLL is modified in solution by a RAFT agent to create a macroinitiator. After self-assembly of this macroinitiator onto the surface, the HPMA is polymerized from the surface by RAFT. In the third and last route, the whole PLL-HPMA bottlebrush is initially synthesized in solution. To this end, HPMA is polymerized from the macroinitiator in solution and the PLL-HPMA bottlebrush is then self-assembled onto the surface in just one step (grafting-to). Additionally, in this third route, we also design and synthesize a bottlebrush polymer with a PLL backbone and HPMA side chains, with the latter containing 5% carboxybetaine (CB) monomers that eventually allow for additional (bio)functionalization in solution or after surface immobilization. These three routes are evaluated in terms of: ease of synthesis, scalability, ease of characterization and a preliminary investigation of their antifouling performance. All three coating procedures result in coatings that show antifouling properties in single-protein antifouling tests. This method thus presents a new, simple, versatile and highly scalable approach for the manufacturing of PLL-based bottlebrush coatings that can be synthesized partly or completely on the surface or in solution, depending on the desired production process and/or application.

5.1 Introduction

The non-specific adsorption of proteins on a surface, *i.e.* fouling, is an initial step in the process of accumulation of unwanted biomaterial on that surface. The adsorption of such biomolecules and biomaterials impairs the functions of biotechnological and biomedical devices, whose correct functioning is crucially dependent on the availability of a non-fouled surface.[1] Surface modification by means of the application of antifouling coatings is advantageous for, *e.g.*, manufacturing biosensors,[2] implants,[3,4] bioactive surfaces,[5] and even big objects like the hull of a ship.[6]

Especially for sensing low concentrations of a target analyte in complex media, there is a demand for facile surface modifications to impart biosensors with antifouling properties in order to prevent non-specific interactions and thereby enhance the signal-to-noise ratio.[7] Antifouling coatings frequently consist of polyethyleneglycol (PEG)[8,9] or zwitterionic polymers.[10–15] More recently, however, also poly(*N*-(2-hydroxypropyl)methacrylamide) (polyHPMA) brushes grown by controlled radical polymerizations have been reported to result in stable and highly antifouling coatings, on a par with – and in some cases outperforming– zwitterionic coatings.[7,13,16–19] Although the antifouling properties of poly(HPMA) brushes are not entirely understood, the reported fouling levels are extremely low.[16,18] These polymeric coatings can be created via a *grafting-from* approach, in which a polymer is grown from the surface.[20,10,11] This is currently considered a highly promising route towards antifouling coatings in terms of long-term antifouling properties, as it leads to a high-density brush structure on the surface with tunable thickness.[21–23] However, despite these advantageous properties of polymer brushes grown via the *grafting-from* method, there is a major hurdle to be overcome if these antifouling coatings are to be applied reproducibly on large, industrially relevant scales.[24] Namely, these *grafting-from* polymer brushes are typically fabricated by surface-initiated, controlled living polymerization in the presence of a metal catalyst and in an oxygen-free environment.[11,13,18,25,26] Since this is typically a rather critical technique, it is difficult to scale up and implement in, *e.g.*, industrial production lines in a reproducible manner.[20,23] For this reason, there is a need to investigate other macromolecular coatings that can potentially match the antifouling properties of these coatings, but at the same time allow easy and reproducible fabrication.[11,13,20,25]

To this aim, one-step coatings using zwitterionic antifouling polymer brushes with a catechol end group were developed for *grafting-to* surface anchoring.[27,28] In addition, Honda *et al.* created randomly composed block copolymers of zwitterionic antifouling groups, combined with triethoxy silanes for surface binding, to create antifouling coatings on glass.[23] Another well-known example of combining antifouling groups with polydentate surface anchoring moieties are poly(L-lysine)-*graft*-poly(ethylene glycol) (PLL-*g*-PEG) polymers, which are known to assemble onto silicon oxide, metal oxide and polymeric surfaces.[29–34] PLL-*g*-PEG self-assembles on silicon oxide at pH > 2 through multiple electrostatic attractions between the negatively charged surface (SiO_2 isoelectric point (IEP) ~ 2.2)[35] and the positively charged pendant amine groups present in PLL (IEP ~9.5),[36] leaving the PEG chains oriented away from the surface.[34]

Despite the ease of application and good antifouling properties of such PLL-*g*-PEG coatings, their use under certain circumstances can be limited due to properties inherent to PEG chains: PEG is known to undergo oxidative degradation, which may yield toxic compounds and leads to degradation of the coating, and has been shown to elicit antibody expression *in vivo*.[37–41]

In response to these limitations, in 2018 Morgese *et al.* published a study on polymers with PLL backbones that were grafted with other types of antifouling polymer brushes, such as poly(2-oxazines) and poly(2-oxazolines) to create bio-interfaces that resist protein adsorption.[31] However, the promising HPMA polymer was not included as a candidate in this study, and the authors only considered the *grafting to* approach. Therefore, we aimed to develop and investigate a bottlebrush macromolecule with poly(HPMA) grafted side chains for antifouling properties, together with a PLL backbone for multivalent surface interactions to achieve strong surface anchoring to silicon oxide surfaces.[28] Previously, PLL and HPMA-based polymers have been combined in hybrid macromolecules for the synthesis of gene delivery agents,[42] or as transfection reagents with minimized toxicity.[43] However, to the best of our knowledge, PLL-HPMA bottlebrushes have not yet been used for the creation of antifouling coatings. The overall goal of this project is to construct PLL bottlebrush coatings in an easy and highly scalable manner without loss of antifouling performance, and the current paper is the first step in this approach for PLL-HMPA bottlebrushes as antifouling coatings.

In this study, silicon oxide was used as a model substrate because of its relevance in, *e.g.*, biosensors[44] and microfluidic devices.[45] We explored three different routes towards such a coating with varying degrees of *grafting-to* and *grafting-from* components (Figure 5.1).

- *Route A*: a coating was completely *grafted-from* the surface. First, PLL was self-assembled on the surface. The RAFT agent that allows for polymerization was subsequently reacted to the PLL coating, after which HPMA side chains were RAFT-polymerized from the PLL backbone.

- *Route B*: a coating that was partly *grafted-from* the surface. The RAFT agent (RA) was coupled to PLL in a solution to synthesize a PLL-RA macroinitiator. The PLL-RA was self-assembled on the surface and HPMA was finally RAFT-polymerized from the RA-modified PLL coating.

- *Route C*: a completely pre-synthesized, *grafted-to* coating. HPMA was RAFT-polymerized from the PLL-RA macroinitiator in solution to create PLL-HPMA bottlebrushes. These bottlebrushes were then self-assembled on the surface in one single step.

For the growth of the poly(HPMA) brushes, photoinduced electron transfer–reversible addition-fragmentation chain transfer (PET-RAFT) technique was applied. This polymerization technique is oxygen tolerant, metal-free and can be applied to polymerizations in water,[46,47] works with an accessible and affordable organic photocatalyst (EosinY),[46,45] and has been shown to be also applicable to the surface-initiated polymerization of different monomers.[48] Especially this final feature makes PET-RAFT very suitable for our purpose, as it works well both in solution as well as from a surface. Subsequently, we determined and evaluated the various properties of the thus formed coatings in detail, including ease of synthesis, scalability, reproducibility, modularity, and ease of characterization. Finally, we performed a preliminary investigation of the antifouling performance obtained for these three coating approaches, and provide a perspective on the use of such PLL-HPMA bottlebrush coatings for antifouling purposes.

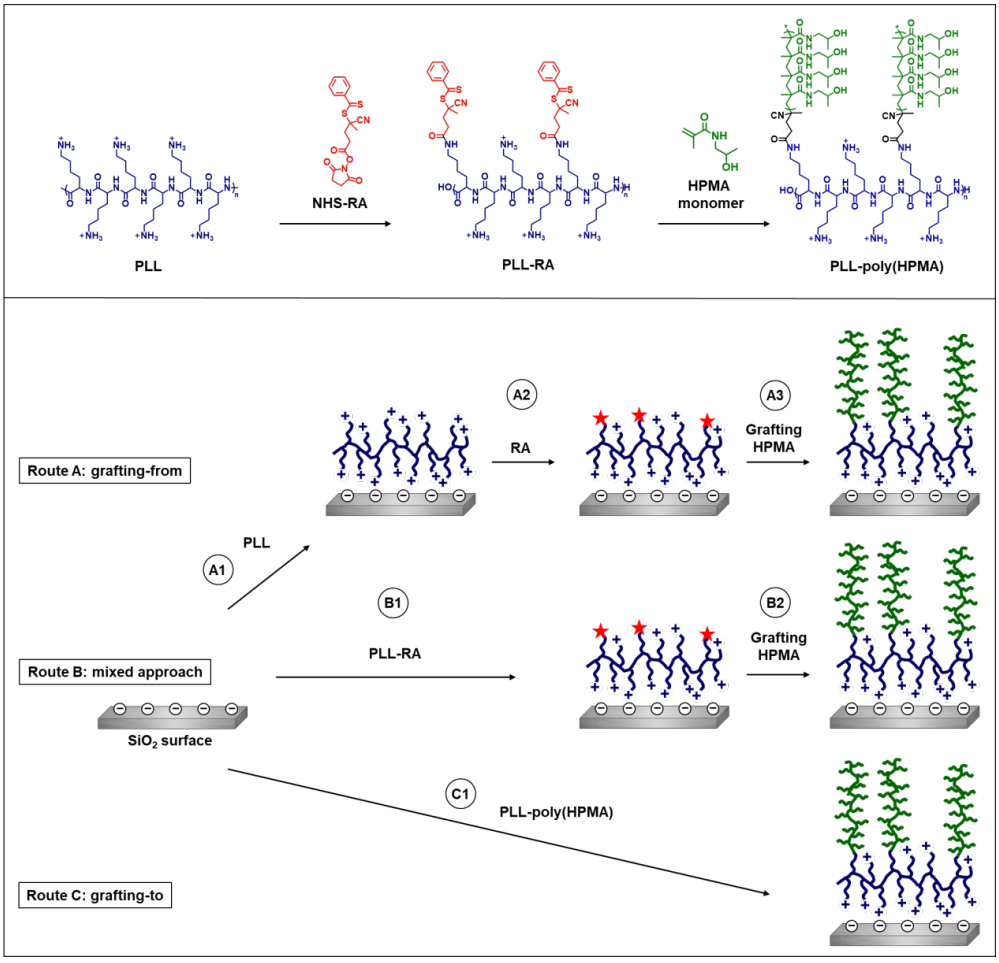

Figure 5.1 Schematic overview of the solution-based synthesis of the macroinitiator (PLL-RA) and PLL-HPMA bottlebrush structure (top). The three investigated routes A–C towards surface-immobilized PLL-HPMA bottlebrushes (bottom). PLL is poly(L-lysine), RA is RAFT agent, HPMA is 2-hydroxypropyl methacrylamide.

5.2 Results and Discussion

We will first discuss the synthesis of the PLL-HPMA bottlebrush-based coatings on silicon oxide surfaces, as obtained via the three different routes presented in Figure 5.1. Afterwards, the results of antifouling studies on the coatings prepared by these different routes will be discussed and evaluated.

5.2.1 Route A: PLL-poly(HPMA) coating via the *grafting-from* procedure

In route A, the poly(HPMA)-based coating was completely *grafted-from* the surface. First, PLL was self-assembled on the surface, followed by coupling of the surface-bound PLL to the RAFT agent (RA), and finally, the polymerization of the poly(HPMA) side chains from the PLL backbone (Figure 5.2).

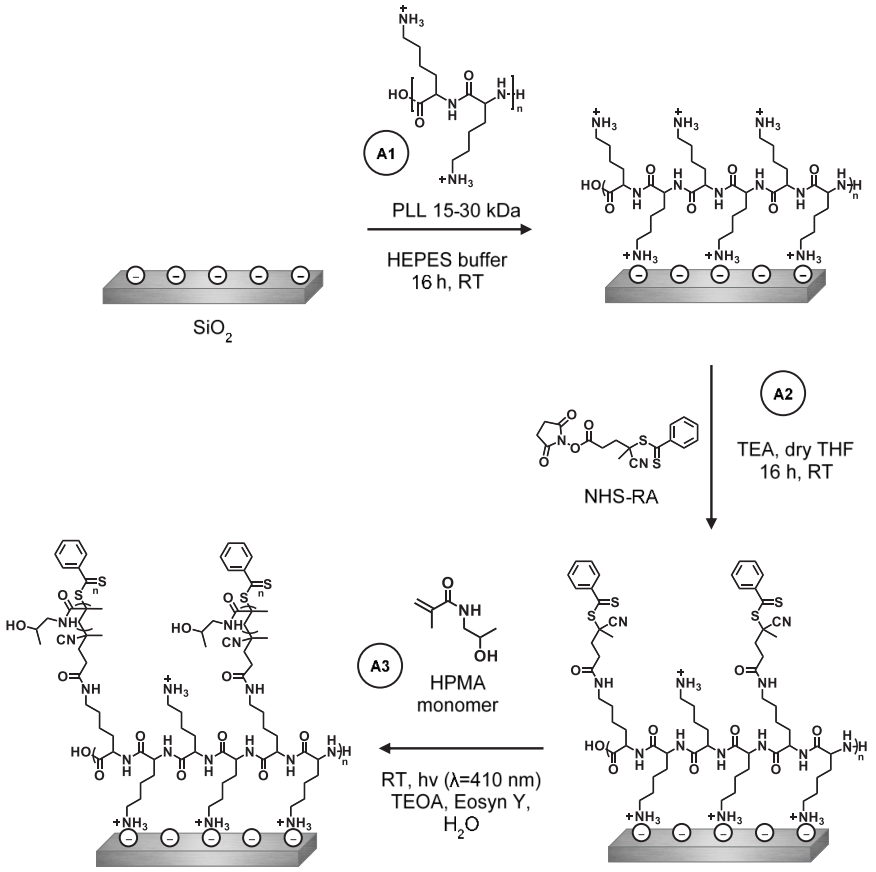

Figure 5.2 Schematic depiction of the construction of the PLL-RA coating via a grafting-from approach, followed by SI-PET-RAFT to grow poly(HPMA) brushes.

A1: Self-assembly of Poly(L-lysine) on SiO_2

PLL-HPMA bottlebrush-coated surfaces were prepared in this first route by building the layer from the surface upwards. To this end, PLL (MW = 15-30 kDa) was self-assembled to form a monolayer by overnight immersion of freshly cleaned, negatively charged silicon oxide surfaces in a 0.1 mg/ml solution of PLL in HEPES buffer (following the procedure reported by Morgese *et al.*[31]). Upon modification of the silicon oxide surfaces with PLL, the presence of a thin layer of polymers on the surfaces was confirmed by analytical techniques. Firstly, by X-ray photoelectron spectroscopy (XPS) we found signals corresponding to the presence of nitrogen (at 400 eV) and carbon (285 eV) on the surface (Figure 5.3, top). Furthermore, the C_{1s} narrow scan measurements showed the characteristic signals for the amide carbonyls (C=O, 288.4 eV), and for the C–N and C–C=O carbon atoms (both at 286.4 eV). Since these monolayers were too thin to be measured by ellipsometry (*vide infra*), we used the Si/C ratio in the XPS wide scan to calculate the average thickness of the layer,[49,50] which was approximately 0.5 nm, which is in good agreement with values reported in the literature.[51,52] The static water contact angle (SWCA) of the PLL-coated surfaces was < 20°, displaying the very hydrophilic character of the coating due to the charges on the protonated terminal amines. These combined data suggest that PLL was deposited as a monolayer on the SiO_2 surfaces.

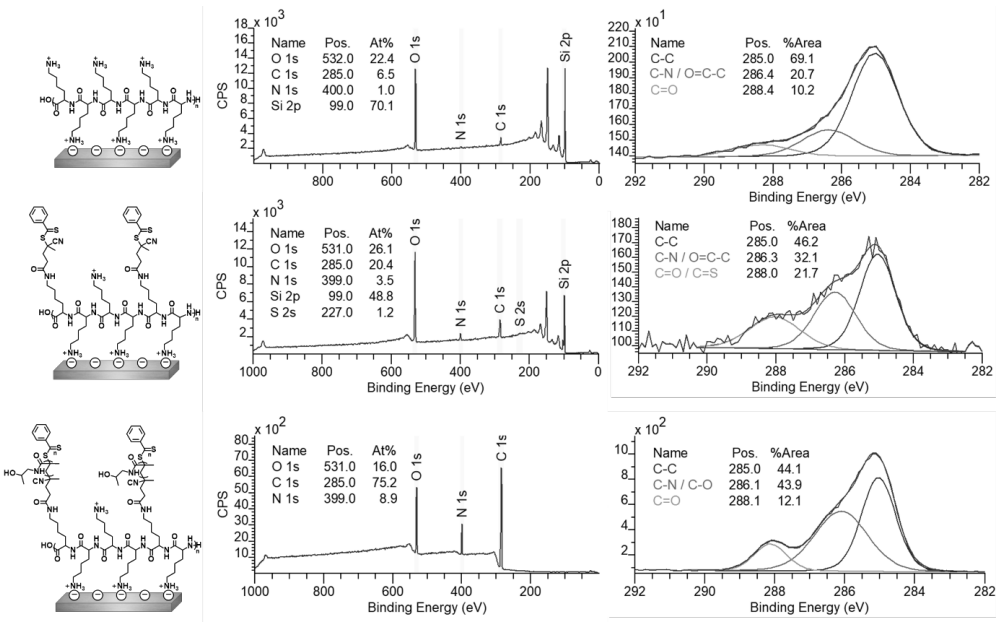

Figure 5.3 XPS wide scan spectrum and C_{1s} narrow scan spectrum of self-assembled PLL on silicon oxide (top), surface-bound PLL, functionalized with RAFT agent (middle) and poly(HPMA) grafted from RAFT agent-modified silicon oxide (after 80 min polymerization) (bottom). On the left, the chemical structure of the analyzed surface is depicted.

A2: Surface immobilization of RAFT agent on PLL-modified SiO_2

While a fraction of the pendant amine groups of PLL was involved in surface binding, the remaining free primary amines of the PLL coating can be used to immobilize a RAFT agent to allow in the following step the polymerization from the surface. To this end, an NHS-activated RAFT agent was reacted with the surface-bound PLL overnight in dry THF (see Figure 5.2, step A2). In the XPS spectrum of the thus prepared surface (Figure 5.3, middle), we found an expected increase in both the C_{1s} (285 eV) and N_{1s} (399 eV) signals in the wide scan, since these elements are predominantly present in the RAFT agent. Moreover, indicatively, we detected sulfur (S_{2s}, 227 eV), which confirms the presence of the RAFT agent. Based on the N/S ratio obtained from XPS wide spectra, roughly 40% of all PLL primary amines have reacted to hold a RAFT agent moiety (Figure 5.18). Taking into account that also a portion of the primary amines is involved in surface binding by electrostatic interactions, this conversion can be considered relatively high, compared to what would be maximally feasible for still strongly surface-bound PLL. The conversion was also confirmed in the C_{1s} narrow scan, which showed that the carbonyl signal at 288 eV became more dominant, which can be attributed to the introduced carbonyl and thiocarbonyls. As expected, the thickness of the coating increased upon the addition of the RAFT agent to approximately 1.3 nm. The SWCA of the RAFT-modified surfaces increased to 42°, in line with the more hydrophobic nature of the RAFT agent.

A3: PET-RAFT polymerization of HPMA on RAFT agent modified SiO_2

Poly(HPMA) side chains were grown from the RAFT-modified, PLL-covered silicon oxide surfaces by surface-initiated PET-RAFT in water using visible light and Eosyn Y as an oxygen tolerant photocatalyst, which allowed polymerization in air.[46,48] Triethanolamine (TEOA) was used as a co-catalyst,[46] and also acted as a sacrificing electron donor to reduce oxygen in the polymerization system.[48] The study of the polymer growth kinetics showed a linear growth for the first 40 min (Figure 5.4), which indicates the controlled nature of this surface-initiated polymerization. The leveling off after 40 min might indicate a reduced availability of the RAFT groups by either increased steric hindrance or chemical degradation.

The chemical composition of the grown poly(HPMA) brushes was studied using XPS, while ellipsometry was used to determine the layer thickness of the polymer brushes. After 80 min of polymerization, the coating reached a total thickness of 32.0 ± 0.2 nm. Similar growth rates have been reported for this HPMA monomer using PET-RAFT on silane anchoring layers.[48] This implies that from a self-assembled polymeric PLL starting layer, the polymerization works equally well compared to well-defined silane monolayers. Figure 5.3 shows the XPS spectra for the polymer brushes that were grown for 80 min. In the wide scan, only three main peaks are observed, namely O_{1s} (531 eV), N_{1s} (388 eV), and C_{1s} (285 eV) in a 1.8 : 1 : 8.3 ratio. This is in reasonable agreement with the elemental composition of the poly(HMPA) structure (2 : 1 : 7) and previously published papers on HPMA brushes, which report a ratio of 1.8 : 1 : 7.6,[48] given the possibility of atmospheric contamination.
In the C_{1s} narrow scan, a clear, more intense signal around 286 eV could be discerned, compared to the RAFT agent-terminated surfaces from before the polymerization. This indicates the increase of C–heteroatom species, which is in agreement with the structure of the HPMA polymer. The SWCA of the polymer layers reached a stable SWCA of ~50° after 40 min of polymerization. Additionally, after 80

min of polymerization, the layers showed a low roughness (Figure 5.22) as could been expressed by a root mean square roughness: R_q = 2.44 ± 0.44 nm as measured by AFM (see supporting information). Overall, these data suggest a surface structure that is similar to that previously reported for HPMA polymer brushes grown by different surface-initiated controlled polymerization methods.[13,18,48]

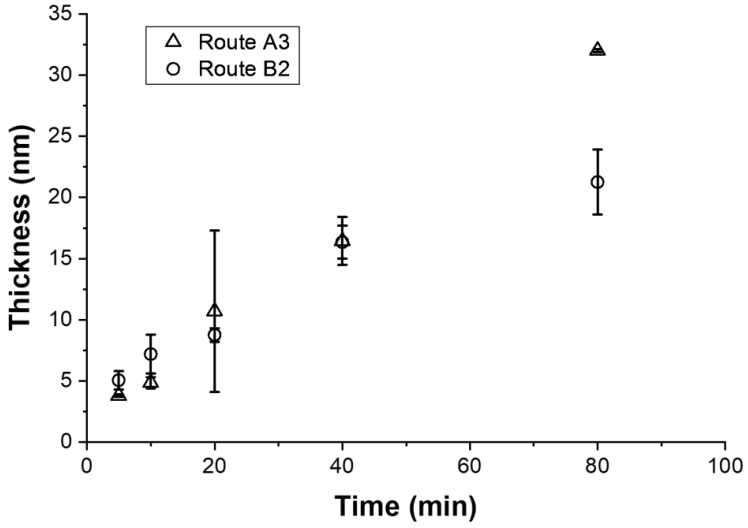

Figure 5.4 Polymerization kinetics of both on-surface PET-RAFT polymerizations of HPMA: Route A3: polymerization on RAFT agent-modified surfaces that were obtained by reacting NHS-RAFT with surface-immobilized PLL. Route B2: polymerization on RAFT agent-modified surfaces that were obtained by the self-assembly of a PLL-RA macroinitiator. Thicknesses were measured *in duplo* by ellipsometry.

5.2.2 Route B: Synthesis and self-assembly of a PLL-RA macroinitiator and HPMA polymerization from PLL-RA-modified surfaces.

In route B the coating was only partly *grafted-from* the surface. The RA was first coupled to PLL in a solution to synthesize a PLL-RA macroinitiator. This PLL-RA macroinitiator was then self-assembled on the surface, after which HPMA was polymerized from the RA-modified PLL side chains (Figure 5.5).

B1: Synthesis and self-assembly of PLL-RA macroinitiator on SiO_2

Route B started with the synthesis of a RAFT agent-functionalized PLL polymer macroinitiator that could afterward be immobilized on the surface (Figure 5.5). By reacting a part of the amine end groups with an NHS-activated RA, we envisioned that enough lysine moieties would be left unreacted to achieve efficient binding of PLL to the silicon oxide surface in the subsequent self-assembly process. Therefore, we chose a 1 : 3 ratio of NHS-RA : lysine monomer in the synthesis of PLL-RA.

The synthesized PLL-RA macroinitiator was first of all characterized by ^{1}H NMR spectroscopy, also allowing for the determination of the actual achieved RA : lysine ratio, which was found to be 1 : 9.8 (Figure 5.11). This ratio was also supported by the elemental composition of the PLL-RA after immobilization on a silicon oxide surface: by comparing the ratios between the N_{1s} and S_{2s} signals in

XPS we found the RAFT : lysine ratio to be 1 : 8.5, which is comparable to the ratio found by ^{1}H-NMR (see Figure 5.19 in the Supporting Information). Several reasons could account for the lower observed degree of RAFT agent incorporation. First of all, the reaction was stopped after 16 h, which might be before full conversion had been reached. The lower degree might have also been affected by the relatively low solubility of PLL and NHS-activated RAFT agent in a common solvent (HEPES buffer with 10 v/v% DMSO), or by partial hydrolysis of the NHS ester. Finally, partial protonation of the amine end groups might have lowered the conversion of the reaction.

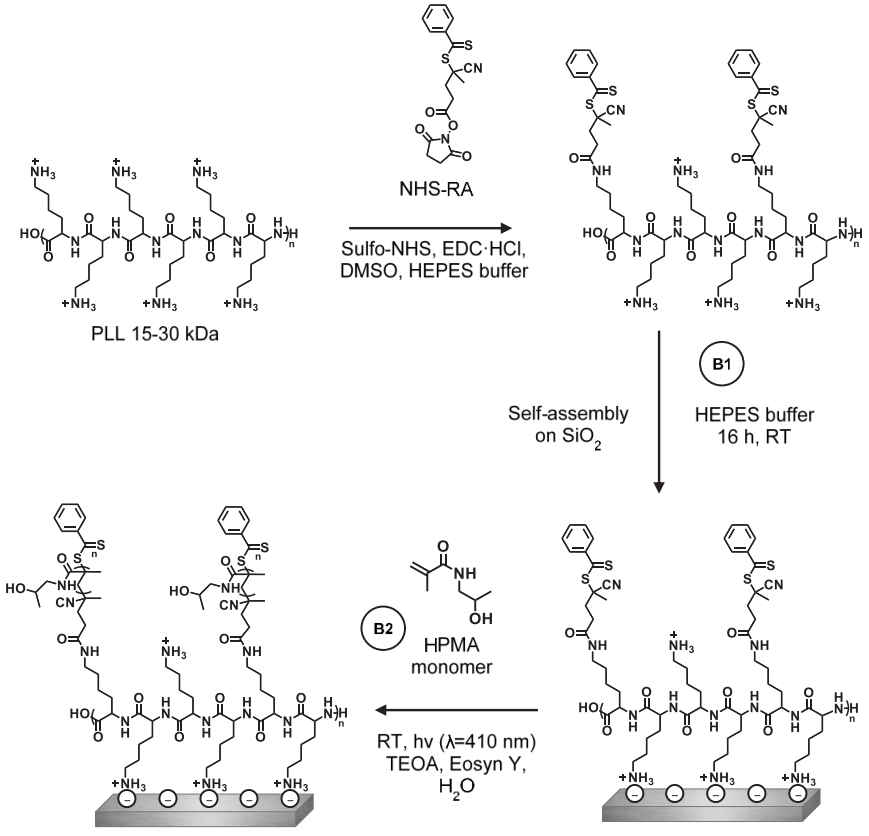

Figure 5.5 Schematic depiction of the build-up of the PLL-RA coating in a partly *grafting-to* approach, followed by SI-PET-RAFT to grow polyHPMA brushes.

Nevertheless, having approximately 9 out of 10 lysines available for surface anchoring likely leads to a more stable coating, while still having enough initiation points for the growth of relatively long polymer brushes. This was demonstrated by the successful growth of poly(HPMA) brushes from silicon oxide surfaces that were coated by the PLL-RA macroinitiator, as discussed below. The PLL-RA macroinitiator formed a monolayer by self-assembly on a freshly cleaned silicon oxide surface using the same protocol as in route A1 (Figure 5.5). XPS analysis of this coating revealed signals for the elements N (at 400 eV), C (285 eV) and S (231 eV) on the surface. In addition, the C_{1s} narrow scan showed the characteristic

signals for the amide carbonyls (N–C=O, 288.2 eV), and the nitrogen- and carbonyls-bound carbon atoms (C–N and C–C=O), both at 286.2 eV (Figure 5.6).

The layer thickness of the PLL-RAFT macroinitiator coating was calculated using the Si_{2p} : C_{1s} ratio from the XPS wide scan, and was found to be approximately 2.2 nm, which thicker than the value obtained in route A (1.3 nm), in which an analogous coating was created by reacting the NHS-RA moiety on pre-assembled PLL. The assembled PLL-RA coating (in route B) had a SWCA of 36°, which is slightly less hydrophobic than the PLL-RA coating from route A (SWCA of 42°). This could be ascribed to the fact that the coupling of the RAFT agent to PLL in solution (step B1) occurs randomly on the entire polymer, while the coupling on the surface (step A2) predominantly occurs on the top (solution-exposed) part of the PLL coating. Therefore, in route B a smaller fraction of the RAFT moieties could have an upward orientation compared to the PLL-functionalized polymer discussed in route A, which would explain the reduced increase in the hydrophobic character of the overall coating for route B.

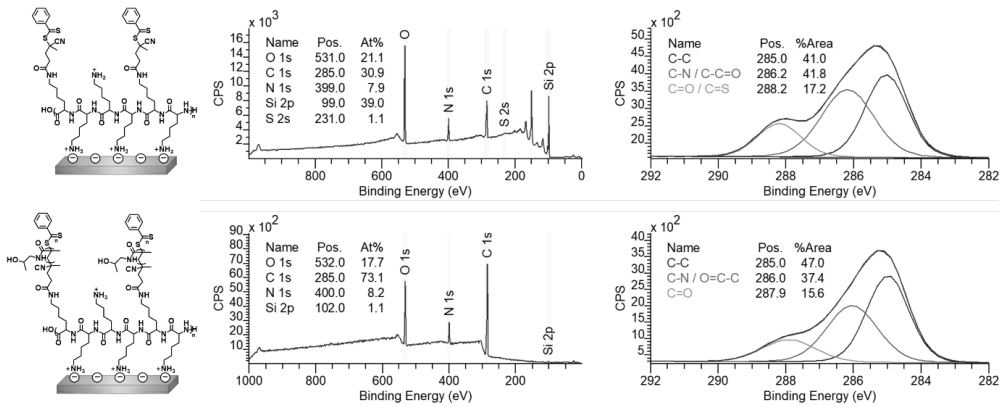

Figure 5.6 XPS wide scan spectrum and C_{1s} narrow scan spectrum of self-assembled macroinitiator PLL-RA (top) and poly(HPMA) grafted from these surfaces (80 min polymerization) (bottom). On the left, the chemical structure of the analyzed surface is depicted.

B2: PET-RAFT polymerization of HPMA on PLL-RA macroinitiator-modified SiO_2

Once the PLL-RA macroinitiator was immobilized on the surface, poly(HPMA) brushes were grown using PET-RAFT conditions, as described in the previous paragraph (Figure 5.5). The layer thicknesses of the polymer coatings that were grown for different time intervals were measured using ellipsometry, allowing the comparison of the kinetics of the polymerization for routes A and B (Figure 5.4). The rate of polymerization is similar for the first 40 min, which implies that the amount of RAFT agent and hydrophilicity of the surface are not rate-determining. After 40 min, the polymerization in route A seems to continue, while the route B polymerization seems to level off. This might be due to the different availability of RA at the surface as discussed in step B1.

Figure 5.6 shows the XPS data of a polymer brush that was grown for 80 min, and which had a thickness of 21 nm, as determined from ellipsometry. In the wide scan, we see three main peaks, namely for the elements O_{1s} (532 eV), N_{1s} (400 eV) and C_{1s} (285 eV) in a 2.3 : 1 : 9.1 ratio, which is in reasonable agreement with the ratios found in the full *grafting-from* procedure in route A (1.8 : 1 : 8.3). In this case, also a very small signal is visible from the silicon oxide surface (Si_{2p}, 102 eV), which confirms the slightly thinner coating as already measured by ellipsometry. Also, the C_{1s} narrow scan gave a very similar spectrum as previously observed for the poly(HPMA) coating in route A. The SWCA stabilized after 30 min polymerization of HPMA to ~50°. AFM topology measurements of the surfaces after 80 min of polymerization revealed a somewhat higher roughness *Rq* = 5.47 ± 0.75 nm compared to surface A3 (2.44 ± 0.44 nm). This is probably due to the more hydrophobic, hence less soluble, character of the initial PLL-RA. Overall, it can be concluded that the polymerization by PET-RAFT from the PLL-RA macroinitiator-modified surfaces was possible in only two surface modification steps. The coupling of the RAFT agent to the PLL polymer in solution did not significantly affect the final polymerization step, which implies that the surface modification procedure can be shortened by one step.

5.2.3 Route C: PLL-HPMA coating via the *grafting-to* procedure

Route C comprises a completely pre-synthesized, *grafted-to* coating. HPMA was first polymerized from the PLL-macroinitiator in solution to create PLL-HPMA bottlebrushes. These bottlebrushes were then self-assembled on the surface in one single step (Figure 5.7). Furthermore, bottlebrushes with carboxybetaine groups that offer the possibility for later biofunctionalization (PLL-HPMA/CBMA) were also synthesized and immobilized on a surface using the method presented in route C.

C1: Solution synthesis and surface immobilization of PLL-HPMA by PET-RAFT polymerization of HPMA from PLL-RA macroinitiator

The previously discussed routes (A and B) required two or three consecutive surface modification steps to create a PLL-HPMA coating on silicon oxide. While route B is thus certainly attractive in terms of scalability, we considered it to be of even more interest to further decrease the number of surface modifications steps, so as to have a one-step procedure for the coating of silicon oxide surfaces by PLL-HPMA bottlebrush polymers. In such a route, the full polymer, a backbone polymer (PLL) with polymeric poly(HPMA) side chains is pre-synthesized in solution, and only subsequently applied to the surface. To this aim, poly(HPMA) side chains were grown from the PLL-RA macroinitiator, which was already synthesized for route B, in solution (Figure 5.7). From the RAFT agent side groups of this macroinitiator, poly(HPMA) chains were grown by PET-RAFT polymerization in water using visible light, Eosyn Y as an oxygen tolerant photocatalyst and triethanolamine (TEOA) as a co-catalyst, in line with the conditions used in route B to grow the poly(HPMA).[48] Extensive dialysis allowed the isolation of the PLL-HPMA bottlebrush that could then be characterized by ^{1}H NMR spectroscopy (Figure 5.8). In the ^{1}H NMR spectrum, peaks at δ 3.08 ppm and δ 3.84 ppm confirm the presence of the poly(HPMA) side chains of the bottlebrush. From the ratio between the ^{1}H signal at δ 4.15 ppm from the PLL backbone and the ^{1}H signal at δ 3.84 ppm from HPMA, the ratio between HPMA monomer : lysine monomer was found to be 1.4 : 1. Combining this ratio, with the previously determined RA : lysine ratio of the PLL-RA macroinitiator, the average chain length of the each HPMA side chain could be

calculated to be roughly 14 repeating monomers, corresponding to approximately 2 kDa. The total weight of the PLL-HPMA bottlebrush was calculated to be 41 kDa (see calculations in Supporting Information).

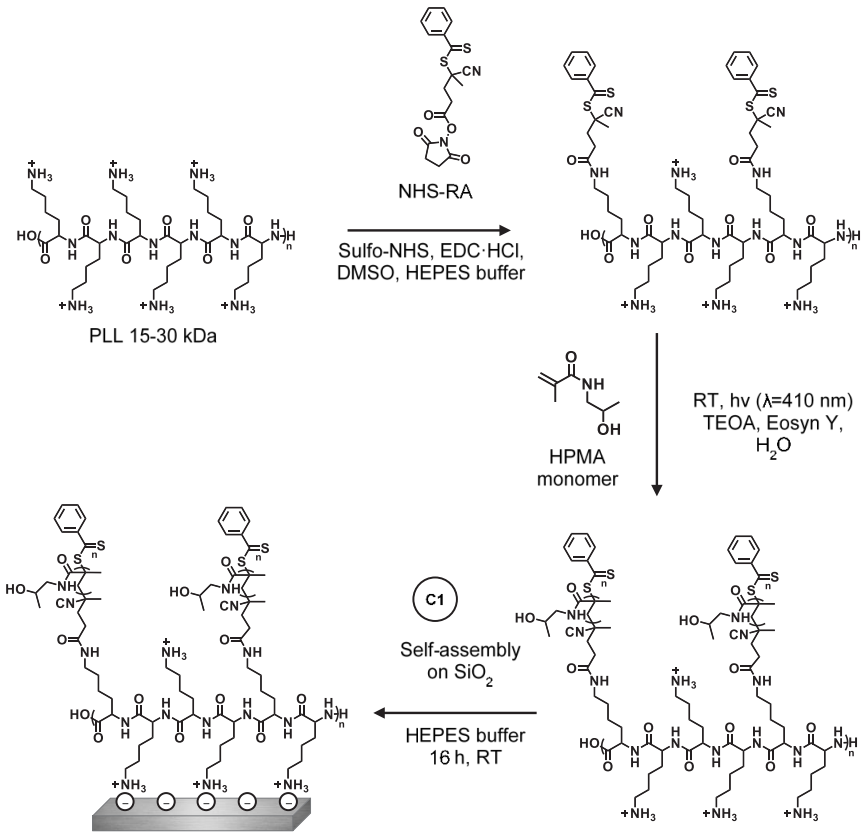

Figure 5.7 Schematic depiction of the build-up of the PLL-HPMA coating in a completely *grafting-to* approach.

The polymer molecular weight and polydispersity index (PDI) were determined by gel permeation chromatography (GPC) in water. Based on calibration by a set of poly(ethylene glycol) standards and a poly(HPMA) standard, a molecular weight of approximately 43 kDa was found, *i.e.* close to the NMR-derived value. Furthermore, from GPC a polydispersity index (PDI) of 1.4 was determined. Further characterization by dynamic light scattering (DLS) revealed a narrow size distribution with an intensity peak maximum at a hydrodynamic radius of 77 nm in water (Figure 5.21).

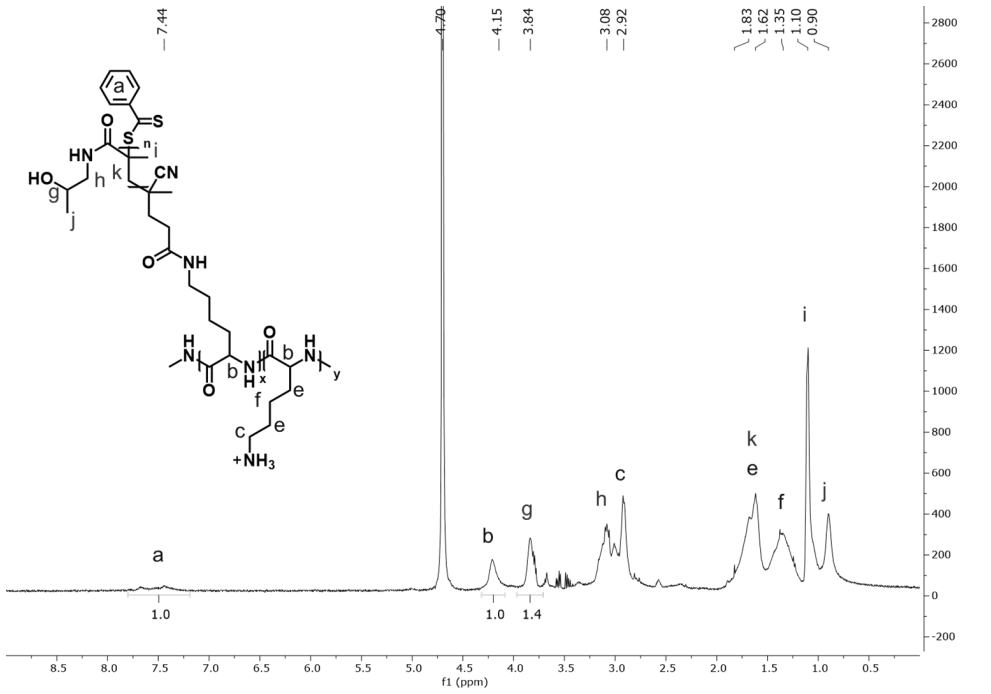

Figure 5.8 ^{1}H-NMR spectrum of the PLL-HPMA bottlebrush synthesis in solution (in D_2O, 400 MHz, 298 K).

The synthesized PLL-HPMA bottlebrushes were allowed to self-assemble on silicon oxide surfaces by overnight immersion of in a 0.1 mg·mL^{-1} solution of PLL-HPMA in HEPES buffer. XPS analysis of this coating (Figure 5.9) showed signals for N (at 399 eV) and C (285 eV) on the silicon oxide surfaces, which is in agreement with the presence of a monolayer of PLL-HPMA. The C_{1s} narrow scan measurements showed the expected signals for the amide carbonyls (*C*=O, 288.2 eV), and carbon-nitrogen and carbon-carbonyls (*C*–N and *C*–C=O), both at 286.2 eV). The layer thickness of the PLL-HPMA coating was calculated using the Si_{2p} : C_{1s} ratio from the XPS wide scan and was found to be approximately 0.9 nm. While this is a rather low layer thickness for a surface-immobilized bottlebrush polymer, it should be pointed out that the XPS thickness measurements were taken under ultra-high vacuum conditions, creating a collapsed polymer layer (which will expand upon immersion). Furthermore, the found dry thickness is in agreement with other types of surface-immobilized PLL-based bottlebrushes reported in literature.[29–31] The self-assembly of PLL-HPMA lead to the formation of a smooth layer (**Figure 5.22**), as the reported roughness by AFM was R_q = 2.37 ± 0.05.

The SWCA of this PLL-HPMA coating was approximately 20°. This hydrophilic character might be due to the polar (partially charged) amine groups of the PLL within the coating that are close to the solvent interface due to relatively low layer thickness of the overall coating. However, the SWCA of the PLL-HPMA self-assembled coating is higher than for the PLL monolayer with comparable thickness observed for step A1 (which has a reported SWCA below 20° for a 0.5 nm surface-immobilized brush) due to the presence of poly(HPMA).

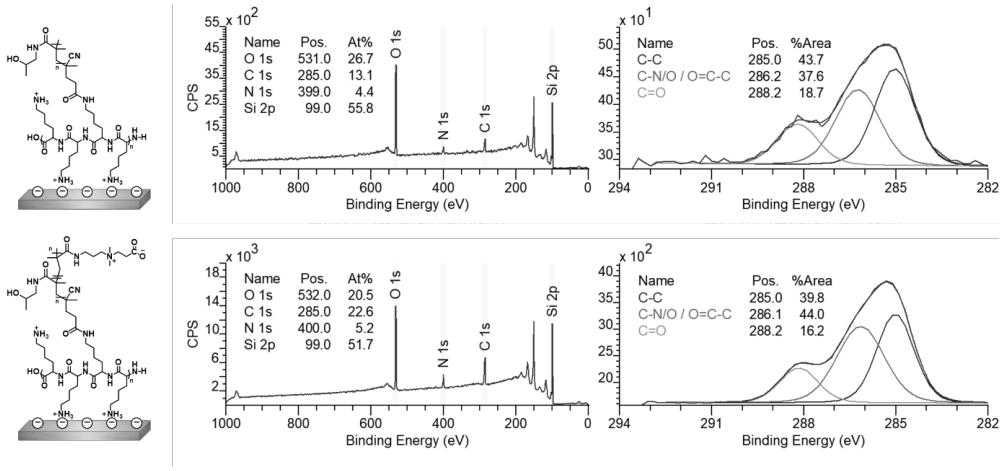

Figure 5.9 XPS wide scan spectrum and C_{1s} narrow scan spectrum of self-assembled PLL-HPMA (top) and PLL-HPMA/CBMA (bottom). On the left, the chemical structure of the analyzed surface is depicted.

Carboxybetaine-doped HPMA brushes for biofunctionalization purposes

We have further improved the concept of PLL-HPMA one-step antifouling coatings by incorporating the possibility for biomolecule immobilization, which is highly desirable for selective binding in, *e.g.*, biosensors and tissue engineering.[7,53,54] The polymerization of HPMA from the PLL-RA macroinitiator was also performed in the presence of a second antifouling monomer that contains a carboxylate group to allow for easy activation by conventional coupling strategies, *e.g.* NHS/EDC, to couple bioactive moieties. To this end, we selected a zwitterionic carboxybetaine (CBMA) monomer that was also used previously for surface functionalization.[7,10,13,55] To this aim, 5% of CBMA monomer was used for this polymerization, keeping the conditions the same as described for the PET-RAFT solution polymerization. The obtained PLL-HPMA/CBMA polymer was analyzed by ^{1}H NMR spectroscopy (see Figure 5.15). We observed the expected additional signals coming from the CBMA monomers, when comparing to the PLL-HPMA bottlebrush spectrum. Based on ^{1}H NMR integration, the content of CBMA was calculated to be 7.7%. The somewhat higher incorporation of CBMA monomer likely stems from the previously reported difference in reactivity between the monomers.[48] The polymer molecular weight and PDI were approximated using GPC and gave an MW of approximately 53 kDa and a PDI of 1.6. In addition, DLS gave a narrow size distribution in water with a maximum at a hydrodynamic radius of 111 nm (Figure 5.22).

The synthesized PLL-HPMA/CBMA bottlebrushes were allowed to self-assemble on silicon oxide surfaces under similar conditions as described above. XPS analysis of this coating (Figure 5.9), revealed signals for the elements N (at 400 eV) and C (285 eV) on the silicon oxide surfaces. The layer thickness of the PLL-HPMA/CBMA coating was calculated using the Si_{2p} : C_{1s} ratio from the XPS wide scan and was found to be approximately 1.3 nm, which is in accordance with the formation of a monolayer of PLL-HPMA/CBMA. The C_{1s} narrow scan measurements showed the expected signals for the amide

carbonyls (*C*=O, 288.2 eV), carbon-nitrogen and carbon-carbonyls (*C*–N and *C*–C=O, both at 286.1 eV). The higher amount of carbon-nitrogen and carbon-carbonyl signals compared to the PLL-HPMA layer (44% vs. 38%) could be explained by the presence of the CBMA monomer that contains an additional carbonyl group. The layer thickness of the PLL-HPMA/CBMA coating was calculated using the Si_{2p} : C_{1s} ratio from the XPS wide scan, and was found to be approximately 1.3 nm. This layer was thus slightly thicker than the PLL-HPMA monolayer, which might be explained by the longer side chains. The SWCA of the PLL-HPMA/CBMA coating was approximately 22°, which is very similar to the PLL-HPMA analog. The self-assembly of the PLL-HPMA/CMBA lead to the formation of a smooth layer (see (**Figure 5.22**), as the reported roughness by AFM was R_q = 1.16 ± 0.05.

Having successfully incorporated CBMA in the PLL-HPMA bottlebrushes, a broad and versatile platform for (bio)functionalization was created. For both poly(HPMA) and poly(CBMA), the antifouling properties are most probably related to the strong binding of water molecules.[56] The combination of these polymers was previously utilized in polymer brush systems which showed good antifouling properties.[14,57] By activation of the carboxylate groups – either in solution or on the surface – antibodies or other bioactive molecules can be installed for monitoring specific interactions in, *e.g.*, biosensor platforms.[7,14,58–60]

5.2.4 Antifouling properties of PLL-HPMA coatings

Having successfully immobilized the three different PLL-HPMA bottlebrush coatings on the silicon oxide surface, a preliminary investigation of their antifouling properties was performed. We quantified the amount of protein adsorption by fluorescence microscopy, by exposing the PLL-HPMA bottlebrush coatings to fluorescently labeled protein solutions.[13,23,28] This method allows for a limit of fluorescent protein detection of 300 pg·mm^{-1} and thus suffices for initial testing.[48] For this study, lysozyme (LYS) and bovine serum albumin (BSA) were used as model proteins at concentrations of 0.1 mg·mL^{-1} in PBS and contacted with the surfaces for 15 min before washing with PBS. BSA was chosen since it is one of the most common proteins in blood plasma with an overall negative charge at pH 7.4 (PBS buffer).[61] LYS is a relatively small, hydrophilic protein and was used because of its overall positive charge at pH 7.4 (PBS buffer).[62] As controls for the protein adsorption experiments, we used bare silicon oxide surfaces, PLL-modified surfaces, and surfaces modified with commercially available PLL-PEG, which is known to have good antifouling properties.[30]

The unmodified silicon oxide surface showed high fluorescence intensities from both solutions (Figure 5.10), indicating significant fouling. PLL-coated silicon oxide was used as a control and already showed less fouling compared to the bare silicon oxide surface, probably due to the hydrophilic and charged nature of the sample, which contributes to the antifouling properties.[20] However, there still is a significant amount of fouling by BSA visible on the PLL-coated silicon oxide, likely due to the oppositely charged nature of BSA and PLL. The PLL-PEG-coated silicon oxide control sample, showed the expected low fluorescence intensities, which confirms the functioning of the procedure and antifouling behavior. The fluorescent intensities for PLL-HPMA-based antifouling coatings were observed on the background level. These data show that PLL-HPMA coatings that were synthesized in different ways (route A, B, or C) show antifouling properties close to the limit of detection.

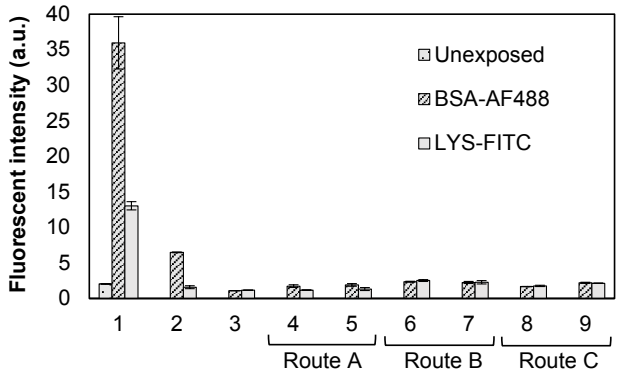

#	Route / Step	Surface – polymerization time
1	-	Bare silicon oxide
2	A1	PLL
3	-	PLL-PEG
4	A3	PLL-RAFT - 40 min HPMA
5	A3	PLL-RAFT - 80 min HPMA
6	B2	PLL-RAFT - 40 min HPMA
7	B2	PLL-RAFT - 80 min HPMA
8	C1	PLL-HPMA
9	C1	PLL-HPMA/CBMAA

Figure 5.10 Fluorescence intensities of different uncoated and coated silicon oxide surfaces (see table) after exposure to solution containing BSA-AF488 and LYS-FITC.

5.2.5 Comparing the different routes towards PLL-HPMA bottlebrush coatings

Coatings made by routes A, B and C showed very similar antifouling properties in single-protein solutions, irrespectively of any possible difference in their built-up, thickness, surface topology and/or brush density. However, depending on the to-be-coated surface and application, one can foresee that a certain route might be preferred over the other two. Both routes A and B led to relatively thick and dense coatings since the HPMA was *grafted-from* an initiator-modified surface. This could be beneficial for stability and long term use since the underlying anchoring layer is better shielded from the environment.

Route A showed the straightforward application of PLL as a multivalent, amine-terminated anchoring layer, on which a polymerization agent can be attached (step A1). PLL could, therefore, be an alternative to the often used silanes.[63–65] The follow-up steps are versatile with regard to the polymerization agent, technique, and monomer of choice.

In route B, the number of on-surface reactions is reduced to one. In solution, a macroinitiator is synthesized by a one-step coupling method. After that, the macroinitiator can be easily self-assembled on the surface, after which polymers can be grafted on the surface. This approach has also been used by Jain *et al.,*[66] who modified a polymer with polymerization initiator groups and embedded this new polymer in a layer-by-layer assay on porous membranes, to eventually grow polymer brushes from these membranes in a *grafting-from* approach. The pre-synthesis of the macroinitiator in solution, allows for precise control over the amount of embedded polymerization agent, and could be specifically beneficial in cases were the anchoring layer (PLL) and the to be polymerized monomer are impossible to synthesize in solution because of opposite polarities (or other properties that are challenging to combine in synthesis). Both route B and C might result in less long-term stable coatings compared to route A since the electrostatic interactions, that assure surface binding, are partly sacrificed by attaching the RAFT agent (route B) or poly(HPMA) side chains (route C) prior to surface binding.

Route C is easiest to apply on a surface and by far the easiest to scale-up, because of the one-step self-assembly and lack of on-surface reactions. The complete synthesis in solution allows control and

knowledge of the composition, weight and dimensions of the formed polymer. Also, this approach allows precise and quantifiable immobilization of (bio)molecules in solution, which typically requires smaller quantities of the (bio)molecule of interest in the overall coating process or on the surface. The synthesis procedure in solution takes time and requires purification. However, once synthesized, only very small amounts of PLL-HPMA (as little as 0.1 $mg \cdot mL^{-1}$) are needed to coat a surface, which makes it very desirable and cost-effective when a coating needs be applied to multiple or large surfaces.

5.3 Conclusion

In this work, we developed three different routes (A–C) to prepare effective antifouling coatings that consist of PLL-HPMA bottlebrushes. In these coatings, the poly(L-lysine) (PLL) backbone self-assembles onto a silicon oxide surface by charge-based interactions between the lysine groups and the negatively charged surface, whereas the poly(*N*-(2-hydroxypropyl)methacrylamide) (HPMA) side chains contribute to the antifouling properties. The PLL-HPMA bottlebrush polymer coatings were produced using *grafting-from* techniques by polymerizing HPMA from the surface (route A and B) and *grafting-to* of a pre-synthesized PLL-HMA bottlebrush (route C); the latter case – taking place fully under ambient conditions with only water as solvent – is both very easy for repeated and/or large-scale use, and allows detailed characterization of the finally polymer in solution, while methods A and B have to rely on surface-sensitive analytical methods for characterization. Additionally, in route C, a bottlebrush was synthesized that contains 5% carboxybetaine (CB) in its side chains, which offers the possibility for further functionalization after an ester activation step. Overall, all surface modification routes (A–C) yield coatings that show single-protein antifouling properties and are worthy of further, more detailed antifouling studies.

5.4 Acknowledgements

The authors thank Hans Beijleveld, Remko Fokkink and Lucas Teunissen for helpful discussions and instrumental support. This project was supported by Netherlands Organization for Scientific Research (NWO; LIFT program, grant 731.015.042) with Surfix BV as a partner and the Science PPP Fund research program with project number 741.018.105, which is partly financed by NWO.

5.5 References

1. Wisniewski, N.; Reichert, M. Methods for Reducing Biosensor Membrane Biofouling. *Colloids Surfaces B Biointerfaces* **2000**, *18* (3–4), 197–219.
2. Rodriguez-Emmenegger, C.; Avramenko, O. A.; Brynda, E.; Skvor, J.; Alles, A. B. Poly(HEMA) Brushes Emerging as a New Platform for Direct Detection of Food Pathogen in Milk Samples. *Biosens. Bioelectron.* **2011**, *26* (11), 4545–4551.
3. Huang, N.; Michel, R.; Voros, J.; Textor, M.; Hofer, R.; Rossi, A.; Elbert, D. L.; Hubbell, J. a; Spencer, N. D. Poly (l-Lysine)-g-Poly (Ethylene Glycol) Layers on Metal Oxide Surfaces : Surface-Analytical Characterization and Resistance to Serum and Fibrinogen Adsorption Poly (L-Lysine)-g-Poly (Ethylene Glycol) Layers on Metal Oxide Surfaces : Surface-An. *Langmuir* **2001**, No. 6, 489–498.
4. Yu, Y.; Cirelli, M.; Li, P.; Ding, Z.; Yin, Y.; Yuan, Y.; de Beer, S.; Vancso, G. J.; Zhang, S. Enhanced Stability of Poly(3-

Sulfopropyl Methacrylate Potassium) Brushes Coated on Artificial Implants in Combatting Bacterial Infections. *Ind. Eng. Chem. Res.* **2019**, *58* (47), 21459–21465.

5. Thissen, H.; Gengenbach, T.; du Toit, R.; Sweeney, D. F.; Kingshott, P.; Griesser, H. J.; Meagher, L. Clinical Observations of Biofouling on PEO Coated Silicone Hydrogel Contact Lenses. *Biomaterials* **2010**, *31* (21), 5510–5519.
6. Rosenhahn, A.; Schilp, S.; Kreuzer, H. J.; Grunze, M. The Role of "'Inert"' Surface Chemistry in Marine Biofouling Prevention. *Phys. Chem. Chem. Phys.* **2010**, *12* (17), 4273–4274.
7. Baggerman, J.; Smulders, M. M. J.; Zuilhof, H. Romantic Surfaces: A Systematic Overview of Stable, Biospecific, and Antifouling Zwitterionic Surfaces. *Langmuir* **2019**, *35* (5), 1072–1084.
8. Joshi, S.; Pellacani, P.; van Beek, T. A.; Zuilhof, H.; Nielen, M. W. F. Surface Characterization and Antifouling Properties of Nanostructured Gold Chips for Imaging Surface Plasmon Resonance Biosensing. *Sens. Actuators B* **2015**, *209*, 505–514.
9. Kuzmyn, A. R.; De Los Santos Pereira, A.; Pop-Georgievski, O.; Bruns, M.; Brynda, E.; Rodriguez-Emmenegger, C. Exploiting End Group Functionalization for the Design of Antifouling Bioactive Brushes. *Polym. Chem.* **2014**, *5* (13), 4124–4131.
10. van Andel, E.; de Bus, I.; Tijhaar, E. J.; Smulders, M. M. J.; Savelkoul, H. F. J.; Zuilhof, H. Highly Specific Binding on Antifouling Zwitterionic Polymer-Coated Microbeads as Measured by Flow Cytometry. *ACS Appl. Mater. Interfaces* **2017**, *9* (44), 38211–38221.
11. Nguyen, A. T.; Baggerman, J.; Paulusse, J. M. J.; Rijn, C. J. M. Van; Zuilhof, H. Stable Protein-Repellent Zwitterionic Polymer Brushes Grafted from Silicon Nitride. *Langmuir* **2011**, *27* (6), 2587–2594.
12. Yang, W.; Chen, S.; Cheng, G.; Vaisocherová, H.; Xue, H.; Li, W.; Zhang, J.; Jiang, S. Film Thickness Dependence of Protein Adsorption from Blood Serum and Plasma onto Poly(Sulfobetaine)-Grafted Surfaces. *Langmuir* **2008**, *24* (17), 9211–9214.
13. Kuzmyn, A. R.; Nguyen, A. T.; Zuilhof, H.; Baggerman, J. Bioactive Antifouling Surfaces by Visible-Light-Triggered Polymerization. *Adv. Mater. Interfaces* **2019**, *6* (12), 1900351.
14. Lísalová, H.; Brynda, E.; Houska, M.; Víšová, I.; Mrkvová, K.; Song, X. C.; Gedeonová, E.; Surman, F.; Riedel, T.; Pop-Georgievski, O.; Homola, J. Ultralow-Fouling Behavior of Biorecognition Coatings Based on Carboxy-Functional Brushes of Zwitterionic Homo- and Copolymers in Blood Plasma: Functionalization Matters. *Anal. Chem.* **2017**, *89* (6), 3524–3531.
15. Schönemann, E.; Laschewsky, A.; Wischerhoff, E.; Koc, J.; Rosenhahn, A. Surface Modification by Polyzwitterions of the Sulfabetaine-Type, and Their Resistance to Biofouling. *Polymers (Basel).* **2019**, *11* (6).
16. Van Andel, E.; Lange, S. C.; Pujari, S. P.; Tijhaar, E. J.; Smulders, M. M. J.; Savelkoul, H. F. J.; Zuilhof, H. Systematic Comparison of Zwitterionic and Non-Zwitterionic Antifouling Polymer Brushes on a Bead-Based Platform. *Langmuir* **2019**, *35* (5), 1181–1191.
17. Vorobii, M.; de los Santos Pereira, A.; Pop-Georgievski, O.; Kostina, N. Y.; Rodriguez-Emmenegger, C.; Percec, V. Synthesis of Non-Fouling Poly[N-(2-Hydroxypropyl)Methacrylamide] Brushes by Photoinduced SET-LRP. *Polym. Chem.* **2015**, *6* (23), 4210–4220.
18. Rodriguez-Emmenegger, C.; Brynda, E.; Riedel, T.; Houska, M.; Šubr, V.; Alles, A. B.; Hasan, E.; Gautrot, J. E.; Huck, W. T. S. Polymer Brushes Showing Non-Fouling in Blood Plasma Challenge the Currently Accepted Design of Protein Resistant Surfaces. *Macromol. Rapid Commun.* **2011**, *32* (13), 952–957.
19. Surman, F.; Riedel, T.; Bruns, M.; Kostina, N. Y.; Sedláková, Z.; Rodriguez-Emmenegger, C. Polymer Brushes Interfacing Blood as a Route toward High Performance Blood Contacting Devices. *Macromol. Biosci.* **2015**, *15* (5), 636–646.
20. Jiang, S.; Cao, Z. Ultralow-Fouling, Functionalizable, and Hydrolyzable Zwitterionic Materials and Their Derivatives for Biological Applications. *Adv. Mater.* **2010**, *22* (9), 920–932.
21. Yang, W.; Xue, H.; Li, W.; And, J. Z.; Jiang, S. Pursuing "Zero" Protein Adsorption of Poly(Carboxybetaine) from Undiluted Blood Serum and Plasma. *Langmuir* **2009**, *25* (19), 11911–11916.
22. Blaszykowski, C.; Sheikh, S.; Thompson, M. A Survey of State-of-the-Art Surface Chemistries to Minimize Fouling from Human and Animal Biofluids. *Biomater. Sci.* **2015**, *3* (10), 1335–1370.
23. Honda, T.; Nakao, A.; Ishihara, K.; Higaki, Y.; Higaki, K.; Takahara, A.; Iwasaki, Y.; Yusa, S. I. Polymer Coating Glass to Improve the Protein Antifouling Effect. *Polym. J.* **2018**, *50* (5), 381–388.
24. Michalek, L.; Barner, L.; Barner-Kowollik, C. Polymer on Top: Current Limits and Future Perspectives of Quantitatively Evaluating Surface Grafting. *Adv. Mater.* **2018**, *30* (21), 1–18.
25. Lange, S. C.; Van Andel, E.; Smulders, M. M. J.; Zuilhof, H. Efficient and Tunable Three-Dimensional Functionalization of Fully Zwitterionic Antifouling Surface Coatings. *Langmuir* **2016**, *32* (40), 10199–10205.
26. Vorobii, M.; De Los Santos Pereira, A.; Pop-Georgievski, O.; Kostina, N. Y.; Rodriguez-Emmenegger, C.; Percec, V. Synthesis of Non-Fouling Poly[N-(2-Hydroxypropyl)Methacrylamide] Brushes by Photoinduced SET-LRP. *Polym. Chem.* **2015**, *6* (23), 4210–4220.

27. Sundaram, H. S.; Han, X.; Nowinski, A. K.; Ella-Menye, J. R.; Wimbish, C.; Marek, P.; Senecal, K.; Jiang, S. One-Step Dip Coating of Zwitterionic Sulfobetaine Polymers on Hydrophobic and Hydrophilic Surfaces. *ACS Appl. Mater. Interfaces* **2014**, *6* (9), 6664–6671.
28. Xu, L. Q.; Pranantyo, D.; Neoh, K. G.; Kang, E. T.; Teo, S. L. M.; Fu, G. D. Synthesis of Catechol and Zwitterion-Bifunctionalized Poly(Ethylene Glycol) for the Construction of Antifouling Surfaces. *Polym. Chem.* **2016**, *7* (2), 493–501.
29. Kenausis, G. L.; Vo, J.; Elbert, D. L.; Huang, N.; Hofer, R.; Ruiz-taylor, L.; Textor, M.; Hubbell, J. A.; Spencer, N. D. Poly (L-Lysine)-g-Poly(Ethylene Glycol) Layers on Metal Oxide Surfaces: Attachment Mechanism and Effects of Polymer Architecture on Resistance to Protein Adsorption. *J. Phys. Chem. B* **2000**, *104* (14), 3298–3309.
30. Paul, S. M. De; Vo, J.; Spencer, N. D.; Textor, M. Poly(L-Lysine)-Graft-Poly (Ethylene Glycol) Assembled Monolayers on Niobium Oxide Surfaces : A Quantitative Study of the Influence of Polymer Interfacial Architecture on Resistance to Protein Adsorption by ToF-SIMS and in Situ OWLS. *Langmuir* **2003**, *19* (20), 9216–9225.
31. Morgese, G.; Verbraeken, B.; Ramakrishna, S. N.; Gombert, Y.; Cavalli, E.; Rosenboom, J. G.; Zenobi-Wong, M.; Spencer, N. D.; Hoogenboom, R.; Benetti, E. M. Chemical Design of Non-Ionic Polymer Brushes as Biointerfaces: Poly(2-Oxazine)s Outperform Both Poly(2-Oxazoline)s and PEG. *Angew. Chem. Int. Ed.* **2018**, *57* (36), 11667–11672.
32. Perry, S. S.; Yan, X.; Limpoco, F. T.; Lee, S.; Müller, M.; Spencer, N. D. Tribological Properties of Poly(l -Lysine)- Graft -Poly(Ethylene Glycol) Films: Influence of Polymer Architecture and Adsorbed Conformation. *ACS Appl. Mater. Interfaces* **2009**, *1* (6), 1224–1230.
33. Huang, W. M.; Gibson, S. J.; Facer, P.; Gu, J.; Polak, J. M. Improved Section Adhesion for Immunocytochemistry Using High Molecular Weight Polymers of L-Lysine as a Slide Coating. *Histochemistry* **1983**, *77* (2), 275–279.
34. Yan, X.; Perry, S. S.; Spencer, N. D.; Pasche, S.; De Paul, S. M.; Textor, M.; Lim, M. S. Reduction of Friction at Oxide Interfaces upon Polymer Adsorption from Aqueous Solutions. *Langmuir* **2004**, *20* (2), 423–428.
35. Parks, G. A. The Isoelectric Points of Solid Oxides, Solid Hydroxides, and Aqueous Hydroxo Complex Systems. *Chem. Rev.* **1965**, *65* (2), 177–198.
36. Weber, D.; Torger, B.; Richter, K.; Nessling, M.; Momburg, F.; Woltmann, B.; Müller, M.; Schwartz-Albiez, R. Interaction of Poly(L-Lysine)/Polysaccharide Complex Nanoparticles with Human Vascular Endothelial Cells. *Nanomaterials* **2018**, *8* (6), 358.
37. Herold, D. A.; Keil, K.; Bruns, D. E. Oxidation of Polyethylene Glycols by Alcohol Dehydrogenase. *Biochem. Pharmacol.* **1989**, *38* (1), 73–76.
38. Lubich, C.; Allacher, P.; de la Rosa, M.; Bauer, A.; Prenninger, T.; Horling, F. M.; Siekmann, J.; Oldenburg, J.; Scheiflinger, F.; Reipert, B. M. The Mystery of Antibodies Against Polyethylene Glycol (PEG) - What Do We Know? *Pharm. Res.* **2016**, *33* (9), 2239–2249.
39. Garay, R. P.; El-Gewely, R.; Armstrong, J. K.; Garratty, G.; Richette, P. Antibodies against Polyethylene Glycol in Healthy Subjects and in Patients Treated with PEG-Conjugated Agents. *Expert Opin. Drug Deliv.* **2012**, *9* (11), 1319–1323.
40. Armstrong, J. K.; Hempel, G.; Koling, S.; Chan, L. S.; Fisher, T.; Meiselman, H. J.; Garratty, G. Antibody against Poly(Ethylene Glycol) Adversely Affects PEG-Asparaginase Therapy in Acute Lymphoblastic Leukemia Patients. *Cancer* **2007**, *110* (1), 103–111.
41. Branden, R.; Matthew, G.; Anirudha, S.; Janis, T.; Cecilia, F.; Melissa, M.; Jennifer, E. PEG Hydrogel Degradation and the Role of the Surrounding Tissue Environment. *J. Tissue Eng. Regen. Med.* **2015**, *9*, 315–318.
42. Johnson, R. N.; Chu, D. S. H.; Shi, J.; SChellinger, J. G.; Carlson, P. M.; Pun, S. H. HPMA-Oligolysine Copolymers for Gene Delivery: Optimization of Peptide Length and Polymer Molecular Weight Russell. *J Control Release* **2011**, *155* (2), 303–311.
43. Tappertzhofen, K.; Weiser, F.; Montermann, E.; Reske-Kunz, A.; Bros, M.; Zentel, R. Poly-L-Lysine-Poly[HPMA] Block Copolymers Obtained by RAFT Polymerization as Polyplex-Transfection Reagents with Minimal Toxicity. *Macromol. Biosci.* **2015**, *15* (8), 1159–1173.
44. Thomson, D.; Zilkie, A.; Bowers, J. E.; Komljenovic, T.; Reed, G. T.; Vivien, L.; Marris-Morini, D.; Cassan, E.; Virot, L.; Fédéli, J. M.; Hartmann, J. M.; Schmid, J. H.; Xu, D. X.; Boeuf, F.; O'Brien, P.; Mashanovich, G. Z.; Nedeljkovic, M. Roadmap on Silicon Photonics. *J. Opt.* **2016**, *18* (7), 1–20.
45. Qi, Z. B.; Xu, L.; Xu, Y.; Zhong, J.; Abedini, A.; Cheng, X.; Sinton, D. Disposable Silicon-Glass Microfluidic Devices: Precise, Robust and Cheap. *Lab Chip* **2018**, *18* (24), 3872–3880.
46. Niu, J.; Lunn, D. J.; Pusuluri, A.; Yoo, J. I.; O'Malley, M. A.; Mitragotri, S.; Soh, H. T.; Hawker, C. J. Engineering Live Cell Surfaces with Functional Polymers via Cytocompatible Controlled Radical Polymerization. *Nat. Chem.* **2017**, *9* (6), 537–545.
47. Lueckerath, T.; Strauch, T.; Koynov, K.; Barner-Kowollik, C.; Ng, D. Y. W.; Weil, T. DNA-Polymer Conjugates by Photoinduced RAFT Polymerization. *Biomacromolecules* **2019**, *20* (1), 212–221.
48. Kuzmyn, A. R.; Nguyen, A. T.; Teunissen, L. W.; Zuilhof, H.; Baggerman, J. Antifouling Polymer Brushes via Oxygen-Tolerant Surface-Initiated PET-RAFT. *Langmuir* **2020**, *36* (16), 4439–4446.

49. Wallart, X.; Henry de Villeneuve, C.; Allongue, P. Truly Quantitative XPS Characterization of Organic Monolayers on Silicon: Study of Alkyl and Alkoxy Monolayers on H-Si(111). *J. Am. Chem. Soc.* **2005**, *127* (21), 7871–7878.
50. Scheres, L.; Giesbers, M.; Zuilhof, H. Organic Monolayers onto Oxide-Free Silicon with Improved Surface Coverage: Alkynes versus Alkenes. *Langmuir* **2010**, *26* (7), 4790–4795.
51. Morga, M.; Adamczyk, Z.; Gödrich, S.; Oćwieja, M.; Papastavrou, G. Monolayers of Poly-l-Lysine on Mica - Electrokinetic Characteristics. *J. Colloid Interface Sci.* **2015**, *456*, 116–124.
52. Elbert, D. L.; Herbert, C. B.; Hubbell, J. A. Thin Polymer Layers Formed by Polyelectrolyte Multilayer Techniques on Biological Surfaces. *Langmuir* **1999**, *15* (16), 5355–5362.
53. Xiao, A.; Dhand, C.; Leung, C. M.; Beuerman, R. W.; Ramakrishna, S.; Lakshminarayanan, R. Strategies to Design Antimicrobial Contact Lenses and Contact Lens Cases. *J. Mater. Chem. B* **2018**, *6* (15), 2171–2186.
54. Poręba, R.; de los Santos Pereira, A.; Pola, R.; Jiang, S.; Pop-Georgievski, O.; Sedláková, Z.; Schönherr, H. "Clickable" and Antifouling Block Copolymer Brushes as a Versatile Platform for Peptide-Specific Cell Attachment. *Macromol. Biosci.* **2020**, *20* (4), 1900354.
55. Krishnamoorthy, M.; Hakobyan, S.; Ramstedt, M.; Gautrot, J. E. Surface-Initiated Polymer Brushes in the Biomedical Field: Applications in Membrane Science, Biosensing, Cell Culture, Regenerative Medicine and Antibacterial Coatings. *Chem. Rev.* **2014**, *114*, 10976–11026.
56. Yang, W.; Xue, H.; Li, W.; And, J. Z.; Jiang, S. Pursuing "Zero" Protein Adsorption of Poly(Carboxybetaine) from Undiluted Blood Serum and Plasma. *Langmuir* **2009**, *25* (19), 11911–11916.
57. Vaisocherová, H.; Surman, F.; Víšová, I.; Vala, M.; Špringer, T.; Ermini, M. L.; Šípová, H.; Šedivák, P.; Houska, M.; Riedel, T.; Pop-Georgievski, O.; Brynda, E.; Homola, J. Copolymer Brush-Based Ultralow-Fouling Biorecognition Surface Platform for Food Safety. *Anal. Chem.* **2016**, *88* (21), 10533–10539.
58. Wang, Y. S.; Yau, S.; Chau, L. K.; Mohamed, A.; Huang, C. J. Functional Biointerfaces Based on Mixed Zwitterionic Self-Assembled Monolayers for Biosensing Applications. *Langmuir* **2019**, *35* (5), 1652–1661.
59. Lin, X.; Jain, P.; Wu, K.; Hong, D.; Hung, H. C.; O'Kelly, M. B.; Li, B.; Zhang, P.; Yuan, Z.; Jiang, S. Ultralow Fouling and Functionalizable Surface Chemistry Based on Zwitterionic Carboxybetaine Random Copolymers. *Langmuir* **2019**, *35* (5), 1544–1551.
60. Carr, L. R.; Xue, H.; Jiang, S. Functionalizable and Nonfouling Zwitterionic Carboxybetaine Hydrogels with a Carboxybetaine Dimethacrylate Crosslinker. *Biomaterials* **2011**, *32* (4), 961–968.
61. Kowalczyńska, H. M.; Nowak-Wyrzykowska, M.; Szczepankiewicz, A. A.; Dobkowski, J.; Dyda, M.; Kamiński, J.; Kołos, R. Albumin Adsorption on Unmodified and Sulfonated Polystyrene Surfaces, in Relation to Cell-Substratum Adhesion. *Colloids Surf. B Biointerfaces* **2011**, *84* (2), 536–544.
62. Price, W. S.; Tsuchiya, F.; Arata, Y. Lysozyme Aggregation and Solution Properties Studied Using PGSE NMR Diffusion Measurements. *J. Am. Chem. Soc.* **1999**, *121* (49), 11503–11512.
63. Zhu, L. J.; Zhu, L. P.; Jiang, J. H.; Yi, Z.; Zhao, Y. F.; Zhu, B. K.; Xu, Y. Y. Hydrophilic and Anti-Fouling Polyethersulfone Ultrafiltration Membranes with Poly(2-Hydroxyethyl Methacrylate) Grafted Silica Nanoparticles as Additive. *J. Memb. Sci.* **2014**, *451*, 157–168.
64. Alswieleh, A. M.; Cheng, N.; Canton, I.; Ustbas, B.; Xue, X.; Ladmiral, V.; Xia, S.; Ducker, R. E.; Zubir, O. El; Cartron, M. L.; Hunter, C. N.; Leggett, G. J.; Armes, S. P. Zwitterionic Poly(Amino Acid Methacrylate) Brushes. *J. Am. Chem. Soc.* **2014**.
65. Chai, C.; Lee, J.; Park, J.; Takhistov, P. Antibody Immobilization on a Nanoporous Aluminum Surface for Immunosensor Development. *Appl. Surf. Sci.* **2012**, *263*, 195–201.
66. Jain, P.; Dai, J.; Grajales, S.; Saha, S.; Baker, G. L.; Bruening, M. L. Completely Aqueous Procedure for the Growth of Polymer Brushes on Polymeric Substrates. *Langmuir* **2007**, *23* (23), 11360–11365.
67. Cao, Z.; Yu, Q.; Xue, H.; Cheng, G.; Jiang, S. Nanoparticles for Drug Delivery Prepared from Amphiphilic PLGA Zwitterionic Block Copolymers with Sharp Contrast in Polarity between Two Blocks. *Angew. Chem. Int. Ed.* **2010**, *49* (22), 3771–3776.
68. Nečas, D.; Klapetek, P. Gwyddion: An Open-Source Software for SPM Data Analysis. *Cent. Eur. J. Phys.* **2012**, *10* (1), 181–188.
69. Stephanek, P. Data Analysis in Dynamic Light Scattering. In *Dynamic light scattering: the method and some applications*; Brown, W., Ed.; Oxford Science Publication: Oxford, 1993; pp 177–241.

5.6 Supporting Information

5.6.1 Experimental Section

5.6.1.1 Materials

Milli-Q water was purified by a Barnsted water purification system, with a resistivity of <18.3 MΩ·cm. Commercially available reagents were used without purification unless mentioned otherwise. Poly-l-lysine hydrobromide (PLL MW 15,000–30,000 by viscosity, average MW of 20.9 kDa, with a degree of polymerization of 100, Sigma Aldrich1); 4-(2-hydroxyethyl)piperazine-1-ethanesulfonic acid (HEPES, ≥99.5% by titration, Sigma Aldrich); hydrogen peroxide solution (H_2O_2, 50 wt.% in H_2O, Honeywell); Sulfuric acid (H_2SO_4, 95.0-97.0%); 4-cyano-4-(phenylcarbonothioylthio)pentanoic acid N-succinimidyl ester (RAFT-NHS, Sigma Aldrich); triethanolamine (TEOA, Sigma Aldrich); eosin Y (EY, Sigma Aldrich); triethylamine (TEA, Sigma Aldrich); tetrahydrofuran (THF, dry, 99.9%, Sigma Aldrich); phosphate-buffered saline (PBS, Sigma-Aldrich); ethanol (EtOH, absolute, Merck); acetone (semiconductor grade, Honeywell); Poly(N-(2-hydroxypropyl)methacrylamide (average Mn 30,000–50,000, PDI ≤1.3, Sigma Aldrich); N-(2-hydroxypropyl) methacrylamide (HPMA, Polysciences, Inc); (3-acryloylamino-propyl)-(2-carboxy-ethyl)-dimethyl-ammonium (CBMA, was synthetized according to a previously described procedure)[67]; Bovine serum albumin-Alexa488 (BSA-Alexa488, Fisher Thermo Scientific); Lysozyme, FITC labeled (LYS-FITC, NANOCS); Silicon single side polished (Si(111), N-type, phosphorus-doped, Siltronix); deuterium oxide (D_2O, 99.9 atom% D, Sigma Aldrich).
The surfaces were plasma-cleaned by a Diener Femto plasma system. Sonication steps were performed in an Elmasonic P 30 H ultrasonic unit. Cellulose membrane dialysis tubing (25 mm flat width, Digma-Aldrich) was used for ≥8 mL volume dialyses. Float-a-lyzer G2 8 mL dialysis membranes with a 3.5–5 kD MWCO (VWR) were used for the final purification step of the bottlebrush polymers. LEDs with a maximum intensity at 410 nm (Intelligent LED Solutions product number: ILH-XO01-S410-SC211-WIR200) were used for polymerization. The current was set at 700 mA, corresponding to a total radiometric power of 2.9 W, according to manufacturer specifications.

5.6.1.2 Characterization methods

Nuclear Magnetic Resonance Spectroscopy (NMR)
^{1}H NMR measurements were recorded on a Bruker Avance III NMR at 400 MHz, ^{13}C NMR spectra were recorded at 100 MHz. Chemical shifts are reported in parts per million (ppm), and are referred to the methyl signal of the sodium salt of 3-(trimethylsilyl)-1-propanesulfonic acid-d_6 (δ = 0).

Infrared Spectroscopy (IR)
IR analyses were performed on a Bruker Tensor 27 spectrometer with platinum ATR accessory.

Ellipsometry
The dry thickness of the brushes was measured using an Accurion Nanofilm_ep4 Imaging Ellipsometer. The ellipsometry data were acquired in air at room temperature using light in the wavelength range of λ = 400.6 – 761.3 nm at an angle of incidence of 50°. The data were fitted with EP4 software using a multilayer model.

X-ray Photoelectron Spectroscopy (XPS)
XPS spectra were obtained using a JPS-9200 photoelectron spectrometer (JEOL, Japan) with monochromatic Al-Kα X-Ray radiation at 12 kV and 20 mA. The obtained spectra were analyzed using CASA XPS software (version 2.3.16 PR 1.6). In C1s and N1s narrow-range spectra, the positions are set to 285 eV and 400 eV for the C–C and N–C signals, respectively. For layers <15 nm, the thickness was calculated based on the attenuation of the Si signal in XPS, according to a published procedure.[50]

Gel Permeation Chromatography (GPC)
The polymer molecular weight and polydispersity index (PDI) were determined using gel permeation chromatography (Agilent G5654A quaternary pump, G7162A refractive index detector), where a PSS SUPREMA Combination medium (P/N 206-0002) 1000 Å single porosity column was employed (0.05% NaN_3 in Milli-Q water

[1] P7890 Certificate of Analysis (accessed 2020/05/19)
https://www.sigmaaldrich.com/Graphics/COfAInfo/SigmaSAPQM/COFA/P7/P7890/P7890-BULK_____SLCF0233__.pdf

as eluent, 0.4 mL/min). Polymer solutions were freshly prepared in Milli-Q and sonicated for 5 min to assure full dissolution. An injection volume of 20 µL was used for each analysis. An Agilent PL2080-0101 PEG calibration kit was used for calibration purposes. Commercially available poly(HPMA) with a molecular weight of 30–50 kDa was used as a secondary calibration standard to account for the stronger hydrophilic character of the poly(HPMA) polymer. The PEG calibration curve was adjusted to account for those interactions on a factor equal to 3.3.

Dynamic Light Scattering (DLS)
Analyses were performed with an ALV/CGS-3 Compact Goniometer analyzer at room temperature in Milli-Q water. Solutions of modified PLL in fresh Milli-Q water were freshly prepared and sonicated to assure solvation.

Fluorescence microscopy
A Leica TCS SP8 confocal laser scanning microscope (CLMS) (Leica Microsystems, Mannheim, Germany) was used to measure protein fouling and specific interactions of the coated surfaces. A Leica HyDTM hybrid detector was used in photon counting mode to measure the intensity of the fluorescence signal. The fluorescence was measured in the wavelength range from 500 to 535 nm with laser excitation wavelength at 488 nm. A 10× objective was used, and the samples were set in focus by maximizing the reflected light intensity from the laser. Fluorescence images were obtained by accumulating ten consecutive images. Images were analyzed with the Leica LAS X Life Science software.

Atomic force microscopy. AFM surface topography images were acquired by an Asylum Research MFP-3D SA AFM (Oxford Instruments, United Kingdom). Gwyddion software was used to process and analyze the AFM topography images.[68] The average root mean square roughness (*Rq)* was calculated from topography images from 2 independent surfaces.

5.6.1.3 Syntheses

Synthesis of macroinitiator PLL-RAFT agent
The PLL-RA macroinitiator synthesis was based on a previously published method.[31] Firstly, the following solutions were prepared in falcon tubes:

1) 50 mg PLL (2.4 mmol polymer, 0.24 mmol lysine monomer) in 2.0 mL HEPES buffer (10 mM) and sonicate for 5 min to assure full solvation;
2) 17.4 mg sulfo-NHS (80 mmol) in 2.0 mL HEPES buffer (10 mM);
3) 153.5 mg EDC·HCl (0.80 mmol) in 2.0 mL HEPES buffer (10 mM);
4) 30.1 mg NHS-RAFT (80 mmol) in 2.0 mL dry DMSO.

Solutions 1–3 were combined and mixed in a falcon tube. Solution 4 was freshly prepared and added, after which the mixture was shaken in an end-over-end shaker overnight (16 hour) at room temperature. The day after, the pink, slightly opaque solution was dialyzed against Milli-Q water for 3 days with 3 medium exchanges using dialysis membranes with a 14 kDa MWCO. After evaporation of the solvent and lyophilization, 52.4 mg (MW 24 kDa, 2.2 mmol) of a fluffy slightly ping/orange powder was obtained with a yield of 92%.

PLL-RA characterization:
^{1}H-NMR (400 MHz, D_2O, 298K) δ 1.35 (H_f; t, 2H), δ 1.6 (H_e; t, 2H), δ 1.81 (H_d; s, 3H), δ 2.90 (H_c; t, 2H), δ 4.20 (H_b; t, 1H), δ 7.41-7.58 (H_a; m, 5H) see Figure 5.11; **^{13}C-NMR** (100 MHz, D_2O, 298K) due to poor solubility it was not possible to get a ^{13}C NMR spectrum, instead a **^{1}H-^{13}C-HSQC** (100 MHz, D_2O, 298K) was recorded (see Figure 5.12); **IR** 3279 cm^{-1} (N–H stretch); 3064 cm^{-1} (aromatic C–H stretch); 2933 cm^{-1} (C–H stretch); 1641 cm^{-1} (carbonyl C=O stretching; Amide I band); 1533 cm^{-1} (carbonyl N–H bending; Amide II band); 1038 cm^{-1} (thiocarbonyl C=S stretch). See also Figure 5.17; **XPS** Surface immobilized PLL-RA (Figure 6 and Figure 5.19).

PET-RAFT synthesis of polymer brushes
A stock solution with photocatalyst was prepared to contain: EY (25 mg, 39 µmol), TEOA (160 mg, 1.6 mmol) in 10 mL of Milli-Q water. The PLL-RAFT macroinitiator (2 mg, $8.4 \cdot 10^{-2}$ µmol) was dissolved in Milli-Q water 1.0 mL and sonicated for 1 hour. The monomer HPMA (61 mg, 0.4 mmol) or mixture of monomers HPMA (58 mg, 0.38 mmol) and CBMA (5 mg, 20 µmol) and subsequently 10 µL of the stock solution were added. Then the polymerization was conducted by irradiating the vials with visible light from an LED light source for 80 minutes. In these experiments, the light source was placed 3–4 cm from the substrates. The polymerization was stopped by turning off the light. The samples were dialyzed against demi water for 3 days with 3 medium exchanges using dialysis membranes with a 3.5–5 kDa MWCO. After evaporation of the solvent and lyophilization, fluffy, slightly orange powders were obtained.

PLL-HPMA characterization:
^{1}H-NMR (400 MHz, D_2O, 298K) δ 0.90 (H_j; d-overlapping, 3H), δ 1.10 (H_i; s,), δ 1.35 (H_f; t, 2H), δ 1.62 (H_k and H_e overlapping; m), δ 2.92 (H_c; t, 2H), δ 3.08 (H_h; d-overlapping, 2H), δ 3.84 (H_g; t, 1H), δ 4.15 (H_b; t, 1H), δ 7.44 (H_a; m, 5H) see Figure 5.13 and Figure 5.11; **^{13}C-NMR** (100 MHz, D_2O, 298K) due to poor solubility it was not possible to get a ^{13}C NMR spectrum, instead a **^{1}H-^{13}C-HSQC** (100 MHz, D_2O, 298K) was recorded (see Figure 5.14); **IR** 3288 cm^{-1} (N–H stretch); 3064 cm^{-1} (aromatic C–H stretch); 2933 cm^{-1} (C–H stretch); 1641 cm^{-1} (carbonyl C=O stretching; Amide I band); 1533 cm^{-1} (carbonyl N–H bending; Amide II band); 1038 cm^{-1} (thiocarbonyl C=S stretch). See also Figure 5.17; **GPC** M_n = 32000, M_w = 43000, PDI = 1.4 (see Figure 5.20); **DLS** R_{avg} = 111 nm (see Figure 5.21); **XPS** Surface immobilized PLL-HPMA (Figure 5.19).

PLL-HPMA/CBMA characterization:
^{1}H-NMR (400 MHz, D_2O, 298K) δ 0.98 (H_j; d-overlapping, 3H), δ 1.11 (H_i; s,), δ 1.35 (H_f; t, 2H), δ 1.68 (H_k and H_e overlapping; m), δ 1.85 (H_d; m, 3H), δ 1.89 (H_p; t, 2H), δ 2.62 (H_o; t, 2H), δ 3.01 (H_c; t, 2H), δ 3.09 (H_l and H_h overlapping, m), δ 3.24 (H_n; d, 2H), δ 3.39 (H_m; d, 2H), δ 3.88 (H_g; t, 1H), δ 4.17 (H_b; t, 1H), δ 7.43 (H_a; m, 5H) see Figure 5.15; **^{13}C-NMR** (100 MHz, D_2O, 298K) due to poor solubility it was not possible to get a ^{13}C NMR spectrum, instead a **^{1}H-^{13}C-HSQC** (100 MHz, D_2O, 298K) was recorded (see Figure 5.16); **IR** 3327 cm^{-1} (N–H stretching); 3060 cm^{-1} (aromatic C–H stretch); 2929 cm^{-1} (C–H stretching); 1631 cm^{-1} (carbonyl C=O stretching; Amide I band); 1527 cm^{-1} (carbonyl N–H bending; Amide II band); 1037 cm^{-1} (thiocarbonyl C=S stretching). See also Figure 5.17; **GPC** M_n = 34000, M_w = 53000, PDI = 1.6 (see Figure 5.20); **DLS** R_{avg} = 111 nm (see Figure 5.21); **XPS** Surface immobilized PLL-HPMA/CBMA (Figure 5.19).

5.6.1.4 Surface chemistry

Preparation of PLL coatings
Silicon wafers were cut into 1×1 cm pieces and cleaned by sonication in acetone for 5 min and drying in a argon stream, subsequently oxidized by air plasma for 5 min and cleaned in a piranha solution (3 : 1 mixture by volume of H2SO4 : H2O2) for 15 minutes, after which they were soaked in and extensively rinsed with Milli-Q water and finally dried by a stream of nitrogen. The freshly cleaned surfaces were immediately used for modification by being covered with a 0.1 mg/mL (sonicated, 5 min) solution of PLL or modified PLL in HEPES buffer (10 mM, pH 7.4) and stored in a humidity chamber overnight at room temperature. Afterwards, they were again extensively rinsed with Milli-Q water and dried by a stream of nitrogen.

Immobilization of NHS-RAFT on PLL-modified surfaces
The procedure was performed according to a previously published procedure.[48] Freshly prepared PLL-modified surfaces were submerged in a solution of RAFT-NHS (20 mg, 53 µmol) and TEA (7.3 mg, 10 µL, 72 µmol) in 1 mL of dry THF at RT for 16 h. The substrates were subsequently rinsed with THF, acetone, EtOH, and Milli-Q water and dried by a stream of nitrogen. The substrates were immediately used for polymerization or stored under argon atmosphere before use.

Surface initiated PET-RAFT
The procedure was performed according to a previously published procedure.[48] A stock solution with photocatalyst was prepared to contain: EY (25 mg, 39 µmol), TEOA (160 mg, 1.6 mmol) in 10 mL of Milli-Q water. The monomer HPMA (200 mg, 1.4 mmol) was dissolved in Milli-Q water (1 mL), and subsequently, 10 µL of the stock solution was added. The mixture was vortexed and added to the vials containing surfaces with an immobilized RAFT agent. Immediately after this, the polymerization was conducted by irradiating the vials with visible light from an LED light source for different periods of time. The thickness of the polymerization solution on top of the surfaces was 2 mm. In these experiments, the light source was placed 3–4 cm from the substrates. The polymerization was stopped by turning off the light. The samples were removed from the solution and subsequently rinsed with Milli-Q water and ethanol and blown dry under a stream of argon.

5.6.1.5 Protein fouling studies

Fouling of the coated surfaces was investigated by incubating surfaces in the single-protein solution of fluorescein isothiocyanate labeled lysozyme (LYS-FITC) (0.1 mg·mL^{-1}) or Alexa488 labeled bovine serum albumin (BSA-Alexa488) (0.1 mg·mL^{-1}) 15 min at room temperature according to a published procedure.[48] The surfaces were then washed with PBS buffer (pH 7.4) and Milli-Q water and subsequently dried in a stream of argon. Subsequently, the samples were mounted on microscope slides using double sides tape and fluorescence intensity of the adsorbed proteins was measured. Each sample was produced and measured *in duplo*.

5.6.2 NMR data

PLL-RA macroinitiator

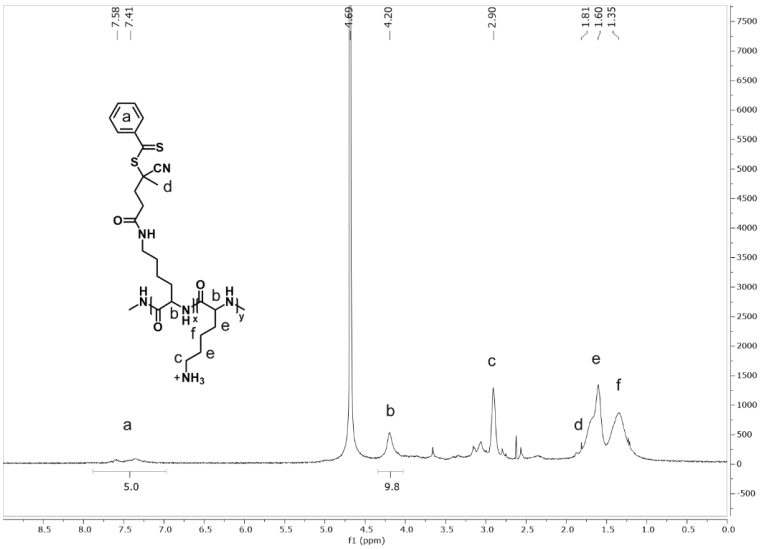

Figure 5.11 ^{1}H-NMR spectrum of PLL-RA measured in D_2O (400 MHz, 298 K).
The protons on the benzyl group of the RA gave a broad signal around at δ = 7.5 ppm. When comparing the integral to the ^{1}H PLL backbone signal at δ = 4.2 ppm (which is not changed upon binding to the RA), we could determine the ratio of RAFT agent : lysine to be 1 : 9.8. That is, approximately 10% of pendant amine groups of PLL were functionalized with the RAFT agent. Based on the NMR-based conversion and the average MW of the PLL starting material is 20.9 kDa with a degree of polymerization of 100, the MW of the synthesized PLL-RA was estimated to be 24 kDa.

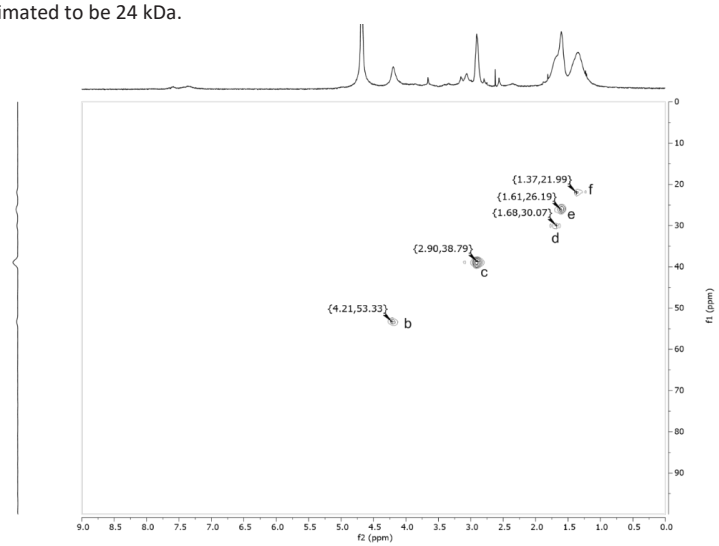

Figure 5.12 ^{1}H-^{13}C-HSQC NMR spectrum of macroinitiator PLL-RA measured in D_2O (100 MHz, 298 K). Peaks were assigned following the labelling of the structure as shown in Figure 5.11.

PLL-HPMA bottlebrush

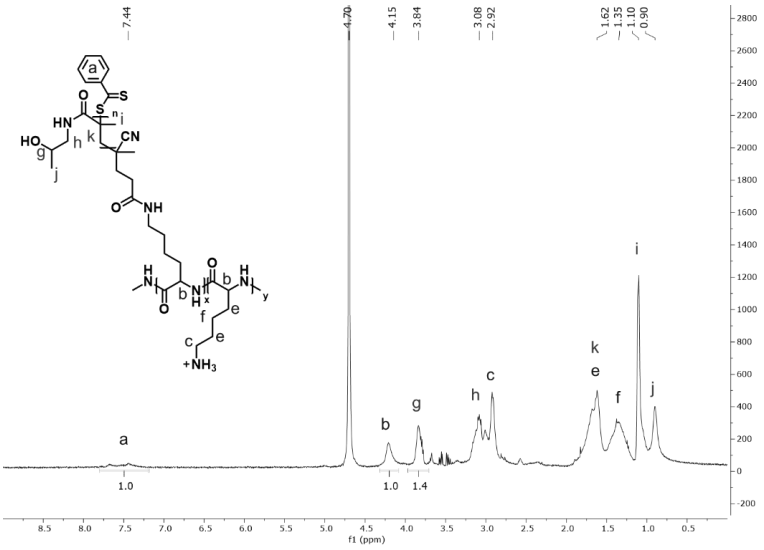

Figure 5.13 ^{1}H-NMR spectrum of PLL-HPMA (D_2O, 400 MHz, 298 K). (Figure is also placed in main text and copied here to support calculations).

From the integrals of the ^{1}H signal at δ = 4.15 ppm and δ = 3.84 ppm, the ratio between HPMA monomer : lysine monomer was determined to be 1.4 : 1. Combined with the 1 : 9.8. ratio of RA : lysine of the PLL-RA macroinitiator, the average chain length of the each HPMA side chain was calculated to be 14 repeating monomers (MW 143 g·mol^{-1}), corresponding to approximately 2 kDa. Based on this information and assuming the average MW of the PLL starting material is 20.9 kDa with a degree of polymerization of 100, the molar ratio lysine : HPMA in the bottlebrush was calculated to be approximately 1 : 1 with a total weight of 40.9 kDa.

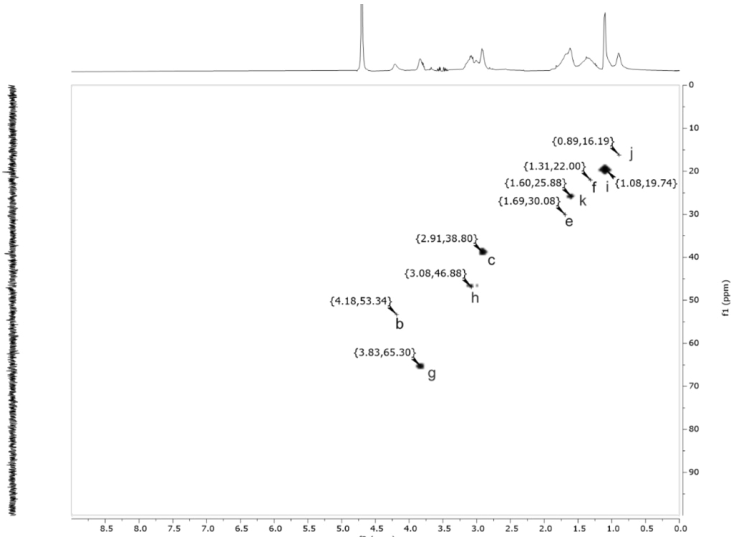

Figure 5.14 ^{1}H-^{13}C-HSQC NMR spectrum of PLL-HPMA measured in D_2O (100 MHz, 298 K). Peaks were assigned following the labelling of the structure as shown in Figure 5.13.

PLL-HPMA/CBMA bottlebrush

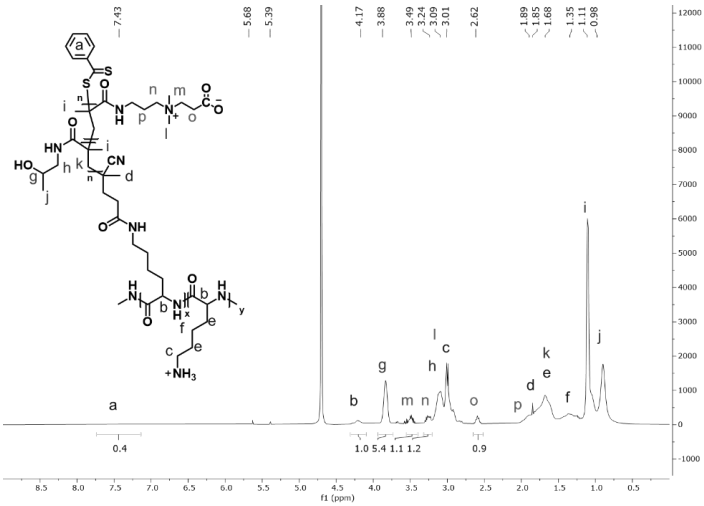

Figure 5.15 ^{1}H-NMR spectrum of PLL-HPMA/CBMA (D_2O, 400 MHz, 298 K).
The isolated 1H peak at δ = 2.62 ppm originates from the CBMA monomers and was used to determine the ratio between HPMA and CBMA in the bottlebrush side chains. By comparing this CBMA signal at δ = 2.62 ppm to the HPMA signal at δ = 3.88 ppm, we found the content of CBMA to be 7.7%. The 1H-NMR spectrum was used to estimate the average HPMA/CBMA side chain length by comparing their combined integrals to the isolated the PLL backbone signal at δ = 4.17 ppm. Since it is known from the NMR data of PLL-RA macroinitiator, that the ratio between RAFT : lysine is roughly 1 : 9.8, the average chain length of the HPMA/CBAA side chains could be calculated to be roughly 100 repeating monomers. The average weight of the HPMA/CBMA monomer was estimated 150 g·mol^{-1} (7.7% CBMA 242 g·mol^{-1} and 92.3% HPMA 143 g·mol^{-1}) which brings the total MW of the side chains to 15 kDa. The difference in side chain weight is partly explained due to the higher molecular weight of the CBMA monomer (242 g·mol^{-1}) compared to HPMA (143 g·mol^{-1}) and the difference in reactivity.

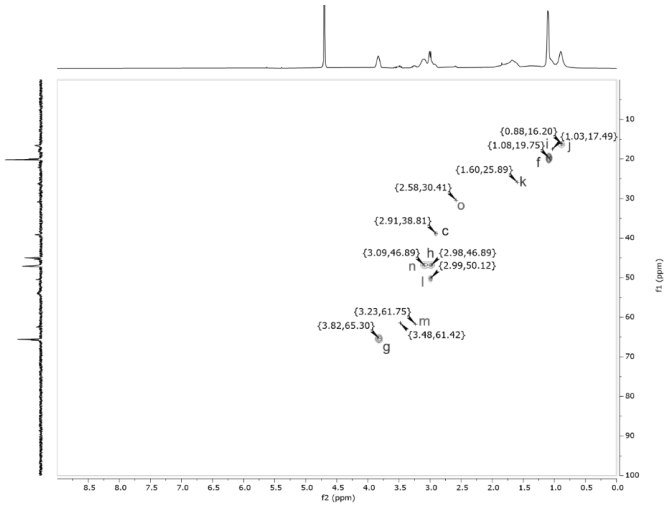

Figure 5.16 ^{1}H-^{13}C-HSQC NMR spectrum of PLL-HPMA/CBMA measured in D_2O (100 MHz, 298 K). Peaks were assigned following the labelling of the structure as shown in Figure 5.15.

5.6.3 Infrared spectra

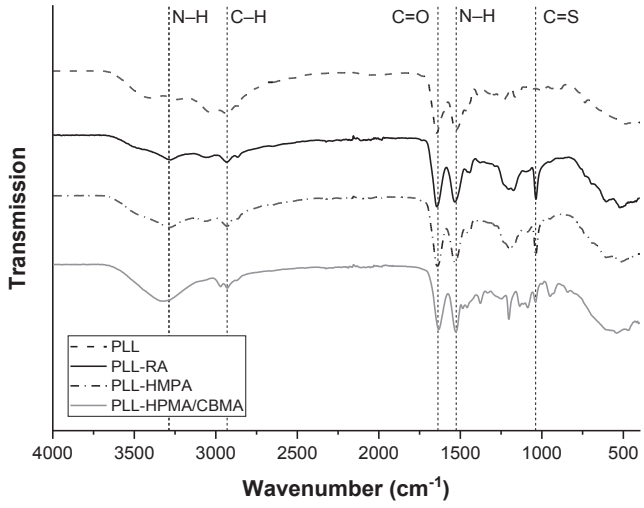

Figure 5.17 IR spectra of PLL, PLL-RA, PLL-HPMA and PLL-HPMA/CBMA. On the *y*-axis the spectra are shown with an offset with respect to each other.

5.6.4 XPS data and calculations

PLL-RA conversion (route A, step A2)

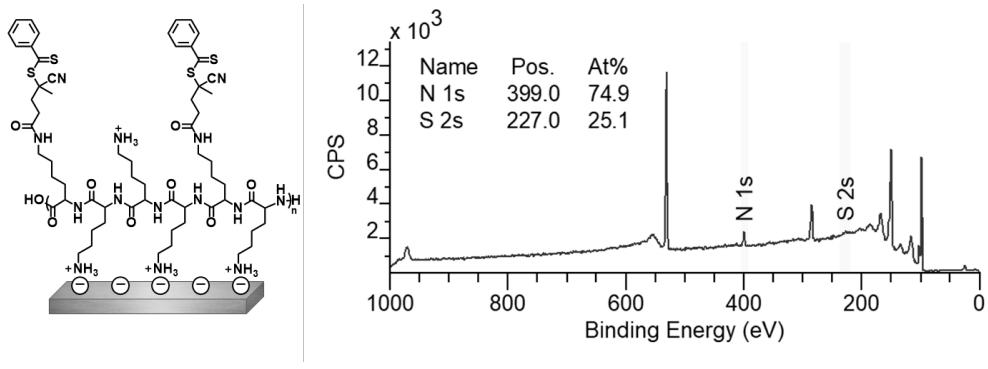

Figure 5.18 Structure and XPS wide scan of surface-immobilized PLL, modified by NHS-RAFT (according to route A, step 2). From the XPS spectrum, the conversion of the reaction in which the terminal amine groups of the PLL were equipped with the RAFT agent can directly be calculated by considering the N/S atomic ratio. This $N_{1s} : S_{2p}$ ratio was found to be 74.9 : 25.1, which equals 6N : 2S. Since the RAFT initiator contains 1N, this leaves 5N originating from PLL, corresponding to 2.5 lysine monomers. This gives a RAFT : lysine ratio of 1 : 2.5, which translates to an on-surface conversion of roughly 40%.

PLL-RAFT conversion (route B, step B1)

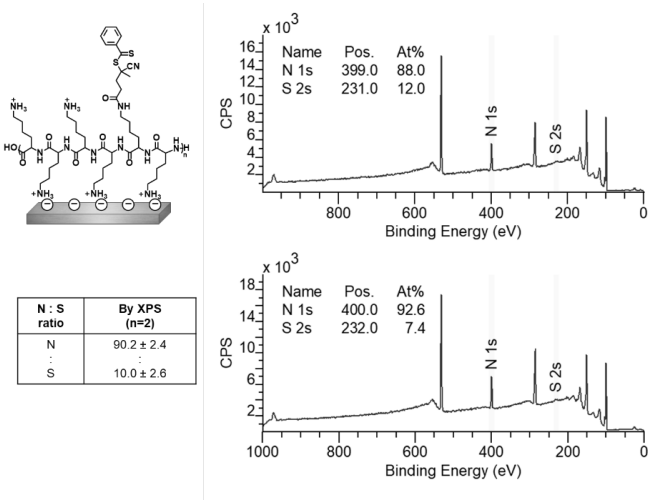

N : S ratio	By XPS (n=2)
N	90.2 ± 2.4
:	:
S	10.0 ± 2.6

Figure 5.19 Structure and XPS wide scan spectra data of B1) surface immobilized PLL-RA, *in duplo*. The table contains the average atomic ratios as determined by XPS.
The found N_{1s} : S_{2p} ratio was found to be approximately 90 : 10, which equals 18N : 2S. Since the RAFT agent contains 1N, this leaves 17N originating from PLL, corresponding to 8.5 lysine monomers. This gives a RAFT : lysine ratio of 1 : 8.5.

5.6.5 GPC data

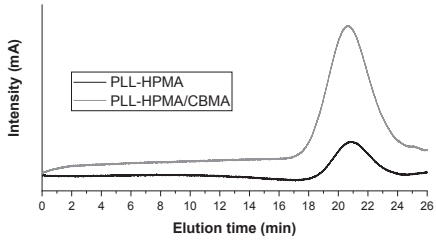

Figure 5.20 GPC traces of both bottlebrush polymers PLL-HPMA and PLL-HPMA/CBMA.

Table 5.1 Number-averaged and weight-averaged molecular weight and polydispersity index (PDI) of the synthesized bottlebrush polymers by GPC.

Bottlebrush polymer	M_n (g/mol)	M_w (g/mol)	PDI
PLL-HPMA	32000	43000	1.4
PLL-HPMA/CB	34000	53000	1.6

5.6.6 DLS data and calculations

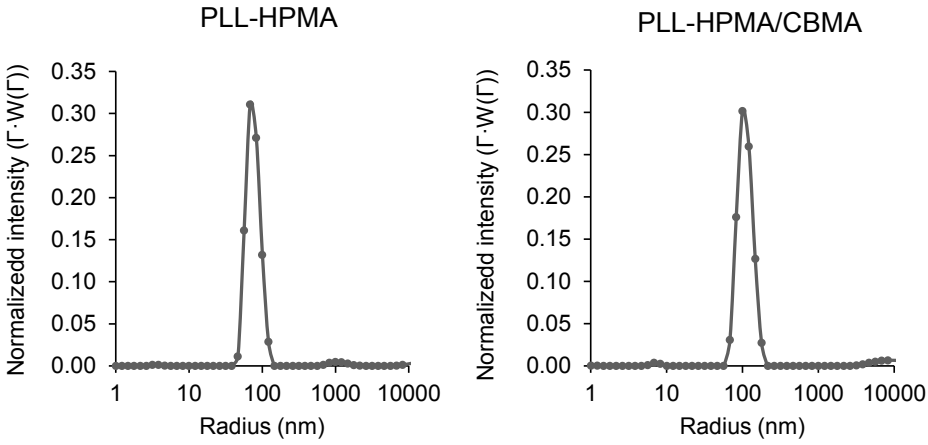

Figure 5.21 DLS data of PLL-HPMA and PLL-HPMA/CBAA bottlebrushes in Milli-Q water (prepared via route C). The contribution to the scattering is plotted against the hydrodynamic radius as intensity-based equal area representation as previously published.[69]

The average radius (R_{avg}) was calculated by applying the following equation:

$$\boldsymbol{R_{avg}} = \frac{\sum_i \boldsymbol{n_i \cdot R_i}}{\sum_i \boldsymbol{n_i}}$$

with:

R_{avg} = average radius
n_i = normalized intensity at given radius
R_i = radius at given intensity

Applying this equation, radiuses of 77 nm and 111 nm were found for PLL-HPMA and PLL-HPMA/CBMA, respectively.

2.7 AFM data

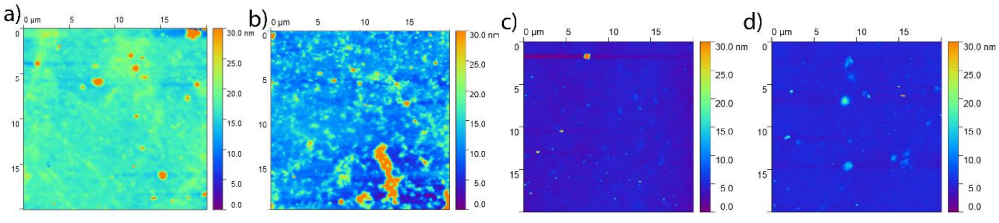

Figure 5.22 AFM surface topology; a) coating A3, b) coating B2, c) route C1 PLL-HPMA, d) route C1 PLL-HPMA/CBMA. The polymerization time for all three routes was 80 minutes.

Chapter 6

General Discussion

Abstract

In the research described in this Thesis, we combined the fields of organic chemistry and surface chemistry for the development of antifouling coatings: from the synthesis of the macromolecular building blocks, via the application in surface coatings to the testing of antifouling properties. This chapter gives an overview of the findings of this Thesis. The most important achievements, and several remaining questions and recommendations for future research will be discussed.

6.1 Introduction

As stated before in this Thesis, currently best performing antifouling coatings need to be prepared by the use of sensitive *grafting-from* methods,[1–5] which is a major hurdle to be overcome when applying these antifouling coatings on large, industrially relevant scales.[6–12] Therefore, in this work, pre-synthesized macromolecules were developed as building blocks for coatings that can be applied on a surface under mild conditions.[1–3,11] Pre-synthesis of building blocks in solution has the benefit of the possibility of careful design and extensive characterization by various methods whereas on-surface synthesized coatings are often limited in terms of characterization because of, *e.g.*, limited analysis dept and low quantities of material. However, the main challenge of the *grafting-to* method is to reach a sufficient grafting-density of the resulting coating, usually depending on the affinity of the polymer towards the surface.[9]

6.2 The Synthesis of Charge Neutral, Zwitterionic Dendrimers

In this work, the synthesis and use of zwitterionic dendrimers (ZID) as building blocks for antifouling coatings is described. Within this project, PPI dendrimers were found to be interesting candidates because of their high density of quaternizable amine groups and commercial availability.[13,14] Noting that complete charge neutrality of the ZIDs plays an important role in the antifouling properties of zwitterionic coating,[15] the synthesis of the ZID was designed carefully in order to develop fully zwitterionic, charge neutral ZIDs.

A straightforward route towards exteriorly zwitterionic modification could have been reacting only the outer primary amines with zwitterionic monomers (Figure 6.1C)[16–18] However, this would have left the interior tertiary amines unreacted and prone to protonation, leading to an overall positively charged dendrimer, which would have been to the detriment of the performance of the ZID as an antifouling coating or bio-material. Another considered one-step route towards interior- *and* exterior ZID could have been the alkylation of PPI dendrimers' primary and tertiary amines with, *e.g.*, 1,3-propane sultone or 1,3-propiolacton, which would automatically yield positive and negative charges in a single step. However, the conversion of such reactions is typically poor (below 50%),[19] likely because the solvent of is not compatible with the formed highly zwitterionic product, leading to premature precipitation before the fully zwitterionic product can be formed. To circumvent this problem, alkylation of the PPI dendrimer in water was considered with a compatible precursor such as an alkyl halide with a carboxylate- of sulfonate group. However, direct alkylation of both the primary and tertiary amines of the PPI dendrimer with an appropriate alkyl halide (providing the negative charge) would have made the dendrimers over-alkylated since the alkylation agent would alkylate the primary amines up to three times and thus resulted an overall negative charge. For example, a generation 2 PPI dendrimer would have an overall charge of –16 (Figure 6.1D-E).

Another possible strategy was performing a Michael addition on the PPI dendrimers with a precursor containing a protected carboxylate (which would later be deprotected), followed by *N*-alkylation using methyl iodide.[20] This approach would have led to an overall charge of –2 (two non-compensated carboxylate negative charges), regardless of the size of the initial dendrimer (Figure 6.1B).

Since we specifically aimed for the design of fully zwitterionic, charge neutral dendrimers, it was crucial that the installation of the negatively charged group had to occur intrinsic simultaneously with the creation of the positivity charge. Therefore, we chose the first step in the modification of the PPI dendrimer to be the double methylation of the outer, primary amines using the Eschweiler-Clarke reaction, as this can be run to full conversion to yield –still charge-neutral– dendrimers with tertiary amines only.[21,22] The methylated dendrimers were subsequently be made zwitterionic by reacting all the tertiary amines with an alkyl halide with a protected or free anionic group (Figure 6.1A).[23]

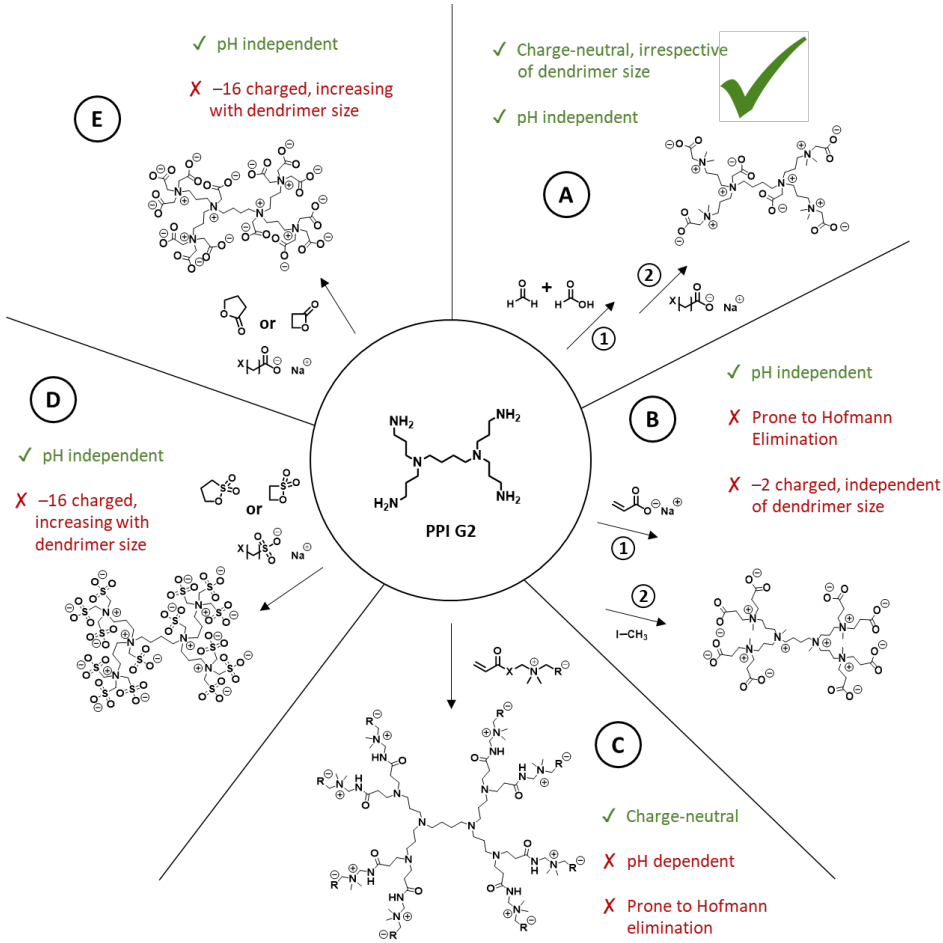

Figure 6.1 Overview of the considered options (A-E) for the synthesis of zwitterionic dendrimers with their pros (green) and cons (red) with the chosen route (A) highlighted. For clarity, a PPI generation 2 (G2) is used as example.

As the conversion of the alkylation step was not 100%, (namely 87%) there were tertiary amines left that could be protonated under physiological conditions, which would lead to dendrimers that are not permanently charge neutral since the carboxylate group is needed to compensate for the positively

charged amine. In order to further increase the yield of this second reaction step, the following parameters are suggested to optimize:

- *Choice of leaving group:* Since we found a clear difference in conversion when comparing sodium iodo- and bromoacetate (87% vs. 54%) in water, the use of better leaving groups such as, *e.g.*, tosylates or mesylates could improve the conversion. However, since this reaction needs to be carried out in water in order to dissolve the zwitterionic product, the choice of the leaving group is limited by hydrolysis.
- *Type of solvent*: The use of both methyl- and *tert*-butyl-protected carboxylates allows to use an aprotic polar solvent since both the reactant and the intermediate product (before deprotection) are soluble in such a solvent, enhancing the stability of the alkyl halide precursors. An increase in conversion up to roughly 90% was observed when using protected acids, possibly due to the stability of the halide precursors in an aprotic solvent. However, when using this approach, an additional deprotection step is necessary in order to yield the negatively charged group, which then again needs to be quantitative to yield a charge-neutral ZID.

Subsequently, a modular synthetic approach was developed to incorporate a variable number of alkyne or azide functional groups, which allow for covalent (bio)functionalization and/or surface-anchoring. Proof-of-principle coupling of an azide-biotin conjugate by click chemistry showed that the ZID indeed can be further functionalized. The fact that multiple, or ultimately even different, functional groups can be incorporated, will further enhance the (bio)applicability of this kind of zwitterionic dendrimers for, *e.g.*, drug delivery purposes. One could imagine coupling both a recognition moiety and a functional drug to a ZID which would be non-toxic due to the zwitterionic modification.

Interestingly, the developed PPI-zwitterionization method could also be applied to other poly-amine macromolecules such as branched polyethylenimine (PEI) (Figure 6.2).[24] This type of polymer is less well defined than PPI dendrimers, but because of its branched nature, once modified, it might make a good candidate to form a coating with similar properties as PPI dendrimers. PEI contains primary, secondary and tertiary amines in a mixed ratio. However, since our approach is based on first converting all present amines into tertiary amines using the Eschweiler-Clarke methylation,[21,22] a subsequent alkylation reaction, introducing both the positive- and negative charge of the zwitterion pairs, will yield charge-neutral zwitterionic polymer, which will still be useful for surface modification purposes. In literature, examples of the zwitterionic modification of polymers are available, however none that yield charge-neutral products.[25,26] Having control over the number of functional groups per molecule will be challenging since PEI is not as well defined as PPI dendrimers.

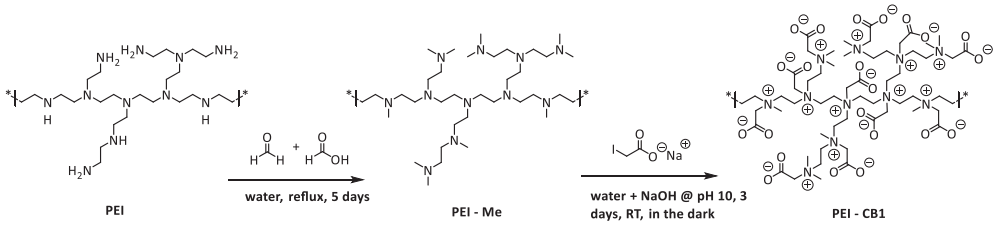

Figure 6.2 Proposed synthetic pathway towards zwitterionic polyethyleneimine (PEI).

6.3 Zwitterionic Dendrimer-Based Antifouling Coatings

While zwitterionic dendrimers (ZID) are interesting building blocks for antifouling coatings, they needed to be immobilized on a surface in order to be able to use them as such. Hence, in we investigated several strategies to do so. The first explored methods were based on covalent binding of single ZIDs on a pre-functionalized surfaces, hinging on amide bond formation, Cu^{I}-catalyzed azide/alkyne cycloaddition (CuAAC), or thiol-yne click chemistry. The two "click" chemistry variants yielded higher levels of immobilized ZID, likely because of the higher reactivity.
One other observed effect was the hydrophilicity of the surface to which the ZIDs needed to be coupled: the more hydrophilic the pre-functionalized starting layer, the higher the subsequent immobilization load of the ZIDs. Possibly, the more hydrophilic starting layers are easier wetted with the aqueous reaction mixture, containing the ZIDs.
It is known from literature that zwitterionic polymer brush layer outperform their monolayer analogues.[27] Hence, we also explored an approach that could potentially form multilayers. By polymerizing ZIDs that contain polymerizable groups, incorporating a functional group on the surface in this polymerization process, coatings were formed in a *grafting-through* fashion.[28,29] Via this approach, mono- and multilayer coatings were formed that showed increasing thicknesses and hydrophilicity with each newly formed layer, and antifouling properties slightly better than their reference (oligoethylene oxide monolayers). Unfortunately, the thickness increase of the coating per layer was only moderate, which was unexpected for methacrylate-containing precursors. Possibly, increasing the number of polymerizable groups per ZID (>2) would increase the polymerization efficiency. Furthermore, the use of acrylate-based monomers instead of methacrylates could be tested since the increased stability of tertiary radicals (in the case of methacrylates) might lower the reactivity of the methacrylates, which could have hampered / slowed the inter-dendrimer crosslinking.[30]

The developed polymerization reactions needed to be carried out in an oxygen-free atmosphere since oxygen inhibits radical-induced polymerization reactions, which is undesired in case of scaling up such an approach. To overcome this problem, additives that reduce oxygen inhibition could be used. For polymerization in aqueous matrices, this can, *e.g.*, be additives that produce new propagating centers for polymerization, or additives or enzymes that scavenge oxygen.[31–33]

Since the synthesized ZID are extremely polar, we envisioned that it would be thermodynamically unfavorable for the ZIDs to move from the aqueous reaction mixture, to an only moderately hydrophilic surface. Therefore, we decided to couple the ZIDs to poly(L-lysine) (PLL), which has an intrinsic affinity for, *e.g.*, silicon oxide, metal oxide and polymeric surfaces.[28–33] This allowed us to apply the *grafting-to* method to immobilized our ZID. The newly developed PLL-ZID macrostructures consisted of randomly crosslinked PLL-ZID networks, and more organized linear PLL-ZID macromolecules. Especially the linear variant exhibited a decent resistance to fouling from single-protein solutions as well as diluted human serum. While the ZID-PLL platform does not yet meet the ultralow fouling levels as described in literature for the currently best performing coatings,[34–42] the results are actually a relevant starting point for further improvement. This is because these results are a) obtained with physiologically relevant protein concentrations (10 mg/mL) and reasonably long

contact times (30 min), on b) a platform that involves only a single, simple self-assembly step using c) only small amounts of pre-synthesized macromolecules that d) spontaneously self-assembled on a surface from e) an aqueous solution in an ambient atmosphere. Given this combination of a)-e), the results, while not excellent, are valuable. For comparison, in literature, extremely low antifouling levels of <1 ng·cm^{-2} in single-protein solutions have frequently been shown for relatively thick (>30 nm) zwitterionic polymer brush coatings using lower concentrations of proteins, such as 0.1 mg/mL and 1.0 mg/mL and shorter fouling exposure times.[41,43–45] Considering that our newly developed coatings are only thin (~1 nm), we envision that increasing the ZID-load on the surface will lead to coatings with improved antifouling properties.[22] However, also for us, the main challenge of this method was to reach a sufficient grafting density of the resulting coating.[34,49–52] Parameters to be varied are, *e.g.*, different (lengths of) polymer backbones, number of cross-coupling agents, and/or different dendrimer generations.

6.4 Poly(HPMA) Bottlebrush-Based Antifouling Coatings

Poly(*N*-(2-hydroxypropyl)methacrylamide) (HPMA) polymer brush coatings are known for having excellent antifouling properties.[4,7,8] Hence, in we developed a method to create such a coating without having to perform sensitive polymerization reactions on-surface. We pre-synthesized HPMA polymers onto a PLL backbone to create a so-called “bottlebrush” branched polymer which proved to self-assemble onto a surface likewise to the PLL-ZID copolymers. Since the currently best performing poly(HPMA) coatings are *grafted-from* the surface, we compared three routes ranging from “classic” *grafting-from* to entirely *grafting-to* in order to compare differences in outcome and overall antifouling performance of the coatings. Additionally, we designed and synthesized a bottlebrush polymer that eventually allowed for additional (bio)functionalization in solution or after surface immobilization. Remarkably, coatings made by the various routes – varying from *grafting-from* to entirely *grafting-to* – showed very similar antifouling properties in single-protein solutions, irrespectively of any possible difference in their built-up, thickness, surface topology and/or brush density. However, it should be kept in mind that the used fluorescence method might be close to the limit of detection, which makes it more difficult to study mutual differences between data.

Grafted-from routes led to relatively thick and dense coatings, which could be beneficial for stability and long-term use since the underlying anchoring layer is better shielded from the environment. As a aside, also the straightforward application of PLL as a multivalent, amine-terminated anchoring layer was shown. PLL could, therefore, be an alternative to the often used amino-silanes.[46–48]

Logically, complete *grafting-to* is the easiest method to apply on a surface and by far the easiest to scale-up, because of the one-step self-assembly and lack of on-surface reactions. The complete synthesis in solution allows control and knowledge of the composition, molecular weight and weight distribution, and dimensions of the formed polymer. Also, this approach allows precise and quantifiable immobilization of (bio)molecules in solution, which typically requires smaller quantities of the (bio)molecule of interest in the overall coating process or on the surface. As such I would recommend such *grafting-to* approach using PLL-HMPA brushes as starting point for further studies that aim for affordable and practical applications.

6.5 The Future of Antifouling Coatings

Taken together, this Thesis combined the fields of organic chemistry and surface for the development of antifouling coatings: from the synthesis of the macromolecular building blocks to the application in surface coatings and testing of antifouling properties. Most of the work in this Thesis was performed on silicon oxide. However, changing the anchoring group chemistry of the pre-coating, the methods as described in Chapter 3 are also applicable to other surface materials. With perhaps slightly adjusted conditions, the PLL-based anchoring of the building blocks in Chapters 4 and 5 will likely also be successful on metal oxide surfaces and polymeric surfaces.[28–33]
The synthesis of the developed building blocks contained multiple steps and involved critical processes. However, it eventually resulted in application methods that are robust, reproducible and possible under ambient conditions. Overall, the synthesis procedure in solution takes time and requires careful purification. However, once synthesized, only very small amounts of the building blocks are needed to coat a surface, which eventually makes it highly cost-effective when a coating needs be applied to multiple or large surfaces.

Antifouling coatings have shown to be valuable in a wide variety of applications, from medical implants and biosensors, all the way to marine coatings. However, their implementation is often challenging and requires laboratory conditions and set-ups. Hence, to be able to use those excellent-performing coatings to their full potential, in the future, focus should also be given to the ease of implementation. It is my estimate that the ease of surface coating and scalability has been underestimated, and that in the coming decade the biggest strides will be made with easy-to-apply materials that allow large-scale coatings at the price of minor loss of antifouling properties, in other words that this part of surface science can, should, and will move from 'ideal' to 'real'.

References

1. Lange, S. C.; Van Andel, E.; Smulders, M. M. J.; Zuilhof, H. Efficient and Tunable Three-Dimensional Functionalization of Fully Zwitterionic Antifouling Surface Coatings. *Langmuir* **2016**, *32* (40), 10199–10205.
2. Nguyen, A. T.; Baggerman, J.; Paulusse, J. M. J.; Rijn, C. J. M. Van; Zuilhof, H. Stable Protein-Repellent Zwitterionic Polymer Brushes Grafted from Silicon Nitride. *Langmuir* **2011**, *27* (6), 2587–2594.
3. Kuzmyn, A. R.; Nguyen, A. T.; Zuilhof, H.; Baggerman, J. Bioactive Antifouling Surfaces by Visible-Light-Triggered Polymerization. *Adv. Mater. Interfaces* **2019**, *6* (12), 1900351.
4. Rodriguez-Emmenegger, C.; Brynda, E.; Riedel, T.; Houska, M.; Šubr, V.; Alles, A. B.; Hasan, E.; Gautrot, J. E.; Huck, W. T. S. Polymer Brushes Showing Non-Fouling in Blood Plasma Challenge the Currently Accepted Design of Protein Resistant Surfaces. *Macromol. Rapid Commun.* **2011**, *32* (13), 952–957.
5. Vorobii, M.; De Los Santos Pereira, A.; Pop-Georgievski, O.; Kostina, N. Y.; Rodriguez-Emmenegger, C.; Percec, V. Synthesis of Non-Fouling Poly[N-(2-Hydroxypropyl)Methacrylamide] Brushes by Photoinduced SET-LRP. *Polym. Chem.* **2015**, *6* (23), 4210–4220.
6. Lísalová, H.; Brynda, E.; Houska, M.; Víšová, I.; Mrkvová, K.; Song, X. C.; Gedeonová, E.; Surman, F.; Riedel, T.; Pop-Georgievski, O.; Homola, J. Ultralow-Fouling Behavior of Biorecognition Coatings Based on Carboxy-Functional Brushes of Zwitterionic Homo- and Copolymers in Blood Plasma: Functionalization Matters. *Anal. Chem.* **2017**, *89* (6), 3524–3531.
7. Van Andel, E.; Lange, S. C.; Pujari, S. P.; Tijhaar, E. J.; Smulders, M. M. J.; Savelkoul, H. F. J.; Zuilhof, H. Systematic Comparison of Zwitterionic and Non-Zwitterionic Antifouling Polymer Brushes on a Bead-Based Platform. *Langmuir* **2019**, *35* (5), 1181–1191.

8. Vorobii, M.; de los Santos Pereira, A.; Pop-Georgievski, O.; Kostina, N. Y.; Rodriguez-Emmenegger, C.; Percec, V. Synthesis of Non-Fouling Poly[N-(2-Hydroxypropyl)Methacrylamide] Brushes by Photoinduced SET-LRP. *Polym. Chem.* **2015**, *6* (23), 4210–4220.
9. Söder, D.; Garay-Sarmiento, M.; Rahimi, K.; Obstals, F.; Dedisch, S.; Haraszti, T.; Davari, M. D.; Jakob, F.; Heß, C.; Schwaneberg, U.; Rodriguez-Emmenegger, C. Unraveling the Mechanism and Kinetics of Binding of an LCI-EGFP-Polymer for Antifouling Coatings. *Macromol. Biosci.* **2021**, *2100158*, 1–10.
10. Michalek, L.; Barner, L.; Barner-Kowollik, C. Polymer on Top: Current Limits and Future Perspectives of Quantitatively Evaluating Surface Grafting. *Adv. Mater.* **2018**, *30* (21), 1–18.
11. Jiang, S.; Cao, Z. Ultralow-Fouling, Functionalizable, and Hydrolyzable Zwitterionic Materials and Their Derivatives for Biological Applications. *Adv. Mater.* **2010**, *22* (9), 920–932.
12. Honda, T.; Nakao, A.; Ishihara, K.; Higaki, Y.; Higaki, K.; Takahara, A.; Iwasaki, Y.; Yusa, S. I. Polymer Coating Glass to Improve the Protein Antifouling Effect. *Polym. J.* **2018**, *50* (5), 381–388.
13. Boas, U.; Christensen, J. B.; Heegaard, P. M. H. Dendrimers: Design, Synthesis and Chemical Properties. *J. Mater. Chem.* **2006**, *16* (38), 3785–3798.
14. Newkome, G. R.; Shreiner, C. D. Poly(Amidoamine), Polypropylenimine, and Related Dendrimers and Dendrons Possessing Different 1 → 2 Branching Motifs: An Overview of the Divergent Procedures. *Polymer.* **2008**, *49* (1), 1–173.
15. Magin, C. M.; Cooper, S. P.; Brennan, A. B. Non-Toxic Antifouling Strategies. *Mater. Today* **2010**, *13* (4), 36–44.
16. Wang, L.; Wang, Z.; Ma, G.; Lin, W.; Chen, S. Reducing the Cytotoxity of Poly(Amidoamine) Dendrimers by Modification of a Single Layer of Carboxybetaine. *Langmuir* **2013**, *29* (28), 8914–8921.
17. Svenningsen, S. W.; Janaszewska, A.; Ficker, M.; Petersen, J. F.; Klajnert-Maculewicz, B.; Christensen, J. B. Two for the Price of One: PAMAM-Dendrimers with Mixed Phosphoryl Choline and Oligomeric Poly(Caprolactone) Surfaces. *Bioconjug. Chem.* **2016**, *27* (6), 1547–1557.
18. Sun, J.; Zeng, F.; Jian, H.; Wu, S. Conjugation with Betaine: A Facile and Effective Approach to Significant Improvement of Gene Delivery Properties of PEI. *Biomacromolecules* **2013**, *14* (3), 728–736.
19. Hu, J.; Su, Y.; Zhang, H.; Xu, T.; Cheng, Y. Design of Interior-Functionalized Fully Acetylated Dendrimers for Anticancer Drug Delivery. *Biomaterials* **2011**, *32* (36), 9950–9959.
20. Carr, L. R.; Zhou, Y.; Krause, J. E.; Xue, H.; Jiang, S. Uniform Zwitterionic Polymer Hydrogels with a Nonfouling and Functionalizable Crosslinker Using Photopolymerization. *Biomaterials* **2011**, *32* (29), 6893–6899.
21. Pine, S. H.; Sanchez, B. L. Formic Acid-Formaldehyde Methylation of Amines. *J. Org. Chem.* **1971**, *36* (6), 829–832.
22. Zhou, X.; Chen, Y.; Han, J.; Wu, X.; Wang, G.; Jiang, D. Betaine Ester-Shell Functionalized Hyperbranched Polymers for Potential Antimicrobial Usage: Guest Loading Capability, PH Controlled Release and Adjustable Compatibility. *Polymer (Guildf).* **2014**, *55* (24), 6261–6270.
23. Wu, L.; Jasinski, J.; Krishnan, S. Carboxybetaine, Sulfobetaine, and Cationic Block Copolymer Coatings: A Comparison of the Surface Properties and Antibiofouling Behavior. *J. Appl. Polym. Sci.* **2012**, *124* (3), 2154–2170.
24. Jäger, M.; Schubert, S.; Ochrimenko, S.; Fischer, D.; Schubert, U. S. Branched and Linear Poly(Ethylene Imine)-Based Conjugates: Synthetic Modification, Characterization, and Application. *Chem. Soc. Rev.* **2012**, *41* (13), 4755–4767.
25. Sahiner, N.; Demirci, S. Can PEI Microgels Become Biocompatible upon Betainization? *Mater. Sci. Eng. C* **2017**, *77*, 642–648.
26. Zheng, L.; Sundaram, H. S.; Wei, Z.; Li, C.; Yuan, Z. Applications of Zwitterionic Polymers. *React. Funct. Polym.* **2017**, *118* (March), 51–61.
27. Ladd, J.; Zhang, Z.; Chen, S.; Hower, J. C.; Jiang, S. Zwitterionic Polymers Exhibiting High Resistance to Nonspecific Protein Adsorption from Human Serum and Plasma. *Biomacromolecules* **2008**, *9* (5), 1357–1361.
28. Mohammadi Sejoubsari, R.; Martinez, A. P.; Kutes, Y.; Wang, Z.; Dobrynin, A. V.; Adamson, D. H. "Grafting-Through": Growing Polymer Brushes by Supplying Monomers through the Surface. *Macromolecules* **2016**, *49* (7), 2477–2483.
29. Henze, M.; Mädge, D.; Prucker, O.; Rühe, J. "Grafting through": Mechanistic Aspects of Radical Polymerization Reactions with Surface-Attached Monomers. *Macromolecules* **2014**, *47* (9), 2929–2937.
30. Pirman, T.; Ocepek, M.; Likozar, B. Radical Polymerization of Acrylates, Methacrylates, and Styrene: Biobased Approaches, Mechanism, Kinetics, Secondary Reactions, and Modeling. *Ind. Eng. Chem. Res.* **2021**, *60* (26), 9347–9367.
31. Szczepaniak, G.; Fu, L.; Jafari, H.; Kapil, K.; Matyjaszewski, K. Making ATRP More Practical: Oxygen Tolerance. *Acc. Chem. Res.* **2021**, *54* (7), 1779–1790.
32. Enciso, A. E.; Fu, L.; Russell, A. J.; Matyjaszewski, K. A Breathing Atom-Transfer Radical Polymerization: Fully Oxygen-Tolerant Polymerization Inspired by Aerobic Respiration of Cells. *Angew. Chemie - Int. Ed.* **2018**, *57* (4), 933–936.
33. Höfer, M.; Moszner, N.; Liska, R. Oxygen Scavengers and Sensitizers for Reduced Oxygen Inhibition in Radical Photopolymerization. *J. Polym. Sci. Part A Polym. Chem.* **2008**, *46* (20), 6916–6927.
34. Kenausis, G. L.; Vo, J.; Elbert, D. L.; Huang, N.; Hofer, R.; Ruiz-taylor, L.; Textor, M.; Hubbell, J. A.; Spencer, N. D. Poly (L-Lysine)-g-Poly(Ethylene Glycol) Layers on Metal Oxide Surfaces: Attachment Mechanism and Effects of Polymer

Architecture on Resistance to Protein Adsorption. *J. Phys. Chem. B* **2000**, *104* (14), 3298–3309.

35. Morgese, G.; Verbraeken, B.; Ramakrishna, S. N.; Gombert, Y.; Cavalli, E.; Rosenboom, J. G.; Zenobi-Wong, M.; Spencer, N. D.; Hoogenboom, R.; Benetti, E. M. Chemical Design of Non-Ionic Polymer Brushes as Biointerfaces: Poly(2-Oxazine)s Outperform Both Poly(2-Oxazoline)s and PEG. *Angew. Chem. Int. Ed.* **2018**, *57* (36), 11667–11672.
36. Paul, S. M. De; Vo, J.; Spencer, N. D.; Textor, M. Poly(L-Lysine)-Graft-Poly (Ethylene Glycol) Assembled Monolayers on Niobium Oxide Surfaces : A Quantitative Study of the Influence of Polymer Interfacial Architecture on Resistance to Protein Adsorption by ToF-SIMS and in Situ OWLS. *Langmuir* **2003**, *19* (20), 9216–9225.
37. Perry, S. S.; Yan, X.; Limpoco, F. T.; Lee, S.; Müller, M.; Spencer, N. D. Tribological Properties of Poly(l -Lysine)- Graft -Poly(Ethylene Glycol) Films: Influence of Polymer Architecture and Adsorbed Conformation. *ACS Appl. Mater. Interfaces* **2009**, *1* (6), 1224–1230.
38. Huang, W. M.; Gibson, S. J.; Facer, P.; Gu, J.; Polak, J. M. Improved Section Adhesion for Immunocytochemistry Using High Molecular Weight Polymers of L-Lysine as a Slide Coating. *Histochemistry* **1983**, *77* (2), 275–279.
39. Yan, X.; Perry, S. S.; Spencer, N. D.; Pasche, S.; De Paul, S. M.; Textor, M.; Lim, M. S. Reduction of Friction at Oxide Interfaces upon Polymer Adsorption from Aqueous Solutions. *Langmuir* **2004**, *20* (2), 423–428.
40. van Andel, E.; de Bus, I.; Tijhaar, E. J.; Smulders, M. M. J.; Savelkoul, H. F. J.; Zuilhof, H. Highly Specific Binding on Antifouling Zwitterionic Polymer-Coated Microbeads as Measured by Flow Cytometry. *ACS Appl. Mater. Interfaces* **2017**, *9* (44), 38211–38221.
41. Yang, W.; Chen, S.; Cheng, G.; Vaisocherová, H.; Xue, H.; Li, W.; Zhang, J.; Jiang, S. Film Thickness Dependence of Protein Adsorption from Blood Serum and Plasma onto Poly(Sulfobetaine)-Grafted Surfaces. *Langmuir* **2008**, *24* (17), 9211–9214.
42. Koc, J.; Schönemann, E.; Amuthalingam, A.; Clarke, J.; Finlay, J. A.; Clare, A. S.; Laschewsky, A.; Rosenhahn, A. Low-Fouling Thin Hydrogel Coatings Made of Photo-Cross-Linked Polyzwitterions. *Langmuir* **2019**, *35* (5), 1552–1562.
43. Baggerman, J.; Smulders, M. M. J.; Zuilhof, H. Romantic Surfaces: A Systematic Overview of Stable, Biospecific, and Antifouling Zwitterionic Surfaces. *Langmuir* **2019**, *35* (5), 1072–1084.
44. Surman, F.; Riedel, T.; Bruns, M.; Kostina, N. Y.; Sedláková, Z.; Rodriguez-Emmenegger, C. Polymer Brushes Interfacing Blood as a Route toward High Performance Blood Contacting Devices. *Macromol. Biosci.* **2015**, *15* (5), 636–646.
45. Chen, R.; Ma, Y.; Zhao, C.; Lin, Z.; Zhu, X.; Zhang, L.; Yang, W. Construction of DNA Microarrays on Cyclic Olefin Copolymer Surfaces Using Confined Photocatalytic Oxidation. *RSC Adv.* **2014**, *4* (87), 46653–46661.
46. Kuzmyn, A. R.; Nguyen, A. T.; Teunissen, L. W.; Zuilhof, H.; Baggerman, J. Antifouling Polymer Brushes via Oxygen-Tolerant Surface-Initiated PET-RAFT. *Langmuir* **2020**, *36* (16), 4439–4446.
47. Cao, B.; Li, L.; Tang, Q.; Cheng, G. The Impact of Structure on Elasticity, Switchability, Stability and Functionality of an All-in-One Carboxybetaine Elastomer. *Biomaterials* **2013**, *34* (31), 7592–7600.
48. Zhu, L. J.; Zhu, L. P.; Jiang, J. H.; Yi, Z.; Zhao, Y. F.; Zhu, B. K.; Xu, Y. Y. Hydrophilic and Anti-Fouling Polyethersulfone Ultrafiltration Membranes with Poly(2-Hydroxyethyl Methacrylate) Grafted Silica Nanoparticles as Additive. *J. Memb. Sci.* **2014**, *451*, 157–168.
49. Alswieleh, A. M.; Cheng, N.; Canton, I.; Ustbas, B.; Xue, X.; Ladmiral, V.; Xia, S.; Ducker, R. E.; Zubir, O. El; Cartron, M. L.; Hunter, C. N.; Leggett, G. J.; Armes, S. P. Zwitterionic Poly(Amino Acid Methacrylate) Brushes. *J. Am. Chem. Soc.* **2014**.
50. Chai, C.; Lee, J.; Park, J.; Takhistov, P. Antibody Immobilization on a Nanoporous Aluminum Surface for Immunosensor Development. *Appl. Surf. Sci.* **2012**, *263*, 195–201.

Summaries

Summary (English)
Samenvatting (Nederlands)

Summary

The undesired deposition of material onto a surface, also known as *fouling*, is a recurring challenge for many applications. The work described in this Thesis combines the fields of organic chemistry and surface chemistry for the development of antifouling coatings: from the synthesis of the macromolecular building blocks to their application on surfaces as coatings and testing of antifouling properties.

Chapter 1 provides an introduction to the concepts of fouling and antifouling. The most applied antifouling coating are discussed alongside the most promising, state-of-the-art polymer materials that make up these coatings. Furthermore, macromolecules such as polymers and dendrimers that make for interesting candidates to serve as new building blocks for antifouling coatings are discussed. Especially dendrimers represent interesting candidates due to the high level of control over their architecture and the possibility for multivalent interactions. Zwitterionic dendrimers (ZID) are modified with an equal number of oppositely charged groups have found use in many biomedical applications. However, the design of and control over the synthesis of these dendrimers remains challenging, in particular with respect to achieving full charge-neutral modification of the dendrimer. In **Chapter 2** the design, synthesis and characterization of fully zwitterionic, charge-neutral carboxybetaine and sulfobetaine zwitterionic dendrimers is described. Additionally, also the synthesis and characterization of ZIDs that contain a variable number of alkyne and azide groups are presented. Proof-of-principle coupling of an azide-biotin conjugate by click chemistry showed that these ZIDs indeed can be further modified. Especially the functionalized dendrimers are potential candidates for antifouling applications but also for biomedical applications such as drug delivery, since they allow straightforward anchoring or (bio)functionalization via click chemistry.

To form an antifouling coating, the developed ZID needs to be coupled to a surface. **Chapter 3** reports different strategies to enable covalent immobilization of ZIDs on a surface. The first explored method was amide bond-mediated binding of the ZID's carboxylates to amine-terminated surfaces. Next to this, two types of click reactions, copper-catalyzed azide-alkyne cycloadditions (CuAAC) and thiol-yne chemistry, between pre-installed functional groups on the ZIDs and the surfaces were tested. These strategies all resulted in monolayers of ZID, although the two click chemistry-based routes yielded slightly higher levels of immobilized ZID, *i.e.*, thicker and more hydrophilic layers. To further increase the immobilization load of the ZID, a *grafting-through* approach was tested that led to multilayers of ZID by reacting methacrylate-functionalized ZIDs onto a pre-coated surface. The multilayers showed increasing thickness and hydrophilicity with each newly formed layer, and displayed antifouling properties that were slightly better than the oligoethylene oxide monolayers which were used as a reference.

For these immobilization strategies, an undesirable surface pre-functionalization step was needed. To circumvent this, the macromolecules themself were designed to have an intrinsic affinity towards the surface. In the research described in **Chapter 4**, poly(L-lysine) (PLL) was used as a coupling agent. Two different routes were developed to synthesize polymer-dendrimer hybrids by the interconnection of PLL and ZID. The first route led to network-like structures in which PLL and ZIDs were crosslinked by

multiple amide bonds. The second route led to a more defined, linear PLL-ZID macromolecule, which was formed via click coupling of multiple ZIDs to a single PLL backbone. These two different types of PLL-ZID systems were self-assembled onto silicon oxide surfaces from aqueous solutions to form thin, hydrophilic coatings. Especially the linear variant yielded good antifouling properties towards single-protein solutions and diluted human serum, as shown in detail by quartz crystal microbalance (QCM) measurements. The formed coatings could be further bio-functionalized using the remaining carboxylate moieties. An on-surface biofunctionalization step by biotin demonstrated the possibility to use the PLL-ZID hybrids coatings for selective detection of target analytes (streptavidin), while the underlying coating maintained its antifouling properties.

Chapter 5 presents possibilities to create poly(*N*-(2-hydroxypropyl)methacrylamide) (HPMA) polymer brush-based coatings without having to perform sensitive polymerization reactions on-surface. HPMA polymers were grafted form a PLL backbone to create a so-called "bottlebrush" polymer, which could self-assemble onto a surface in a similar fashion like the PLL-ZID copolymers reported in Chapter 4. Three routes towards such PLL-HPMA-coated surfaces were developed ranging from "classic" *grafting-from* to entirely *grafting-to* in order to compare differences in outcome and overall antifouling performance of the coatings. Additionally, a *grafting-to* bottlebrush was synthesized that contained 5% carboxybetaine in its side chains, which offered the possibility for further functionalization after an ester activation step. Eventually, all surface modification routes yielded coatings that showed single-protein antifouling properties.

Finally, in **Chapter 6** the differently developed building blocks and coatings are discussed in terms of synthesis, antifouling properties and ease of application. The findings of this research are placed in a broader context and recommendations for further research are given.

Samenvatting

De onbedoelde afzetting van (bio)materiaal aan oppervlakken, ook wel *fouling* genoemd, is een hardnekkig en terugkerend probleem voor vele uiteenlopende biomedisch en bio analytische toepassingen. Het onderzoek zoals beschreven in dit proefschrift gebruikt de kennis uit zowel de organische chemie, als de oppervlaktechemie om nieuwe *antifouling coatings* te ontwikkelen: van de synthese van nieuwe macromoleculaire bouwstenen, tot de toepassing ervan als coating en het testen van de antifouling eigenschappen.

Hoofdstuk 1 introduceert de concepten fouling en antifouling, een overzicht van de huidige, meest toegepaste coatings, als ook van de verdere ontwikkelingen op het gebied van antifouling coatings. Verder worden macromoleculen zoals polymeren en dendrimeren besproken die kunnen dienen als bouwstenen voor nieuwe antifouling coatings. Dendrimeren zijn bijzonder interessante kandidaten dankzij hun unieke, goed gedefinieerde structuur en hun mogelijkheid om meerdere bindingen aan te gaan. *Zwitterionische* dendrimeren (ZID) zijn dusdanig gemodificeerd dat ze een exact gelijk aantal positieve en negatieve ladingen dragen en daarmee ladingsneutraal zijn. Dit creëert unieke eigenschappen wat deze ZID inzetbaar maakt voor biomedische toepassingen. Echter, het ontwerp en de synthese van ZID blijft een uitdaging, met name wat betreft het voorkomen van een netto lading (positief dan wel negatief) op het gehele dendrimeermolecuul.

In **Hoofdstuk 2** wordt het ontwerp, de synthese en karakterisering van volledig zwitterionische, neutrale carboxybetaine en sulfobetaine ZID beschreven. Tevens wordt de synthese en daaropvolgende karakterisering van een functionele ZID, gemodificeerd met een variabel aantal alkyn of azide groepen, gepresenteerd. De bruikbaarheid hiervan wordt aangetoond door de koppeling met een azide-biotine met behulp van een zogenaamde klik reactie. De mogelijkheid tot koppelen met andere materialen met gebruik van klikchemie maakt deze functionele ZID interessant als bouwsteen voor antifouling coatings, maar ook als drager van medicijnen *in vivo*.

Om een coating te creëren moeten het ZID gebonden worden aan een oppervlak. **Hoofdstuk 3** beschrijft de verschillende strategieën die zijn getest om dit te bewerkstelligen. Allereerst is geprobeerd om het ZID te verbinden door middel van amide bindingen tussen de carboxylaat groepen van het ZID en amine groepen op een oppervlak. Parallel hieraan zijn twee soorten klikchemie met gebruik van de functionele groepen aan het ZID getest, namelijk de koper gekatalyseerde azide-alkyn Huisgen-cycloadditie en de thiol-yn klikreactie. Deze strategieën leidden allemaal tot een coating die bestaat uit een enkelvoudige laag van het ZID, hoewel de twee soorten klikchemie tot iets meer binding van ZID leidden, wat resulteerde in dikkere en meer hydrofiele lagen.
Om de efficiëntie van de vorming van een ZID-gebaseerde coating verder te verbeteren, werd een methacrylaat gemodificeerde ZID herhaaldelijk gepolymeriseerd op een oppervlak met reactieve eindgroepen. De multilagen die hierbij vormden, werden bij iedere uitgevoerde cyclus dikker en hydrofieler, en lieten antifouling eigenschappen zien die het referentieoppervlak (gecoat met een oligoethyleenglycol laag) overtroffen.

De voorgenoemde koppeling strategieën vereisen allen een voorafgaande modificatie van het oppervlak, wat in principe ongewenst is. Om dit te voorkomen is het ZID in **Hoofdstuk 4** gekoppeld aan een polymeer poly(L-lysine) (PLL) dat een intrinsieke affiniteit heeft met het oppervlak. Hierbij zijn twee manieren van verbinden van PLL en ZID gekozen. De eerste was de vorming van een macromoleculair netwerk door willekeurige onderlinge koppeling van PLL en ZID middels amide bindingen. De tweede aanpak leidde tot de vorming van een goed gedefinieerd lineair macromolecuul waarbij meerdere ZID moleculen met één enkel PLL polymeer werden verbonden met behulp van klikchemie.
De resulterende soorten PLL-ZID macromoleculen hechtten spontaan aan het oppervlak vanuit een waterige oplossing, wat resulteerde in dunne, hydrofiele coatings. Met name de coatings gemaakt van lineaire PLL-ZID macromoleculen lieten kwalitatief goede antifouling zien in quartz crystal microbalance (QCM, kwarts-microbalans) tests met eiwit-oplossingen en verdund humaan serum. De gevormde coatings konden vervolgens voorzien worden van biotine groepen met gebruik van de beschikbare carboxylaten, waardoor het mogelijk was om selectief streptavidine te binden zonder verlies van het antifouling karakter.

In **Hoofdstuk 5** wordt de synthese van poly(*N*-(2-hydroxypropyl)methacrylamide)) (HPMA) coatings beschreden zonder daarbij gevoelige polymerisaties uit te hoeven voeren op een oppervlak. Door HPMA polymeren te groeien vanaf een PLL kern, werden zogenaamde PLL-HPMA polymeer-borstels gevormd die spontaan op een oppervlak hechten op een vergelijkbare manier als de PLL-ZID macromoleculen. Deze polymeer-borstel coatings werden op drie manieren gevormd: volledig in oplossing, volledig vanaf een oppervlak en een tussenvariant. Op deze manier konden de gevormde coatings die uit de drie routes voortkwamen onderling vergeleken worden wat betreft antifouling eigenschappen. Verder is er ook een HPMA-PLL polymeer-borstel in oplossing gesynthetiseerd die 5% carboxybetaine bevat in de zijgroepen, wat de mogelijkheid biedt om de polymeer-borstels te kunnen voorzien van andere functionele groepen en (bio)moleculen.

Tenslotte is er in **Hoofdstuk 6** een beschouwing gegeven op de synthese van de ontwikkelde bouwstenen en de toepasbaarheid en antifouling eigenschappen van de gevormde coatings. De belangrijkste bevindingen uit dit proefschrift zijn in een bredere context geplaatst met aanbevelingen voor vervolgonderzoek.

About the Author

Curriculum Vitae

Esther Maria Theodorus Roeven was born on May 11, 1990 in Venlo, The Netherlands. In 2008 she graduated secondary school at Bouwens van der Boije College in Panningen. In the same year, she started studying Applied Sciences at Fontys Eindhoven. During her BSc thesis project at Surfix BV in Wageningen, she got her first experience with surface chemistry by developing nanocoatings for biosensor chips. In 2012, she graduated *cum laude* on the topic Molecular Science and Engineering. After graduating, she worked at Surfix BV as an R&D engineer for four years. In 2016, she got the opportunity to start a collaborative PhD project at the Laboratory of Organic Chemistry at the Wageningen University & Research (The Netherlands) under the supervision of M. M. J. Smulders, L. Scheres and H. Zuilhof with Surfix BV as a partner. The goal of this project was to develop new antifouling coatings that allowed for easy application in a production environment. The most important results of this work are described in this thesis. Parallel to finishing her thesis, Esther started working as a researcher at Canon CPP in Venlo, The Netherlands.

List of Publications

Zwitterionic Dendrimer-Polymer Hybrid Copolymers for Self-Assembling Antifouling Coatings
Roeven, E., Scheres, L.M.W., Smulders, M., Zuilhof, H. *European Polymer Journal* **2021**, 156, 110578

PLL-Poly(HPMA) Bottlebrush-Based Antifouling Coatings: Three Grafting Routes
Roeven, E., Kuzmyn A. R., Scheres, L.M.W., Baggerman J., Smulders, M., Zuilhof, H. *Langmuir*, **2020**, 36, 10187–10199

Synthesis and characterization of functional zwitterionic dendrimers
Roeven, E., Scheres, L.M.W., Smulders, M., Zuilhof, H. *ACS Omega*, **2019**, 4, 3000−3011

Versatility of bromo-terminated porous aluminum oxide for its (bio)functionalization
Debrassi, A. , Roeven, E. , Thijssen, E. , Scheres, L.M.W. , Vos, W.M. de, Wennekes, T. , Beek, T.A. van , Zuilhof, H. *Langmuir,* **2015***,* 31 (20), 5633–5644

Ambient Surface Analysis of Organic Monolayers using Direct Analysis in Real Time Orbitrap Mass Spectrometry
Manova, R.K. , Joshi, S. , Debrassi, A. , Bhairamadgi, N.S. , Roeven, E. , Gagnon, J. , Tahir, M.N. , Claassen, F.W. , Scheres, L.M.W. , Wennekes, T. , Schroën, C.G.P.H. , Beek, T.A. van , Zuilhof, H. , Nielen, M.W.F. *Analytical Chemistry,* **2014**, 86, 2403 - 2411.

List of completed training activities

Discipline-specific activities	**Organizing institute**	**Year**
CHAINS (Chemistry As INnovating Science)	NWO	2016-2018
Advanced Organic Chemistry	ORC	2016-2020
Advanced Chemistry	ORC/PCC/BNT	2016
MicroNano Conference 2016	NanonextNL	2016-2017
DPD (Dutch Polymer Days)	PTN	2018-2019
Intern. Conference on Bio-inspired and Zwitterionic Materials	ICBZM	2019
Brightlands Rolduc Polymer Conference	Brightlands	2019

General courses	**Organizing institute**	**Year**
VLAG PhD Week	VLAG	2016
Scientific Artwork with Photoshop and Illustrator	WUR Library	2017
Scientific Writing	WSG	2018
Presenting with Impact	WSG	2020
Efficient Writing Strategies	WSG	2020

Optionals	**Organizing institute**	**Year**
Preparation PhD research proposal	ORC	2016
Group meetings and seminars	ORC/Surfix	2016-2020
PhD study trips (Denmark/Sweden, Israel)	ORC	2017, 2019

Dankwoord

Dankwoord

Eindelijk is het moment aangebroken: ik schrijf de laatste bladzijden van mijn proefschrift! Na vier jaar onderzoek en ruim een jaar schrijven, parallel aan een andere baan, zijn ook de laatste loodjes achter de rug.

Om jullie niet de indruk te geven dat alleen ik hard heb gewerkt de voorbije jaren, wil ik dat graag weerleggen door de volgende mensen stuk voor stuk te bedanken. Elk op hun eigen manier hebben ze mijn tijd als PhD student heel wat aangenamer gemaakt. Terugkijkend zijn de jaren voorbij gevlogen en ik kijk er heel dankbaar op terug.

Ten eerste wil ik graag mijn promotor bedanken: *Han*, bedankt voor de enorme kans die je me gegeven hebt om via een niet alledaagse route toch aan een PhD traject te mogen beginnen. Bedankt voor je vertrouwen, expertise en begeleiding. Je gevatheid om dingen kort maar correct te formuleren neem ik graag mee in mijn verdere carrière.

Maarten, bedankt voor het feit dat je eigenlijk altijd tijd voor me had. Je deur stond altijd open voor goede adviezen over een breed scala aan onderwerpen, wat je tot een ware mentor maakte. Jouw kennis over de synthese en analyse van macromoleculen hebben de oppervlaktechemie ermee mogelijk gemaakt. De snelle feedback op mijn “schrijfsels” (in welke staat ze ook verkeerden) hebben me enorm geholpen bij het schrijven van dit boekje.

Luc, heel veel dank voor alles! In 2011 koppelde Jan van Geldrop me aan (toen nog eenmanszaak) Surfix voor een afstudeerstage. Jij introduceerde me in de wondere wereld van de nanocoatings en dankzij het mooie project waaraan ik toen mocht werken kreeg ik de smaak te pakken, dit was gaaf werk! Ik bleef enkele jaren met plezier bij Surfix “plakken”. Een sluimerende wens om me verder te ontwikkelen vertaalde zich later in een onderzoek samen met de WUR, wat uiteindelijk tot dit boekje heeft geleid. Bedankt voor alles wat je hieraan hebt bijgedragen. Ook de vele gezamenlijke kilometers waarbij we overal over konden praten hebben zeer veel betekend, zeker in tijden die niet makkelijk voor me waren. In ruil daarvoor kletste ik de reistijd vol en strooide pepernoten door je auto... Inmiddels is Surfix uitgegroeid tot een prachtig bedrijf waar je enorm trots op mag zijn. Als je ooit een vestiging opent in Limburg opent, moet je me bellen!

Also to the members of my thesis committee, *Prof. J.R. de Vries*, *Prof. P.Y.W. Dankers*, *Prof. P. Jonkheijm*, and *dr. C. Rodriguez-Emmenegger*, thank you for finding time in your busy schedules to validate my PhD thesis.

Anke and *Alice* a big thank you for accepting to be my paranymphs. It feels a little more comfortable to defend my thesis knowing you will be next to me on that stage. Dear *Anke*, we started working at Surfix almost simultaneously. Thank you for the fun we had and for

answering my many questions. Dear *Alice*, you made my time at ORC so much more fun. Sharing both an office and lab also meant sharing thoughts, coffee and food. Thanks for all the fun and energy you bring to the group.

Mijn studenten *Margaux*, *Maaike* en *Jaimy* wil ik graag bedanken voor hun bijdrage aan de synthese en analyse van de dendrimeren. Heel veel succes in jullie verdere carrières!

Veel van de data in dit proefschrift was nooit tot stand gekomen zonder hulp van de technische staf. *Hans* en *Elbert*, bedankt voor jullie inzet en geduld om samen de dendrimeren te analyseren op de GPC. *Sidhu* en *Barend*, bedankt dat jullie de XPS toch altijd weer aan de praat kregen als mij dat niet lukte. *Barend* bedankt dat je ondanks vaak laag signaal toch bruikbare spectra uit de NMR wist te persen. Tevens wil ik je bedanken voor de vele niet-onderzoek gerelateerde gesprekken, deze heb ik ook als zeer waardevol ervaren. *Remco,* bedankt voor je hulp bij de DLS metingen, die hebben Hoofdstuk 5 mooi compleet gemaakt. *Pieter*, bedankt voor de ^{15}N-NMR metingen in Hoofdstuk 2. Zonder chemicaliën geen chemie! *Henny* bedankt voor het afhandelen van de vele bestellingen.

Elly, *Aleida*, *Bep*, *Esther*, *Meta*, jullie zorgen ervoor dat wij ons niet ook nog druk hoeven te maken over bureaucratische zaken, heel veel dank daarvoor!

Thank you ORC PhD's, post-docs, staff members, technicians and guest-researchers: *Milou, Ellen, Jordi, Michel, Pepijn, Jorick, Sybren, Sjoerd, Annemieke, Tjerk, Jorin, Kaustub, Rafael, Alyssa, Jay, DJ, Rickdeb, Gina, Ariadni, Pina, Stefani, Jorge, Caroline, DongDong, Sweccha, Natalja, Fred, Medea, Alexandre, Yuri, Andrada, Tunan, Daniele, Simon, Si, Fridolin, Julian, Jasper, Dieuwertje, Judith, Maurice, Hendra, Bauke, Louis, Anne-Marie, Ai* and *Jacob*. I enjoyed the pleasant working atmosphere, the many "borrels", study trips to Scandinavia and Israel, the Friday lunches, lab-trips, barbecues, WE-days and so on...

Andriy, thank you for being a great sparring partner and collaborator. I really appreciate your help characterizing surfaces using the fluorescence microscope and AFM. I am proud of our joined publication and it was a pleasure working with you!

"Andere" *Esther*, ik heb warme herinneringen aan de vele klets-momenten, vaak onder het genot van goede koffie. Buiten dat onze onderzoeken overlap hadden konden we ook over veel andere dingen praten die ons beiden bezig hielden. Ik bewonder je ambitie en doorzettingsvermogen. Heel veel succes met je verdere carrière, we houden contact!

Sevil, many thanks for teaching me how to work with the QCM-D, which enabled me to complete Chapter 4. Good luck finishing your own thesis!

Lucas, bedankt de mooie cover image die je voor me hebt gemaakt!

Ian, ik heb zeer veel bewondering voor je inzet en toewijding en kijk met heel veel plezier terug op een bijna volledige overlap van onze PhD-tijd. Ook een dikke dankjewel dat ik je de afgelopen maanden als “hulplijn” heb mogen gebruiken in de afronding van mijn eigen boekje.

Uiteraard wil ik ook mijn Surfix collega’s bedanken: *Luc, Anke, Carole, Adriaan, Jelmer, Wout, Janneke, Txema, Henk, Rui, Reamon, Kevin, Jeroen, Daan, Hans* en *Samira,* bedankt voor het delen van jullie kennis, de gezellige uitjes en de hele fijne werksfeer.

Irma, bedankt voor de vele gezellige carpool-kilometers. Dat betekende vaak heel vroeg opstaan en een strak schema draaien, maar dat heeft me ook heel efficiënt gemaakt.

Ook mijn huidige collega’s bij Canon in Venlo wil ik graag bedanken voor de ruimte en flexibiliteit die ik heb gekregen om mijn proefschrift tot een goed einde te brengen.

En dan mijn lieve vriendinnen *Maud, Roos, Steffie* en *Laura.* We kennen elkaar al sinds de basisschool en vanuit daar zijn we heel verschillende carrièrewegen gaan bewandelen. Desondanks is onze vriendschap er altijd geweest. Ik ben dankbaar dat we altijd een luisterend oor voor elkaar hebben en dat jullie me ook in dit avontuur gesteund hebben.

Graag wil ik ook mijn familie, schoonfamilie, en alles wat daar inmiddels bij hoort, bedanken voor jullie interesse, steun en vertrouwen. *Mam* & *Johan*, bedankt dat we vaak bij jullie mogen aanschuiven, dat is altijd een genot. *Pap* bedankt voor de tijd en energie die je in onze gezamenlijke hobby, de paardensport, steekt. Ook *Fanny* & *Anton* bedankt, lief zusje, ondanks de grote afstand en onze totaal verschillende levens hebben we tegenwoordig meer aan elkaar dan ooit. Ik ben heel erg trots op je!

Liefste *Sjoerd*, wat ben ik blij dat wij het samen zo fijn hebben. De afgelopen jaren heb je me gesteund en gemotiveerd maar ook gekalmeerd wanneer dat nodig was. Bedankt voor je liefde, humor en goede zorgen. Ik kijk uit naar onze toekomst samen, ik hou van je. ❤

Esther

The research presented in this thesis was financially supported by NWO (LIFT program, grant 731.015.042) with Surfix BV as a partner.

Financial support from Wageningen University for printing this thesis is gratefully acknowledged.
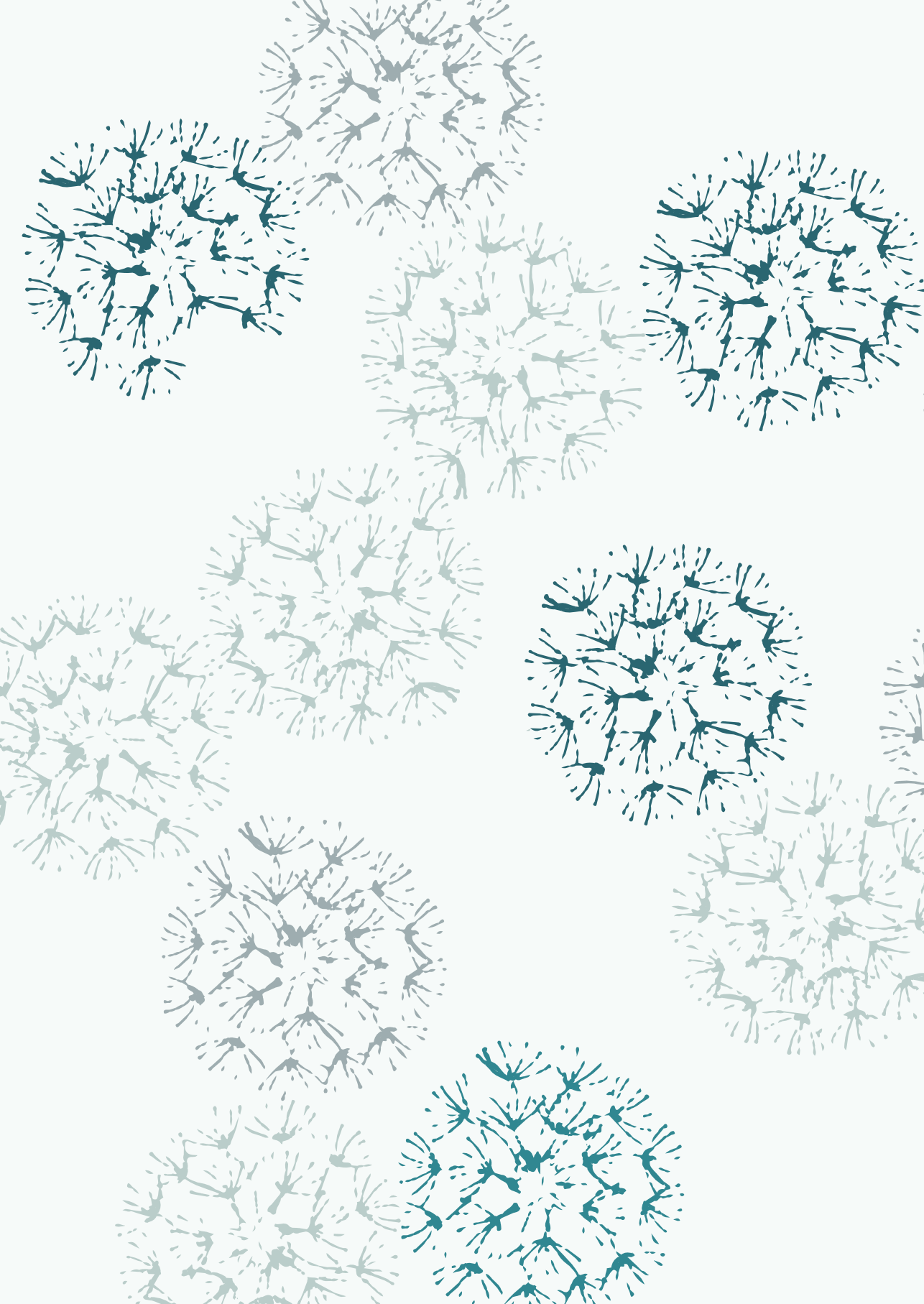
Printed by GVO Drukkers & Vormgevers B.V., Ede, The Netherlands
Design and layout by author
Cover by Loes Kema